



International Agreement Report

Evaluation of TRACE Spacer Grid Model with FLECHT-SEASET Reflood Test

Prepared by:
Byung-Gil HUH, Ae-Ju CHEONG, Kyung Won LEE

Korea Institute of Nuclear Safety
62 Gwahak-ro, Yuseong-gu
Daejeon, 34142, Korea

K. Tien, NRC Project Manager

Division of Systems Analysis
Office of Nuclear Regulatory Research
U.S. Nuclear Regulatory Commission
Washington, DC 20555-0001

Manuscript Completed: December 2016
Date Published: August 2017

Prepared as part of
The Agreement on Research Participation and Technical Exchange
Under the Code Applications and Maintenance Program (CAMP)

Published by
U.S. Nuclear Regulatory Commission

AVAILABILITY OF REFERENCE MATERIALS IN NRC PUBLICATIONS

NRC Reference Material

As of November 1999, you may electronically access NUREG-series publications and other NRC records at the NRC's Public Electronic Reading Room at <http://www.nrc.gov/reading-rm.html>. Publicly released records include, to name a few, NUREG-series publications; *Federal Register* notices; applicant, licensee, and vendor documents and correspondence; NRC correspondence and internal memoranda; bulletins and information notices; inspection and investigative reports; licensee event reports; and Commission papers and their attachments.

NRC publications in the NUREG series, NRC regulations, and Title 10, "Energy," in the *Code of Federal Regulations* may also be purchased from one of these two sources.

1. The Superintendent of Documents

U.S. Government Publishing Office
Mail Stop SSOP
Washington, DC 20402-0001
Internet: <http://bookstore.gpo.gov>
Telephone: 1-866-512-1800
Fax: (202) 512-2104

2. The National Technical Information Service

5301 Shawnee Road
Alexandria, VA 22161-0002
<http://www.ntis.gov>
1-800-553-6847 or, locally, (703) 605-6000

A single copy of each NRC draft report for comment is available free, to the extent of supply, upon written request as follows:

U.S. Nuclear Regulatory Commission

Office of Administration
Publications Branch
Washington, DC 20555-0001
E-mail: distribution.resource@nrc.gov
Facsimile: (301) 415-2289

Some publications in the NUREG series that are posted at the NRC's Web site address <http://www.nrc.gov/reading-rm/doc-collections/nuregs> are updated periodically and may differ from the last printed version. Although references to material found on a Web site bear the date the material was accessed, the material available on the date cited may subsequently be removed from the site.

Non-NRC Reference Material

Documents available from public and special technical libraries include all open literature items, such as books, journal articles, transactions, *Federal Register* notices, Federal and State legislation, and congressional reports. Such documents as theses, dissertations, foreign reports and translations, and non-NRC conference proceedings may be purchased from their sponsoring organization.

Copies of industry codes and standards used in a substantive manner in the NRC regulatory process are maintained at—

The NRC Technical Library

Two White Flint North
11545 Rockville Pike
Rockville, MD 20852-2738

These standards are available in the library for reference use by the public. Codes and standards are usually copyrighted and may be purchased from the originating organization or, if they are American National Standards, from—

American National Standards Institute

11 West 42nd Street
New York, NY 10036-8002
<http://www.ansi.org>
(212) 642-4900

Legally binding regulatory requirements are stated only in laws; NRC regulations; licenses, including technical specifications; or orders, not in NUREG-series publications. The views expressed in contractor-prepared publications in this series are not necessarily those of the NRC.

The NUREG series comprises (1) technical and administrative reports and books prepared by the staff (NUREG-XXXX) or agency contractors (NUREG/CR-XXXX), (2) proceedings of conferences (NUREG/CP-XXXX), (3) reports resulting from international agreements (NUREG/IA-XXXX), (4) brochures (NUREG/BR-XXXX), and (5) compilations of legal decisions and orders of the Commission and Atomic and Safety Licensing Boards and of Directors' decisions under Section 2.206 of NRC's regulations (NUREG-0750).

DISCLAIMER: This report was prepared under an international cooperative agreement for the exchange of technical information. Neither the U.S. Government nor any agency thereof, nor any employee, makes any warranty, expressed or implied, or assumes any legal liability or responsibility for any third party's use, or the results of such use, of any information, apparatus, product or process disclosed in this publication, or represents that its use by such third party would not infringe privately owned rights.



International Agreement Report

Evaluation of TRACE Spacer Grid Model with FLECHT-SEASET Reflood Test

Prepared by:
Byung-Gil HUH, Ae-Ju CHEONG, Kyung Won LEE

Korea Institute of Nuclear Safety
62 Gwahak-ro, Yuseong-gu
Daejeon, 34142, Korea

K. Tien, NRC Project Manager

Division of Systems Analysis
Office of Nuclear Regulatory Research
U.S. Nuclear Regulatory Commission
Washington, DC 20555-0001

Manuscript Completed: December 2016
Date Published: August 2017

Prepared as part of
The Agreement on Research Participation and Technical Exchange
Under the Code Applications and Maintenance Program (CAMP)

Published by
U.S. Nuclear Regulatory Commission

ABSTRACT

The effects of spacer grid model of TRACE V5.0 patch 4 were assessed for the Full-Length Emergency Core Heat Transfer Separate Effects and Systems Effects Tests (FLECHT-SEASET) that were the typical reflood heat transfer tests. The FLECHT-SEASET test section was modeled in the VESSEL component of TRACE and the 161 heated rods in 17x17 assemblies were modeled as a single HTSTR component. The injected flow rates and temperatures were provided as a function of time by a FILL component connecting to the bottom of the lower plenum. The BREAK component was used to set the pressure boundary at the top of the test section. The main parameters of the spacer grid were defined by the experimental design data and eight egg-crate grids were modeled in the VESSEL component of TRACE. The calculations for eight tests of FLECHT-SEASET revealed that when the spacer grid model was used, the rod temperatures decreased and the rods were quenched at an earlier time in most other tests. In addition, as the reflood rate increased, the lower peak rod temperature and the earlier quenching time were predicted. When the test pressure was lower, the higher rod temperature and the later rod quenching were predicted since the liquid approached a relatively lower saturation temperature faster. When the subcooling degree was higher, the reduced degree of quenching time due to the spacer grid was further decreased because the higher subcooling degree enhanced the heat transfer rate. Sensitivity studies were performed to identify the effect of the grid locations and the difference from the spacer grid model of RELAP5. In this study, the effect of the spacer grid model in TRACE is shown well to simulate the FLECHT-SEASET reflood heat transfer tests. However, since the droplet breakup and the grid rewetting models were not fully implemented yet, there were some limitations in quantitatively predicting their effects. The comparison with the RELAP5 revealed that the current RELAP5 version had some errors in implementing the spacer grid model, and the effect of the spacer grid of TRACE could have been over-estimated for the rod temperature behaviors as compared with RELAP5.

TABLE OF CONTENTS

	<u>Page</u>
ABSTRACT	iii
LIST OF FIGURES	vii
LIST OF TABLES	xi
EXECUTIVE SUMMARY	xiii
1 INTRODUCTION	1
2 TEST FACILITY AND MODEL DESCRIPTION	3
2.1 Description of the FLECHT-SEASET Experiment.....	3
2.1.1 Spacer Grid Model in TRACE.....	6
3 EVALUATION OF THE SPACER GRID MODEL FOR FLECHT-SEASET REFLOOD TESTS	9
3.1 TRACE Modeling.....	9
3.2 Evaluation for Spacer Grid Model.....	13
4 SENSITIVITY ANALYSIS	99
4.1 Effect of the Grid Location.....	99
4.1.1 Run No. 31805.....	99
4.1.2 Run No. 31302.....	105
4.2 Comparison with Spacer Grid Model of RELAP5.....	109
5 CONCLUSIONS	129
6 REFERENCES	131

LIST OF FIGURES

		<u>Page</u>
Figure 2-1	FLECHT-SEASET Test Facility.....	4
Figure 2-2	FLECHT-SEASET Test Bundle Cross Section.....	5
Figure 3-1	TRACE Nodalization for FLECHT-SEASET Facility.....	11
Figure 3-2	Axial Power Profile of Heated Rod.....	12
Figure 3-3	Liquid Inlet Flowrate – Run No.31805.....	15
Figure 3-4	Liquid Inlet Temperature – Run No.31805.....	16
Figure 3-5	Heater Rod Temperature at 0.6 m – Run No.31805.....	16
Figure 3-6	Heater Rod Temperature at 1.2 m – Run No.31805.....	17
Figure 3-7	Heater Rod Temperature at 1.8 m – Run No.31805.....	17
Figure 3-8	Heater Rod Temperature at 1.98 m – Run No.31805.....	18
Figure 3-9	Heater Rod Temperature at 2.4 m – Run No.31805.....	18
Figure 3-10	Heater Rod Temperature at 3.0 m – Run No.31805.....	19
Figure 3-11	Heater Rod Temperature at 3.3 m – Run No.31805.....	19
Figure 3-12	Heater Rod Temperature at 3.5 m – Run No.31805.....	20
Figure 3-13	Quench Front Profile – Run No.31805.....	20
Figure 3-14	Differential Pressure for Entire 12 ft – Run No.31805.....	21
Figure 3-15	Differential Pressure at 10~11 ft Elevation – Run No.31805.....	21
Figure 3-16	Vapor Temperature at 1.8 m – Run No.31805.....	22
Figure 3-17	Vapor Temperature at 3.0 m – Run No.31805.....	22
Figure 3-18	Heat Transfer Coefficient at 1.98 m – Run No.31805.....	23
Figure 3-19	Heat Transfer Coefficient at 2.4 m – Run No.31805.....	23
Figure 3-20	Heat Transfer Coefficient at 3.0 m – Run No.31805.....	24
Figure 3-21	Liquid Inlet Flowrate – Run No.31504.....	25
Figure 3-22	Liquid Inlet Temperature – Run No. 31504.....	26
Figure 3-23	Heater Rod Temperature at 0.6 m – Run No.31504.....	26
Figure 3-24	Heater Rod Temperature at 1.2 m – Run No.31504.....	27
Figure 3-25	Heater Rod Temperature at 1.8 m – Run No.31504.....	27
Figure 3-26	Heater Rod Temperature at 1.98 m – Run No.31504.....	28
Figure 3-27	Heater Rod Temperature at 2.4 m – Run No.31504.....	28
Figure 3-28	Heater Rod Temperature at 3.0 m – Run No.31504.....	29
Figure 3-29	Heater Rod Temperature at 3.3 m – Run No.31504.....	29
Figure 3-30	Heater Rod Temperature at 3.5 m – Run No.31504.....	30
Figure 3-31	Quench Front Profile – Run No.31504.....	30
Figure 3-32	Differential Pressure for Entire 12 ft – Run No.31504.....	31
Figure 3-33	Differential Pressure at 10~11 ft Elevation – Run No.31504.....	31
Figure 3-34	Vapor Temperature at 1.8 m – Run No.31504.....	32
Figure 3-35	Vapor Temperature at 3.0 m – Run No.31504.....	32
Figure 3-36	Heat Transfer Coefficient at 1.98 m – Run No.31504.....	33
Figure 3-37	Heat Transfer Coefficient at 2.4 m – Run No.31504.....	33
Figure 3-38	Heat Transfer Coefficient at 3.0 m – Run No.31504.....	34
Figure 3-39	Liquid Inlet Flowrate – Run No.31203.....	35
Figure 3-40	Liquid Inlet Temperature – Run No. 31203.....	36
Figure 3-41	Heater Rod Temperature at 0.6 m – Run No.31203.....	36
Figure 3-42	Heater Rod Temperature at 1.2 m – Run No.31203.....	37
Figure 3-43	Heater Rod Temperature at 1.8 m – Run No.31203.....	37

Figure 3-44	Heater Rod Temperature at 1.98 m – Run No.31203	38
Figure 3-45	Heater Rod Temperature at 2.4 m – Run No.31203	38
Figure 3-46	Heater Rod Temperature at 3.0 m – Run No.31203	39
Figure 3-47	Heater Rod Temperature at 3.3 m – Run No.31203	39
Figure 3-48	Heater Rod Temperature at 3.5 m – Run No.31203	40
Figure 3-49	Quench Front Profile – Run No.31203	40
Figure 3-50	Differential Pressure for Entire 12 ft – Run No.31203	41
Figure 3-51	Differential Pressure at 10~11 ft Elevation – Run No.31203	41
Figure 3-52	Vapor Temperature at 1.8 m – Run No.31203	42
Figure 3-53	Vapor Temperature at 3.0 m – Run No.31203	42
Figure 3-54	Heat Transfer Coefficient at 1.98 m – Run No.31203	43
Figure 3-55	Heat Transfer Coefficient at 2.4 m – Run No.31203	43
Figure 3-56	Heat Transfer Coefficient at 3.0 m – Run No.31203	44
Figure 3-57	Liquid Inlet Flowrate – Run No.31302	46
Figure 3-58	Liquid Inlet Temperature – Run No. 31302	46
Figure 3-59	Heater Rod Temperature at 0.6 m – Run No.31302	47
Figure 3-60	Heater Rod Temperature at 1.2 m – Run No.31302	47
Figure 3-61	Heater Rod Temperature at 1.8 m – Run No.31302	48
Figure 3-62	Heater Rod Temperature at 1.98 m – Run No.31302	48
Figure 3-63	Heater Rod Temperature at 2.4 m – Run No.31302	49
Figure 3-64	Heater Rod Temperature at 3.0 m – Run No.31302	49
Figure 3-65	Heater Rod Temperature at 3.3 m – Run No.31302	50
Figure 3-66	Heater Rod Temperature at 3.5 m – Run No.31302	50
Figure 3-67	Quench Front Profile – Run No.31302	51
Figure 3-68	Differential Pressure for Entire 12 ft – Run No.31302	51
Figure 3-69	Differential Pressure at 10~11 ft Elevation – Run No.31302	52
Figure 3-70	Vapor Temperature at 1.8 m – Run No.31302	52
Figure 3-71	Vapor Temperature at 3.0 m – Run No.31302	53
Figure 3-72	Heat Transfer Coefficient at 1.98 m – Run No.31302	53
Figure 3-73	Heat Transfer Coefficient at 2.4 m – Run No.31302	54
Figure 3-74	Heat Transfer Coefficient at 3.0 m – Run No.31302	54
Figure 3-75	Liquid Inlet Flowrate – Run No.31701	56
Figure 3-76	Liquid Inlet Temperature – Run No. 31701	57
Figure 3-77	Heater Rod Temperature at 0.6 m – Run No.31701	57
Figure 3-78	Heater Rod Temperature at 1.2 m – Run No.31701	58
Figure 3-79	Heater Rod Temperature at 1.8 m – Run No.31701	58
Figure 3-80	Heater Rod Temperature at 1.98 m – Run No.31701	59
Figure 3-81	Heater Rod Temperature at 2.4 m – Run No.31701	59
Figure 3-82	Heater Rod Temperature at 3.0 m – Run No.31701	60
Figure 3-83	Heater Rod Temperature at 3.3 m – Run No.31701	60
Figure 3-84	Heater Rod Temperature at 3.5 m – Run No.31701	61
Figure 3-85	Quench Front Profile – Run No.31701	61
Figure 3-86	Differential Pressure for Entire 12 ft – Run No.31701	62
Figure 3-87	Differential Pressure at 10~11 ft Elevation – Run No.31701	62
Figure 3-88	Vapor Temperature at 1.8 m – Run No.31701	63
Figure 3-89	Vapor Temperature at 3.0 m – Run No.31701	63
Figure 3-90	Heat Transfer Coefficient at 1.98 m – Run No.31701	64
Figure 3-91	Heat Transfer Coefficient at 2.4 m – Run No.31701	64
Figure 3-92	Heat Transfer Coefficient at 3.0 m – Run No.31701	65

Figure 3-93	Liquid Inlet Flowrate – Run No.31108	67
Figure 3-94	Liquid Inlet Temperature – Run No. 31108	67
Figure 3-95	Heater Rod Temperature at 0.6 m – Run No.31108	68
Figure 3-96	Heater Rod Temperature at 1.2 m – Run No.31108	68
Figure 3-97	Heater Rod Temperature at 1.8 m – Run No.31108	69
Figure 3-98	Heater Rod Temperature at 1.98 m – Run No.31108	69
Figure 3-99	Heater Rod Temperature at 2.4 m – Run No.31108	70
Figure 3-100	Heater Rod Temperature at 3.0 m – Run No.31108	70
Figure 3-101	Heater Rod Temperature at 3.3 m – Run No.31108	71
Figure 3-102	Heater Rod Temperature at 3.5 m – Run No.31108	71
Figure 3-103	Quench Front Profile – Run No.31108	72
Figure 3-104	Differential Pressure for Entire 12 ft – Run No.31108	72
Figure 3-105	Differential Pressure at 10~11 ft Elevation – Run No.31108.....	73
Figure 3-106	Vapor Temperature at 1.8 m – Run No.31108	73
Figure 3-107	Vapor Temperature at 3.0 m – Run No.31108	74
Figure 3-108	Heat Transfer Coefficient at 1.98 m – Run No.31108	74
Figure 3-109	Heat Transfer Coefficient at 2.4 m – Run No.31108	75
Figure 3-110	Heat Transfer Coefficient at 3.0 m – Run No.31108	75
Figure 3-111	Liquid Inlet Flowrate – Run No.32013	77
Figure 3-112	Liquid Inlet Temperature – Run No.32013	77
Figure 3-113	Heater Rod Temperature at 0.6 m – Run No.32013	78
Figure 3-114	Heater Rod Temperature at 1.2 m – Run No.32013	78
Figure 3-115	Heater Rod Temperature at 1.8 m – Run No.32013	79
Figure 3-116	Heater Rod Temperature at 1.98 m – Run No.32013	79
Figure 3-117	Heater Rod Temperature at 2.4 m – Run No.32013	80
Figure 3-118	Heater Rod Temperature at 3.0 m – Run No.32013	80
Figure 3-119	Heater Rod Temperature at 3.3 m – Run No.32013	81
Figure 3-120	Heater Rod Temperature at 3.5 m – Run No.32013	81
Figure 3-121	Quench Front Profile – Run No.32013	82
Figure 3-122	Differential Pressure for Entire 12 ft – Run No.32013	82
Figure 3-123	Differential Pressure at 10~11 ft Elevation – Run No.32013.....	83
Figure 3-124	Vapor Temperature at 1.8 m – Run No.32013	83
Figure 3-125	Vapor Temperature at 3.0 m – Run No.32013	84
Figure 3-126	Heat Transfer Coefficient at 1.98 m – Run No.31701	84
Figure 3-127	Heat Transfer Coefficient at 2.4 m – Run No.31701	85
Figure 3-128	Heat Transfer Coefficient at 3.0 m – Run No.31701	85
Figure 3-129	Liquid Inlet Flowrate – Run No.32114	87
Figure 3-130	Liquid Inlet Temperature – Run No. 32114	87
Figure 3-131	Heater Rod Temperature at 0.6 m – Run No.32114	88
Figure 3-132	Heater Rod Temperature at 1.2 m – Run No.32114	88
Figure 3-133	Heater Rod Temperature at 1.8 m – Run No.32114	89
Figure 3-134	Heater Rod Temperature at 1.98 m – Run No.32114	89
Figure 3-135	Heater Rod Temperature at 2.4 m – Run No.32114	90
Figure 3-136	Heater Rod Temperature at 3.0 m – Run No.32114	90
Figure 3-137	Heater Rod Temperature at 3.3 m – Run No.32114	91
Figure 3-138	Heater Rod Temperature at 3.5 m – Run No.32114	91
Figure 3-139	Quench Front Profile – Run No.32114	92
Figure 3-140	Differential Pressure for Entire 12 ft – Run No.32114	92
Figure 3-141	Differential Pressure at 10~11 ft Elevation – Run No.32114.....	93

Figure 3-142	Vapor Temperature at 1.8 m – Run No.32114	93
Figure 3-143	Vapor Temperature at 3.0 m – Run No.32114	94
Figure 3-144	Heat Transfer Coefficient at 1.98 m – Run No.32114	94
Figure 3-145	Heat Transfer Coefficient at 2.4 m – Run No.32114	95
Figure 3-146	Heat Transfer Coefficient at 3.0 m – Run No.32114	95
Figure 3-147	Variation of Peak Rod Temperature at Elevation $z = 1.98$	98
Figure 3-148	Variation of Quenching Time at Elevation $z = 1.98$	98
Figure 4-1	Node Change for Sensitivity of Grid Location.....	101
Figure 4-2	Heater Rod Temperature at 1.2 m – Run No.31805	102
Figure 4-3	Heater Rod Temperature at 1.98 m – Run No.31805	102
Figure 4-4	Heater Rod Temperature at 2.4 m – Run No.31805	103
Figure 4-5	Heater Rod Temperature at 3.3 m – No.31805.....	103
Figure 4-6	Quench Front Profile – Run No.31805.....	104
Figure 4-7	Heat Transfer Coefficient at 1.98 m – Run No.31805	104
Figure 4-8	Heater Rod Temperature at 1.2 m – Run No.31302	106
Figure 4-9	Heater Rod Temperature at 1.98 m – Run No.31302	106
Figure 4-10	Heater Rod Temperature at 2.4 m – Run No.31302	107
Figure 4-11	Heater Rod Temperature at 3.3 m – No.31302.....	107
Figure 4-12	Quench Front Profile – Run No.31302	108
Figure 4-13	Heat Transfer Coefficient at 2.4 m – Run No.31302	108
Figure 4-14	RELAP5 Nodalization for the FLECHT-SEASET Test.....	110
Figure 4-15	Heater Rod Temperature at 1.2 m – Run No.31805	111
Figure 4-16	Heater Rod Temperature at 1.98 m – Run No.31805	112
Figure 4-17	Heater Rod Temperature at 3.0 m – Run No.31805	112
Figure 4-18	Heater Rod Temperature at 1.2 m – Run No.31805	113
Figure 4-19	Heater Rod Temperature at 1.98 m – Run No.31805	113
Figure 4-20	Heater Rod Temperature at 3.0 m – Run No.31805	114
Figure 4-21	Heater Rod Temperature at 1.2 m – Run No.31805	116
Figure 4-22	Heater Rod Temperature at 1.98 m – Run No.31805	116
Figure 4-23	Heater Rod Temperature at 2.4 m – Run No.31805	117
Figure 4-24	Heater Rod Temperature at 3.0 m – Run No.31805	117
Figure 4-25	Heater Rod Temperature at 3.3 m – Run No.31805	118
Figure 4-26	Heater Rod Temperature at 3.5 m – Run No.31805	118
Figure 4-27	Axial Rod Temperature Profile at 150 sec – Run No.31805.....	119
Figure 4-28	Axial Rod Temperature Profile for Sub-models at 150 sec – Run No.31805	119
Figure 4-29	Variation of Heat Transfer Enhancement for Laminar Enhancement Factor.....	120
Figure 4-30	Heater Rod Temperature at 1.2 m – Run No.31302	121
Figure 4-31	Heater Rod Temperature at 1.98 m – Run No.31302	121
Figure 4-32	Heater Rod Temperature at 2.4 m – Run No.31302	122
Figure 4-33	Heater Rod Temperature at 3.0 m – Run No.31302	122
Figure 4-34	Heater Rod Temperature at 3.3 m – Run No.31302	123
Figure 4-35	Heater Rod Temperature at 3.5 m – Run No.31302	123
Figure 4-36	Heater Rod Temperature at 1.2 m – Run No.31805	125
Figure 4-37	Heater Rod Temperature at 1.98 m – Run No.31805	125
Figure 4-38	Heater Rod Temperature at 3.0 m – Run No.31805	126
Figure 4-39	Heater Rod Temperature at 1.2 m – Run No.31805	126
Figure 4-40	Heater Rod Temperature at 1.98 m – Run No.31805	127
Figure 4-41	Heater Rod Temperature at 3.0 m – Run No.31805	127

LIST OF TABLES

	<u>Page</u>
Table 3-1 Test Matrix for TRACE Evaluation.....	13
Table 3-2 Peak Temperature and Quenching Time at Elevation $z = 1.98$	97
Table 4-1 Peak Temperature and Quenching Time at Elevation $z = 1.98$ for Run No. 31805 ..	100
Table 4-2 Peak Temperature and Quenching Time at Elevation $z = 1.98$ for Run No. 31302 ..	105

EXECUTIVE SUMMARY

TRACE implemented spacer grid models in 2010 that enhanced the heat transfer downstream of spacer grids, but a systematic assessment of those models has not been performed for various post-CHF heat transfer tests such as FLECHT-SEASET, THTF, etc. In particular, the FLECHT-SEASET tests are considered representative reflood experiments because the facility is relatively large and well instrumented. In this study, the spacer grid model of TRACE was evaluated for the FLECHT-SEASET test by the TRACE V5.0 patch4.

The Full-Length Emergency Core Heat Transfer Separate Effects and Systems Effects Tests (FLECHT-SEASET) was conducted to identify the thermal hydraulic phenomena of forced and gravity reflooding in a 161-rod bundle without flow blockage. The FLECHT-SEASET test section was modeled in the VESSEL component of TRACE. The test section was divided into 16 axial nodes: one node for the lower plenum, fourteen nodes for the heated section and one node for the upper plenum, and there were two cells between each grid. The 161 heated rods in 17x17 assemblies were modeled as a single HTSTR component. The injected flow rates and temperatures were provided as a function of time by the FILL component, which was connected to the bottom of the lower plenum. The BREAK component was used to set the pressure boundary at the top of the test section. Eight egg-crate grids without a mixing vane were located in the bottom of every other node. The grid parameters were determined by the experimental design data and the general fuel data.

Eight tests were selected for analyses, and tests covered a range of the flooding rate from 2.10 cm/sec to 15.50 cm/sec, the subcooling temperature from 5 °C to 79 °C and the upper plenum pressure from 0.13 MPa to 0.41 MPa. The initial rod power at the peak location was 2.3 kW/m (0.7 kW/ft) in all the tests. As would be expected, the rod temperatures decreased and the rods were quenched at an earlier time in most tests if the spacer grid model was used. In addition, as the reflood rate increased, a lower peak rod temperature and earlier quenching time were predicted. In tests with a high reflood rate, the change in the peak temperature due to the spacer grid was not large, which resulted from a short heat up period and a faster increase in the liquid level by the high reflooding rate. As the test pressure decreased, a higher rod temperature and later rod quenching were predicted since the liquid approached the relatively lower saturation temperature faster. The use of the spacer grid model at a lower pressure showed relatively bigger differences for rod temperature, but not for quenching time. With a higher subcooling degree, the decreased amount of quenching time due to the spacer grid also reduced because the high subcooling degree enhanced the heat transfer rate.

Sensitivity studies were performed to identify the effect of the grid locations and the difference from the spacer grid model of RELAP5. When the locations of spacer grids were changed to the top of every other node, the rod temperature was higher and the rod quenching was delayed at a high power than in the case in which the spacer grids were located in the bottom of the node. It would be more reasonable to predict the experimental data, which would have more conservative results. The RELAP5 code currently implemented the KNF reflood model and the spacer grid model. This spacer grid model considered three sub-models: single-phase heat transfer enhancement, grid rewet, and droplet breakup. However, the current RELAP5 version (Version 3.3jz~3.3kl) may have some errors in implementing the KNF reflood and spacer grid model. It may be because there are some problems with using the KNF reflood model (Option 40) and the spacer grid input (43000000 cards). Therefore, the developmental version of KNF was used to identify the effect of sub-models, and then the droplet breakup model had the biggest effect on the rod temperatures among the three models. The effect of the droplet breakup model was more significant at the higher elevation since the droplet velocity and the number of entrained droplets could be larger at the higher elevation. When the RELAP5 results were compared with the TRACE results, the effect of the spacer grid model in TRACE was more significant even though the single-phase heat transfer enhancement was only implemented in

TRACE. These results may be due to the modeling characteristics and the use of the laminar enhancement factor in TRACE. The convective heat transfer enhancement may be excessively large if the laminar enhancement factor is large.

In conclusion, the effect of the spacer grid model in TRACE was shown well to simulate the FLECHT-SEASET reflood heat transfer experiments. However, there were some limitations in quantitatively predicting the effect of the droplet breakup and the grid rewetting models. The comparison with the RELAP5 revealed that the current RELAP5 version had some errors in implementing the spacer grid model, and the effect of the spacer grid of TRACE may have been over-predicted for the rod temperature behaviors as compared to RELAP5. Therefore, in future studies the current RELAP5 needs to be modified to correct the errors for the spacer grid model and the TRACE code should be improved to implement the droplet breakup and the grid rewetting models.

1 INTRODUCTION

A spacer grid is generally installed in most commercial pressurized light water reactor (PWR) fuel assemblies. The spacer grid was developed by evaluating, among other things, the fuel rod vibration performance, the fretting wear resistance, the heat transfer enhancement, and the pressure drop characteristics. In particular, the spacer grid can influence the analysis for a large break loss of coolant accident (LOCA), is the most severe accident of a PWR because it affects the thermal-hydraulics in the core during the blowdown and reflood phases. After initiating a large break in the cold legs, the two-phase mixture formed by the flashing flows through the core and discharges into the break. The reflood phase typically starts by increasing the subcooled water from the bottom of the core. Large amounts of steam are generated by interacting between the subcooled water and hot fuels. This steam increases the core pressure and then hinders the reflooding of water. Various heat transfer regimes such as single-phase vapor convection, nucleate boiling, transition boiling, and film boiling also appears during this phase [1]. Therefore, the spacer grid can affect the heat transfer mechanism of the core during these phases. However, the effect of the spacer grid has not been evaluated properly in various accident analyses, and it has just been considered by adding the loss coefficient at the location of spacer grid.

The spacer grid was originally designed to maintain a geometrical configuration of the fuel bundles and support fuel rods laterally and vertically. However, the spacer grids affected the fluid dynamics and the heat transfer in the core. The spacer grids can create an obstacle to the fluid flow in the core and then increase the overall pressure losses. The spacer grids can also decrease the flow area by contracting and accelerating the flow, and the mixing vanes of the spacer grid typically promotes turbulence and induces a strong swirling flow in the core, which increases the local heat transfer downstream of the spacer grid. In addition, if the spacer grids are quenched, their surfaces are covered with liquid film and provide an additional interface area between liquid and vapor. Finally, the spacer grids can also break up the entrained droplets into smaller droplets and therefore the downstream vapor temperature decreases due to the enhancement of the evaporative heat transfer of the smaller droplets.

The TRACE code is a thermal-hydraulic system code and was developed by USNRC for a realistic analysis of thermal-hydraulics transients in pressurized water reactors [2]. TRACE implemented the spacer grid model in December 2010 [3]. The spacer grid models in TRACE consists of the single-phase convective enhancement model, the pressure loss model, the droplet breakup model, and the spacer grid rewet model, but the droplet breakup model and the grid re-wetting model have not been fully implemented in the current TRACE. The systematic assessment of those models has not been performed sufficiently with various post-CHF heat transfer tests, such as FLECHT-SEASET, THTF, etc., though the effect of the spacer grid of TRACE was recently evaluated for RBHT [4xx]. In particular, the FLECHT-SEASET tests have been considered as representative reflood experiments because the facility is relatively large and well instrumented [5].

In this study, calculations using TRACE V5.0 patch4 code [2] released in April 2014 and a comparison with experimental data were performed for FLECHT-SEASET reflood heat transfer tests to assess the effect of the spacer grid model of the TRACE code. Some tests were also evaluated using RELAP5 code with the spacer grid model and their results were compared to those of TRACE.

A brief description for FLECHT-SEASET facility and the spacer grid models of TRACE is made in Chapter 2. The comparative assessment of the TRACE spacer grid model against eight FLECHT-SEASET tests is described in Chapter 3. Chapter 4 describes the results for the sensitivity analysis, such as the effect of the grid location and the comparison to the RELAP5. Finally, the conclusions of this study are provided in Chapter 5.

2 TEST FACILITY AND MODEL DESCRIPTION

2.1 Description of the FLECHT-SEASET Experiment

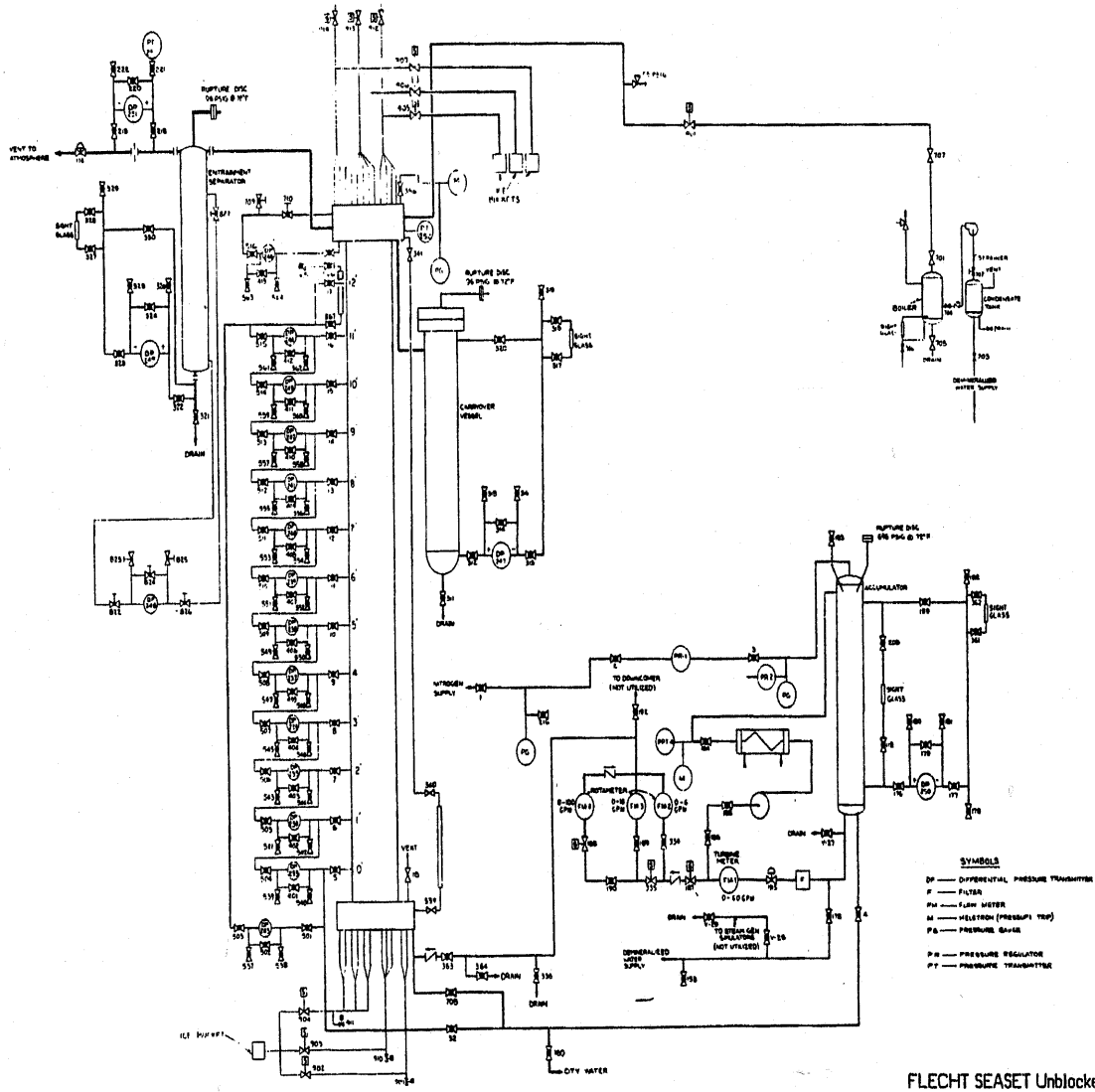
The Full-Length Emergency Core Heat Transfer Separate Effects and Systems Effects Tests (FLECHT-SEASET) was constructed and conducted to identify the thermal hydraulic of forced and gravity reflooding in a 161-rod bundle without flow blockage [5]. The FLECHT-SEASET tests was a large and relatively well instrumented reflood experiments. This test facility was modified from the FLECHT facility to apply a new heater rod bundle of which dimensions were typical of the Westinghouse 17x17 fuel bundle.

Figure 2-1 showed the FLECHT-SEASET test facility schematic. It comprised a cylindrical test section, a coolant accumulator, an entrained liquid separation tank, an external pipe downcomer for the gravity reflood tests, a steam boiler for back-pressure regulation, and the required piping and valves. The low mass housing was designed to minimize the wall effects so that the rods one row or more away from the housing wall [6]. Three hosing windows were installed at 0.91, 1.83, and 2.74 m elevations. A cross section of the test bundle was shown in Figure 2-2. The bundle contained 177 heater rods which consisted of 161 heater rods (93 noninstrumented and 68 instrumented), 16 thimbles, and 12 steam probes [7]. The 177 heater rods were placed in a cylinder of 0.194 m diameter and the heated length was 3.66 m (12 ft). There were also 8 solid triangular fillers and 8 grids in the test bundle. The triangular fillers were welded to the grids to maintain the proper grid location and decreased the amount of flow area from 9.3% to 4.7%.

The fuel rods were simulated with electrically heated rods with a Kanthal heater coil imbedded in boron nitride encased with stainless steel cladding. The outside diameter of heater rod is 9.5 mm (0.374 inch). The heater rod had the wall thickness of 0.64 mm (0.025 inch) and the heated length of 3.66 m (12 ft) and the pitch of 12.6 mm (0.496 inch). The fuel bundle has 8 spacer grids which was the egg-crate type without the mixing vane. The grid locations were similar to a 17x17 PWR fuel assembly. The blockage ratio of the spacer grids was estimated to be 0.29. The axial power profile in the heater rod was considered as the cosine curve with a power peak-to-average ratio of 1.66 and the radial power profile was assumed as uniform.

To determine the experimental conditions, the reflood phase following a LOCA transient was evaluated to start approximately 30 seconds after a hypothetical break. By referring the reflood transient for a standard Westinghouse 17x17 four-loop, the reference test conditions were followed: initial clad temperature (871 °C), peak power (2.4 kW/m), upper plenum pressure (0.28 MPa), Injection rate with lower plenum initially full (25 mm/sec), coolant subcooling (78 °C).

For the reflood experiments, the test bundle was pre-heated to the desired pressure and temperature with dry steam, and then cooling water was delivered to the lower plenum of the bundle by a gas-charged accumulator for the forced reflood tests to quench the rods, simulating the reflood process.



FLECHT SEASET Unblocked Bundle Flow Diagram, Forced Reflood Configuration

Figure 2-1 FLECHT-SEASET Test Facility

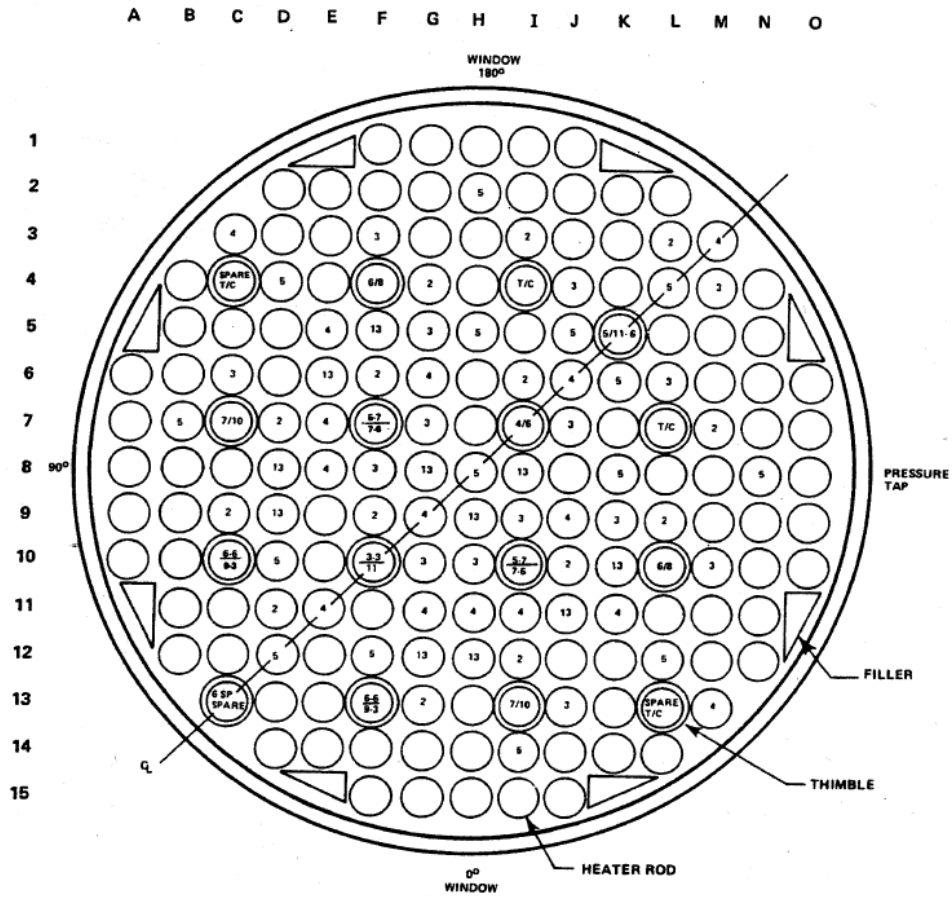


Figure 2-2 FLECHT-SEASET Test Bundle Cross Section

2.1.1 Spacer Grid Model in TRACE

There are the spacer grids in most fuel assembly. The functions of the spacer grid are to support fuel rods vertically and laterally, to maintain the space between rods and to enhance the flow mixing. In the thermal-hydraulic aspect, the spacer grid could provide flow obstacles in a core channel and then influence the heat transfer mechanism in a core. First, the spacer grid reduces the flow area and then the flow acceleration occurs at the location of a spacer grid. This could promote the local convective heat transfer. Second, the spacer grids can be quenched before the fuel rod during a reflood and it may increase the interfacial area between liquid and vapor. Third, the spacer grids can break the entrained droplets into smaller ones and this can increase the interfacial heat transfer to the vapor phase.

Currently, there are 4 sub-models in TRACE, which are for the convective heat transfer enhancement, the pressure drop, the droplet breakup and the grid re-wetting, respectively. In this chapter, 4 sub-models would be described shortly by referring the TRACE theory manual [3].

2.1.1.1 Convective heat transfer enhancement

The Yao, Hochreiter and Leech model [8] was applied in TRACE and it can be used in both egg-crate grids and mixing vane grids. This model consists of two parts; 1) the heat transfer enhancement due to the acceleration of the flow and the increased turbulence due to the spacer grid, and 2) the effects of mixing vanes:

$$\frac{Nu}{Nu_o} = \underbrace{\left[1 + 5.55\beta^2 e^{-0.13\frac{x}{D_H}} \right]}_{\text{Part 1}} \underbrace{\left[1 + a^2 (\tan\phi)^2 e^{-0.034\frac{x}{D_H}} \right]}_{\text{Part 2}}^{0.4} \quad (1)$$

where Nu is the local Nusselt number at the wall with the grid spacer, Nu_o is the local Nusselt number at the wall without the spacer grid, β represents the spacer grid flow blockage area ratio as viewed from upstream, x is the axial distance from the downstream edge of the spacer, and D_H is the hydraulic diameter of the flow channel, a is the mixing vane flow blockage area ratio when viewed from upstream, and ϕ is the angle of the vane with respect to the axial direction.

As shown in Eq. (1), this model depends on the spacer grid blockage ration, the mixing vane blockage ration, and the mixing vane angle. Also, in order to consider the increased enhancement effects for high void fraction, laminar flows, a laminar enhancement factor, F was introduced into this model as shown in TRACE theory manual [3].

2.1.1.2 Pressure losses

In order to consider the pressure drop due to the spacer grids, TRACE adopted the Yao, Loftus and Hochreiter [9] model. The loss coefficient for this model was improved by the Rehme [10] and the 40% increase of the loss factor was also applied to account for the sharp leading edge.

$$\Delta p_{grid} = K_{grid} \frac{\rho}{2} V^2, \quad K_{grid} = 1.4 C_V (\beta + a)^2 \quad (2)$$

$$\text{where, } C_V = \begin{cases} 196 Re_m^{-0.33}, & 10^3 < Re < 10^4 \\ 41 Re_m^{-0.16}, & 10^4 < Re < 10^5 \\ 6.5, & 10^5 < Re \end{cases}$$

2.1.1.3 Droplet breakup

In the dispersed droplets flow, the droplet can split apart by the spacer grid strap. The droplet breakup model in TRACE is based on the study which was conducted by Yao, Hochreiter and Cai [11]. The shattered small droplet ratio could be represented as a function of the droplet Weber number and the ration of the Sauter mean diameter to the initial diameter. If the Weber number is greater than 250, the droplets don't have sufficient surface tension force to overcome the impact with the spacer grid straps and the droplet breakup is possible [3]. The droplet mass flow rate in the downstream cell is followed:

$$\dot{m}_{small} = 0.6(\beta + a)\dot{m}_o, \dot{m}_{large} = \dot{m}_o - \dot{m}_{small} \quad (3)$$

The diameters of the shattered droplets and the remained large droplets are given as:

$$D_{small} = 6.16We_d^{-0.53}D_o, D_{large} = D_o \quad (4)$$

where $We_d = \frac{\rho_l D_d V_d^2}{\sigma_d}$ is the droplet Weber number.

This model is subject to the completion of droplet field equation since droplets shattered from a large group are taken as source and sink terms in the downstream axial cell. However, the droplet breakup model is not currently activated in TRACE and it has been waiting the full implementation of the droplet field.

2.1.1.4 Grid re-wetting

During reflood conditions, the spacer grid with no internal heat generation could fall below the minimum film boiling temperature before the fuel rods. Therefore, the liquid film formed on a spacer grid increases the local interfacial area for heat transfer and then it can result in significant de-superheating of the vapor. In TRACE, the modified radiation model of Paik, Hochreiter, Kelly, and Kohrt [12] was used after several simplifications. This model is about the heat transfer between fuel rods, a spacer grid, and the continuous vapor phase. The heat balance equation for the spacer grid is given as:

$$\rho_{sp} C_p \frac{\partial T_{sp}}{\partial t} = \frac{WP_{grid}}{A_{grid}} (q_{rad}'' - q_{conv}'') \quad (5)$$

The detailed description for this model would refer to TRACE manual [3]. According to this model, the spacer grid temperature was calculated by the spacer grid surface area is obtained as the spacer grid height times the grid wetted perimeter multiplied by two to account for both sides of the spacer grid straps.

However, in current TRACE, the spacer grid re-wetting model is only implemented to calculate the transient spacer grid temperatures and add the spacer grid surface area to the wallFilmArea variable if the spacer grid is quenched. Further work for a critical film thickness will be required for determining the film Nusselt number from which the film interfacial heat transfer coefficient is calculated.

3 EVALUATION OF THE SPACER GRID MODEL FOR FLECHT-SEASET REFLOOD TESTS

In general, when the spacer grid is considered, the flow area is reduced and the convective heat transfer is promoted due to the flow acceleration and the turbulence increases. This is shown in both egg-crate style spacer grids and mixing vane grids. Also, the mixing vane increases the convective heat transfer additionally in the case of mixing vane grids. In this section, the effect of spacer grid model of TRACE was performed on FLECHT-SEASET (Full-Length Emergency Core Heat Transfer – Separate Effects And System Effect Test) reflood tests [7]. The tests comprised of forced and gravity reflood tests to simulate the nuclear fuel arrays of PWR, which was similar to Westinghouse 17x17 assemblies. Especially, the tests were the important data sources to predict the characteristics of reflood phase for large-break (LB) loss-of-coolant accidents (LOCAs) since some tests were conducted at temperatures exceeding the requirement limit (2200 °F). The test facility consisted of the cylindrical test section with a lower plenum, the heater rod bundle and the upper plenum, the cooling water injection system, the entrained water separation tank and the carry-over liquid collection tank as shown in Figure 2-1. This facility has a heated length of 3.66 m (12.0 ft) of typical pressurized water reactor (PWR) fuel assembly. The test section consisted of a 17x17 rod bundle with 161 heated electrical rods and 16 thimble rods. The 68 rods of the 161 heater rods were instrumented and the total power was about 850 KW. The bundle comprised of 8 spacer grids, 12 steam probes and 8 solid triangular fillers which were used to reduce the flow area near the housing wall. The electrical rods have a diameter of 9.5 mm and the wall thickness of 0.64 mm and are arranged in a 17x17 array with a 12.6 mm pitch. Eight forced reflood tests in the TRACE assessment manual [6] were selected to evaluate the effect of spacer grid model of TRACE.

3.1 TRACE Modeling

The FLECHT-SEASET facility was modeled by TRACE to simulate the forced reflood tests. The test facility was made as five components of TRACE to simplify the water injection system and the carry-over liquid collection tank. The FLECHT-SEASET test section was modeled in Vessel and HTSTR components of TRACE as shown in Figure 3-1. TRACE modeling was almost same as that of the previous study [6] beside of some corrections. The Vessel was divided into 16 axial nodes; one node for lower plenum, fourteen nodes for heated section and one node for upper plenum and there were two cells between each grid. As in the TRACE assessment manual [6], the bottom of spacer grid was located in the bottom of corresponding cell. Two PIPE components were modeled as the lower- and the upper- plenum respectively. The 161 heated rods in 17x17 assemblies were modeled as a single heat structure (HTSTR Component 6) while the bundle housing wall was modeled as another heat structure (HTSTR Component 7). The heated length of heater rod was a 3.66 m with a cosine axial power profile as shown in Figure 3-2 and the radial power distribution was uniform. The rod power was designed to represent the decay heat prescribed by 10CFR part 50 Appendix K [13] from 30 sec following LBLOCA, which the transient power was 1.2 times to ANS 71 model.

The heater rod was modeled with 7 radial cells and the material properties of the previous study [6] were also used in this calculation. The injected flow rates and temperatures was provided as a function of time by FILL component connecting to the bottom of the lower plenum. The BREAK component was used to set the pressure boundary at the top of the test section.

For the spacer grid, the grid is the egg-crate type without the mixing vane. Eight spacer grids were installed along 3.6 m heated length in FLECHT-SEASET. The grid straps made by Inconel 718 alloy sheets which are 0.38 mm (0.015 in) thick and are 45.0 mm (1.75 in) in height. Each grid span has two equal distance nodes (~ 10 inch or 10.5 inch) as shown in Figure 3-1. Thus, the grid was located

in the bottom of every other node. The first grid is located 0.57 m (22.25 in) above the test section, which is just under the heated section. Actually, the grid locations were similar to a 17x17 PWR fuel assembly. In order to model the spacer grid, the experimental design data [5, 7] and the general fuel data were considered to determine some parameters. The spacer grid for TRACE was modeled as follows;

*n: Grid- egg-crate style

*

* gridid

101

* spbloc vnbloc phi wetperm

0.29 0.0 0.0 11.8

* height strthick spmatid

0.045 3.8.0E-4 10

Meaning of the grid parameters

- gridid : Grid number ID
- spbloc : Spacer grid flow blockage area ratio
- vnbloc : Mixing vane flow blockage area ratio
- phi : Mixing vane angle measured from parallel with the top of the spacer grid to the mixing vane
- wetperim : Spacer grid wetted perimeter
- height : Spacer grid axial height
- strthick : Grid strap thickness of modeled spacer grid (0.015 inch)
- spmatid : Grid material ID

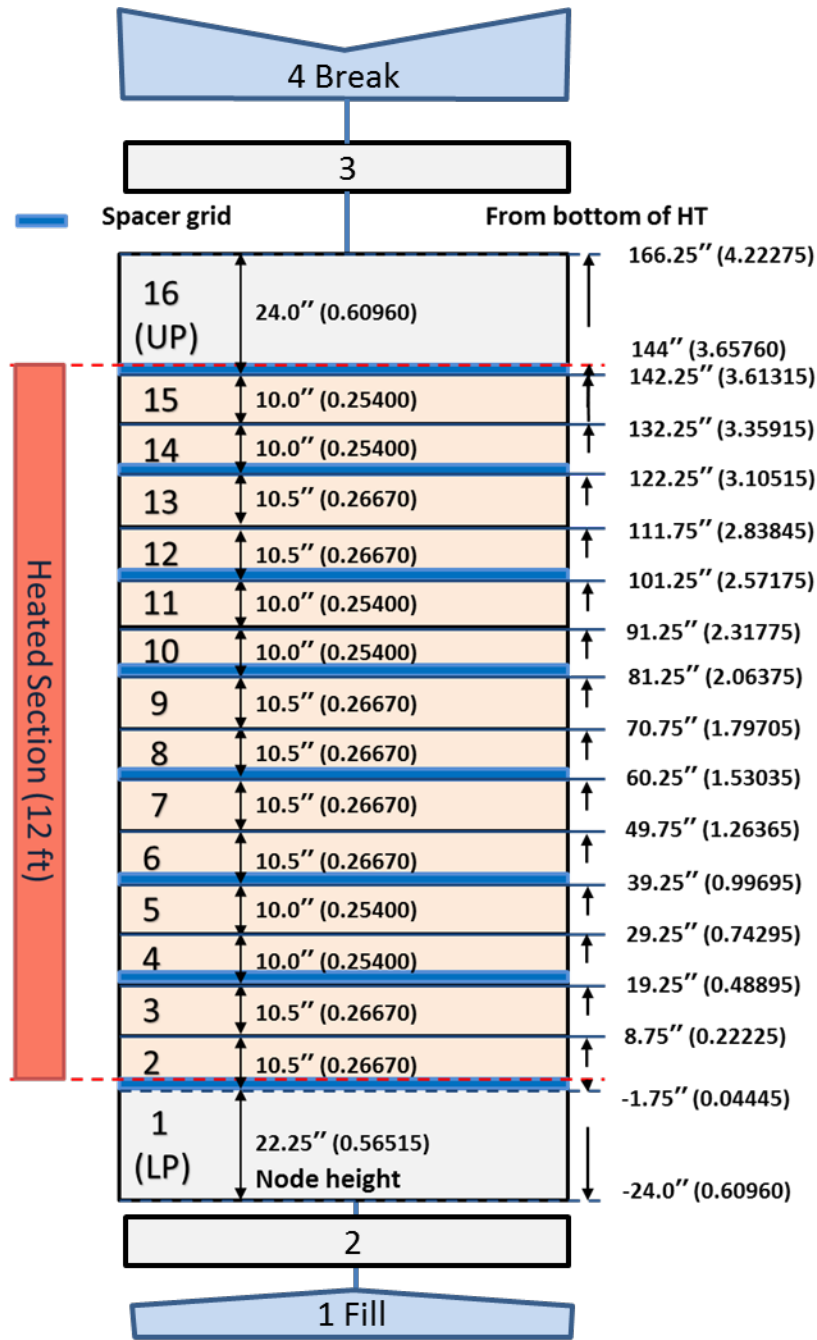


Figure 3-1 TRACE Nodalization for FLECHT-SEASET Facility

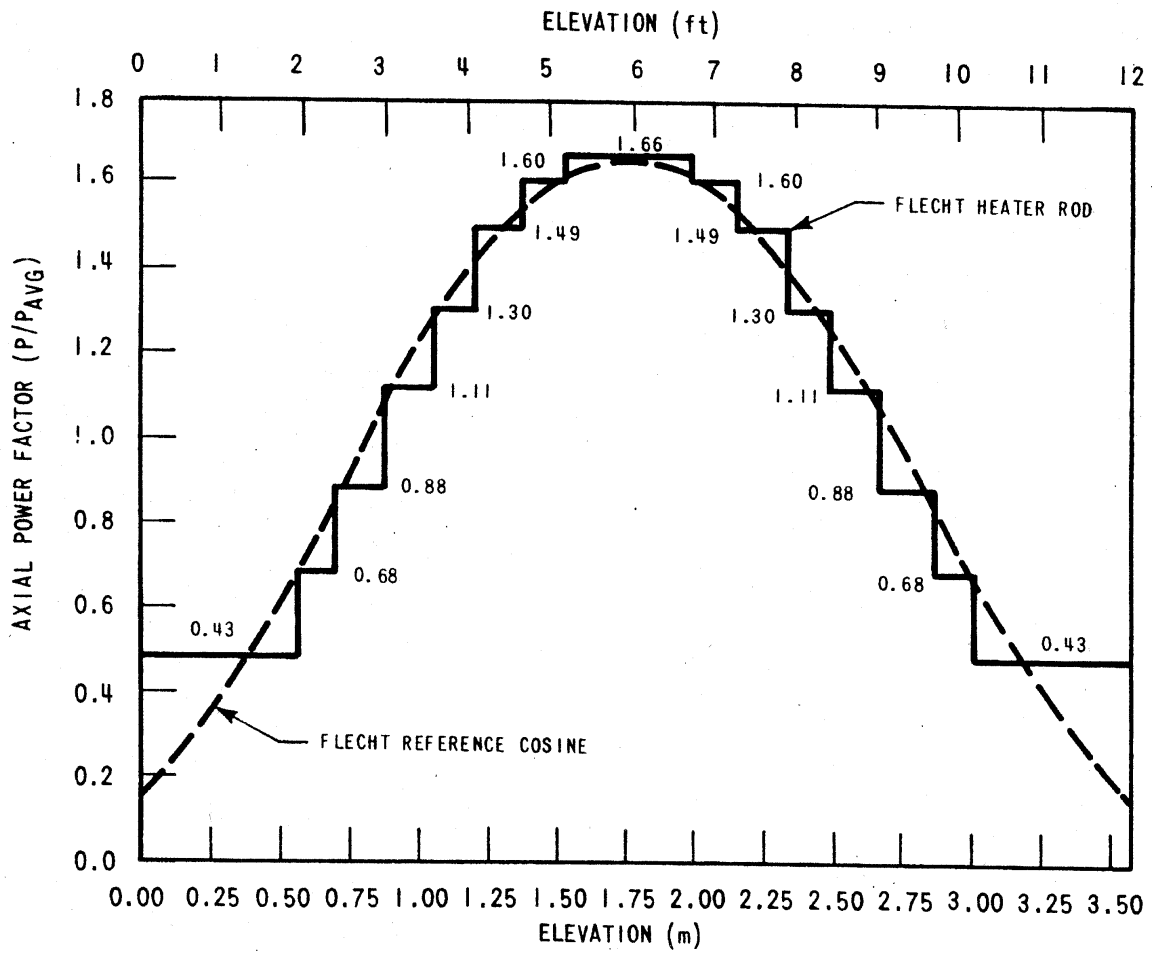


Figure 3-2 Axial Power Profile of Heated Rod

3.2 Evaluation for Spacer Grid Model

As mentioned before, eight tests were chosen for this calculation as shown in Table 3-1. Tests were covering a range of flooding rate from 2.10 cm/sec to 15.50 cm/sec, subcooling temperature from 5 °C to 79 °C and upper plenum pressure from 0.13 MPa to 0.41 MPa. The initial rod power at the peak location is 2.3 KW/m (0.7 KW/ft) in all tests. The test conditions in Table 3-1 were nominal values. The actual values in tests changed with time and then the actual inlet flow rates, temperatures and the upper plenum pressures were used as input with a function of time. Also, the rod power was considered as a function of time that it was reduced with time like the decay heat formula in the Appendix K.

As the general reflood test, the test bundle was pre-heated up to the predetermined pressure and temperature with dry steam. After that, the cooling water was injected to the lower plenum of the test bundle in order to quench the rods.

The instrumentations of the FLECHT-SEASET Facility were very extensive, including 205 heater rod thermocouples, 12 differential pressure transmitters positioned 0.3048 m (1 ft.) apart along the axial direction of the heated section, 12 steam probes, and inlet and outlet flow meters. TRACE simulations in the assessment manual [6] showed the results for rod cladding temperatures, Vapor temperatures, heat transfer coefficients, quench profile, differential pressures and void fraction during a reflood test. In this study, the results for showing the effects of spacer grid well were given for tests as follows;

Table 3-1 Test Matrix for TRACE Evaluation

	Run No.	Flooding Rate	Upper Plenum Pressure	Coolant Inlet Temp.	Coolant Inlet Subcooling Temp.	
		cm/s (in/sec)	MPa (psia)	°C (°F)	°C (°F)	
1	31805	2.10 (0.81)	0.28 (40)	51 (124)	~79 (143)	79 (143)
2	31504	2.40 (0.97)		51 (124)		79 (143)
3	31203	3.84 (1.51)		52 (126)		78 (141)
4	31302	7.65 (3.01)		52 (126)		78 (141)
5	31701	15.5 (6.10)		53 (127)		77 (140)
6	31108	7.90 (3.11)	0.13 (19)	33 (91)		74 (134)
7	32013	2.64 (1.04)	0.41 (60)	66 (150)		79 (143)
8	32114	2.5-3.1 (1.0-1.22)	0.28 (40)	125 (257)		5 (10)

1) Run No. 31805

Run No. 31805 was a test with a flooding rate of 2.1 cm/sec at 0.28 MPa and 79 oC inlet subcooling temperature as shown in Table 3-1. However, as described previously, the actual input conditions changed largely with time and showed the big oscillations. Therefore, the inlet flowrate and temperature were considered as time-dependent variables as shown in Figures 3.3 ~ 3.4. Most initial conditions in the TRACE assessment manual [6] were applied in this study.

The rod temperatures at various elevations are shown in Figure 3-5 through Figure 3-12. These figures showed well the process that the rod was heating up by the initiation of reflood, turning to reduce during the reflood, and finally quenching. In the calculation without the spacer grid model, the predicted peak temperatures agreed reasonably with the experimental data at low elevations ($z \leq 2.4$ m), but showed over predicted results at higher elevations (3.0 m ~ 3.3 m). The maximum peak clad temperature was shown at elevation $z=1.98$ m (6.5 ft). At low elevations ($z \leq 1.2$ m), the quenching time showed a good agreement with the data, but under predicted at higher elevations. For low reflooding rates such as Run No. 31805, the dominant flow regime was a highly dispersed flow film-boiling region in which the heat transfer rates were very low. Therefore, the peak clad temperature usually occurred in this region and the maximum peak clad temperature at elevation $z=1.98$ m had the highest value as compared to following 4 tests. In the spacer grid model of TRACE, Only two models for the convective enhancement and pressure loss models were currently implemented to perform the rod temperature. The droplet breakup and grid rewet models were not fully implemented in TRACE. When the spacer grid model was applied, the effect of mixing vane was not considered since the egg-crate spacer grid was installed in the FLECHT-SEASET. Therefore, the convective Nusselt number was enhanced due to the flow acceleration and the turbulence increase for a spacer grid without the mixing vane. As would be expected, the lower rod temperatures and earlier rod quenches were predicted in the case with a spacer grid model. During a heat up period, the effect of the spacer grid model did not show at lower elevations ($z \leq 2.4$ m), but the earlier rise of rod temperature was predicted at higher elevations. Those predictions for the spacer grid would come from the relatively high vapor temperature due to the promotion of heat transfer from lower elevations. The turnings of rod temperature to reduce were estimated earlier than those without the spacer grid at all elevations since the spacer grid enhanced the increase of collapsed water level and heat transfer. The peak temperatures with the spacer grid model had the lower values at low elevations ($z \leq 3.0$ m) and under predicted the experimental data in comparison with those without the spacer grid model, while the peak temperature with the spacer grid model had the higher value at $z = 3.3$ elevation as shown in Figure 3-11. This might be resulted from the earlier rise of rod temperature during a heat up region. The maximum peak clad temperature at $z=1.98$ m was reduced in case with the spacer grid model. From a previous study [14], the droplet break model among sub-models for the spacer grid would have the largest effect to the rod temperature. Since the droplet break model could influence largely the rod quenching downstream of grid, the full implementation of spacer grid model could predict the lower temperatures at high elevations. At elevation $z=1.98$ with the maximum peak cladding temperature, the decreasing temperature was ~ 57.0 K and the reduction of quenching time was ~ 32 sec due to the spacer grid model. These values would seem to be the significant amount and were the largest values in tests of Table 3-1. This test have the lowest reflood rate in top 5 tests of Table 3-1 and the effect of the spacer grid model was most dominant.

As shown in Figure 3-13, the quench front without the spacer grid model showed a good agreement with data at all elevations. The steep rise at high elevations might be due to the de-entrainment of liquid from the upper part above the heated section. If the spacer grid model was applied, the quench front was increasing slightly faster than that without the spacer grid model as the elevation was higher.

The differential pressure (DP) for entire 12 ft was plotted in Figure 3-14 and the differential pressure between 11 ft and 12 ft was shown in Figure 3-15. The growth of DP for entire test section was related to the collapsed liquid level and the DP increased gradually with the injected water. The DP for entire 12 feet showed a reasonable prediction with the trend of data, but it showed the slight over-estimation of the experimental data. It would be considered to the behaviors of the rod temperature and the quench front. If the spacer grid model was applied, the DP for entire 12 feet was growing slightly faster than that without the spacer grid model as shown in Figure 3-14. As shown well in Figure 3-15, the DP between 11 ft and 12 ft was increased at elevation with the spacer grid and the pressure drop in the spacer grid model was predicted well.

The vapor temperatures at two elevations 1.8 m and 3.0 m were shown in Figures 3.16 and 3.17, respectively. As described in the rod temperature, the vapor temperature at higher elevation 3.0 m was over predicted at the initial heat up period and it would result in the earlier increase of the rod temperature up to its turn-over time. The calculation with the spacer grid model showed the slightly higher vapor temperature during the heat up and the faster quenching due to the enhancement of heat transfer.

The heat transfer coefficients (HTCs) at several elevations is in Figure 3-18 through Figure 3-20. Usually, as the rod was quenched, the heat transfer coefficient was increased suddenly. As shown in Figures, the HTC was reducing or stagnant during the rod heat up and the rod during the reflood phase cooled by the steam cooling and/or water droplets and the HTC increased gradually. TRACE seems to not predict the HTC decrease during the rod heat up beside of the result at elevation 3.0 m. The average HTC during the reflood predicted roughly the data, but the faster rise of HTC was predicted with the data due to the earlier turn-over of the rod temperature. TRACE predicted a sharp increase of HTC much earlier than experimental data since the rod quenching occurred too early. When the spacer grid model was applied, the steep increase of HTC was expedited since the earlier rod quench occurred due to the growth of convective heat transfer.

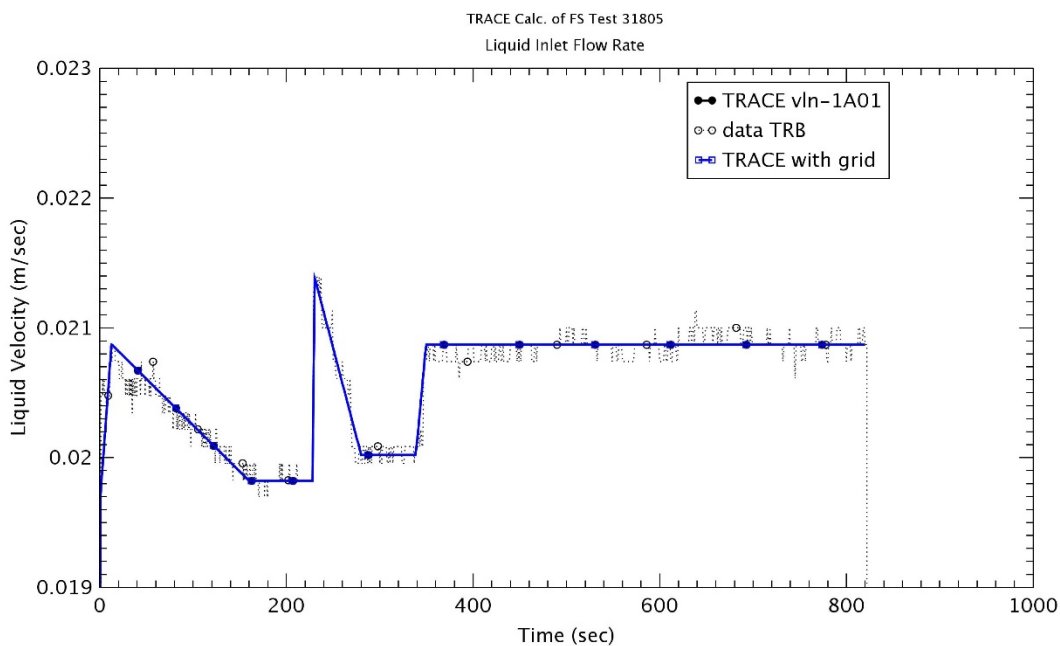


Figure 3-3 Liquid Inlet Flowrate – Run No.31805

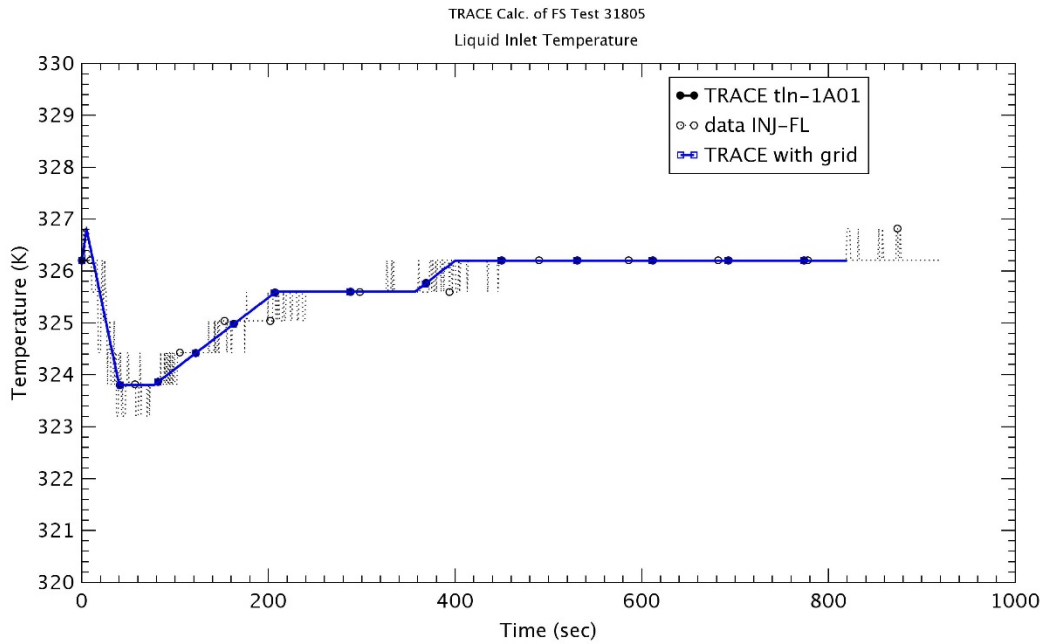


Figure 3-4 Liquid Inlet Temperature – Run No.31805

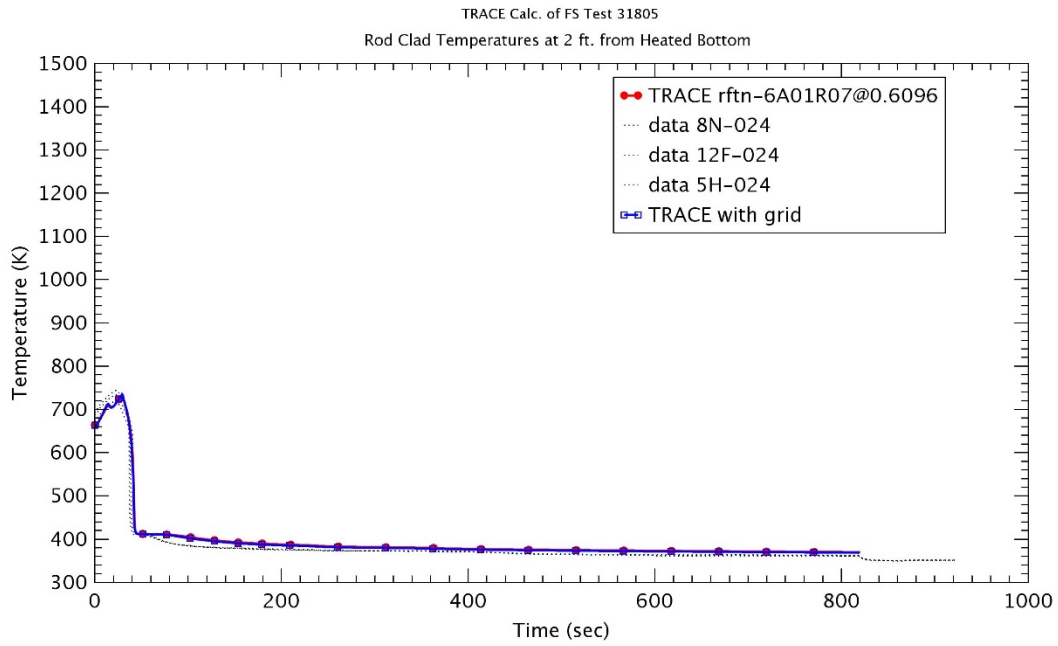


Figure 3-5 Heater Rod Temperature at 0.6 m – Run No.31805

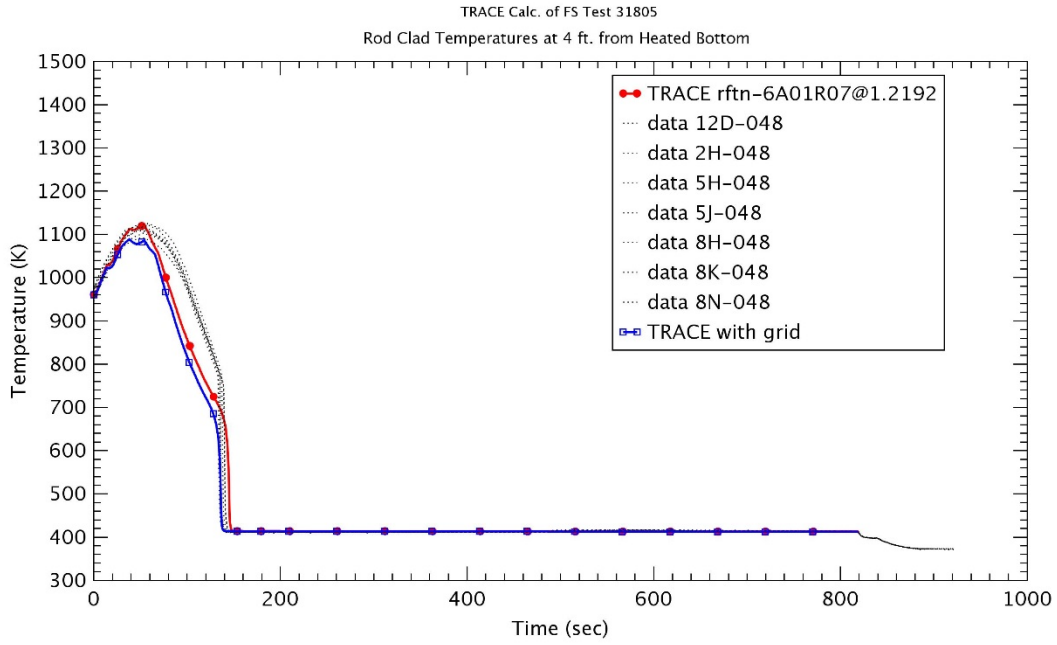


Figure 3-6 Heater Rod Temperature at 1.2 m – Run No.31805

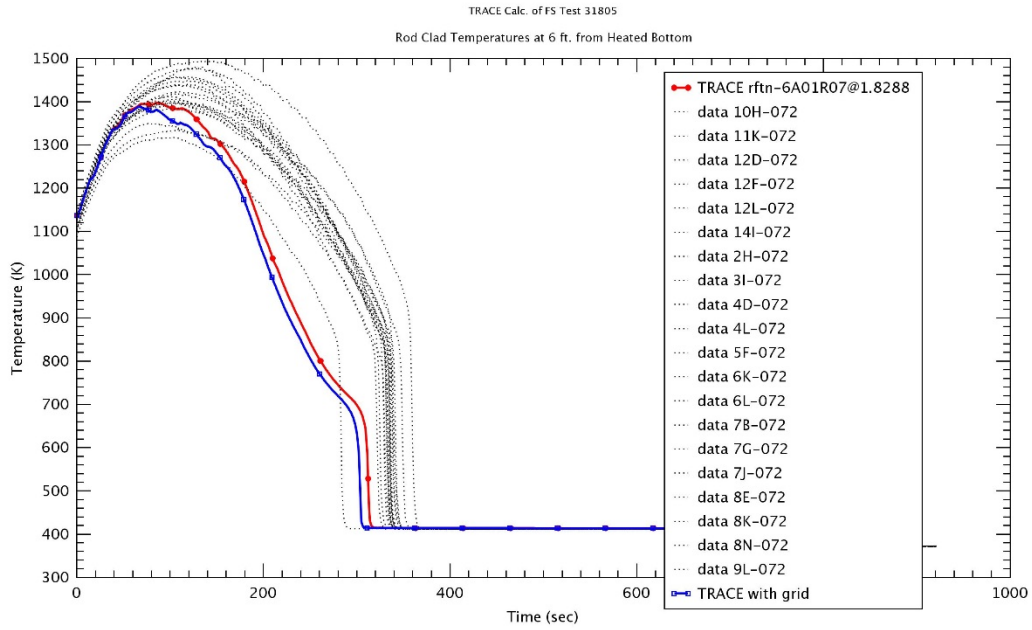


Figure 3-7 Heater Rod Temperature at 1.8 m – Run No.31805

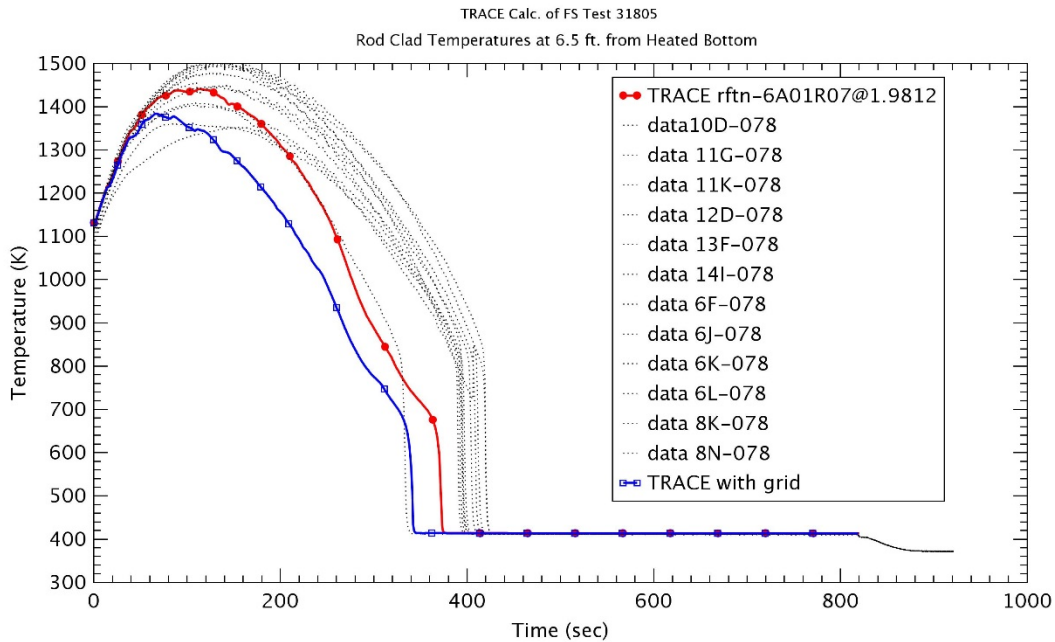


Figure 3-8 Heater Rod Temperature at 1.98 m – Run No.31805

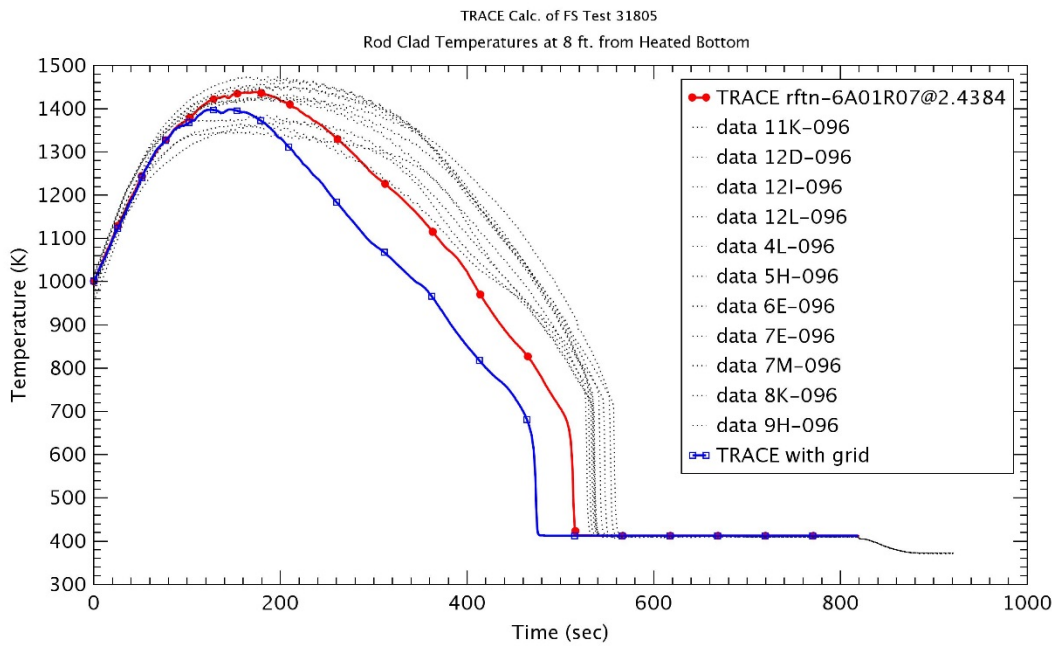


Figure 3-9 Heater Rod Temperature at 2.4 m – Run No.31805

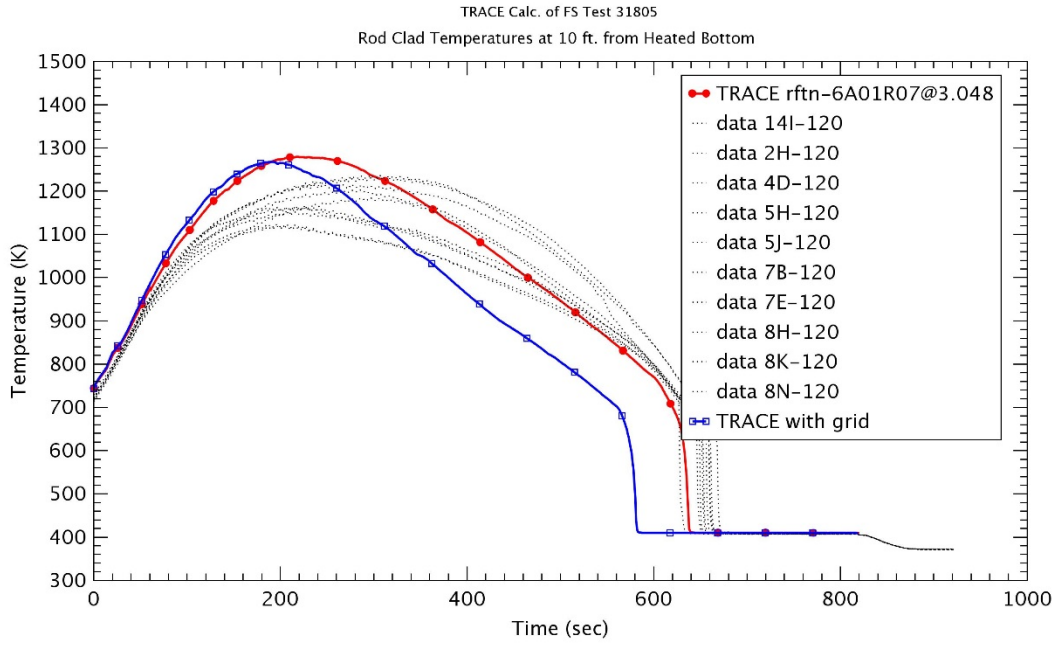


Figure 3-10 Heater Rod Temperature at 3.0 m – Run No.31805

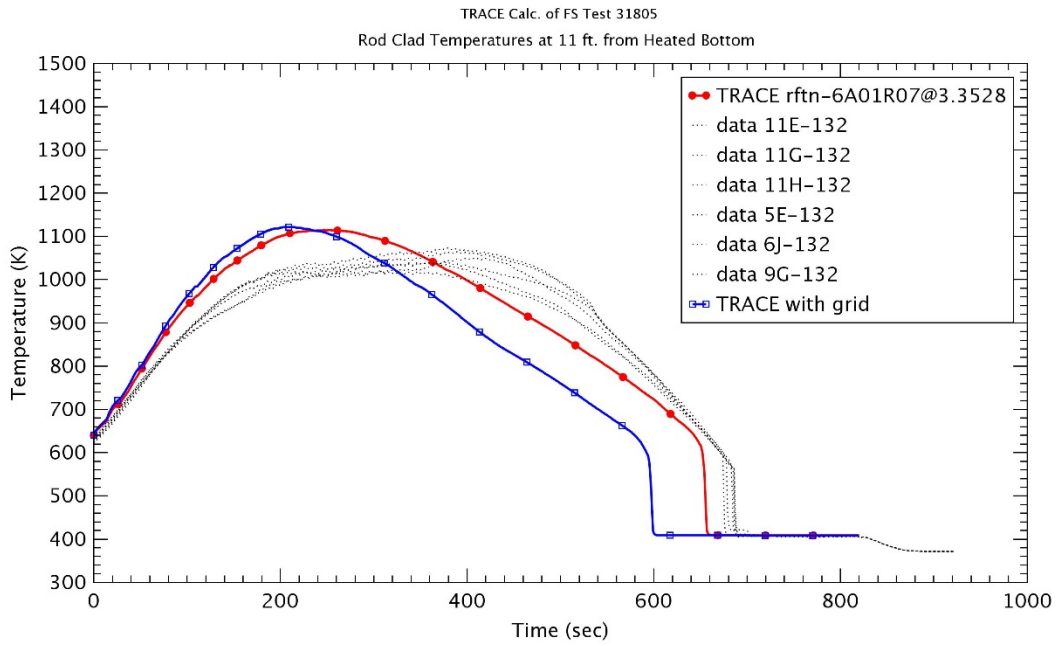


Figure 3-11 Heater Rod Temperature at 3.3 m – Run No.31805

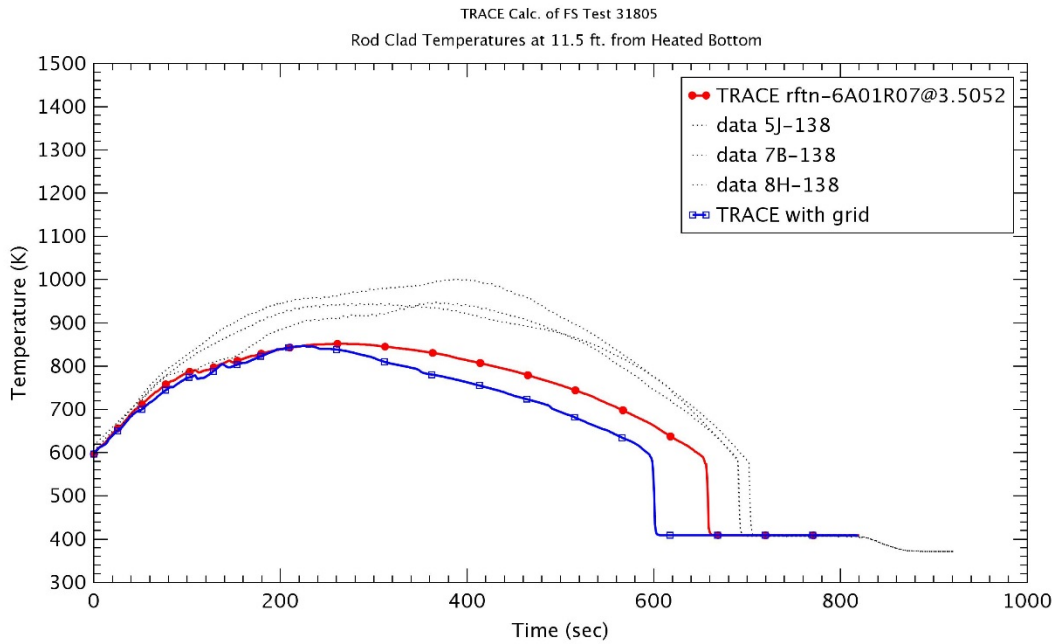


Figure 3-12 Heater Rod Temperature at 3.5 m – Run No.31805

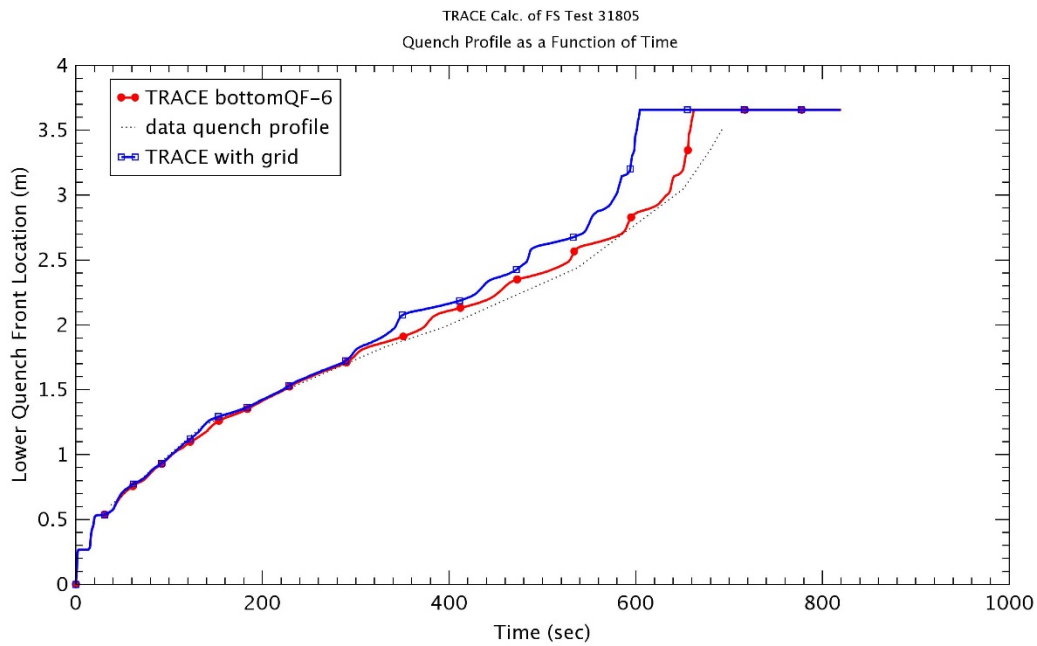


Figure 3-13 Quench Front Profile – Run No.31805

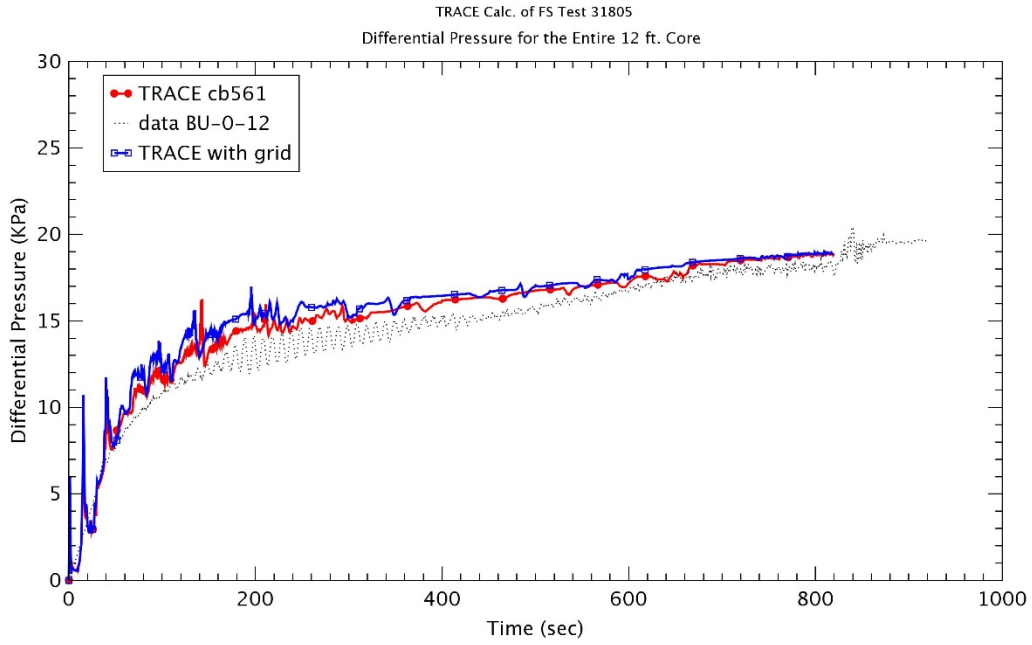


Figure 3-14 Differential Pressure for Entire 12 ft – Run No.31805

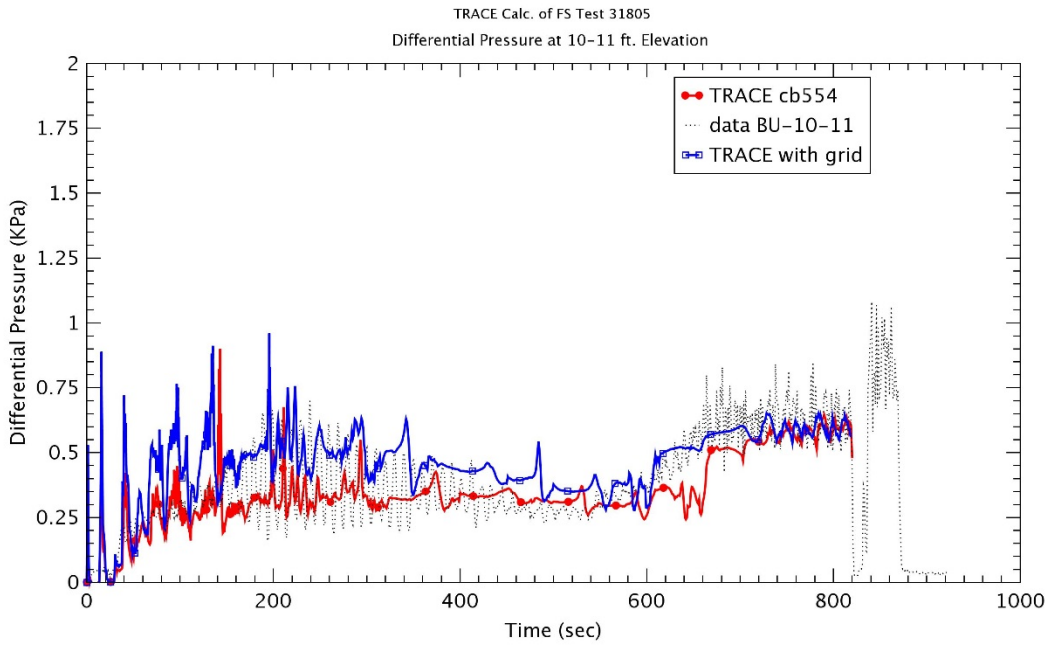


Figure 3-15 Differential Pressure at 10~11 ft Elevation – Run No.31805

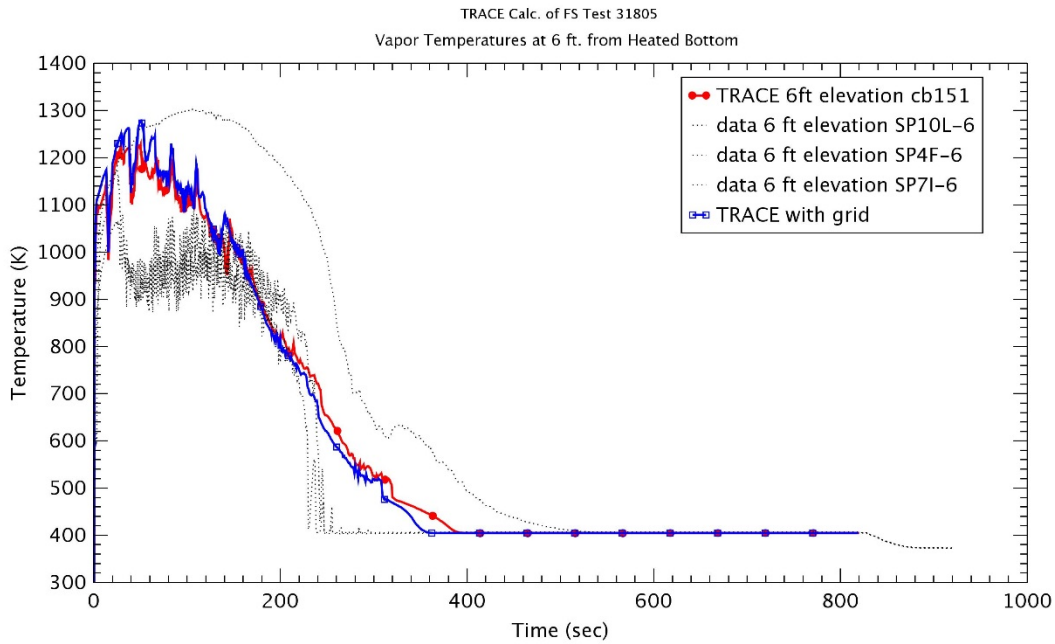


Figure 3-16 Vapor Temperature at 1.8 m – Run No.31805

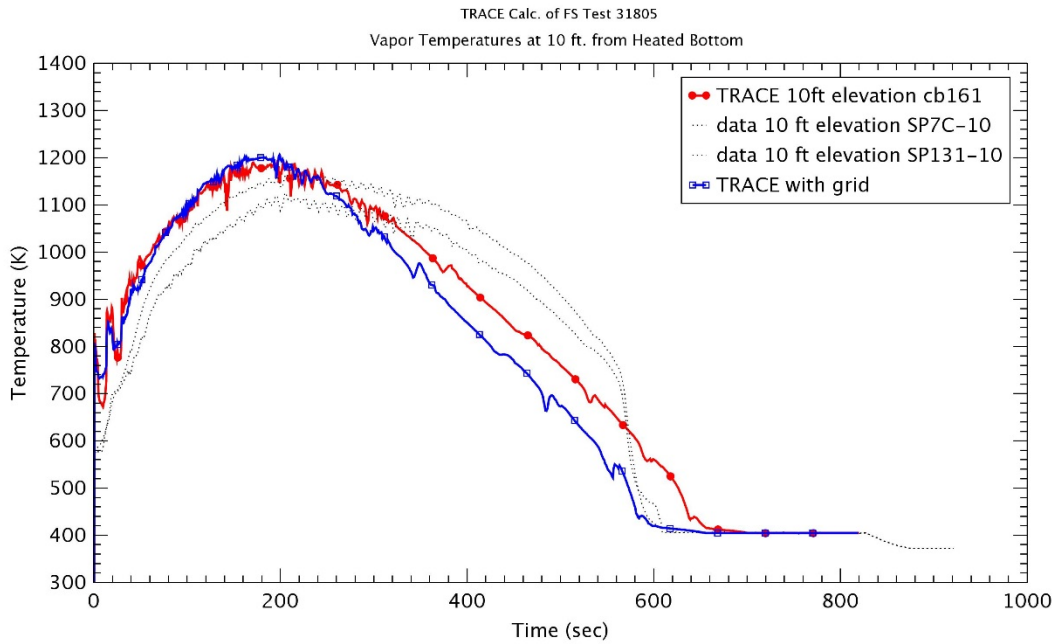


Figure 3-17 Vapor Temperature at 3.0 m – Run No.31805

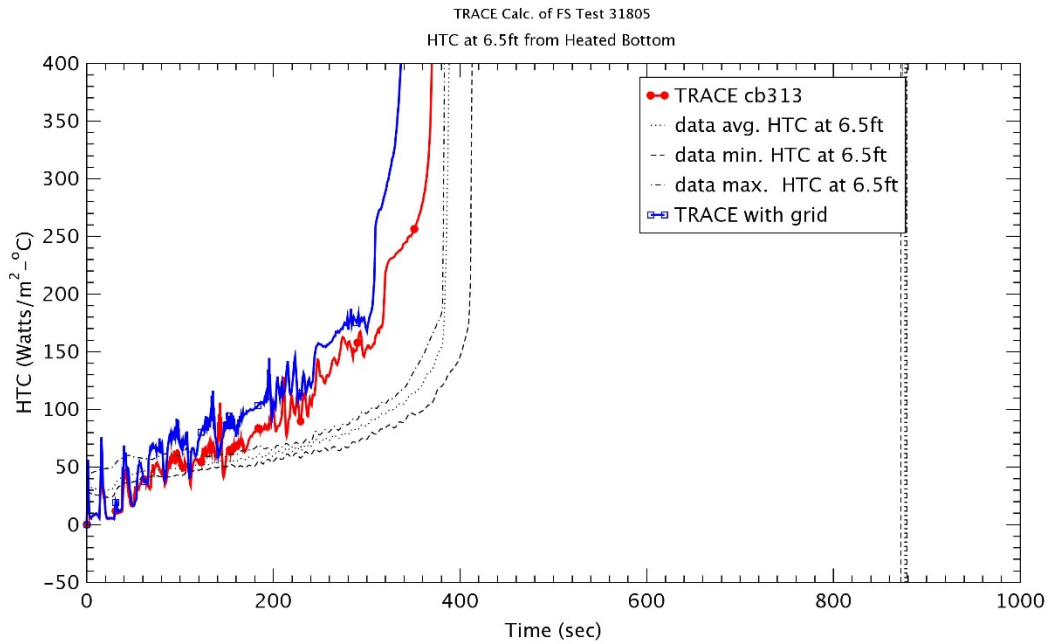


Figure 3-18 Heat Transfer Coefficient at 1.98 m – Run No.31805

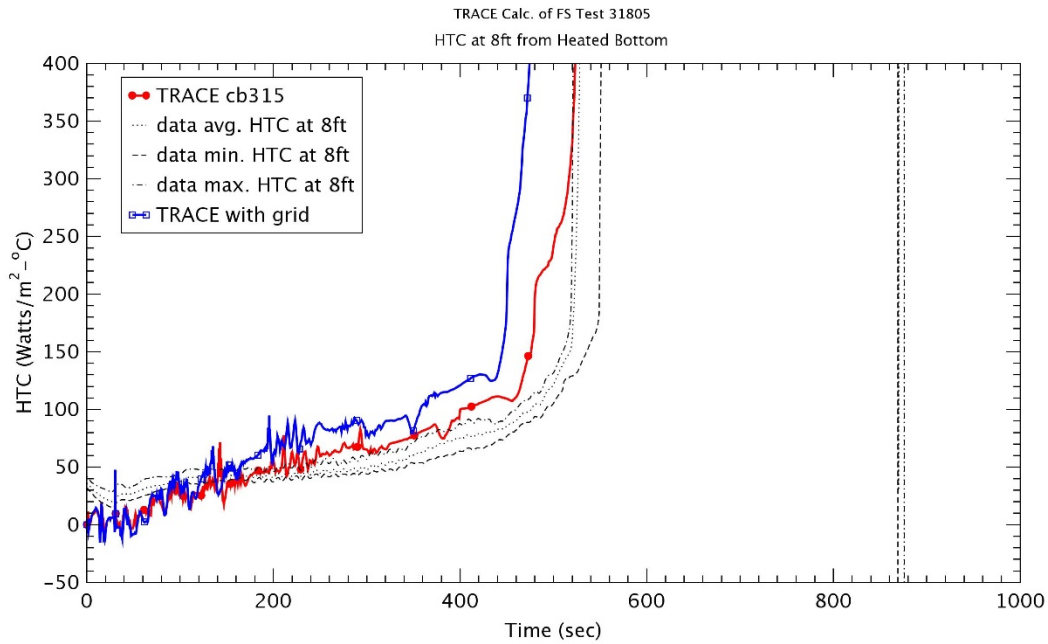


Figure 3-19 Heat Transfer Coefficient at 2.4 m – Run No.31805

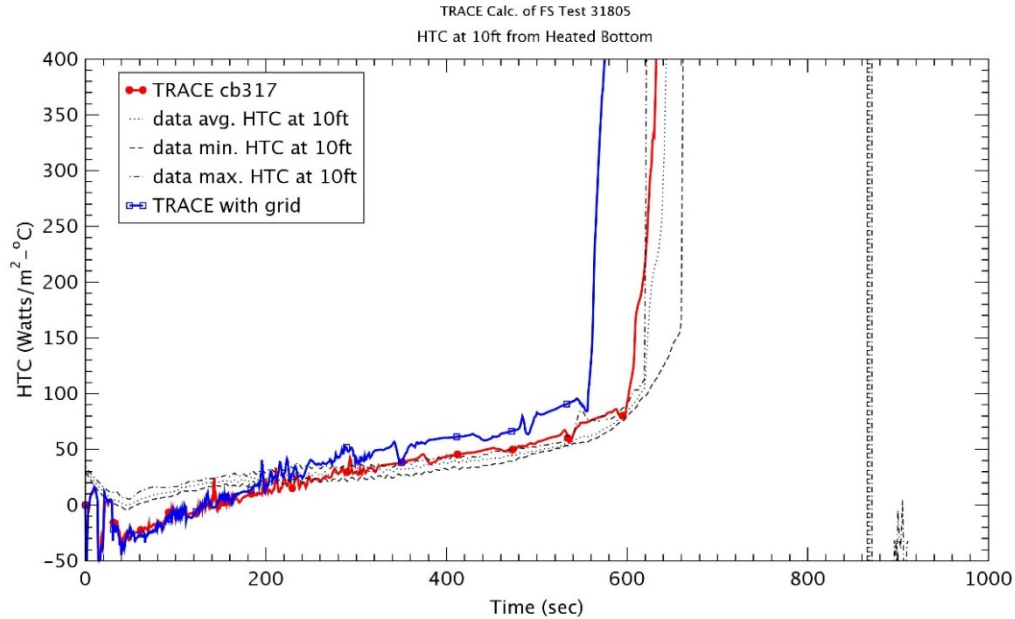


Figure 3-20 Heat Transfer Coefficient at 3.0 m – Run No.31805

3.2.1.1 Run No. 31504

Run No. 31504 was a test with a flooding rate of 2.4 cm/sec at 0.28 MPa and 79 oC inlet subcooling temperature as shown in Table 3-1. This was the same as Run No. 31805, except for an increase of a flooding rate. However, as described previously, the actual input conditions changed largely with time and showed the big oscillations. Therefore, the inlet flowrate and temperature were considered as time-dependent variables as shown in Figures 3.21 ~ 3.22. Most initial conditions in the TRACE assessment manual [6] were applied in this study.

Figure 3-23 through Figure 3-30 represent the rod temperatures at various elevations. These figures showed well the processes such as the heat up, turn-over of rod temperature during a reflow and a final quenching as in Run No. 31805. In the calculation without the spacer grid model, the peak temperatures were fairly predicted with the experimental data at low elevations ($z \leq 2.4$ m), but were over predicted at higher elevations (3.0 m ~ 3.3 m). The maximum peak clad temperature was shown at elevation $z=1.98$ m (6.5 ft) and decreased due to relatively higher reflow rate. The quenching times were reasonably agreed with the data beside of higher elevations ($z > 3.3$ m) and it showed the better results by the higher reflow rate compared to Run No. 31805. When the spacer model was applied, the rod temperatures were reduced and the quenching time was expedited at most elevations. The rod temperature and the quenching time showed the similar trend with Run No. 31805. During a heating up, the effect of the spacer grid model did not show at lower elevations ($z \leq 2.4$ m), but the rod temperatures at higher elevations were increased faster than the case without the spacer grid model. The turn-over time of rod temperature were estimated earlier than those without the spacer grid at all elevations since the spacer grid enhanced the increase of collapsed water level. The peak temperatures with the spacer grid model had the lower values at low elevations ($z \leq 3.0$ m) in comparison with those without the spacer grid model, while the peak temperature with the spacer grid model was similar to that at $z = 3.3$ elevation as shown in Figure 3-29. In the case with the spacer grid model, the decreasing temperature was ~ 10.8 K and the reduction of quenching time was ~ 9 sec due to the spacer grid model at elevation $z=1.98$ with the maximum peak cladding temperature.

As shown in Figure 3-31, the quench front without the spacer grid model showed a very good agreement results at all elevations and this reflected well the quenching time of rod. With the spacer grid model, the quench front was increasing slightly faster than that without the spacer grid model as the elevation was higher.

The differential pressure (DP) for entire 12 ft was shown in Figure 3-32 and the differential pressure between 11 ft and 12 ft was illustrated in Figure 3-33. The rise of DP for entire test section was related to the collapsed liquid level and the DP increased gradually with the injected water. The DP for entire 12 feet showed the large over-prediction with the experimental data. It appeared that TRACE predicted more water in the test section compared to the data. If the spacer grid model was applied, the faster increase of DP for entire 12 feet was predicted which is similar to Run No. 31805. As shown well in Figure 3-33, the DP between 11 ft and 12 ft rose at elevation with the spacer grid and the pressure drop was predicted well. The plots after 600 sec should be ignored because the test is finished at ~ 600 sec.

Figures 3.34 and 3.35 represented the vapor temperatures at two elevations 1.8 m and 3.0 m, respectively. The vapor temperature at higher elevation 3.0 m was largely over predicted at the initial heat up period and it would result in the earlier increase of the rod temperature during the heating up and the earlier turn-over time. The calculation with the spacer grid model showed the higher vapor temperature during the heat up and the faster quenching at high elevation.

The heat transfer coefficients (HTCs) at several elevations is shown in Figure 3-36 through Figure 3-38. As shown in Figures, the HTC was reducing or stagnant during the rod heat up, but TRACE did not predict well the experimental data for the heating up. However, the HTCs were fairly predicted during the reflood phase and the time of steep increase of HTC was agreed well with the experimental data, especially at elevation $z \geq 2.4$. This would correspond with the behaviors of rod temperature. With the spacer grid model, the earlier sharp rise of HTC was predicted due to the earlier rod quench.

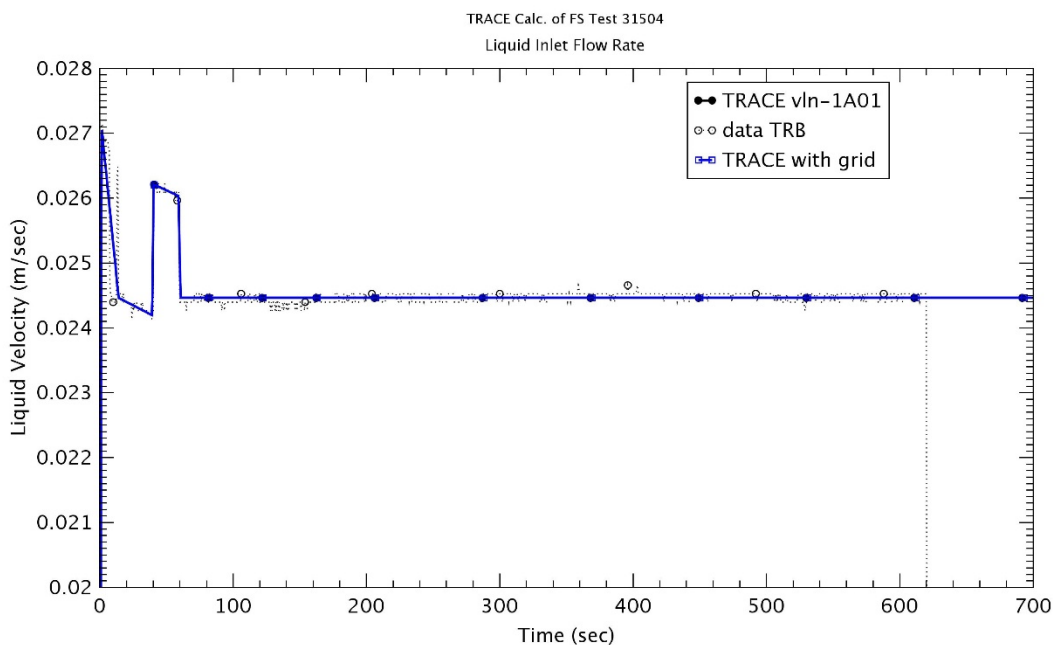


Figure 3-21 Liquid Inlet Flowrate – Run No.31504

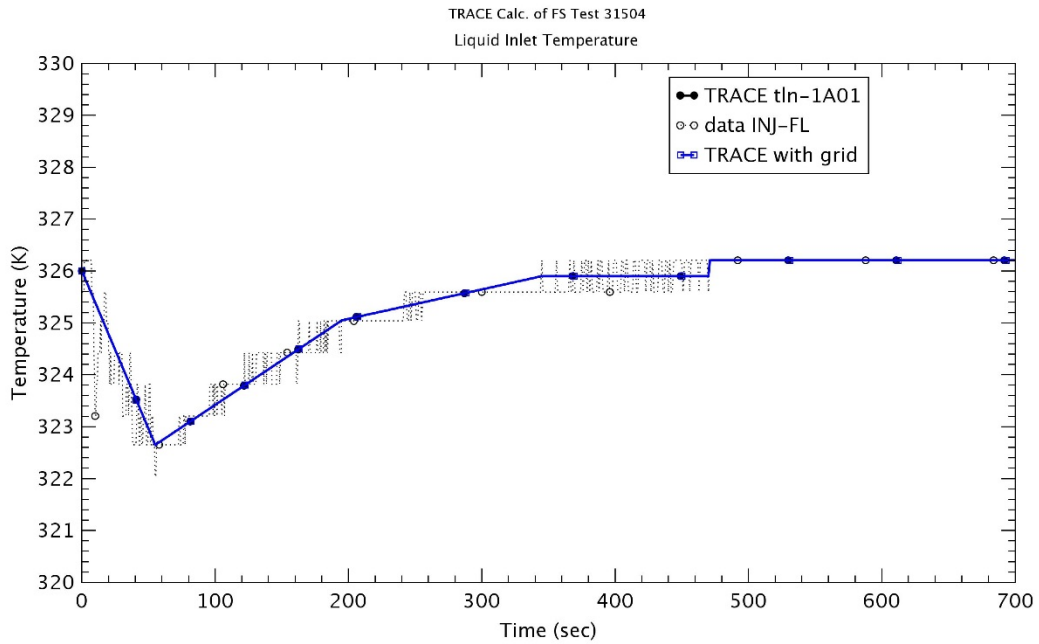


Figure 3-22 Liquid Inlet Temperature – Run No.31504

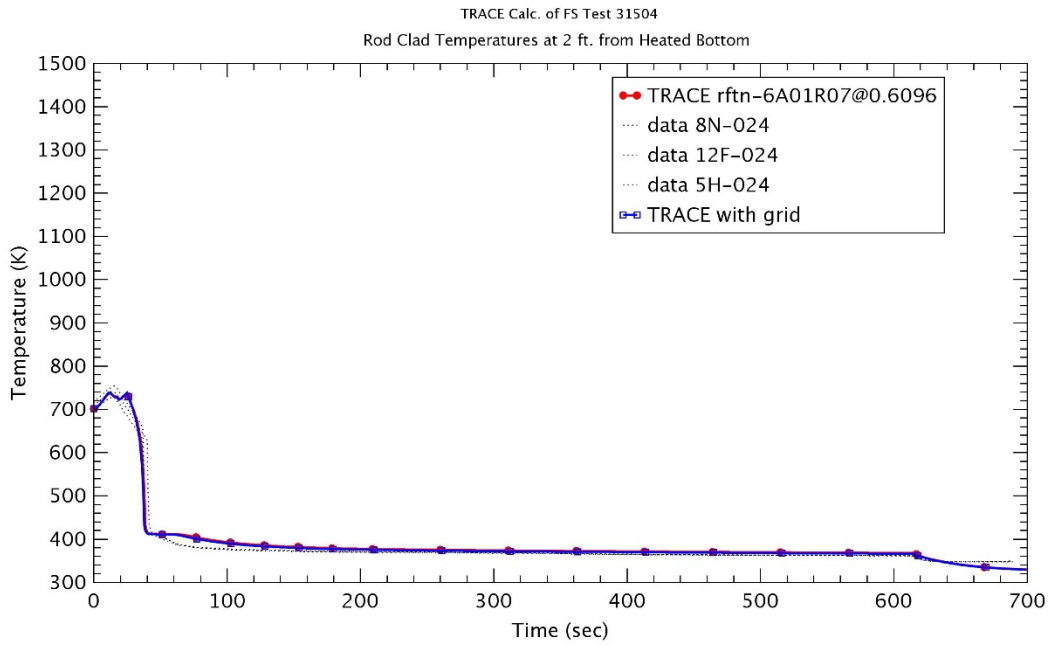


Figure 3-23 Heater Rod Temperature at 0.6 m – Run No.31504

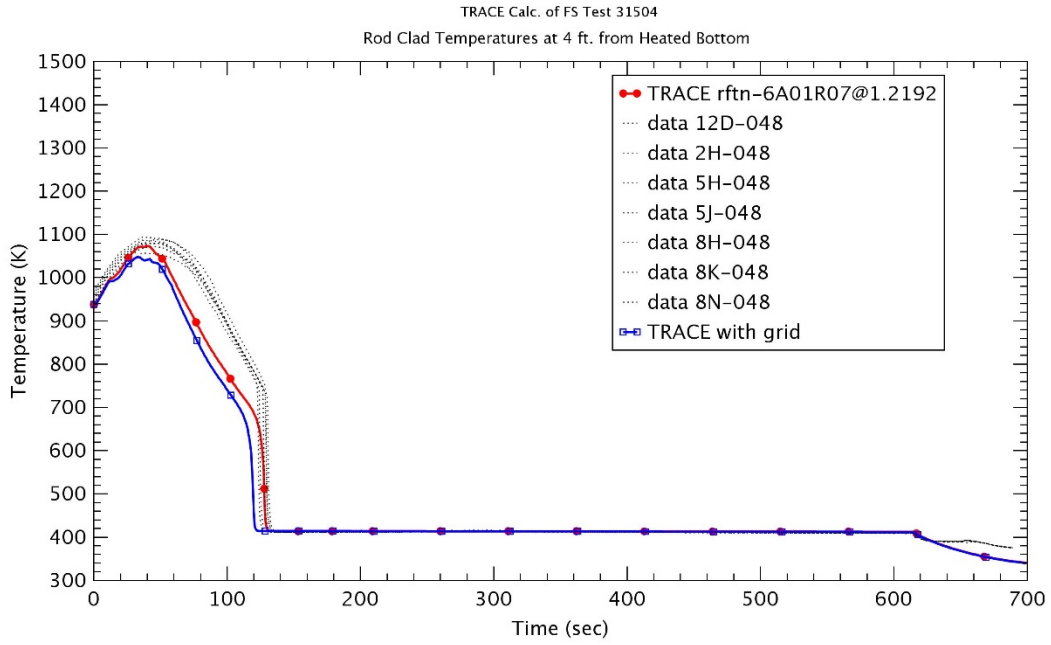


Figure 3-24 Heater Rod Temperature at 1.2 m – Run No.31504

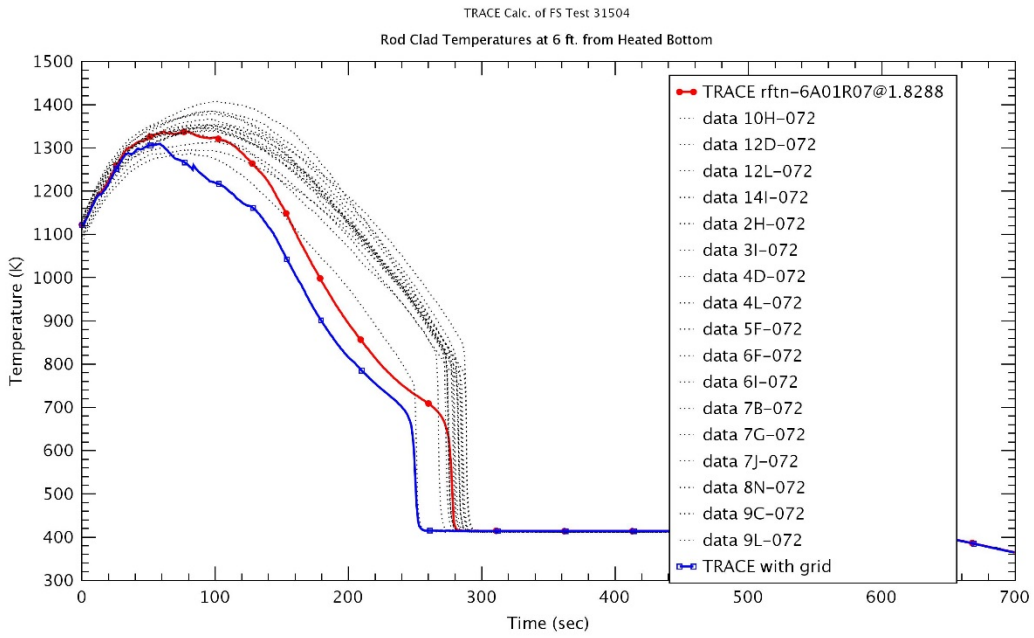


Figure 3-25 Heater Rod Temperature at 1.8 m – Run No.31504

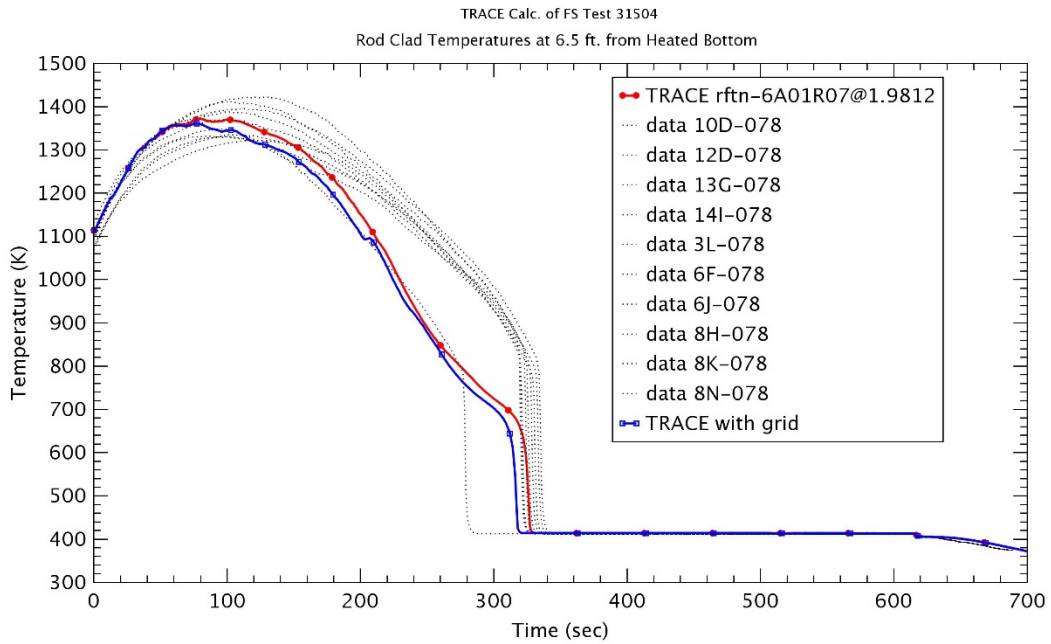


Figure 3-26 Heater Rod Temperature at 1.98 m – Run No.31504

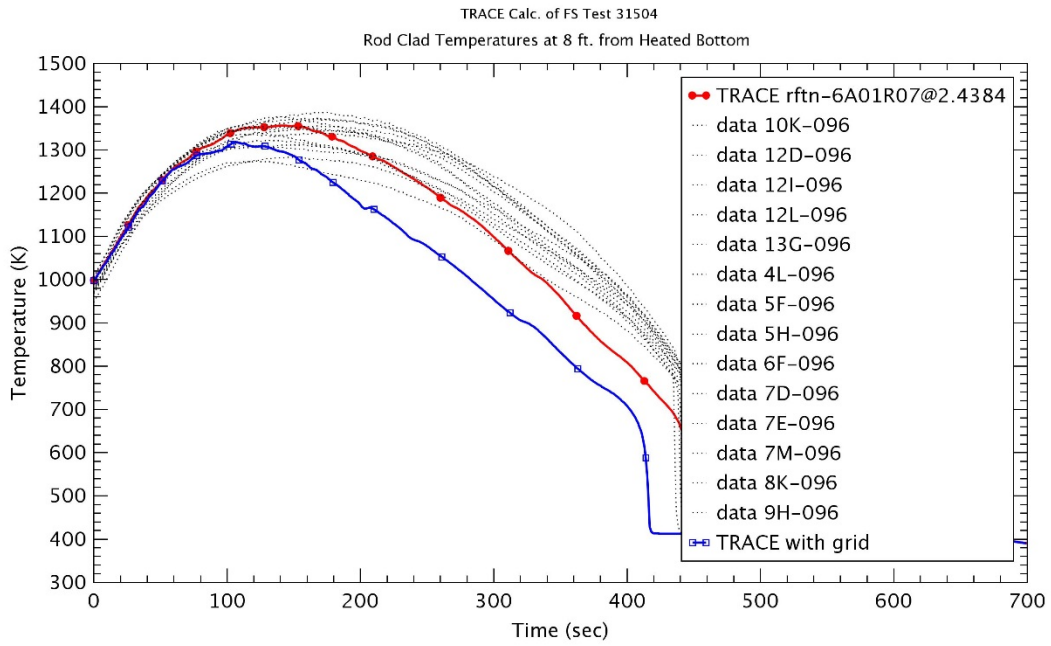


Figure 3-27 Heater Rod Temperature at 2.4 m – Run No.31504

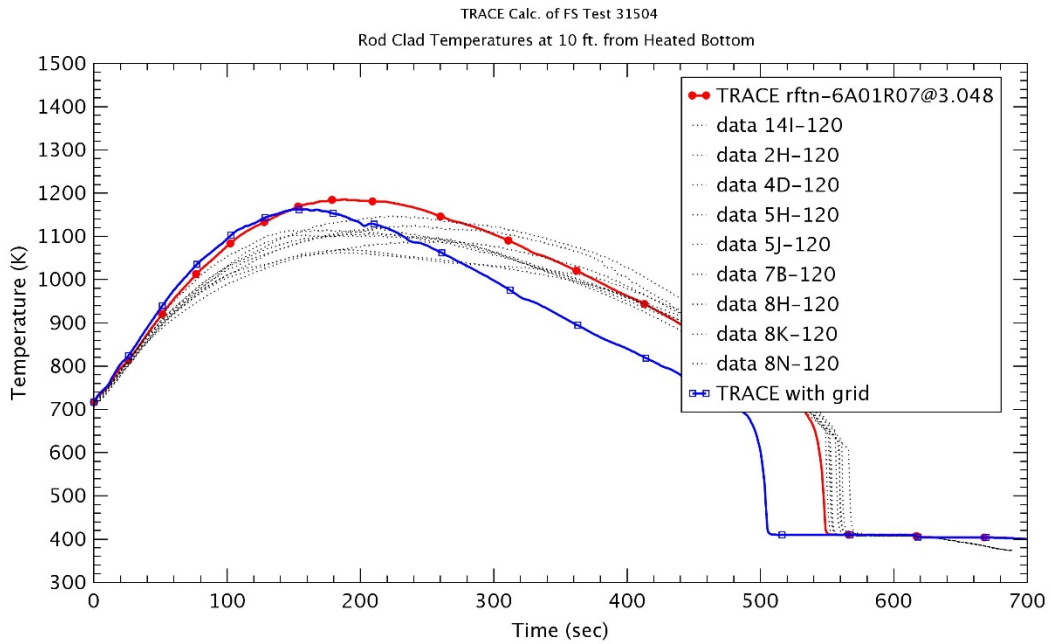


Figure 3-28 Heater Rod Temperature at 3.0 m – Run No.31504

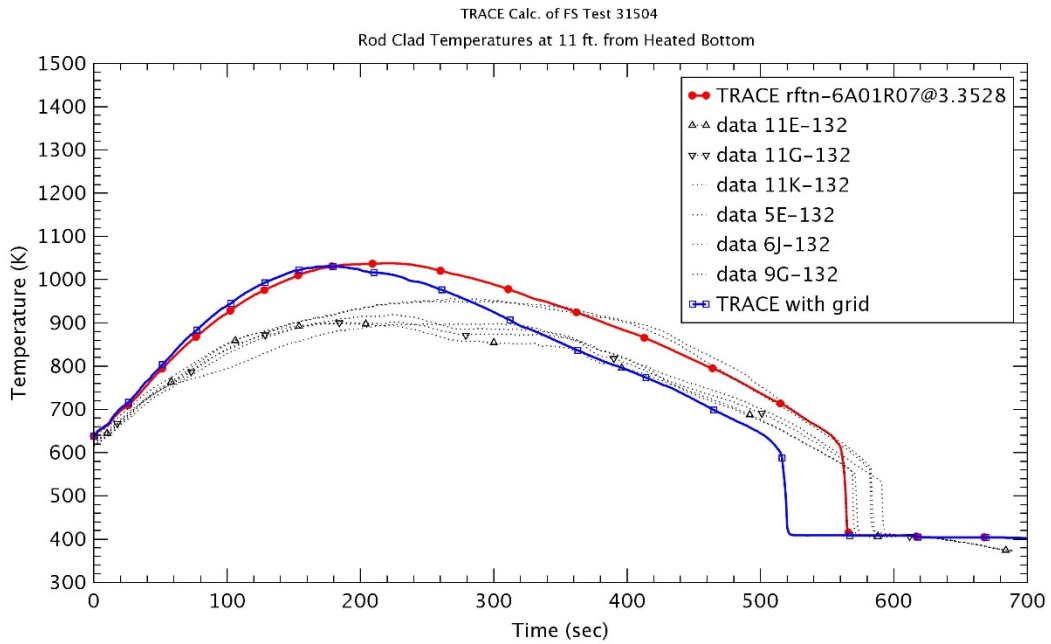


Figure 3-29 Heater Rod Temperature at 3.3 m – Run No.31504

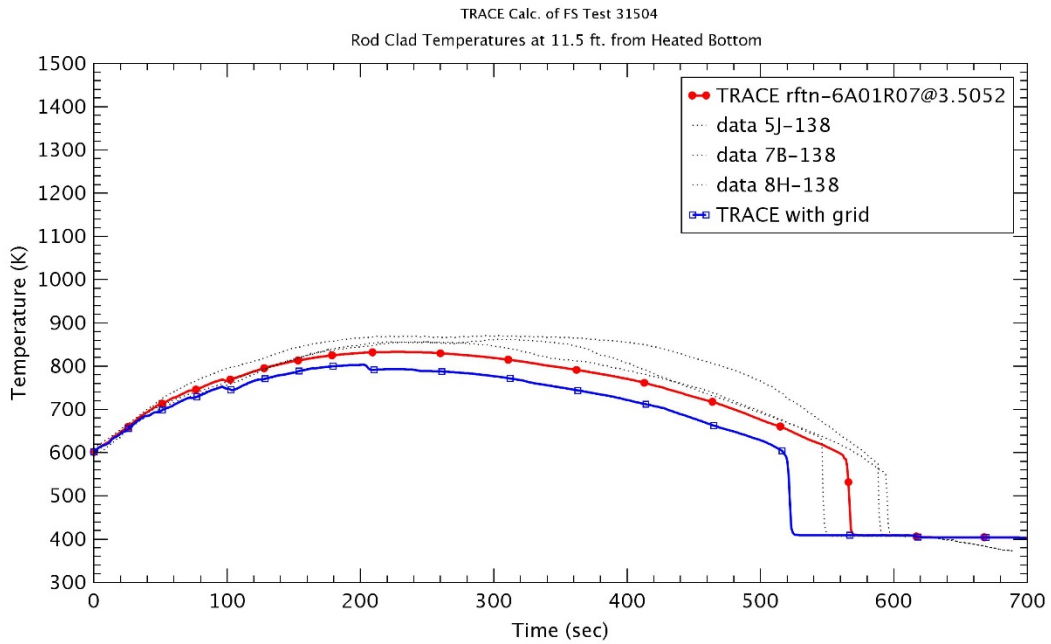


Figure 3-30 Heater Rod Temperature at 3.5 m – Run No.31504

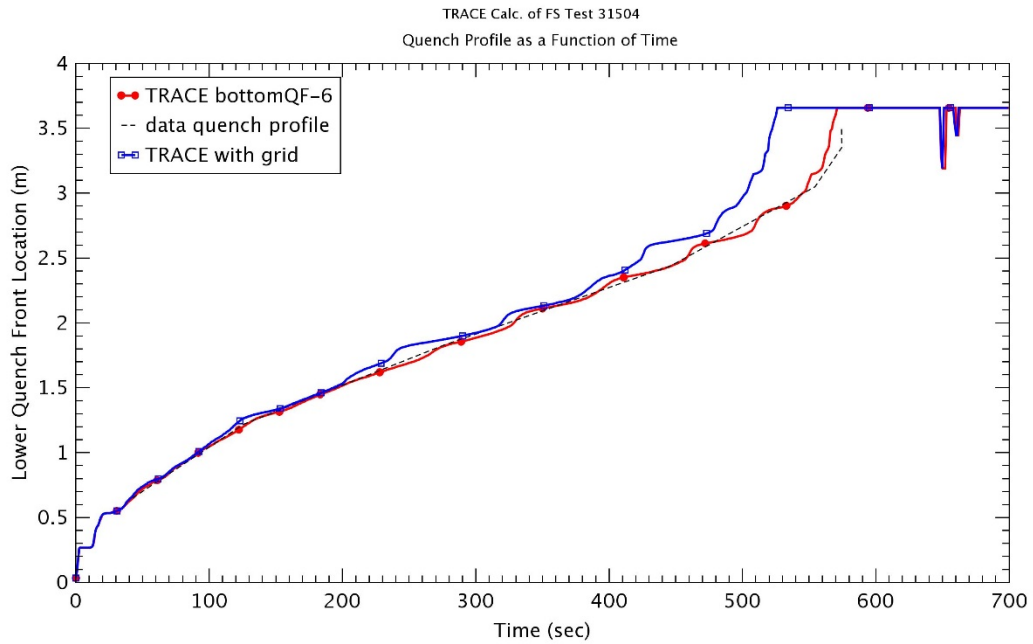


Figure 3-31 Quench Front Profile – Run No.31504

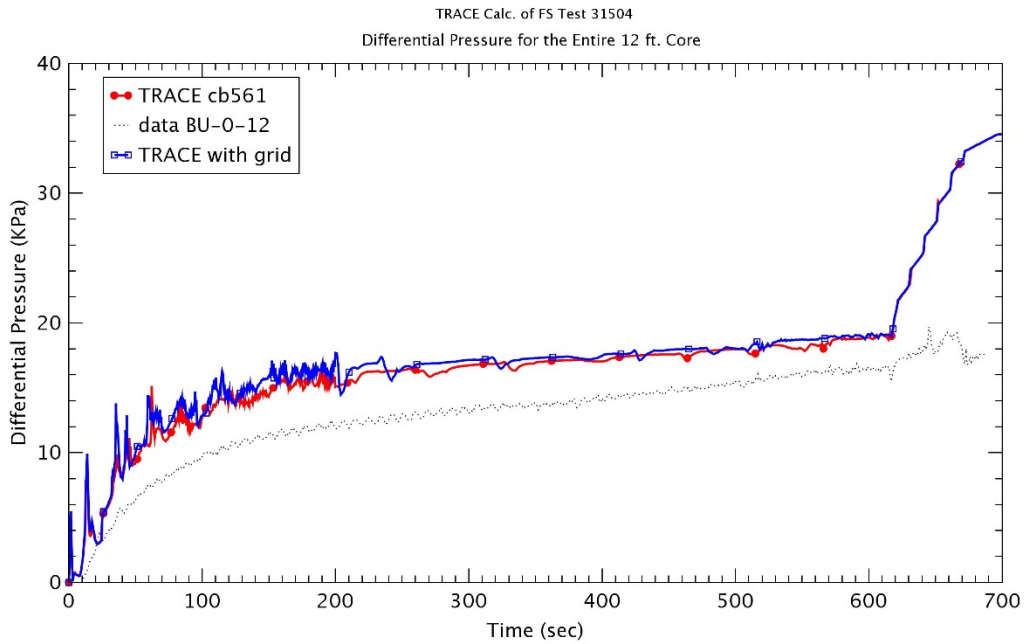


Figure 3-32 Differential Pressure for Entire 12 ft – Run No.31504

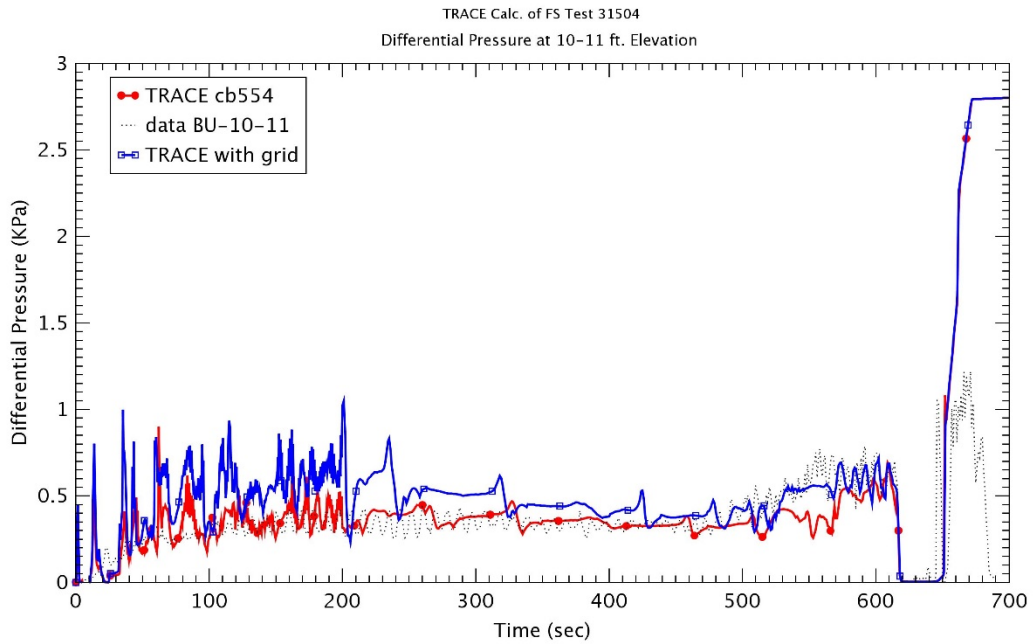


Figure 3-33 Differential Pressure at 10~11 ft Elevation – Run No.31504

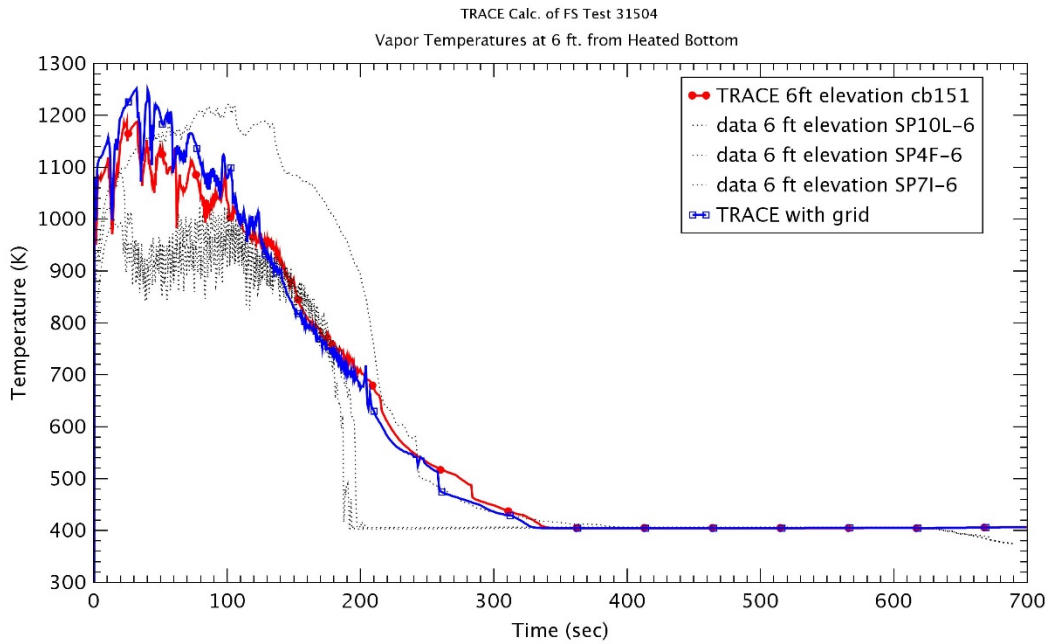


Figure 3-34 Vapor Temperature at 1.8 m – Run No.31504

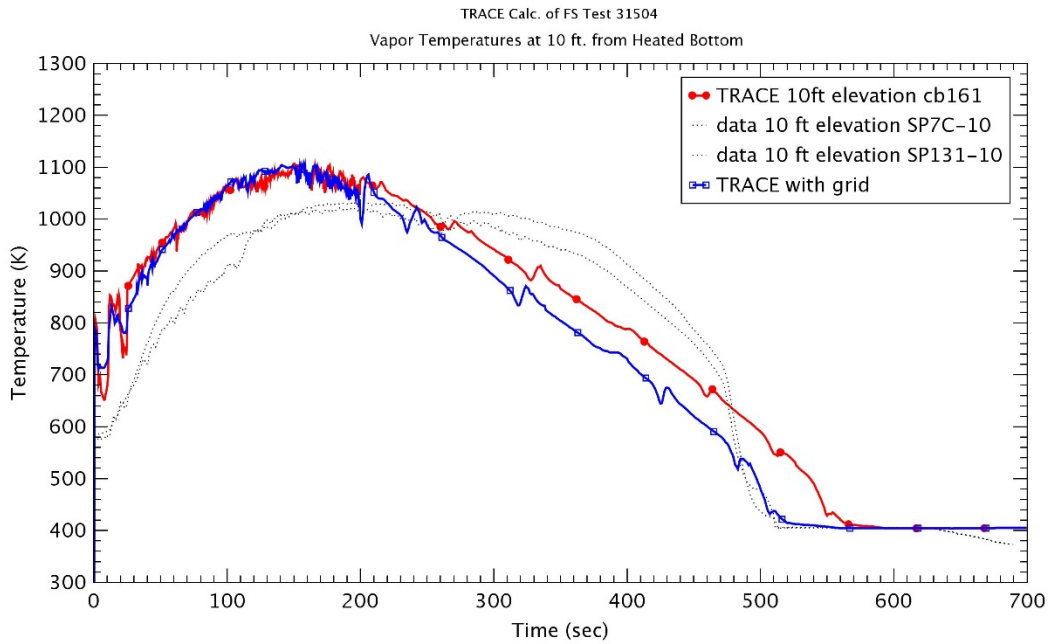


Figure 3-35 Vapor Temperature at 3.0 m – Run No.31504

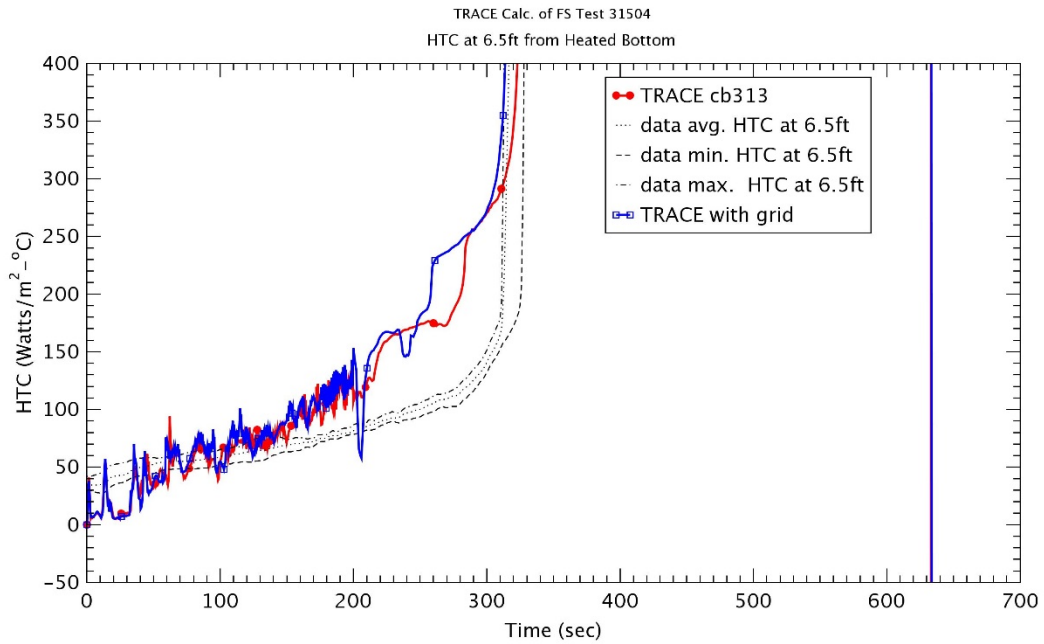


Figure 3-36 Heat Transfer Coefficient at 1.98 m – Run No.31504

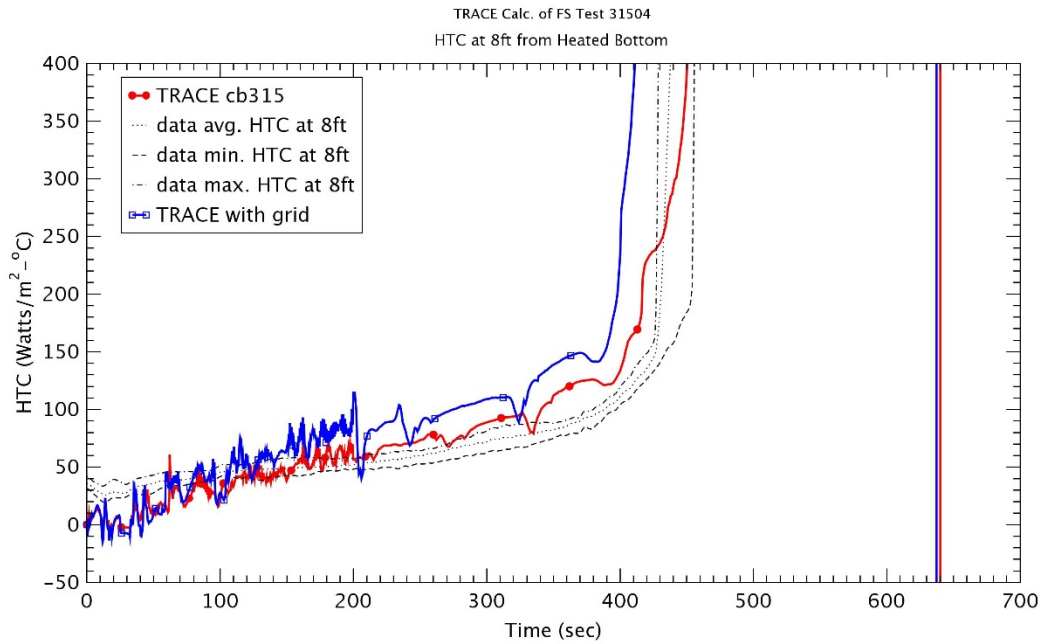


Figure 3-37 Heat Transfer Coefficient at 2.4 m – Run No.31504

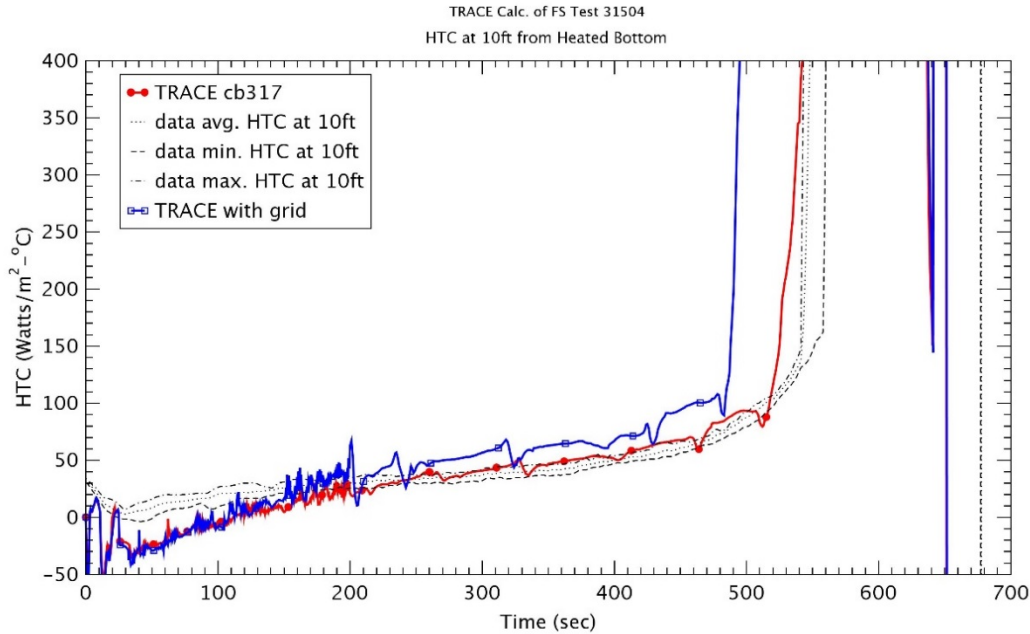


Figure 3-38 Heat Transfer Coefficient at 3.0 m – Run No.31504

3.2.1.2 Run No. 31203

Run No. 31203 was a test with a flooding rate of 3.84 cm/sec at 0.28 MPa and 78 oC inlet subcooling temperature as shown in Table 3-1. This was the same as Run No. 31805, except for an increase of a flooding rate. However, as described previously, the actual input conditions changed largely with time and showed the big oscillations. Therefore, the inlet flowrate and temperature were considered as time-dependent variables as shown in Figures 3.39 ~ 3.40. Most initial conditions in the TRACE assessment manual [6] were applied in this study.

The rod temperatures at various elevations were plotted in Figure 3-41 through Figure 3-48. These figures showed well the processes such as the heat up, turn-over of rod temperature during a reflow and a final quenching as in Run No. 31805. Without the spacer grid model, the peak temperatures were predicted well with the data at low elevations ($z \leq 2.4$ m), but were over predicted at higher elevations ($z = 3.0$ m ~ 3.3 m). Especially, TRACE also over predicted the peak temperatures at $z = 3.5$ m, It was a different result with previous tests. The maximum peak clad temperature was shown at elevation $z=1.98$ m (6.5 ft) and decreased as the reflow rate is higher. The turn-around times were reasonably predicted well in all elevations. The quenching times were fairly agreed with the data at lower elevations ($z < 1.98$ m). When the spacer model was applied, the rod temperatures were decreased and the final quenching time was shortened at all elevations, as expected. The trends of rod temperature and the quenching time were similar with Run No. 31805. During a heating up, the effect of the spacer grid model was not significant at lower elevations ($z \leq 3.0$ m), but the earlier increase of the rod temperatures was predicted at higher elevations in the case with the spacer grid model. The turn-over time of rod temperature with the spacer grid model were expedited at all elevations since the spacer grid enhanced the convective heat transfer. The peak temperatures with the spacer grid model were lower than those without the spacer grid model at most elevations. In the case with the spacer grid model, the decreasing temperature was ~ 5.9 K and the reduction of quenching time was ~ 4 sec due to the spacer grid model at elevation $z=1.98$ with the maximum peak cladding temperature.

As shown in Figure 3-49, the quench front without the spacer grid model was predicted well for the lower 80% elevations. In this test, the data showed a top quench which was probably from the liquid de-entrainment above the active core, but TRACE did not predict this top quenching. The quench front with the spacer grid model was rising faster than that without the model as the elevation was higher.

The differential pressure (DP) for entire 12 ft was plotted in Figure 3-50 and the differential pressure between 11 ft and 12 ft was shown in Figure 3-51. The increase of DP for entire test section was correspond with the collapsed liquid level and the DP increased with the injected water. The DP for entire 12 feet showed the large over-prediction with the experimental data. TRACE predicted more water inventory in the test section compared to the data. If the spacer grid model was applied, the DP for entire 12 feet was increased at slightly earlier time. As shown well in Figure 3-51, the DP between 11 ft and 12 ft rose at elevation with the spacer grid and the large pressure drop was predicted.

Figures 3.52 and 3.53 showed the vapor temperatures at two elevations 1.8 m and 3.0 m, respectively. The vapor temperature at higher elevation 3.0 m was over estimated at the initial heating up and it would result in the earlier increase of the rod temperature and the earlier turn-around time. In the case with the spacer grid model, the higher vapor temperature during the heat up and the faster quenching at high elevation were predicted.

Figure 3-54 through Figure 3-56 showed the heat transfer coefficients (HTCs) at several elevations. The HTC was reducing or stagnant during the rod heat up, but TRACE under predicted the experimental data for the heating up. During the reflood phase, the HTCs were over predicted and increased faster than the experimental data and the time of increase of HTC was expedited at elevations $z \geq 2.4$. If the spacer grid model was applied, the earlier sharp rise of HTC was predicted according to the earlier quenching.

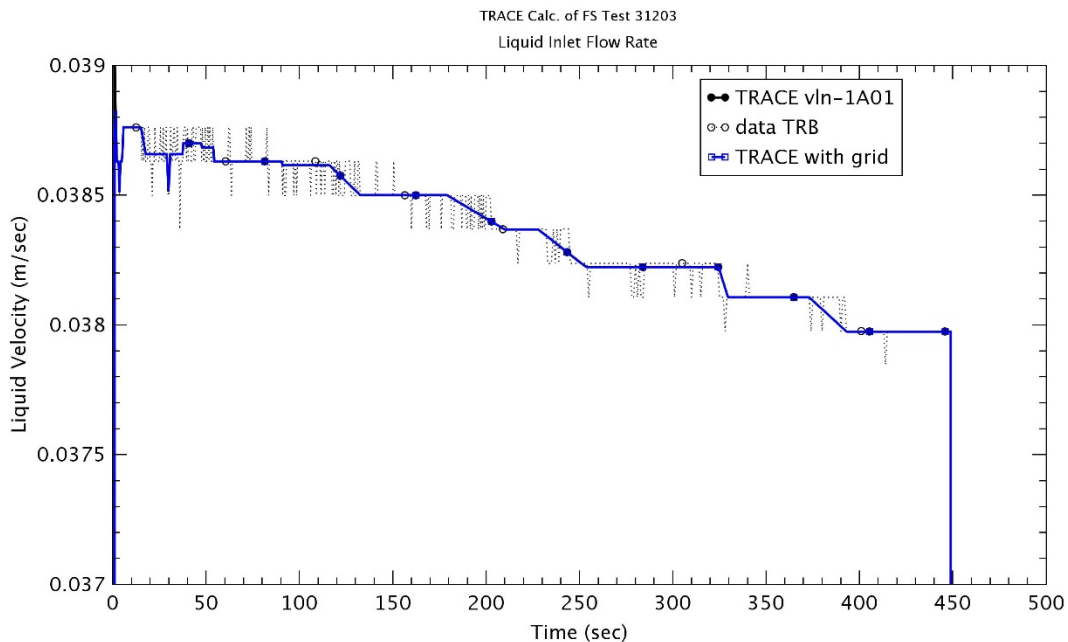


Figure 3-39 Liquid Inlet Flowrate – Run No.31203

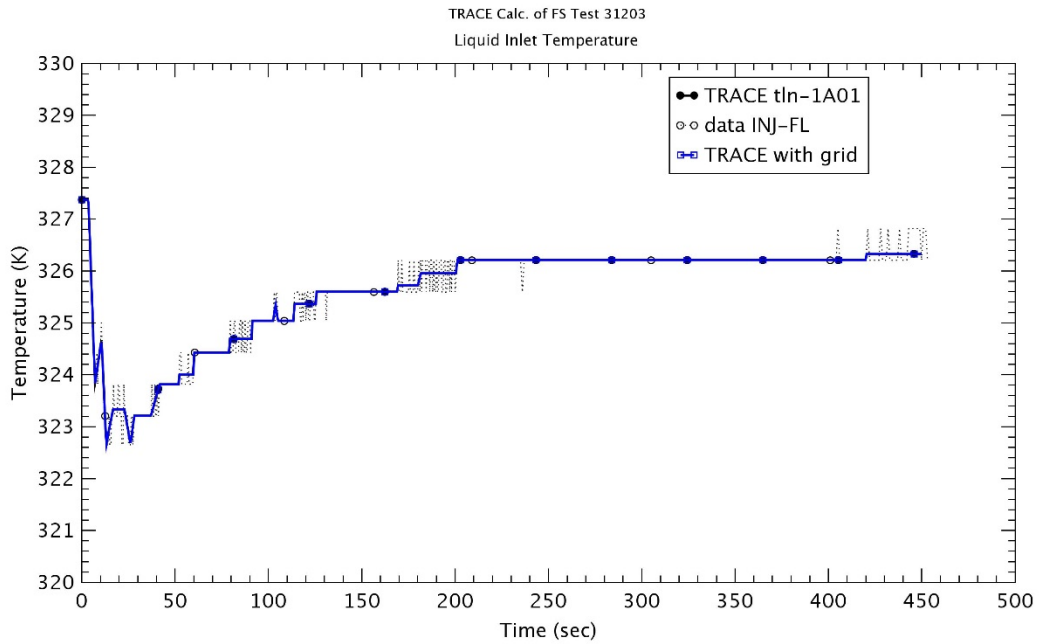


Figure 3-40 Liquid Inlet Temperature – Run No.31203

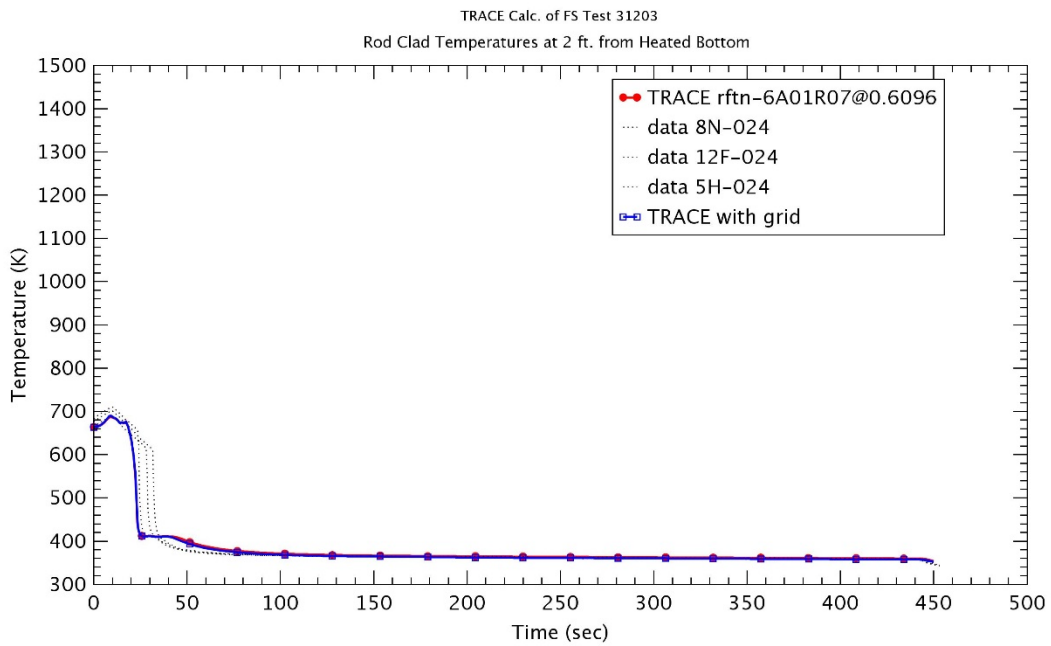


Figure 3-41 Heater Rod Temperature at 0.6 m – Run No.31203

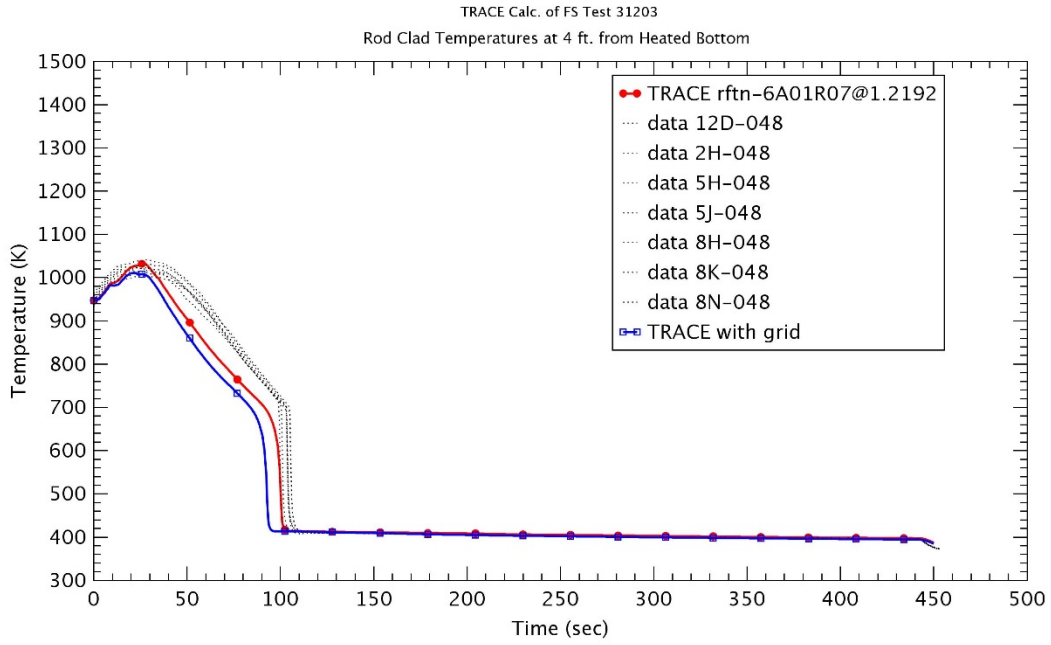


Figure 3-42 Heater Rod Temperature at 1.2 m – Run No.31203

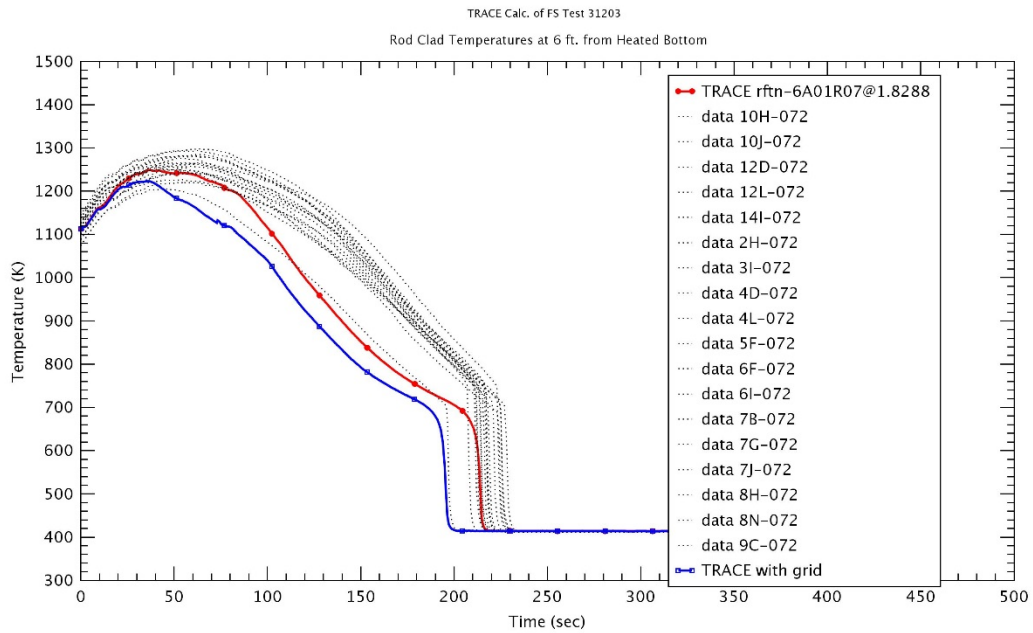


Figure 3-43 Heater Rod Temperature at 1.8 m – Run No.31203

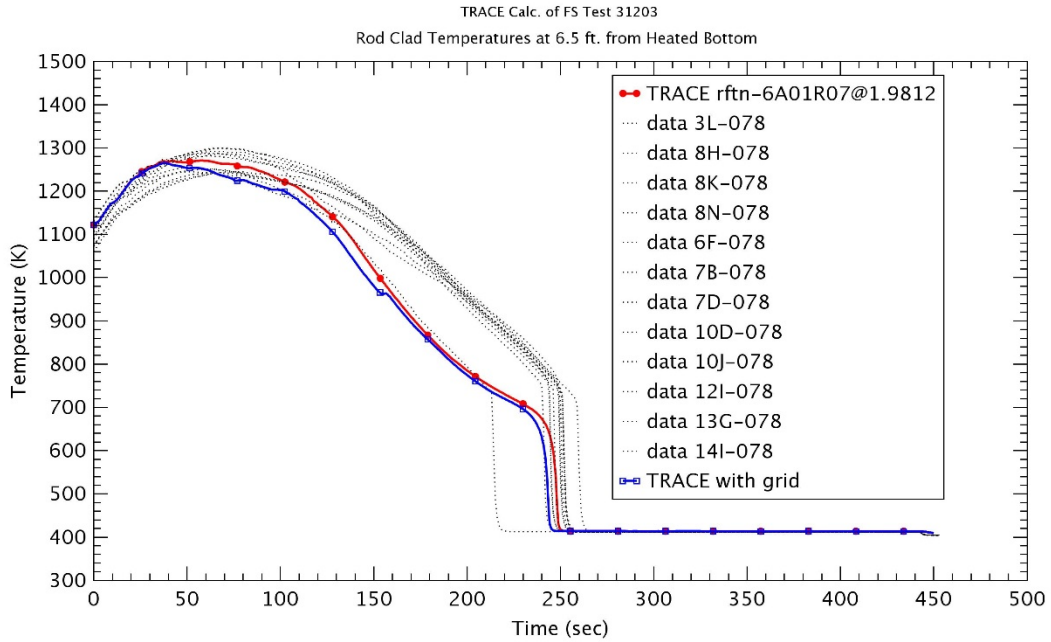


Figure 3-44 Heater Rod Temperature at 1.98 m – Run No.31203

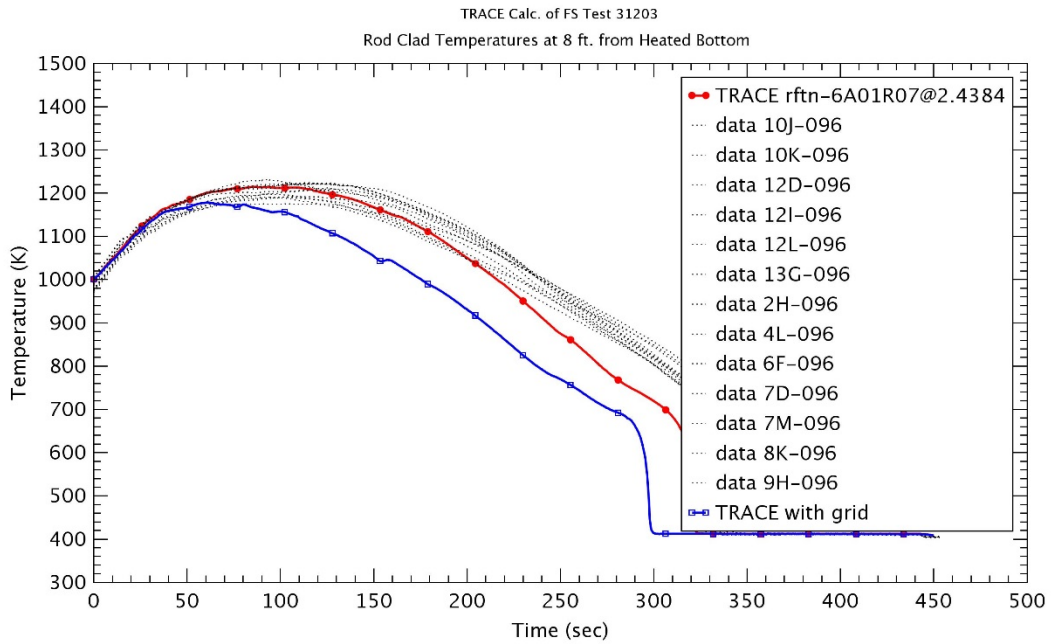


Figure 3-45 Heater Rod Temperature at 2.4 m – Run No.31203

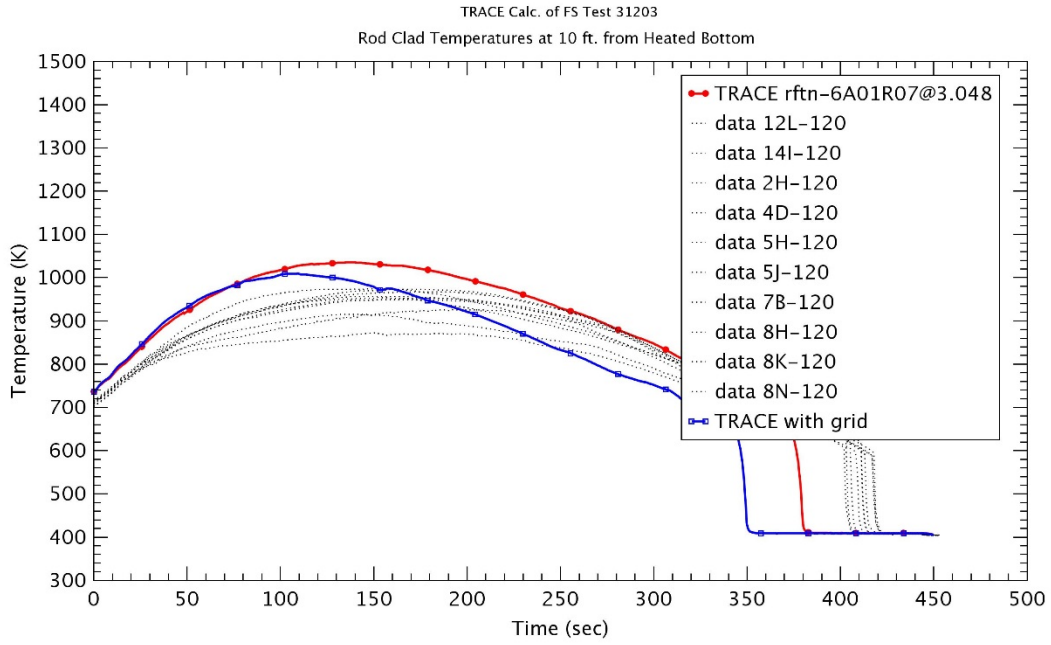


Figure 3-46 Heater Rod Temperature at 3.0 m – Run No.31203

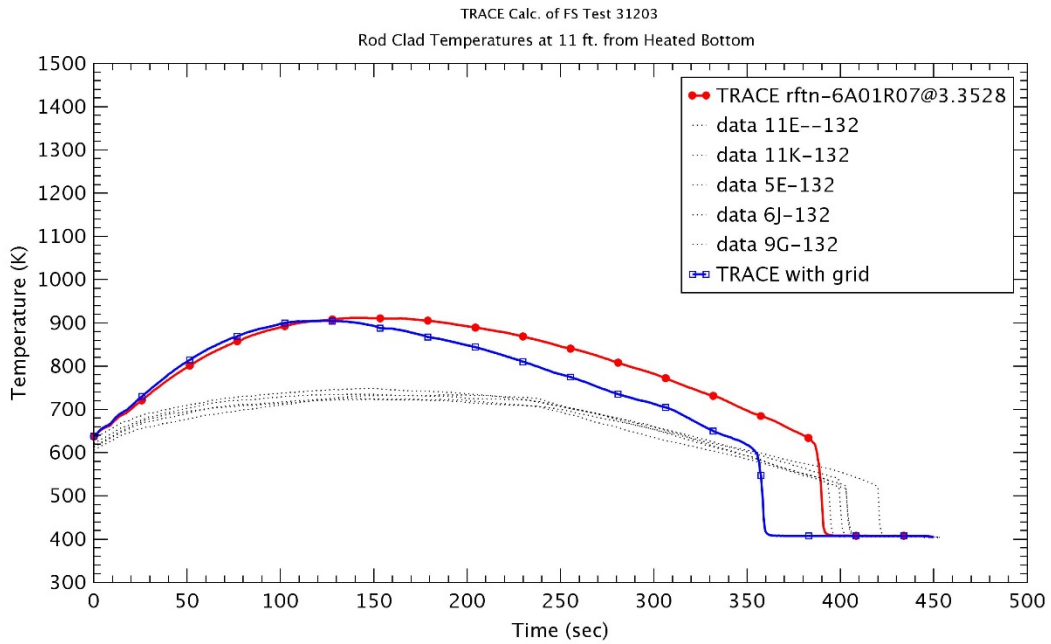


Figure 3-47 Heater Rod Temperature at 3.3 m – Run No.31203

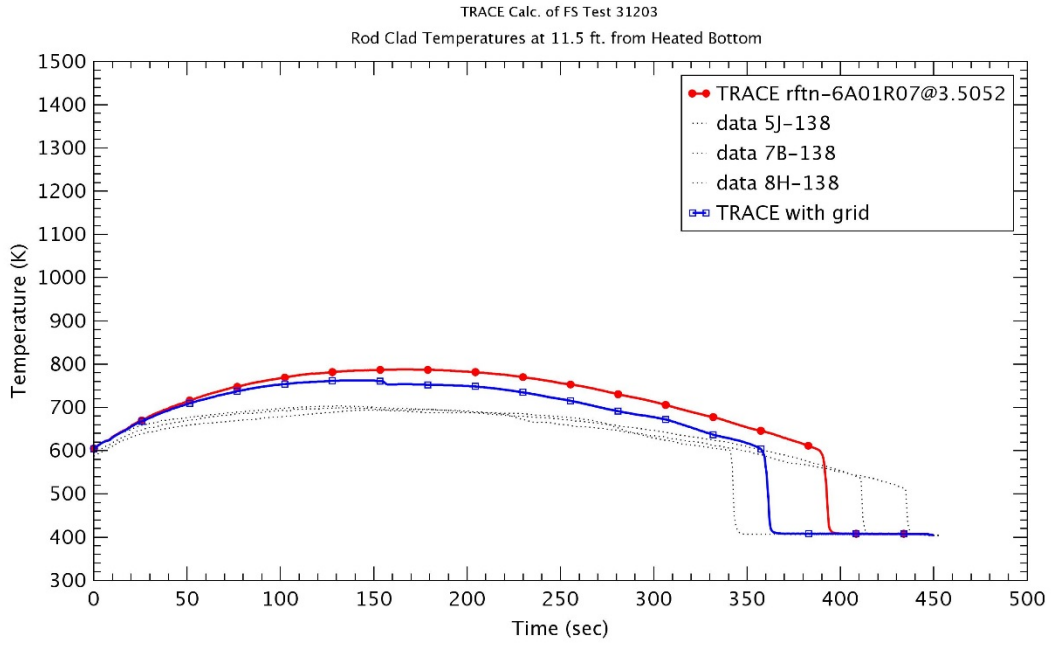


Figure 3-48 Heater Rod Temperature at 3.5 m – Run No.31203

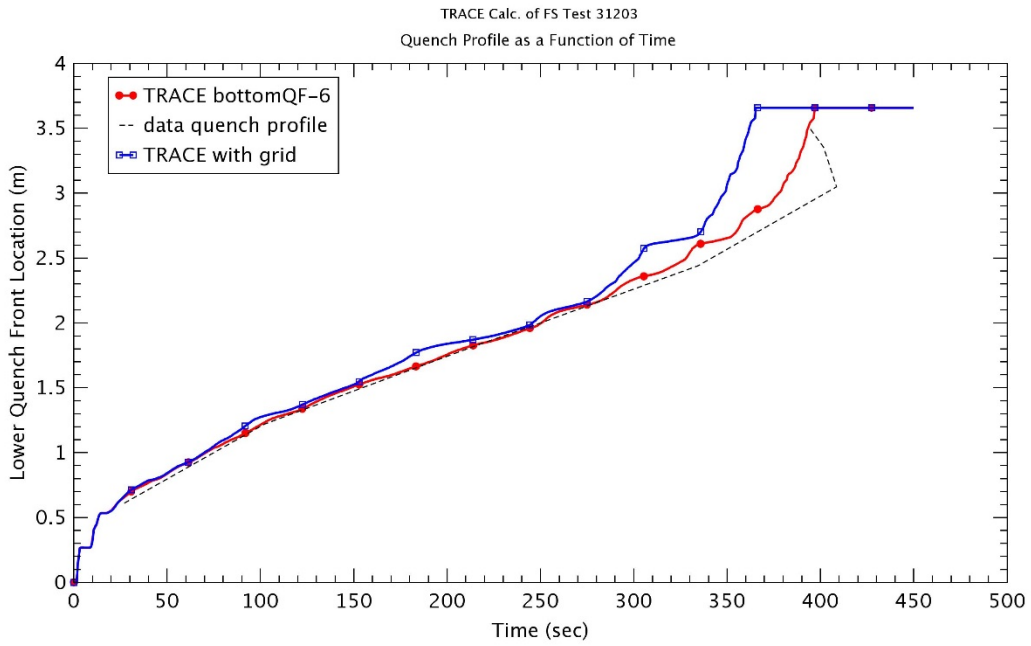


Figure 3-49 Quench Front Profile – Run No.31203

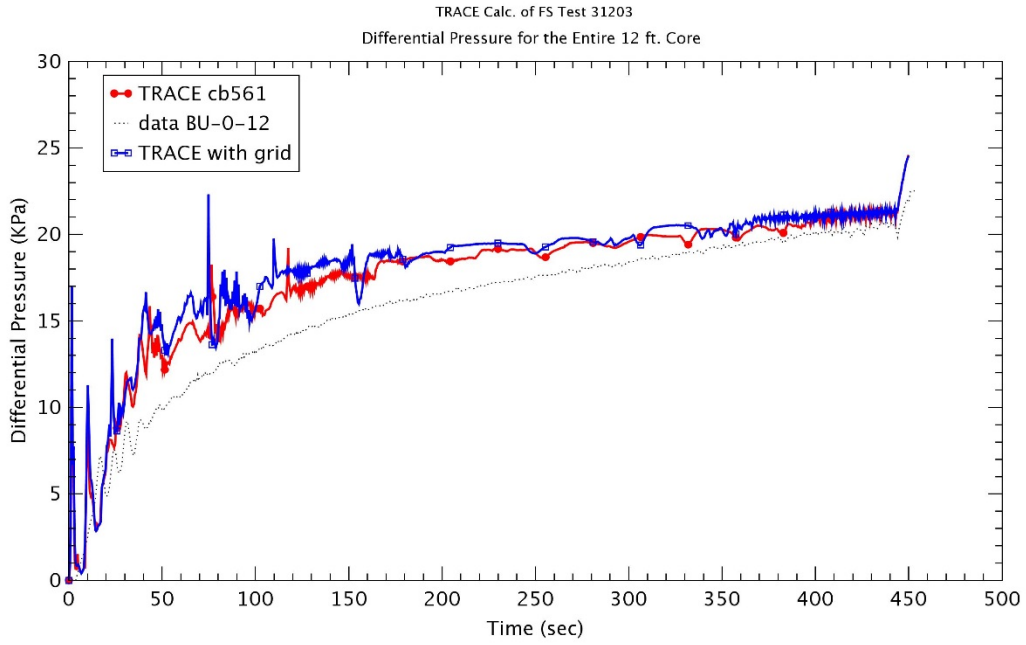


Figure 3-50 Differential Pressure for Entire 12 ft – Run No.31203

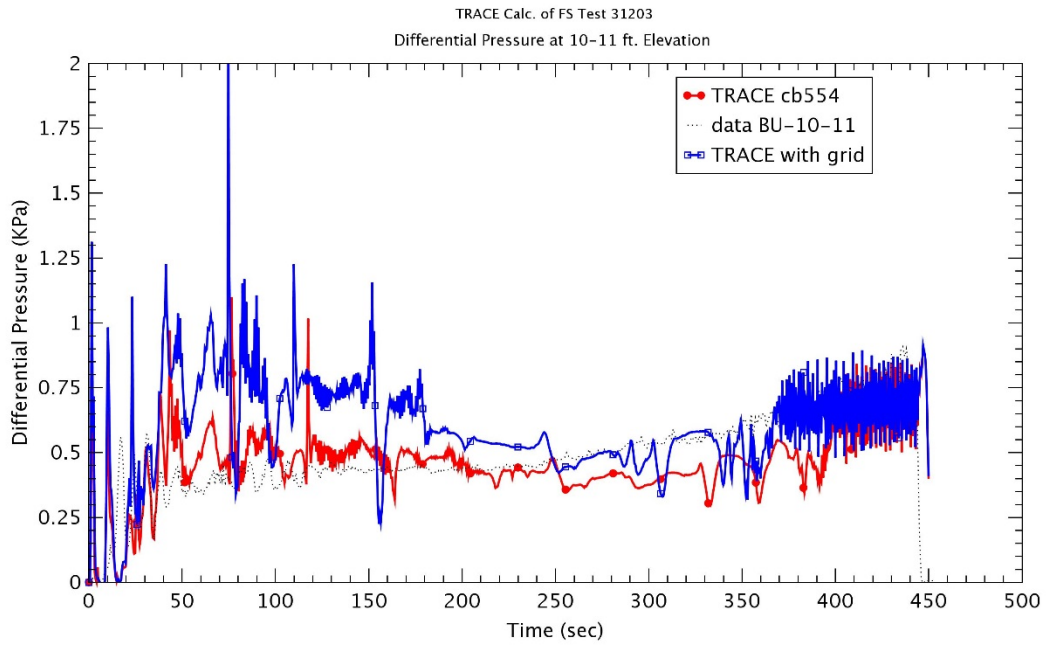


Figure 3-51 Differential Pressure at 10~11 ft Elevation – Run No.31203

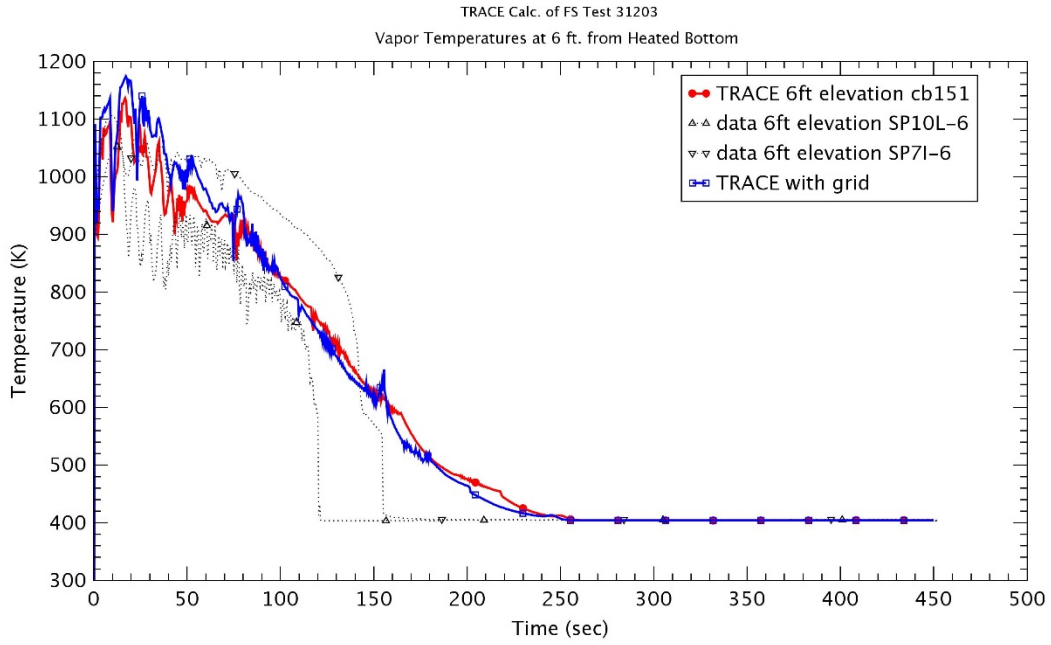


Figure 3-52 Vapor Temperature at 1.8 m – Run No.31203

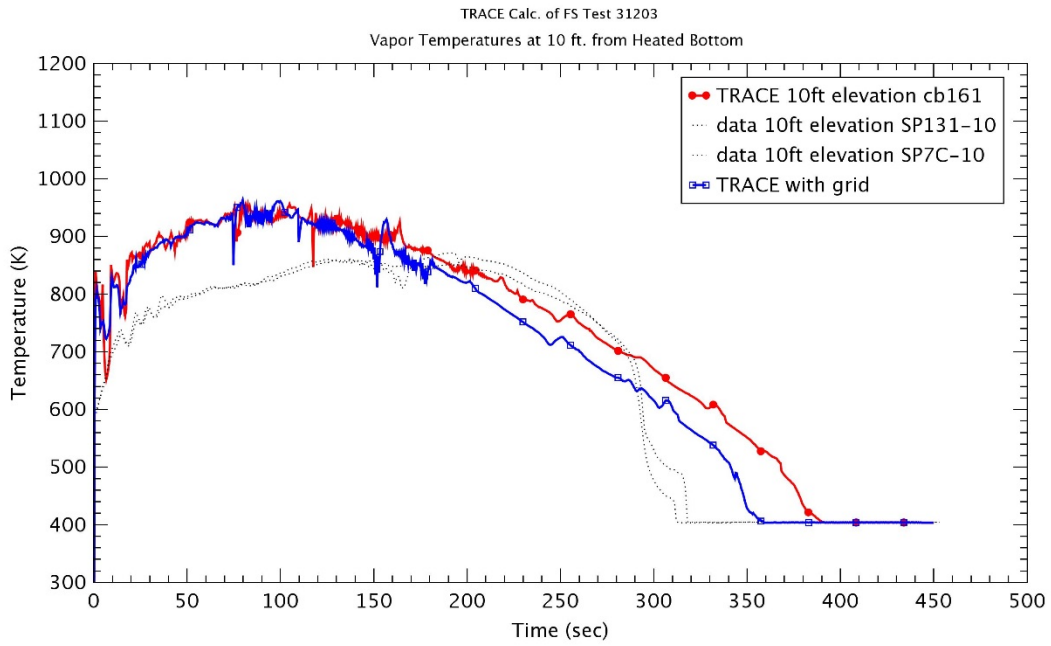


Figure 3-53 Vapor Temperature at 3.0 m – Run No.31203

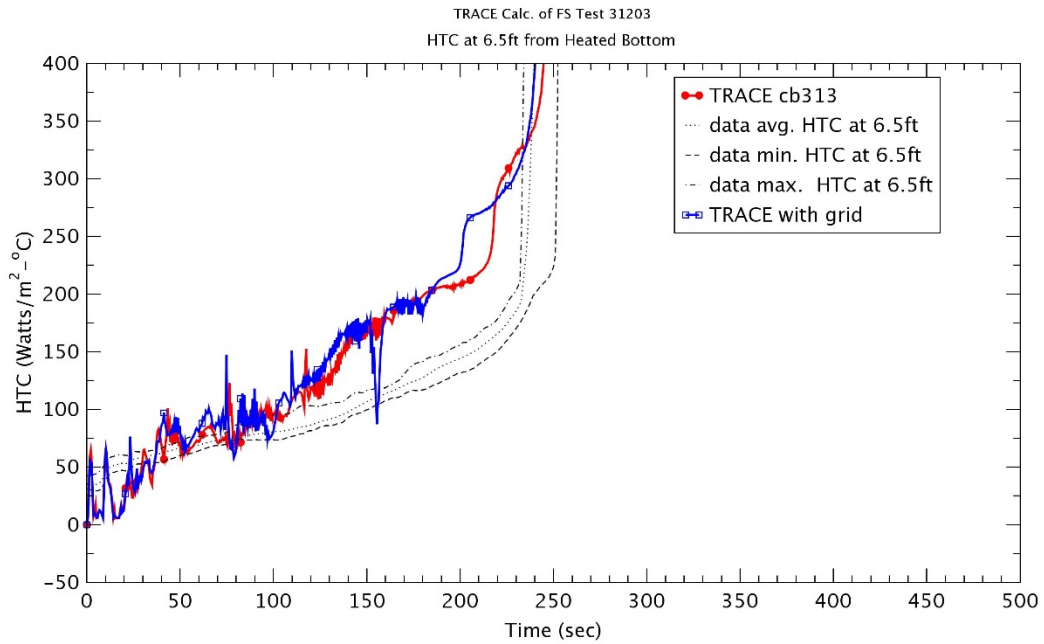


Figure 3-54 Heat Transfer Coefficient at 1.98 m – Run No.31203

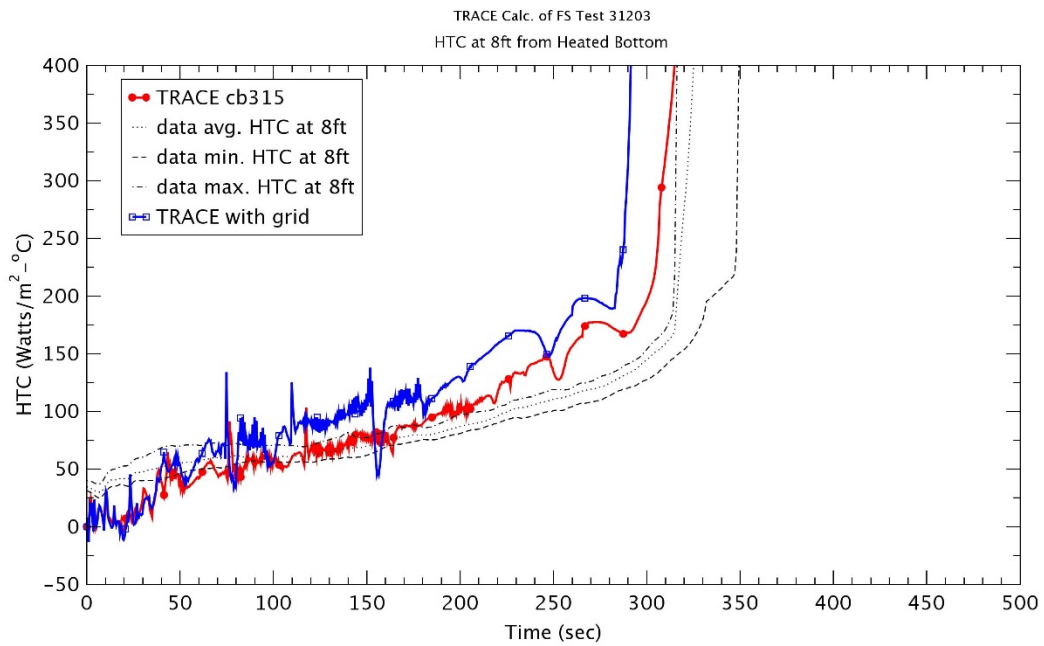


Figure 3-55 Heat Transfer Coefficient at 2.4 m – Run No.31203

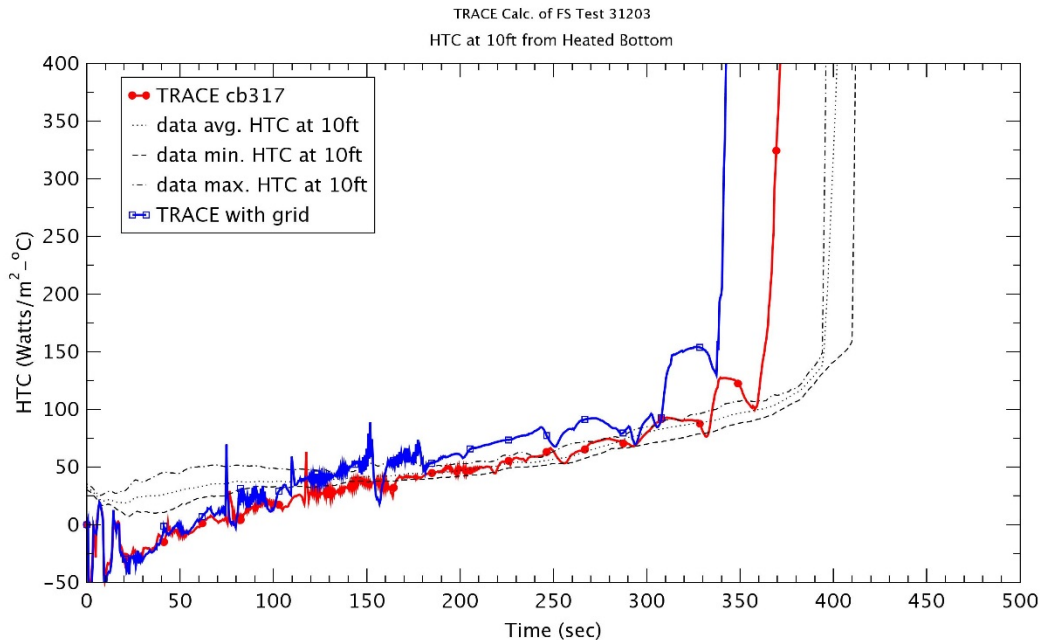


Figure 3-56 Heat Transfer Coefficient at 3.0 m – Run No.31203

3.2.1.3 Run No. 31302

Run No. 31302 was a test with a flooding rate of 7.65 cm/sec at 0.28 MPa and 78 oC inlet subcooling temperature as shown in Table 3-1. This was the same as Run No. 31805 except for increasing the reflood rate. However, as described previously, the actual input conditions varied largely with time and showed the big oscillations. So, the inlet flowrate and temperature were considered as time-dependent variables as shown in Figures 3.57 ~ 3.58. Most initial conditions in the TRACE assessment manual [6] were applied in this study.

The rod temperatures at various elevations were shown in Figures 3.59 ~ 3.66. These figures showed fairly the reflood process that the rod was heating up by the initiation of reflood, turn-over of rod temperature and finally quenching. In the case without the spacer grid model, the predicted peak temperatures under estimated at elevation $z = 0.6$ m with low power density. This test had three times the reflood rate in Run No. 31504, that resulted in the low heat up at $z = 0.6$ m. However, the peak temperatures were over predicted with the data above elevation $z = 1.8$ m. Those predictions were reflected in the relatively high vapor temperature as shown in Figures 3.70 ~ 3.71. The maximum peak clad temperature was predicted at elevation $z = 1.98$ m (6.5 ft). At elevations ($z \leq 3.0$ m), the quenching times were reduced as compared to the experimental data, while it were predicted at the later time at elevation $z > 3.0$ since TRACE did not predict the strong top-down quenching was observed in the experiment. In the case with a spacer grid model, the effect of the spacer grid model during a heat up period was not shown at all elevations, but the earlier turn-around of rod temperature was predicted since the spacer grid enhanced the increase of collapsed liquid level. The peak temperatures with the spacer grid model had the lower values at all elevations in comparison with those without the spacer grid model. The maximum peak clad temperature at $z=1.98$ m was reduced in case with the spacer grid model. At elevation $z=1.98$ with the maximum peak cladding temperature, the decreasing temperature was ~ 2.4 K and the reduction of quenching time was ~ 4 sec due to the spacer grid model.

As shown in Figure 3-67, the quench front without the spacer grid model was predicted well with the data up to elevation $z = 2.0$ m. In this test, TRACE did not predict the top quenching at higher elevations which was from the liquid de-entrainment from the upper part above the active core. If the spacer grid model was applied, the quench front was increasing faster than that without the spacer grid model as the elevation was higher.

The differential pressure (DP) for entire 12 ft was plotted in Figure 3-68 and the differential pressure between 11 ft and 12 ft was shown in Figure 3-69. The growth of DP for entire test section was correspond to the injected water. The DP for entire 12 ft showed a good prediction with the trend of data in spite of the difference of quenching behaviors at higher elevations ($z \geq 3.0$ m). It would result from the top down quenching of test. If the spacer grid model was applied, the DP for entire 12 ft was growing a little faster than that without the spacer grid model as shown in Figure 3-68. As shown well in Figure 3-69, the DP between 11 ft and 12 ft was increased largely due to the spacer grid.

The vapor temperatures at two elevations 1.8 m and 3.0 m were shown in Figures 3.70 and 3.71, respectively. As described in the rod temperature, the vapor temperatures at two elevations was over predicted during all reflood processes. The calculation with the spacer grid model had the slightly higher vapor temperature during the heat up and the faster quenching behaviors.

The heat transfer coefficients (HTCs) at several elevations is in Figure 3-72 through Figure 3-74. As shown in Figures, the HTC was under predicted during the rod heat up and increased faster than the experimental data. TRACE predicted a sharp increase of HTC much earlier than experimental data since the rod quenching occurred too early. When the spacer grid model was applied, the steep rise of HTC was expedited because of the earlier quenching of rod.

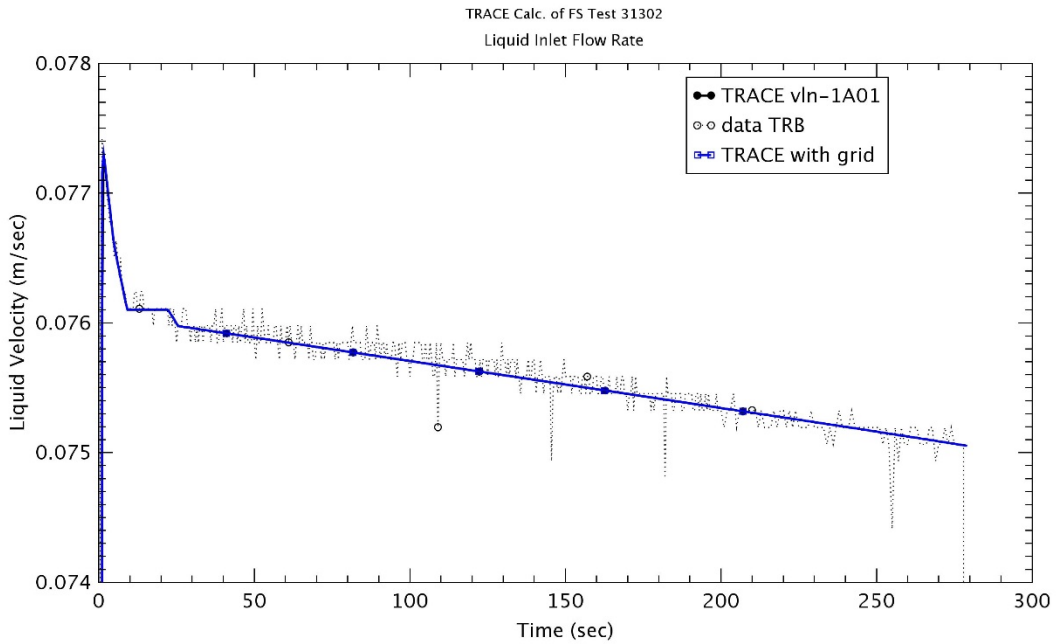


Figure 3-57 Liquid Inlet Flowrate – Run No.31302

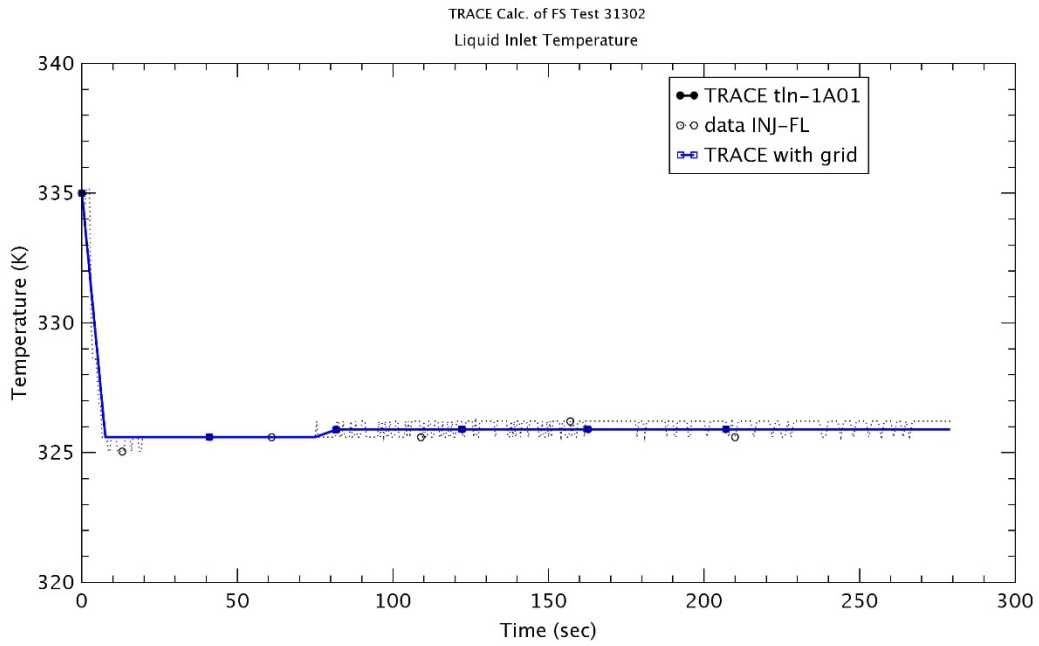


Figure 3-58 Liquid Inlet Temperature – Run No.31302

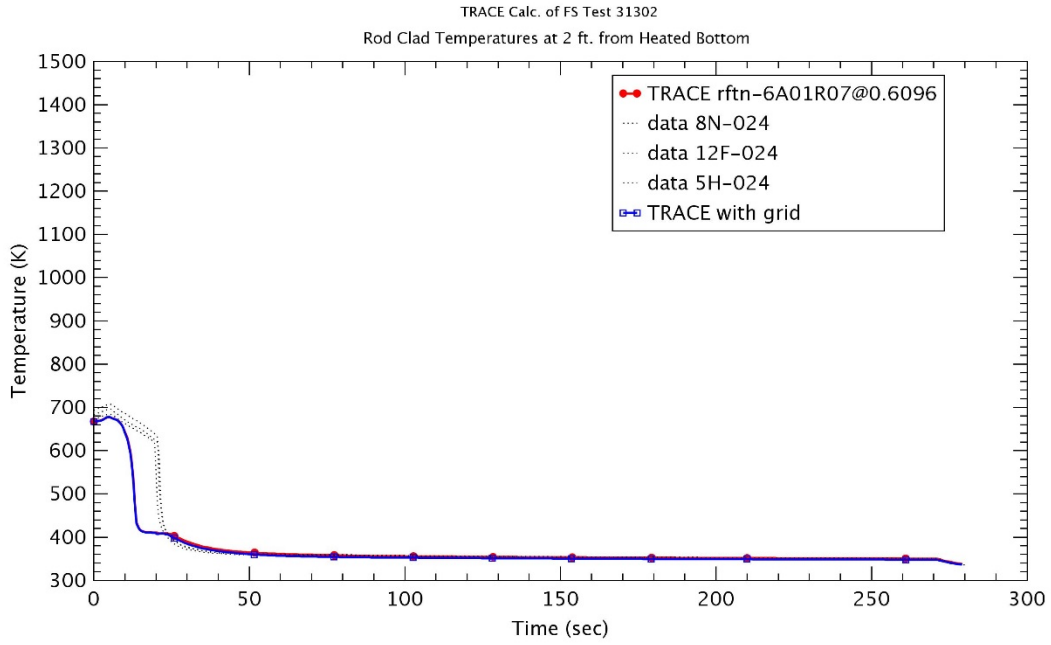


Figure 3-59 Heater Rod Temperature at 0.6 m – Run No.31302

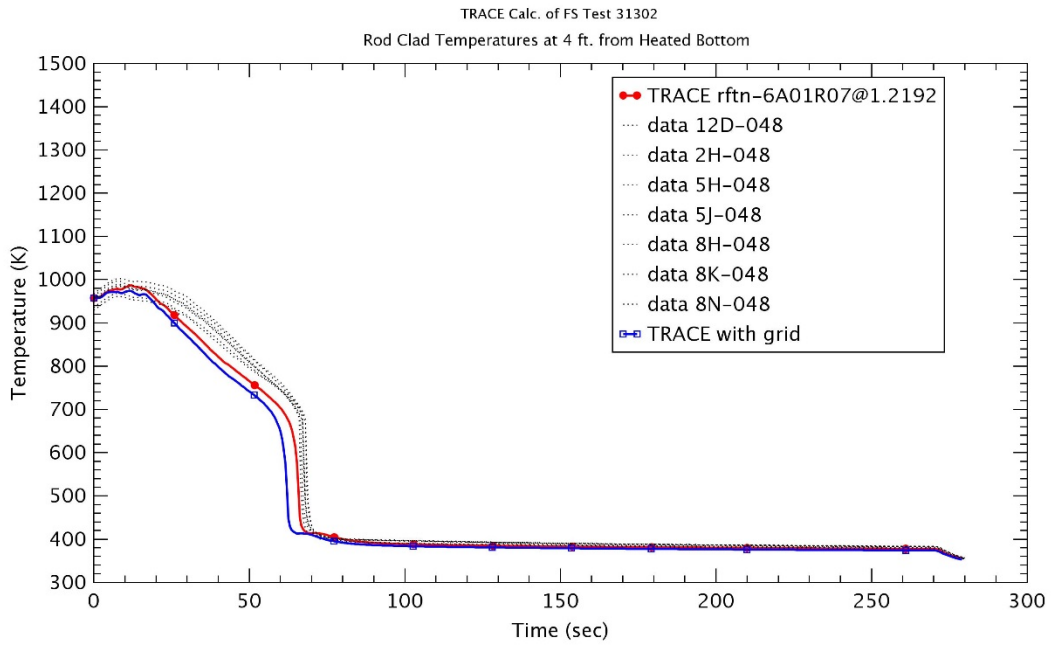


Figure 3-60 Heater Rod Temperature at 1.2 m – Run No.31302

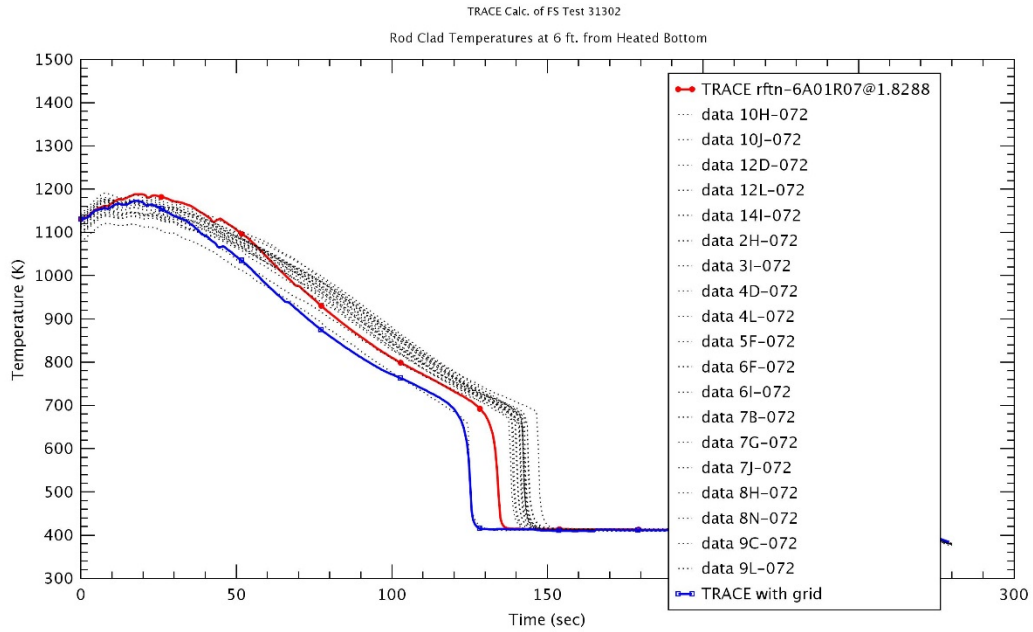


Figure 3-61 Heater Rod Temperature at 1.8 m – Run No.31302

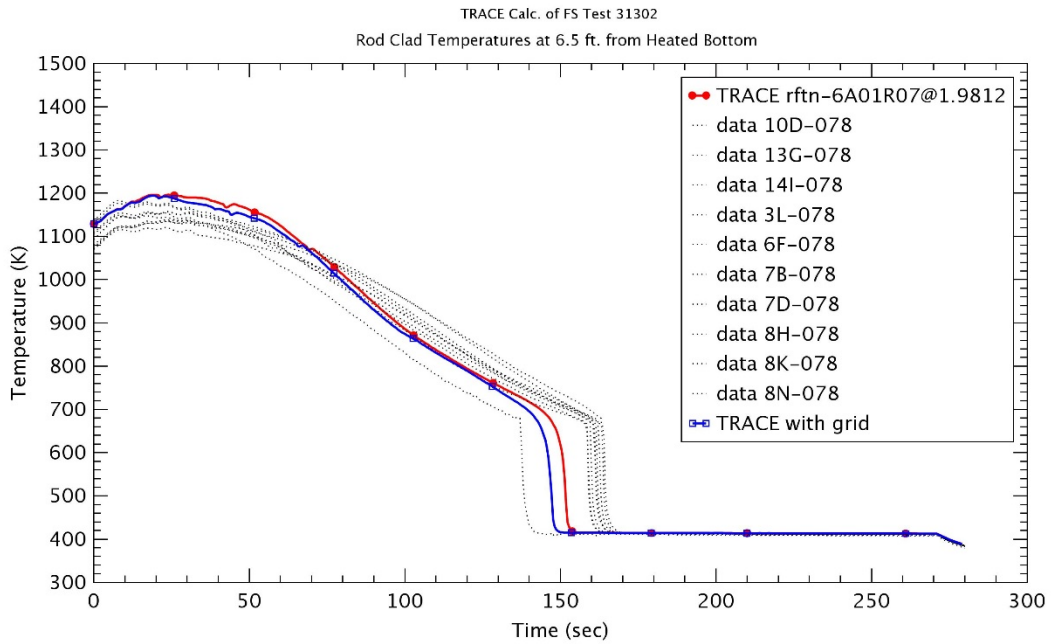


Figure 3-62 Heater Rod Temperature at 1.98 m – Run No.31302

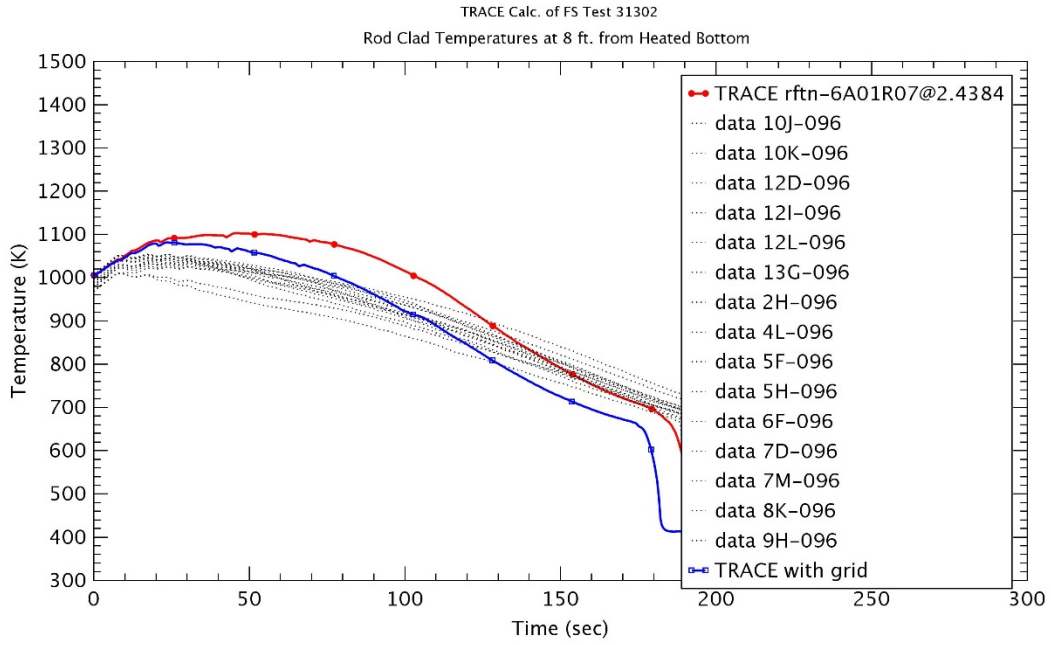


Figure 3-63 Heater Rod Temperature at 2.4 m – Run No.31302

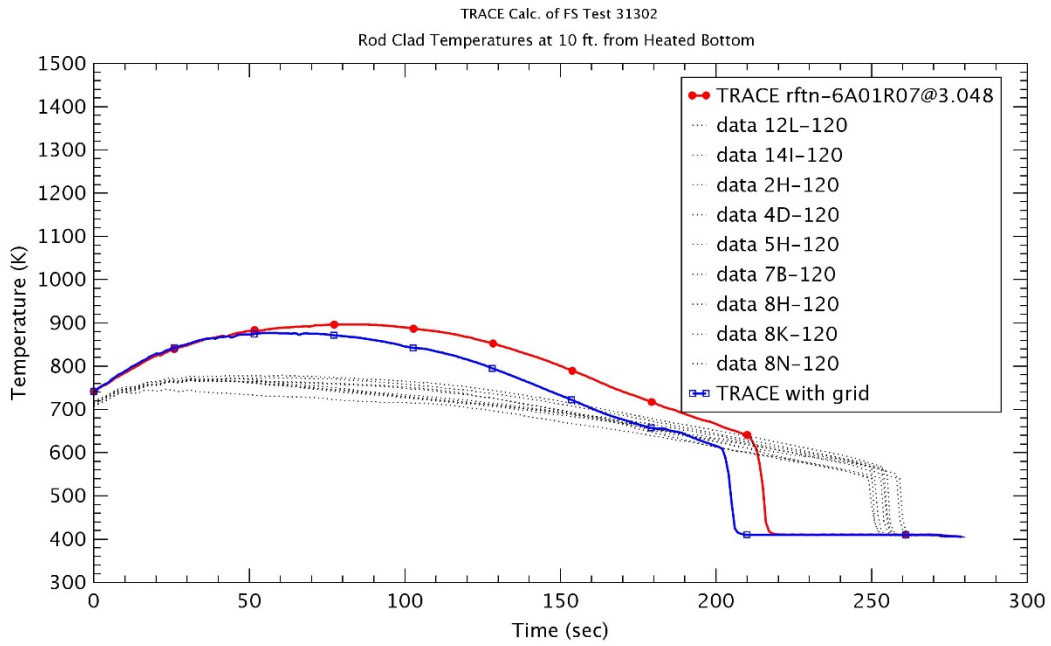


Figure 3-64 Heater Rod Temperature at 3.0 m – Run No.31302

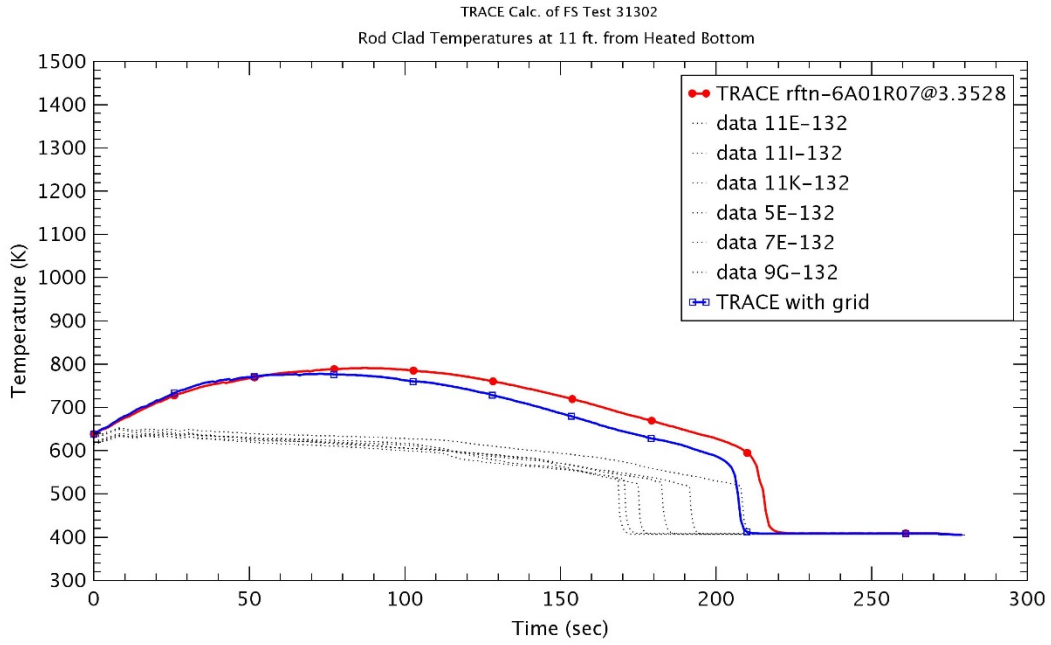


Figure 3-65 Heater Rod Temperature at 3.3 m – Run No.31302

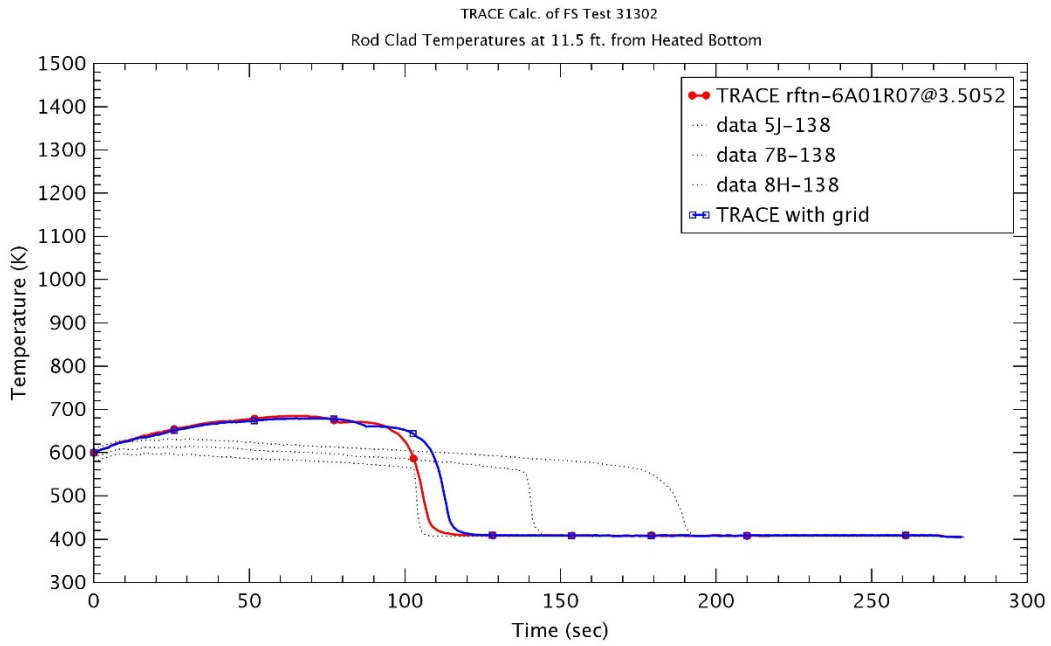


Figure 3-66 Heater Rod Temperature at 3.5 m – Run No.31302

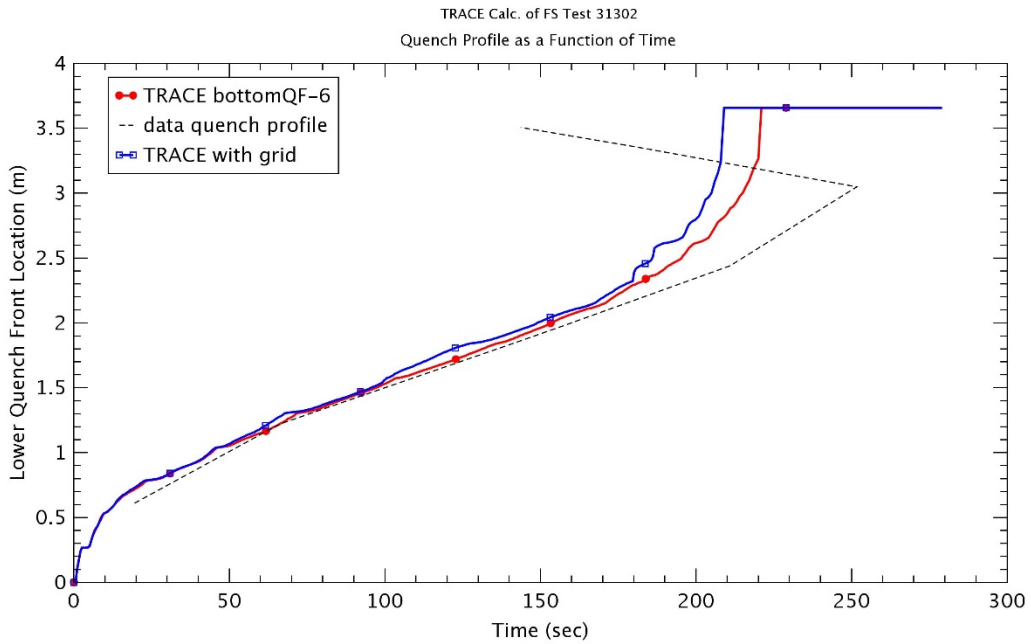


Figure 3-67 Quench Front Profile – Run No.31302

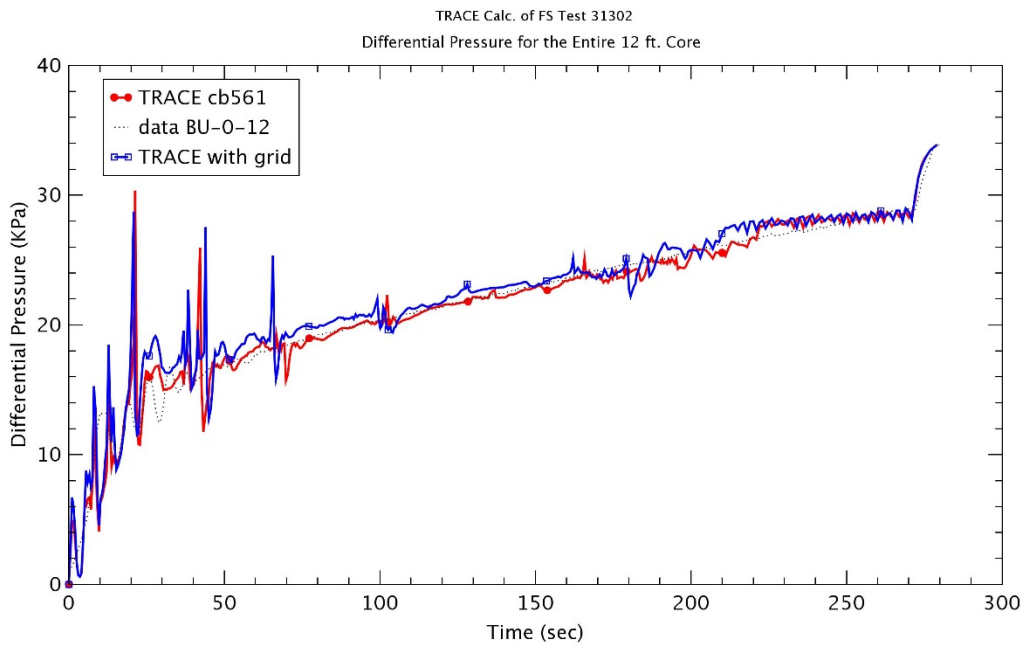


Figure 3-68 Differential Pressure for Entire 12 ft – Run No.31302

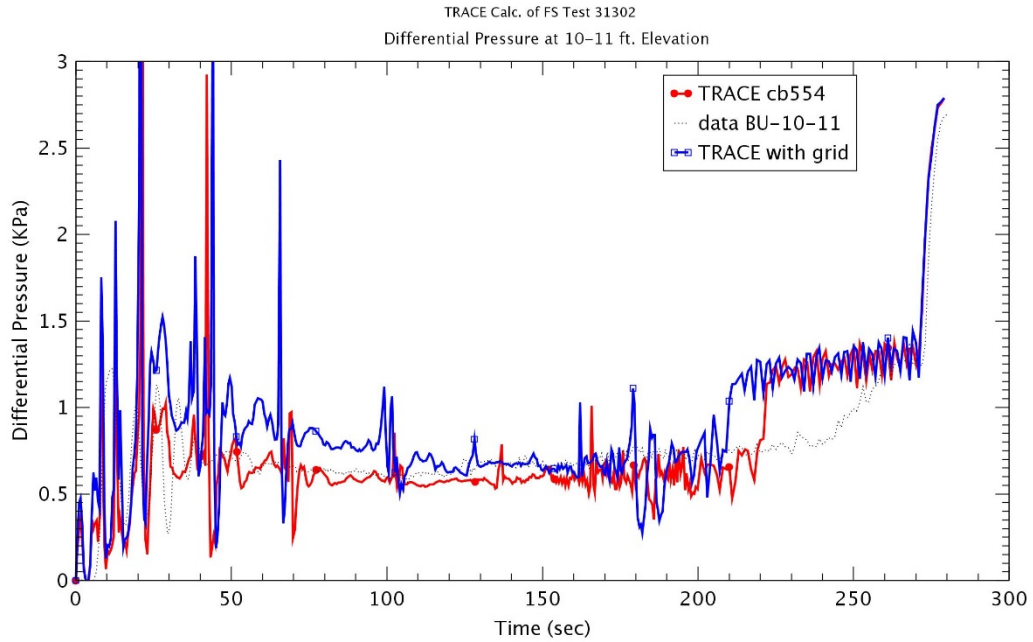


Figure 3-69 Differential Pressure at 10~11 ft Elevation – Run No.31302

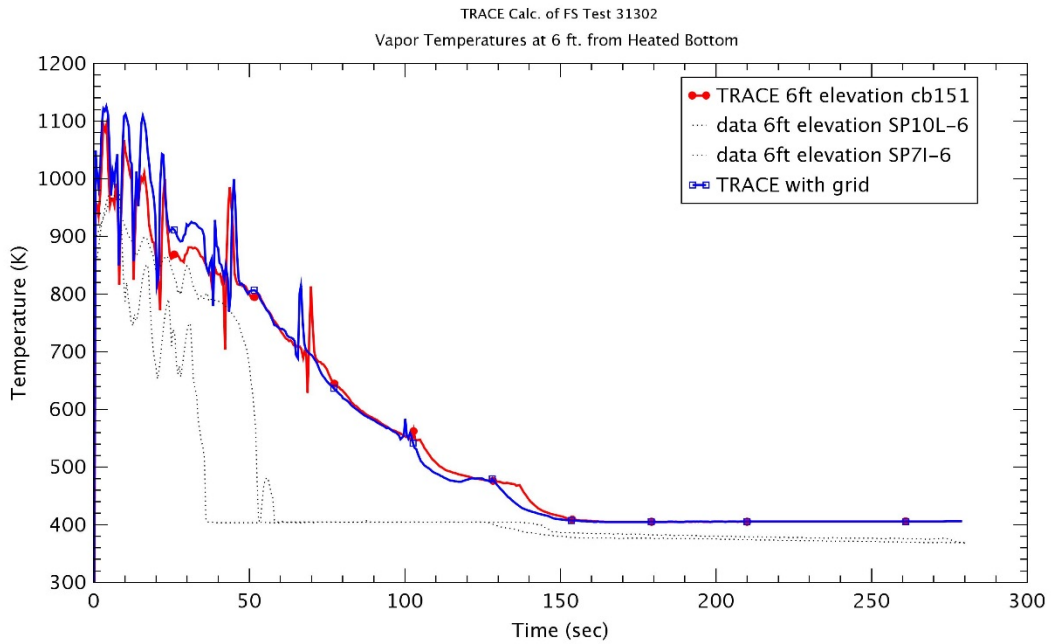


Figure 3-70 Vapor Temperature at 1.8 m – Run No.31302

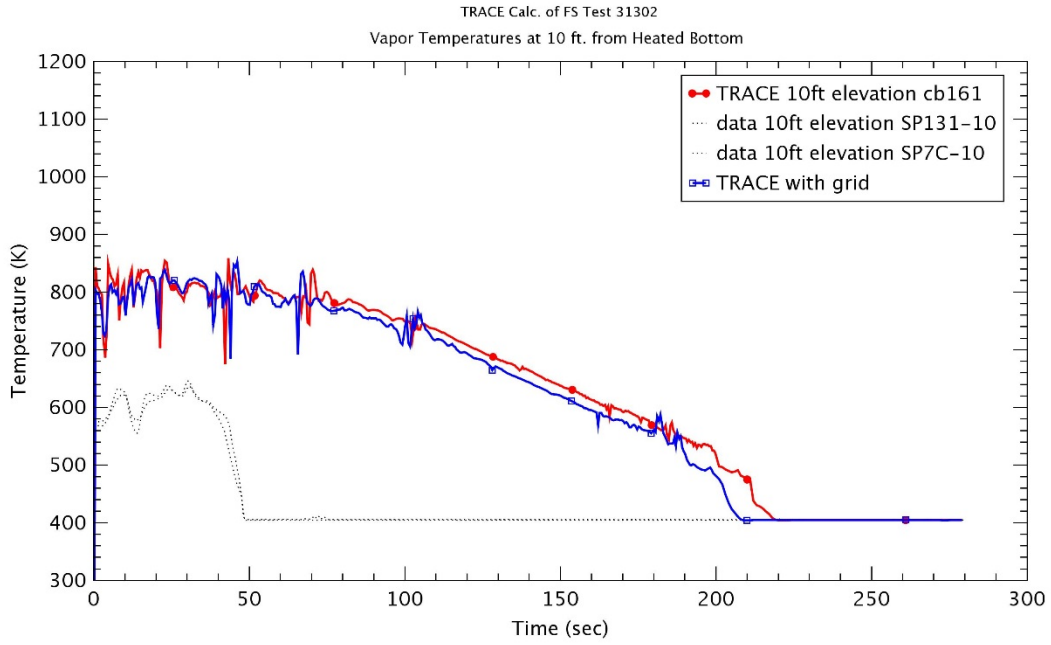


Figure 3-71 Vapor Temperature at 3.0 m – Run No.31302

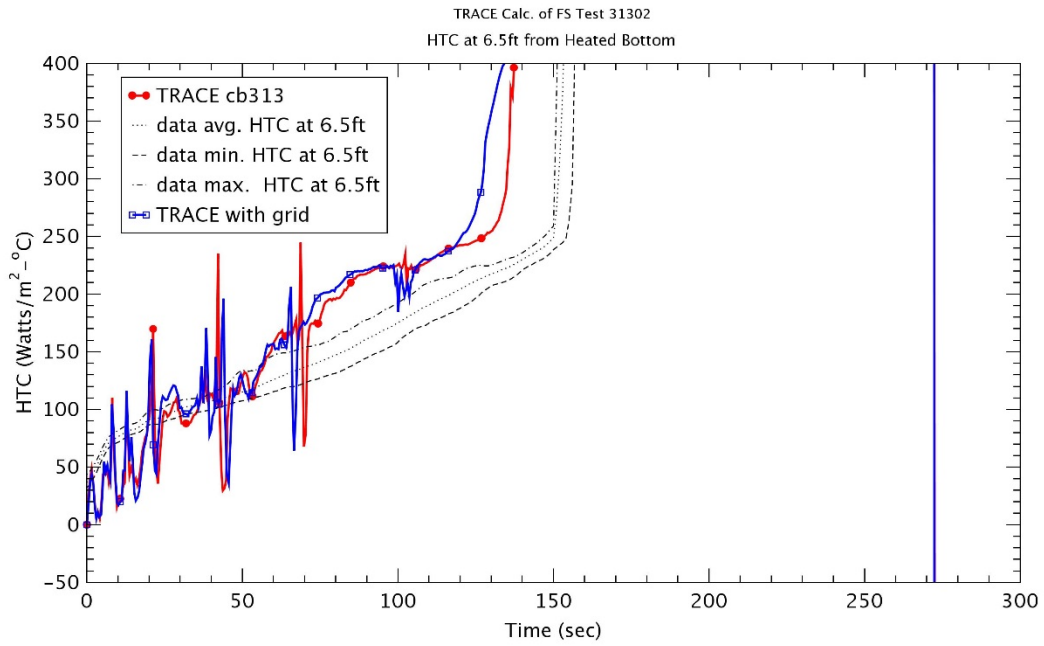


Figure 3-72 Heat Transfer Coefficient at 1.98 m – Run No.31302

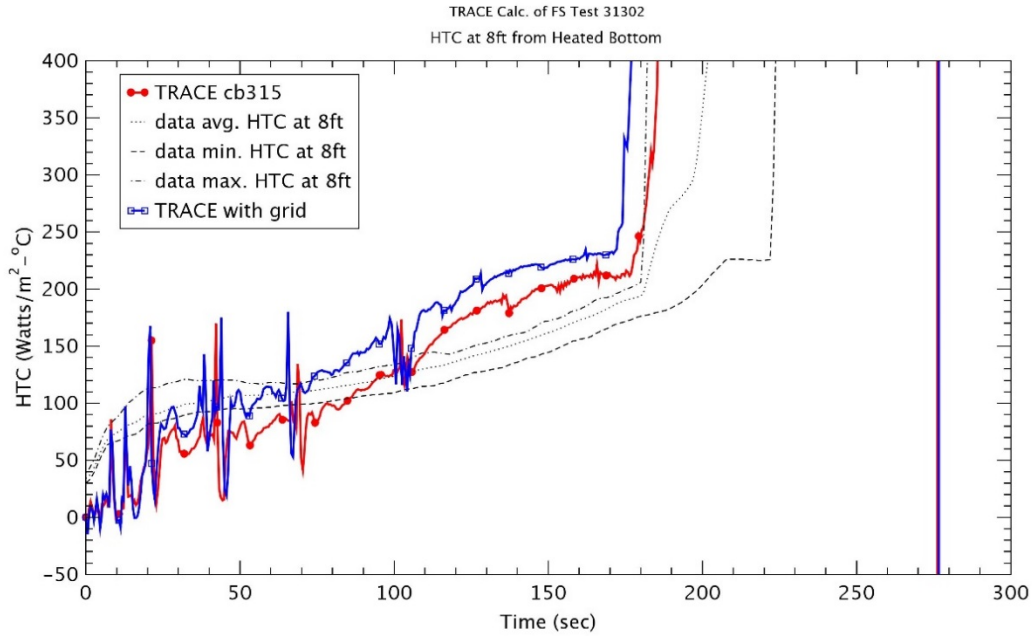


Figure 3-73 Heat Transfer Coefficient at 2.4 m – Run No.31302

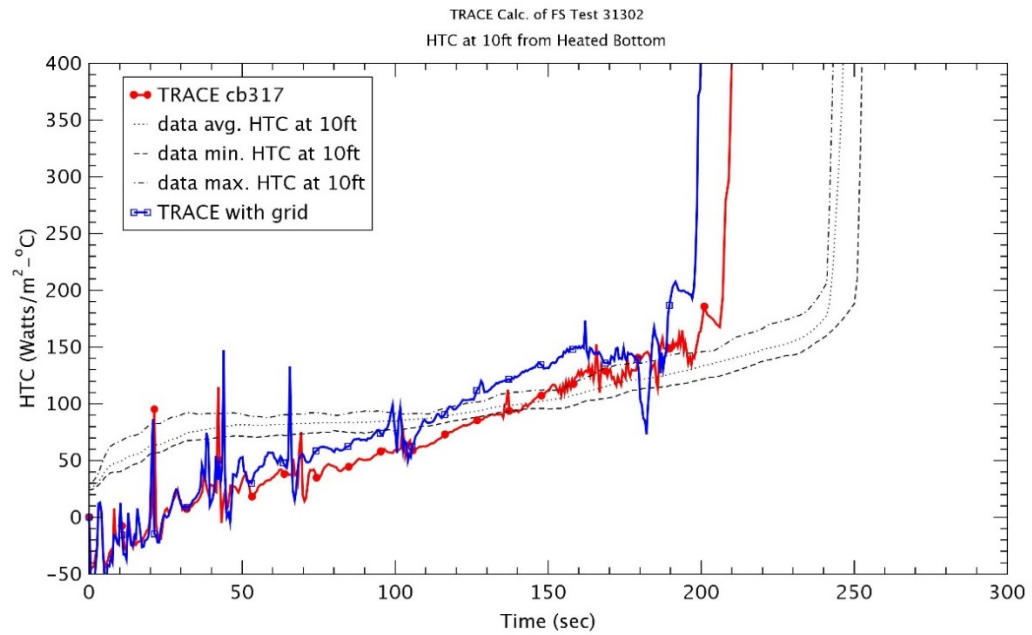


Figure 3-74 Heat Transfer Coefficient at 3.0 m – Run No.31302

3.2.1.4 Run No. 31701

Run No. 31701 was a test with a flooding rate of 15.5 cm/sec at 0.28 MPa and 77 oC inlet subcooling temperature as shown in Table 3-1. This was the same conditions as Run No. 31805, except for increasing of the flooding rate. Compared to the previous 4 tests, this had the largest reflooding rate.

As described before, the actual input conditions changed largely with time and showed the big oscillations. Therefore, the inlet flowrate and temperature were considered as time-dependent variables as shown in Figures 3.75 ~ 3.76. Most initial conditions in the TRACE assessment manual [6] were applied in this study.

Figure 3-77 through Figure 3-84 represented the rod temperatures at various elevations. These figures also showed well the reflood processes such as the heat up, turnover of rod temperature and a final quenching. In the calculation without the spacer grid model, the peak temperatures were under predicted with the experimental data at low elevations ($z \leq 1.2$ m) and were over predicted at higher elevations ($z \geq 1.98$ m). Usually, for high flooding rates above 15 cm/sec (6 in/sec), the dominant flow regime would be an inverted annular regime in bundles and then the heat transfer was very high and the turn-over of cladding temperature occurred immediately. As shown in Figure 3-85, the earlier quenching from the middle elevation ($z \sim 1.0$ m) was observed in the experimental data as compared to TRACE results. This might come from the under predictions for the lumps of liquid from the lower elevations and the de-entrained liquid from the upper parts. It would result in the over prediction of rod temperature at higher elevations. Those predictions were also reflected as the relatively high vapor temperature in Figure 3-88 and Figure 3-89. The maximum peak clad temperature was shown at elevation $z = 1.98$ m (6.5 ft) and had the lowest value due to higher reflood rate as compared to above 4 tests. The quenching times were over-estimated at most elevations due to the under prediction for the top-down quenching in test. The top-down quenching started to be observed from Run No. 31203 and became more dominant as the reflood rate is higher. When the spacer model was applied, the rod temperatures were reduced and the quenching time was expedited at most elevations. However, because of the highest reflood rate, the differences of rod temperature and quenching time were the smallest as compared to 4 tests above. During a heating up, the effect of the spacer grid model was not shown at all elevations. The turn-over times of rod temperature were almost same as those without the spacer grid at all elevations due to the high reflood rate. The quenching time was slightly decreased because of the relatively faster rise of liquid level. In the case with the spacer grid model, the decreasing temperature was ~ 2.5 K and the reduction of quenching time was ~ 2 sec due to the spacer grid model at elevation $z = 1.98$ with the maximum peak cladding temperature.

The quench front profile was shown in Figure 3-85. The quench front without the spacer grid model was predicted well up to elevation $z \sim 1.0$ m. At elevations $z \geq 1.0$ m, TRACE would under-predict the liquid chunks from lower part and/or the de-entrained liquid from upper part of the active core and this might result in the significantly delayed quench front in higher reflood rates. When the spacer grid model was used, the increase of quench front was almost identical up to elevation $z = 2.0$ m and the earlier rise of that was predicted at elevations $z \geq 2.0$ m.

The differential pressure (DP) for entire 12 ft was shown in Figure 3-86 and the differential pressure between 11 ft and 12 ft was illustrated in Figure 3-87. The rise of DP for entire test section corresponded to the collapsed liquid level and the DP increased gradually with the injected water. The DP for entire 12 ft agreed fairly with the data until ~ 100 sec, but slightly under predicted after ~ 100 sec. The DP between 11 ft and 12 ft under predicted for all times of test. It would result from the under prediction of the liquid chunks from upper parts above the active core. If the spacer grid model was applied, the faster increase of DP for entire 12 feet was predicted and the DP between 11 ft and 12 ft reflected well the larger pressure drop of the spacer grid model.

Figures 3.88 and 3.89 represented the vapor temperatures at two elevations 1.8 m and 3.0 m, respectively. As explained in the rod temperature, the vapor temperatures at two elevations was over predicted during all times of test. As shown in other tests, the spacer grid model resulted in the higher vapor temperature during the heat up and the faster quenching at high elevation, but the effect of the spacer grid model would be less, as the reflood rate is higher.

The heat transfer coefficients (HTCs) at several elevations is shown in Figure 3-90 through Figure 3-92. During the heating up, the reduction or stagnant for HTC was not observed in the data due to the high reflood rate and then the HTC was under predicted for this region. According to the over prediction of rod temperature at higher elevations ($z \geq 1.98$ m), the under prediction of HTC was also shown continuously during the reflood phase. TRACE predicted a sharp increase of HTC at the delayed time as compared to experimental data due to the late rod quenching. In the case with the spacer grid model, the relatively higher HTC during the reflood phase and the earlier sharp increase of HTC were predicted.

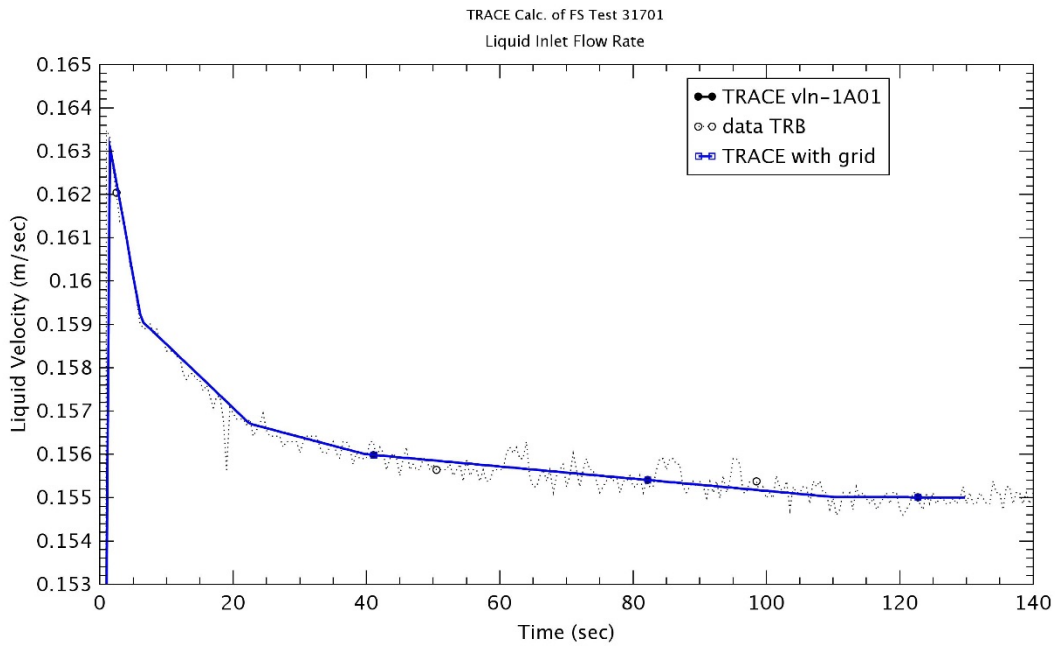


Figure 3-75 Liquid Inlet Flowrate – Run No.31701

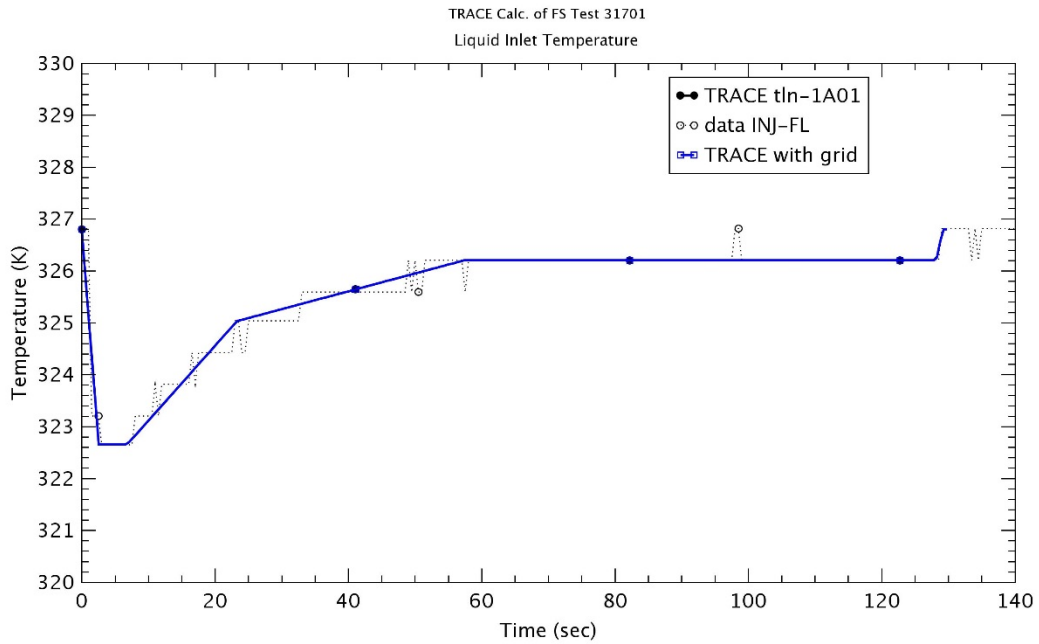


Figure 3-76 Liquid Inlet Temperature – Run No.31701

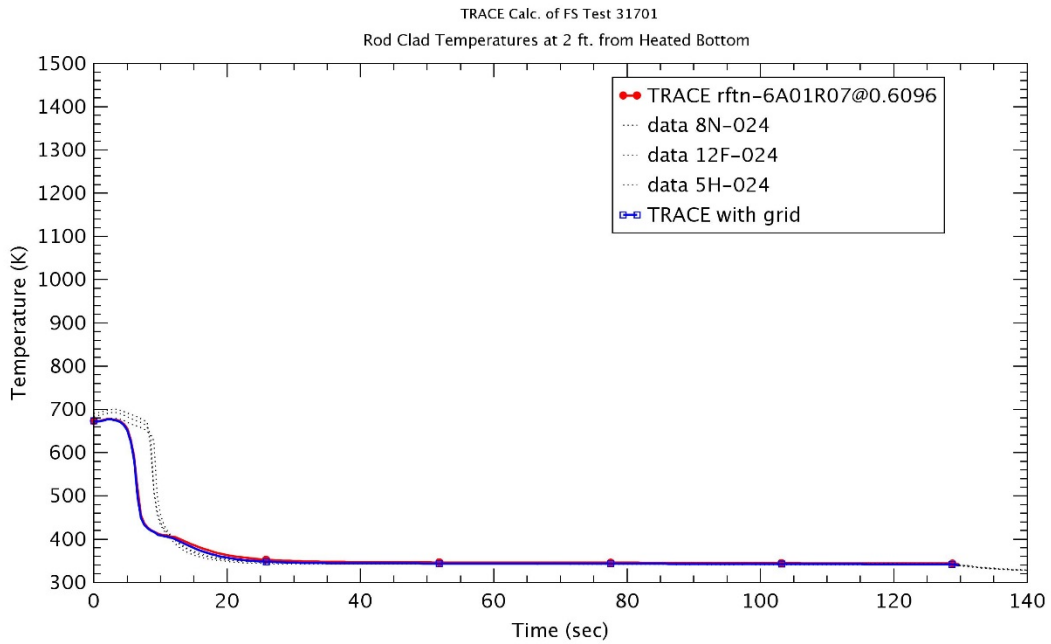


Figure 3-77 Heater Rod Temperature at 0.6 m – Run No.31701

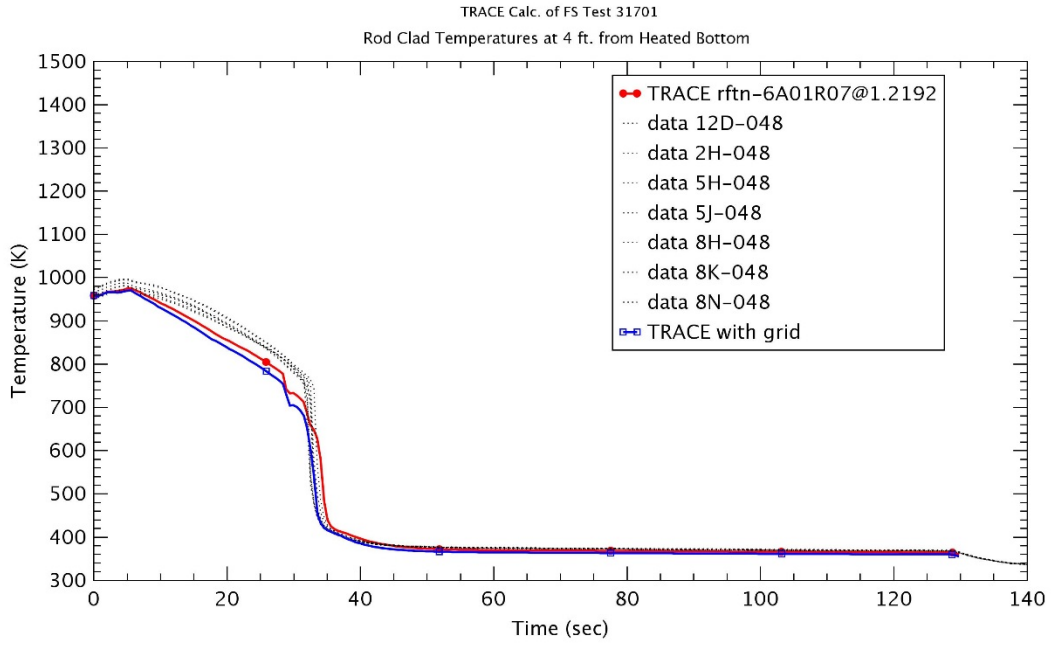


Figure 3-78 Heater Rod Temperature at 1.2 m – Run No.31701

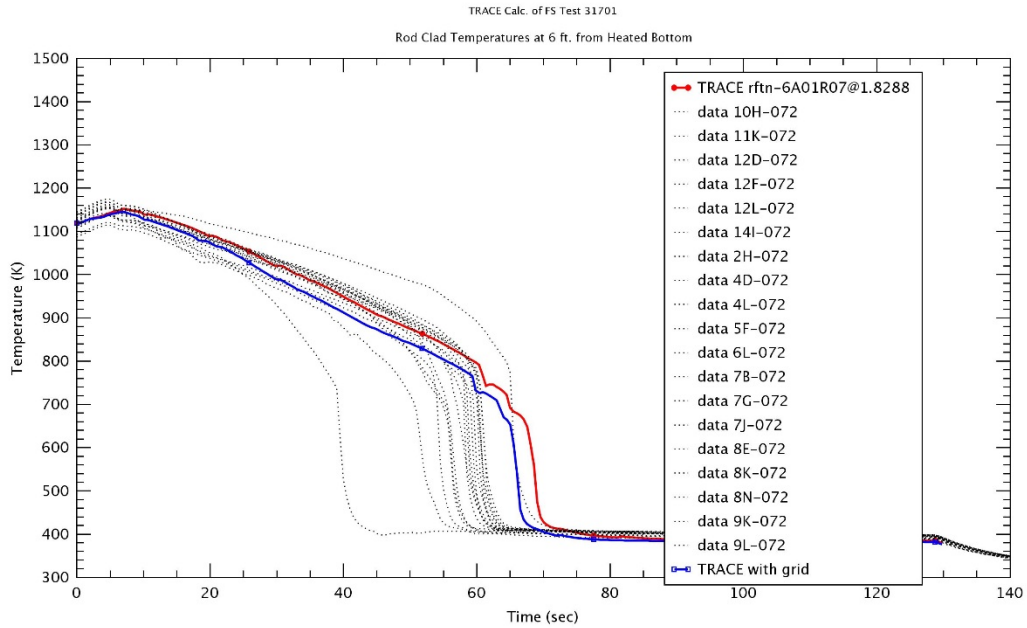


Figure 3-79 Heater Rod Temperature at 1.8 m – Run No.31701

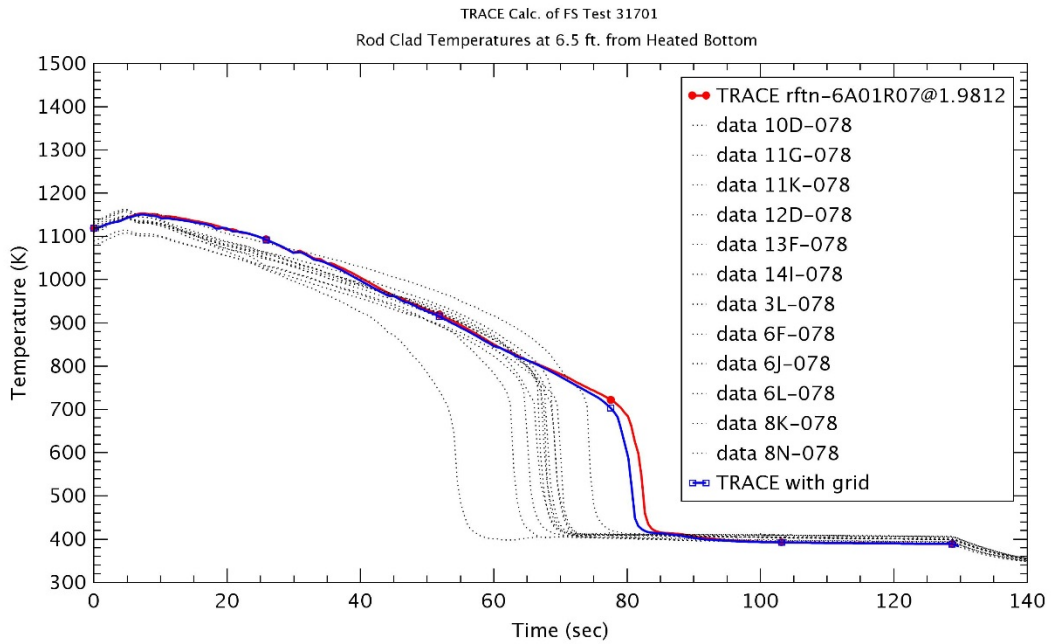


Figure 3-80 Heater Rod Temperature at 1.98 m – Run No.31701

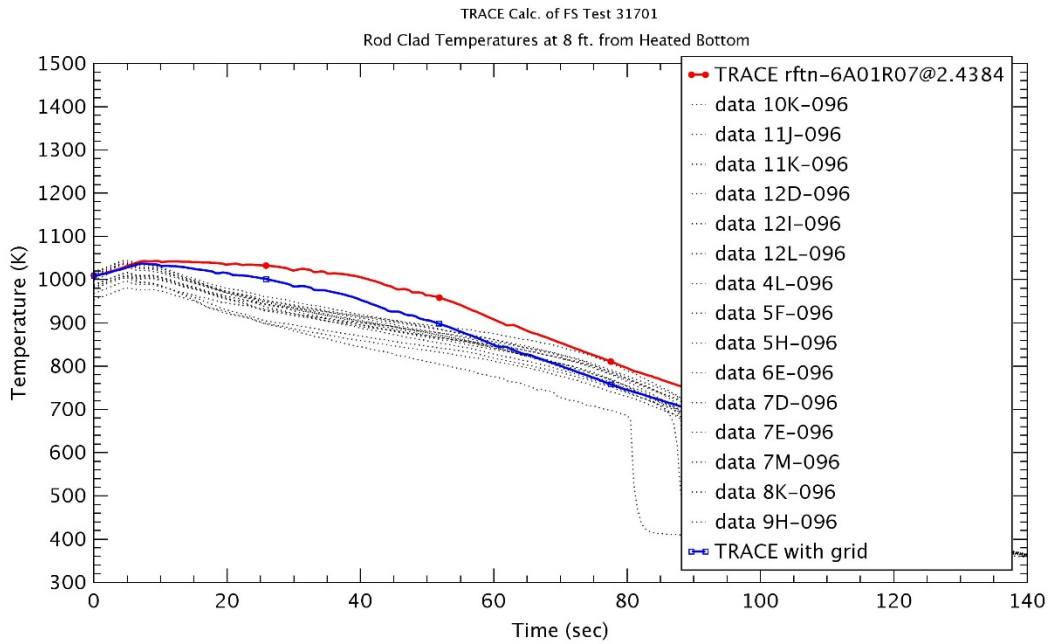


Figure 3-81 Heater Rod Temperature at 2.4 m – Run No.31701

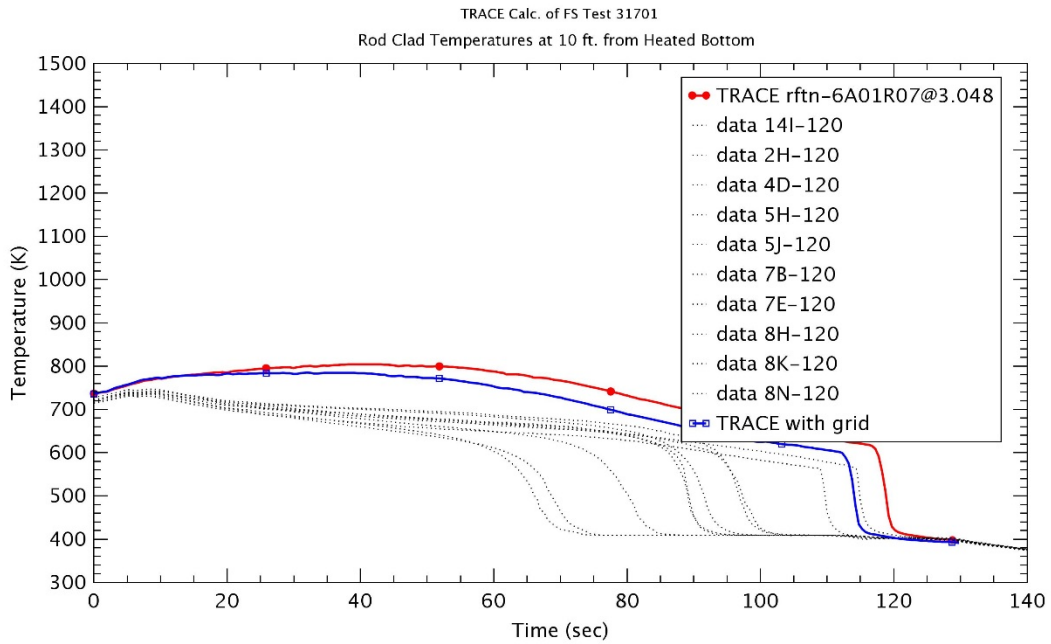


Figure 3-82 Heater Rod Temperature at 3.0 m – Run No.31701

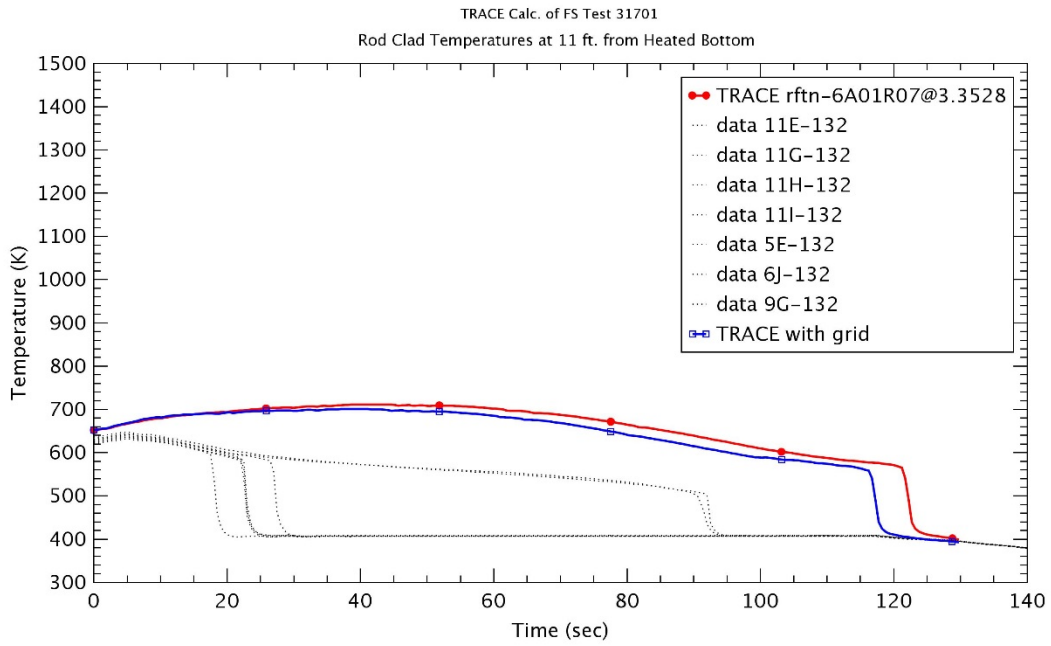


Figure 3-83 Heater Rod Temperature at 3.3 m – Run No.31701

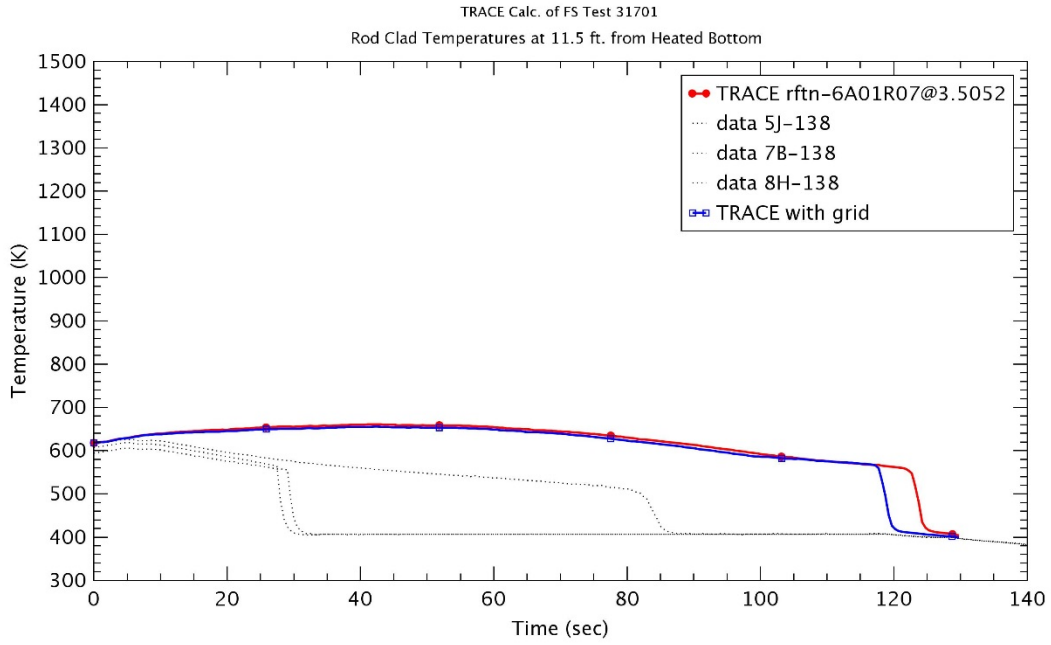


Figure 3-84 Heater Rod Temperature at 3.5 m – Run No.31701

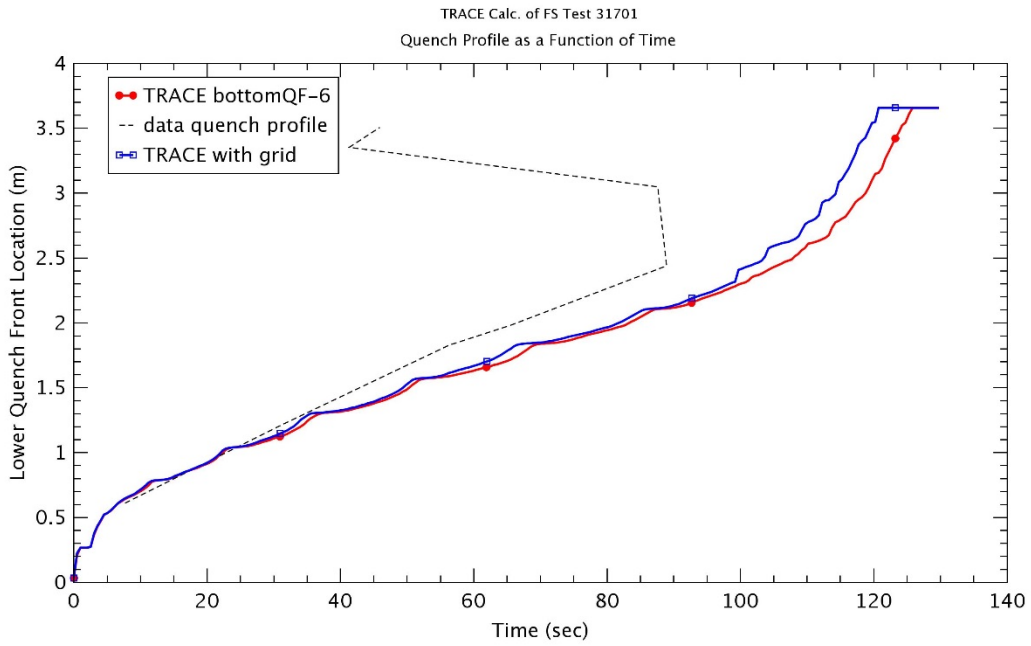


Figure 3-85 Quench Front Profile – Run No.31701

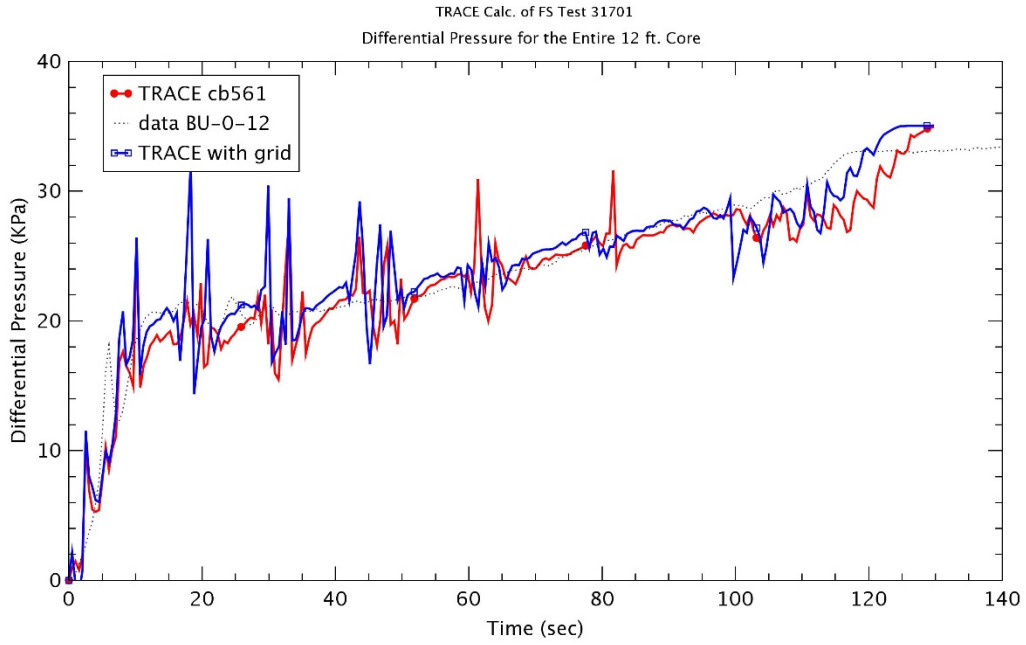


Figure 3-86 Differential Pressure for Entire 12 ft – Run No.31701

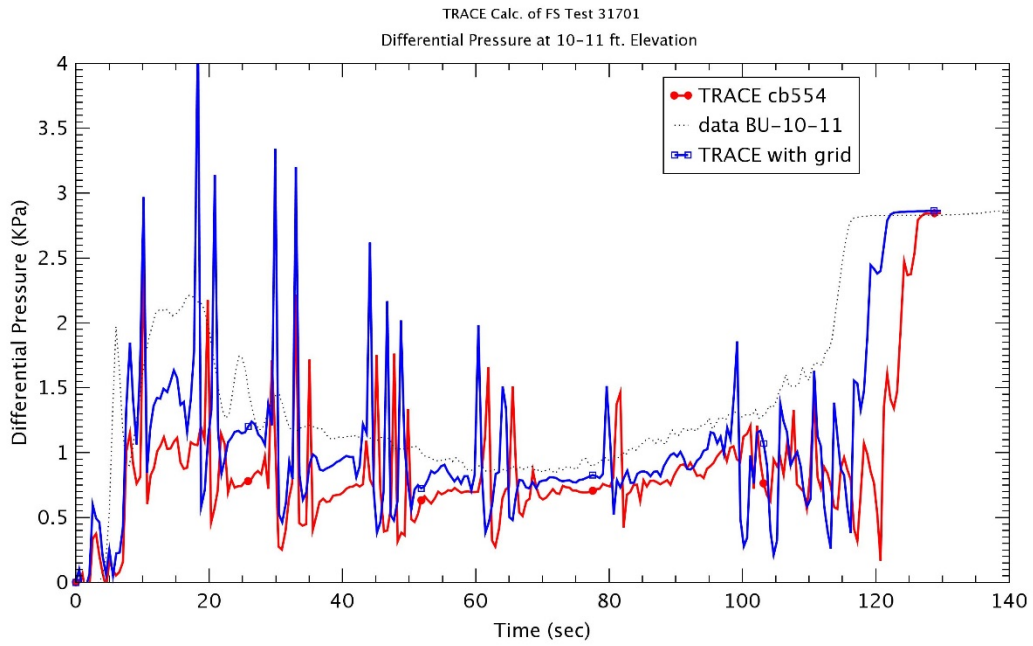


Figure 3-87 Differential Pressure at 10~11 ft Elevation – Run No.31701

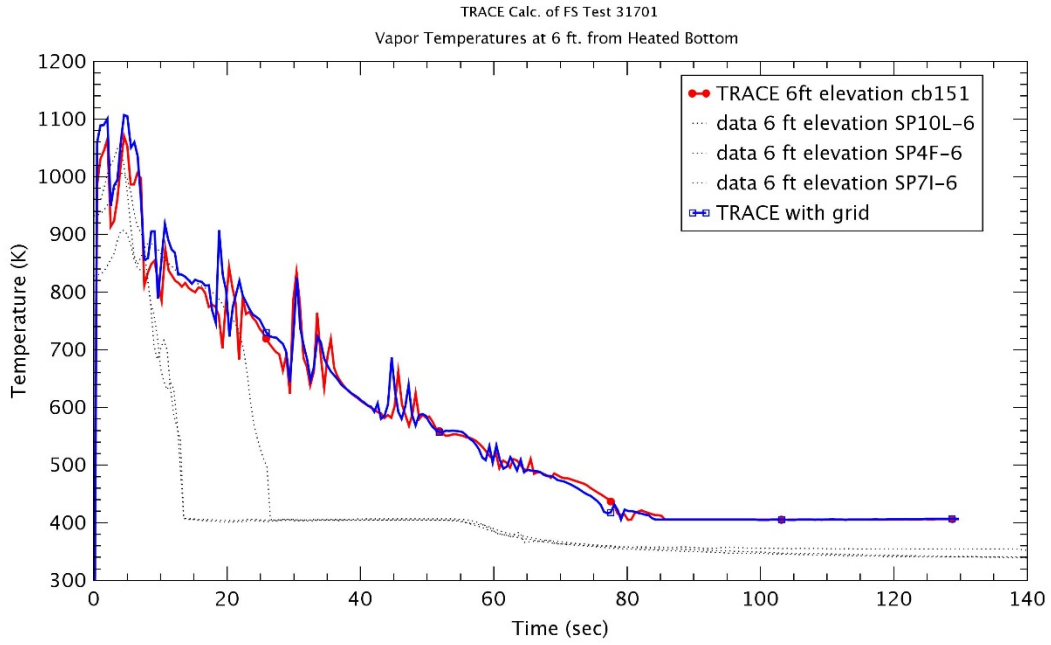


Figure 3-88 Vapor Temperature at 1.8 m – Run No.31701

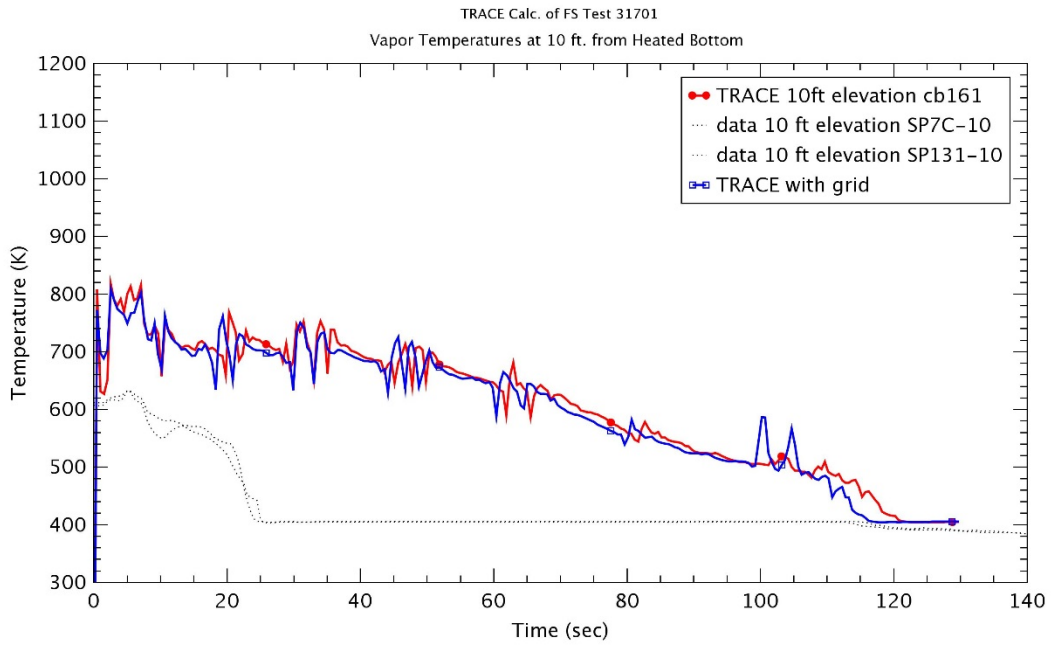


Figure 3-89 Vapor Temperature at 3.0 m – Run No.31701

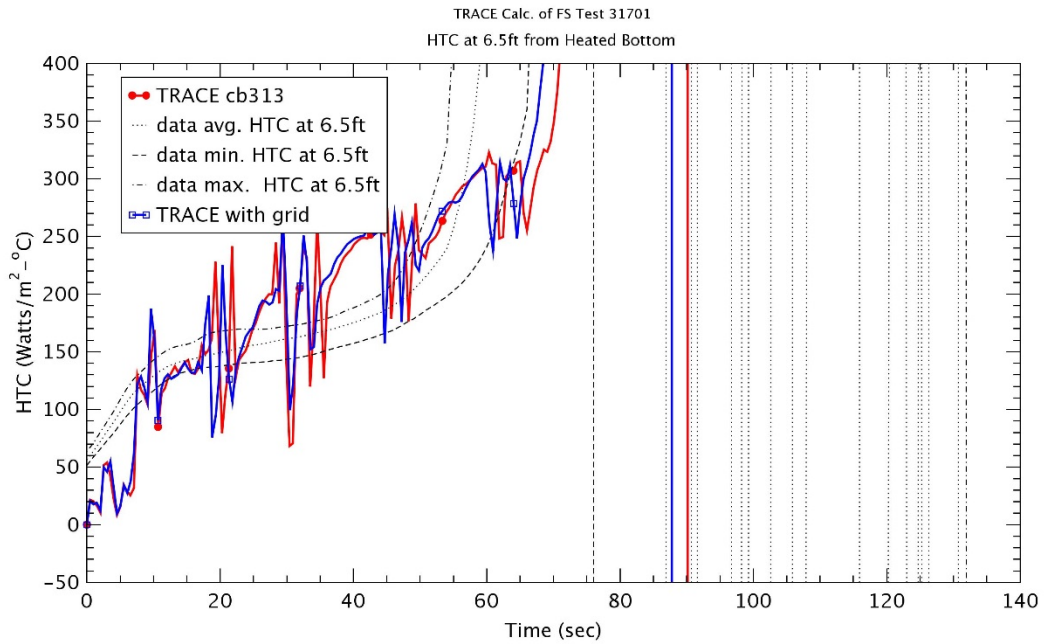


Figure 3-90 Heat Transfer Coefficient at 1.98 m – Run No.31701

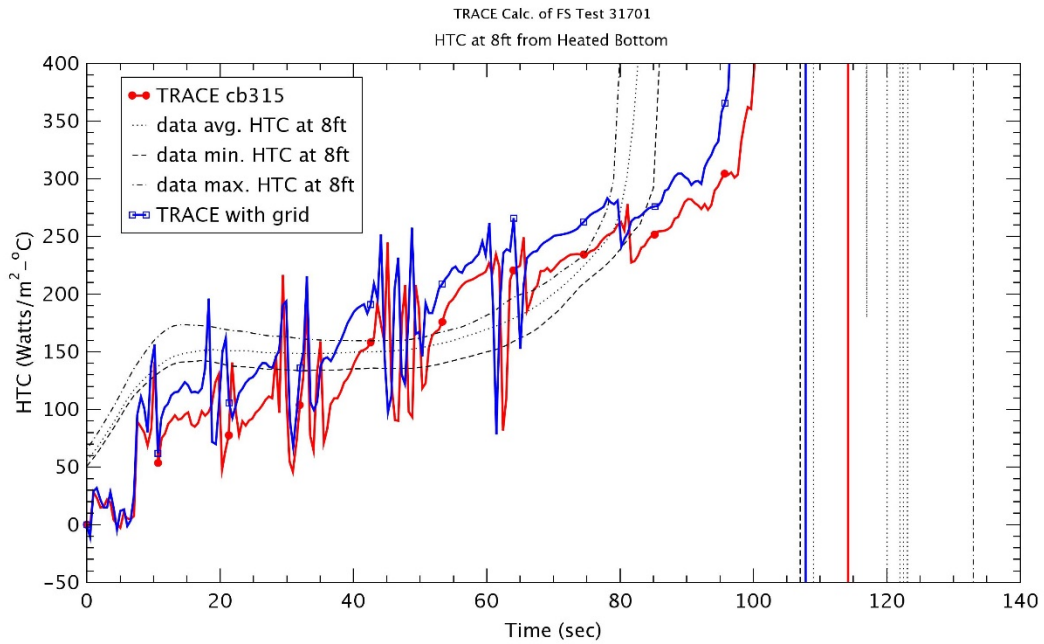


Figure 3-91 Heat Transfer Coefficient at 2.4 m – Run No.31701

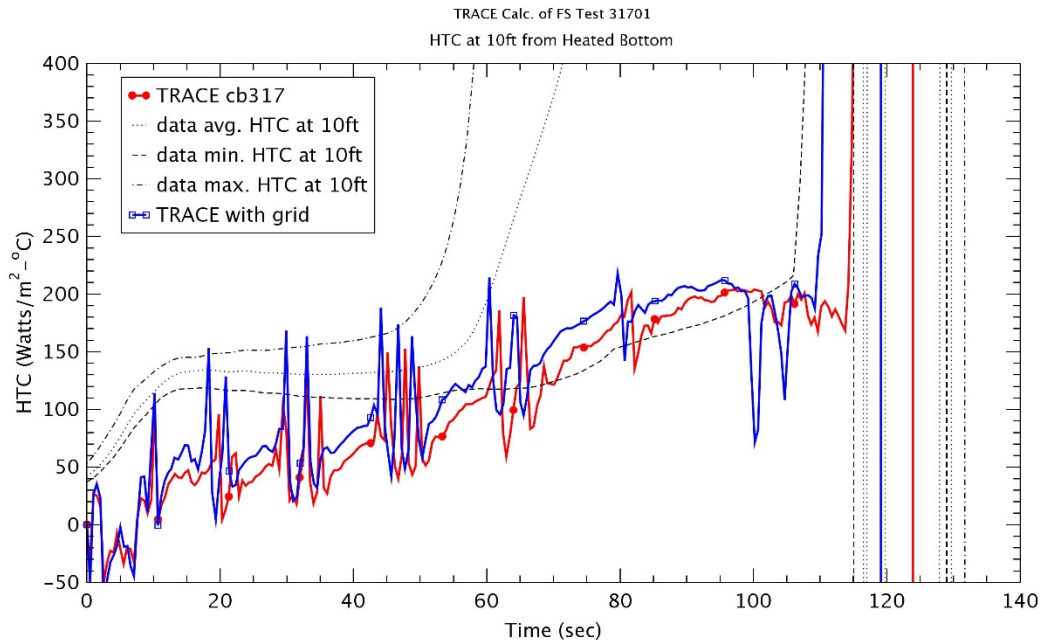


Figure 3-92 Heat Transfer Coefficient at 3.0 m – Run No.31701

3.2.1.5 Run No. 31108

Run No. 31108 was a test with a flooding rate of 7.90 cm/sec at 0.13 MPa and 74 oC inlet subcooling temperature as shown in Table 3-1. This was similar to Run No. 31302 except for decreasing the pressure for the upper plenum. However, as described previously, the actual input conditions varied largely with time and showed the big oscillations. So, the inlet flowrate and temperature were considered as time-dependent variables as shown in Figure 3-93 and 3.94, respectively. Most initial conditions in the TRACE assessment manual [6] were applied in this study.

The rod temperatures at various elevations were plotted in Figures 3.95 ~ 3.102. These figures showed fairly the reflood processes including the initiating heating up, the turn-over of rod temperature and finally quenching. When the spacer grid model was not applied, the predicted peak temperatures were reasonably agreed with the data at elevation $z \leq 1.8$ m. The peak temperatures were over predicted with the data at elevations $z \geq 1.8$ m. This over prediction of rod temperature corresponded to the relatively high vapor temperature as shown in Figures 3.106 ~ 3.107. The maximum peak clad temperature was showed at elevation $z = 1.98$ m (6.5 ft). At elevations ($z \leq 1.98$ m), TRACE predicted fairly the quenching time, but the quenching times became shorten up to elevation $z = 3.0$ m. At elevation $z = 3.0$ m above, the quenching were predicted at the later time since the strong top-down quenching was observed in the experiment as shown in Figure 3-103. This test had the half of the upper plenum pressure of Run No. 31302 and the similar trends for the rod temperatures were shown with Run No. 31302. The rod temperatures at all elevations were slightly higher than those of Run No. 31302 since the saturation temperature would be relatively low due to the lower pressure, but the difference of the rod temperatures would be not significant because of the high reflood rate. When the spacer grid model was applied, the differences of the rod temperatures was not shown well at all elevations during the heat-up phase, but the earlier turn-around of rod temperature was predicted since the spacer grid would enhance the heat transfer. The peak temperatures with the spacer grid model had the lower values at all elevations. The maximum peak clad temperature at $z=1.98$ m was

decreased in case with the spacer grid model. At elevation $z=1.98$ with the maximum peak cladding temperature, the temperature reduction was ~ 16.3 K and the quenching time was decreased with ~ 8 sec due to the spacer grid model.

As shown in Figure 3-103, the quench front without the spacer grid model was predicted well with the data up to elevation $z = 1.8$ m. In this test, TRACE did not predict the top quenching at higher elevations ($z \geq 3.0$ m) which was from the liquid de-entrainment from the upper part above the active core. The transition of quench front for the top quench could be identified in the experiment at around $z = 3.0$ m. If the spacer grid model was applied, the quench front was increasing faster than that without the spacer grid model as the elevation was higher.

The differential pressure (DP) for entire 12 ft was plotted in Figure 3-104 and the differential pressure between 11 ft and 12 ft was shown in Figure 3-105. The growth of DP for entire test section was correspond to the collapsed water level. The DP for entire 12 ft was over predicted at all times of test despite of the top down quenching in test. TRACE predicted more water inventory in the test section. If the spacer grid model was applied, the DP for entire 12 ft was rising slightly earlier than that without the spacer grid model. As shown well in Figure 3-105, the DP between 11 ft and 12 ft was increasing due to the spacer grid.

The vapor temperatures at two elevations 1.8 m and 3.0 m were shown in Figures 3.106 and 3.107, respectively. As described in the rod temperature, the vapor temperatures at two elevations was over predicted during testing. The calculation with the spacer grid model had the slightly higher vapor temperature during the heat up and the quick quenching behaviors.

The heat transfer coefficients (HTCs) at several elevations is in Figure 3-108 through Figure 3-110. As shown in Figures, the HTC was under predicted during the rod heat up and increased faster than the experimental data. TRACE predicted a steep increase of HTC earlier than experimental data because of the earlier prediction of the rod quenching. When the spacer grid model was applied, the steep rise of HTC was expedited because of the earlier quenching of rod.

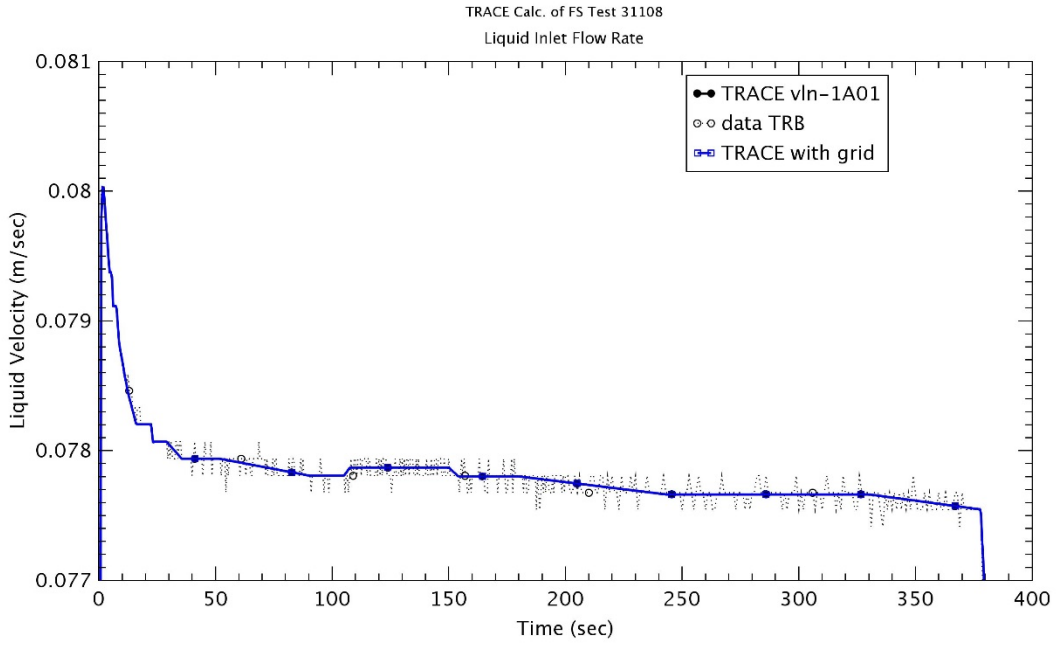


Figure 3-93 Liquid Inlet Flowrate – Run No.31108

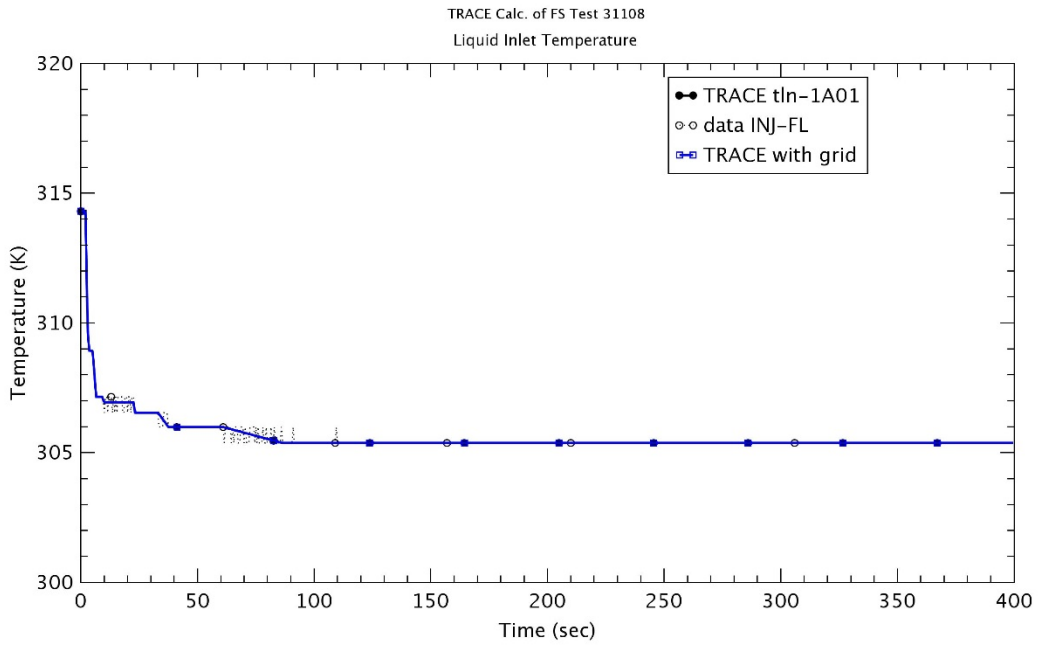


Figure 3-94 Liquid Inlet Temperature – Run No.31108

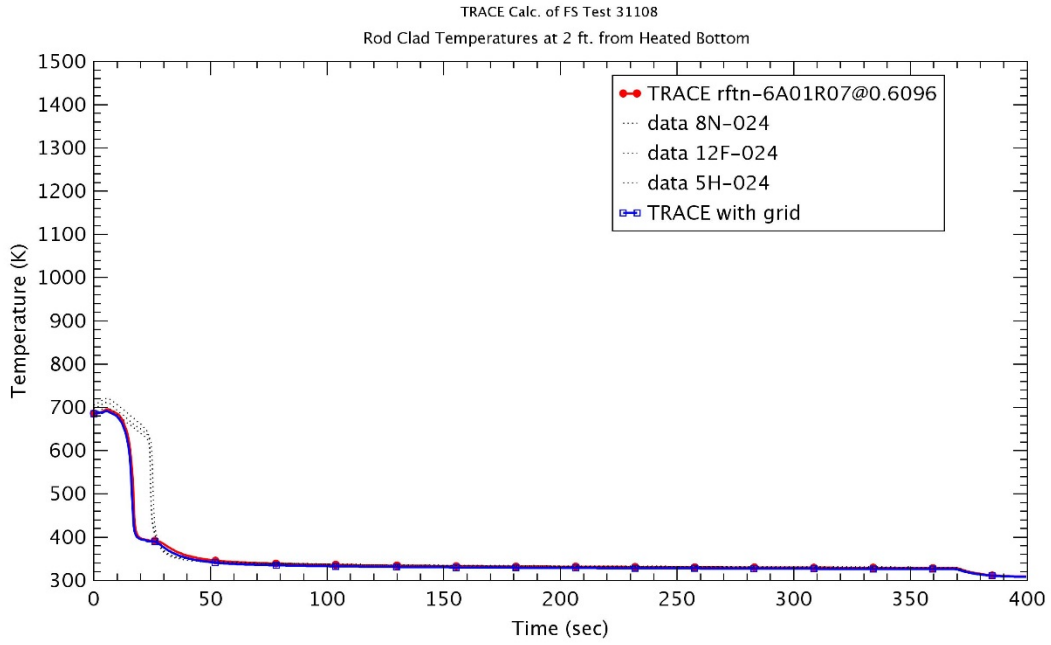


Figure 3-95 Heater Rod Temperature at 0.6 m – Run No.31108

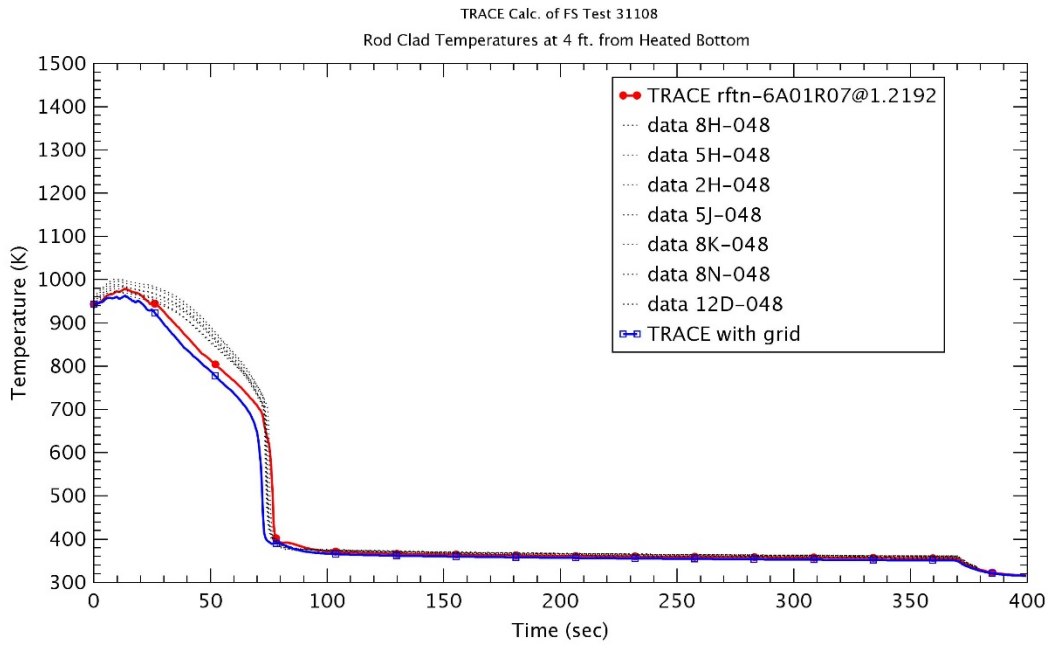


Figure 3-96 Heater Rod Temperature at 1.2 m – Run No.31108

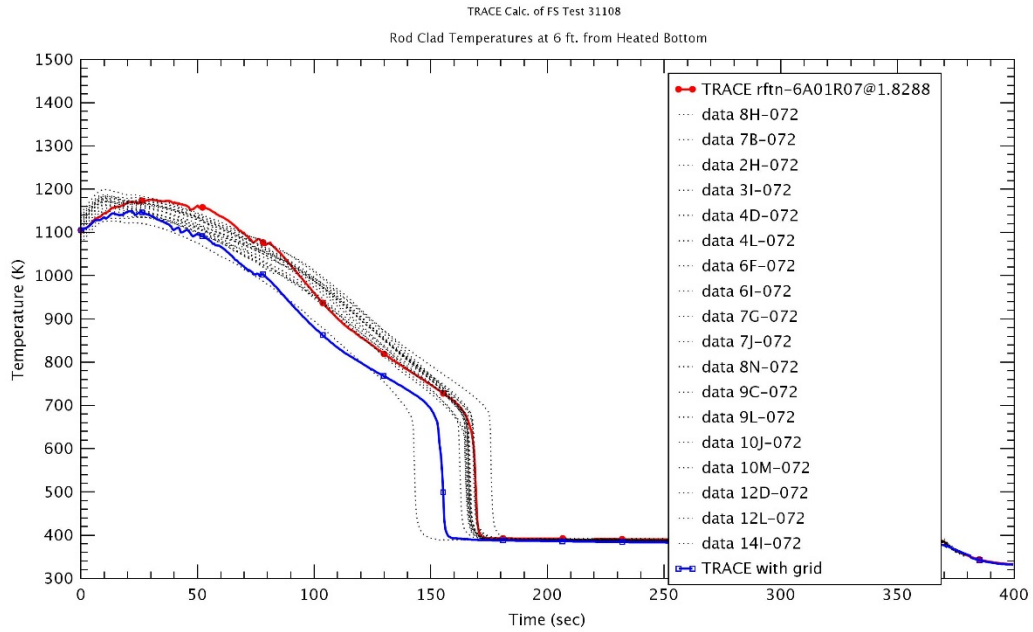


Figure 3-97 Heater Rod Temperature at 1.8 m – Run No.31108

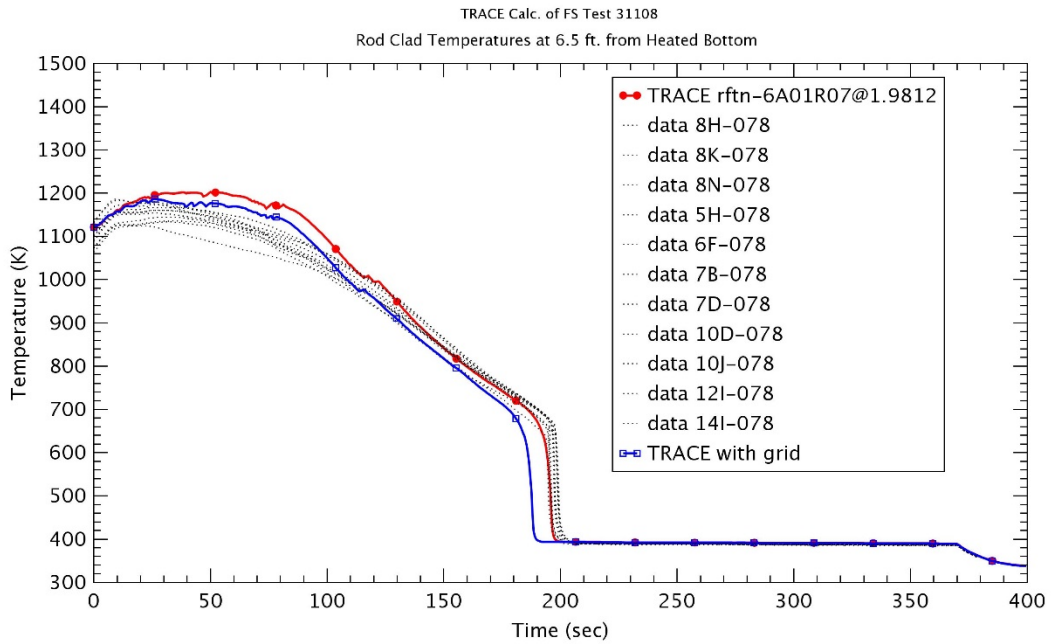


Figure 3-98 Heater Rod Temperature at 1.98 m – Run No.31108

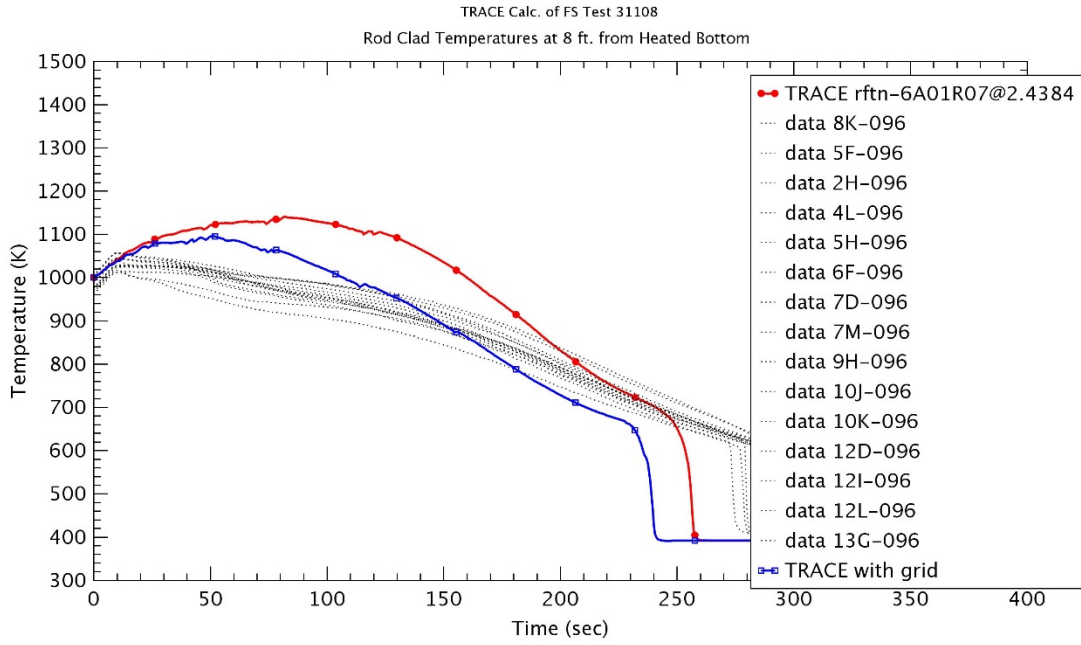


Figure 3-99 Heater Rod Temperature at 2.4 m – Run No.31108

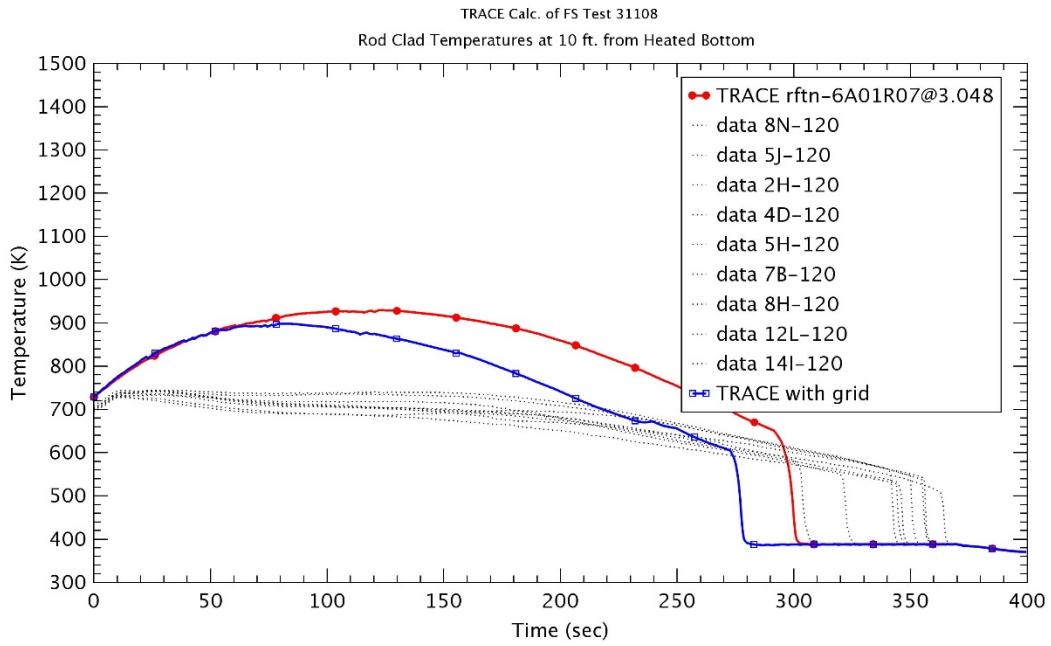


Figure 3-100 Heater Rod Temperature at 3.0 m – Run No.31108

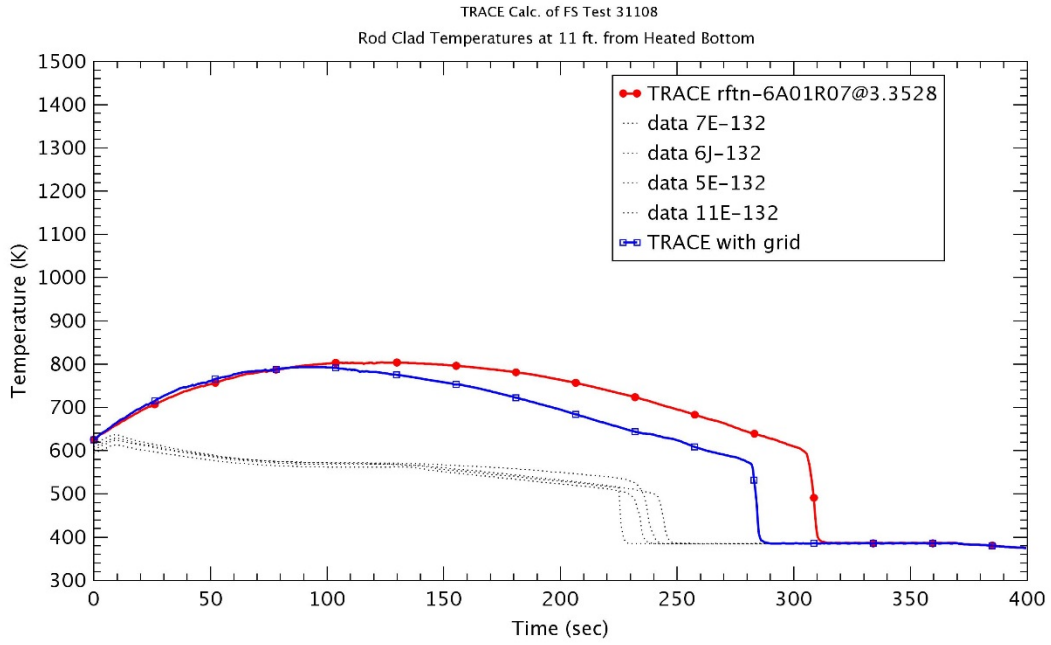


Figure 3-101 Heater Rod Temperature at 3.3 m – Run No.31108

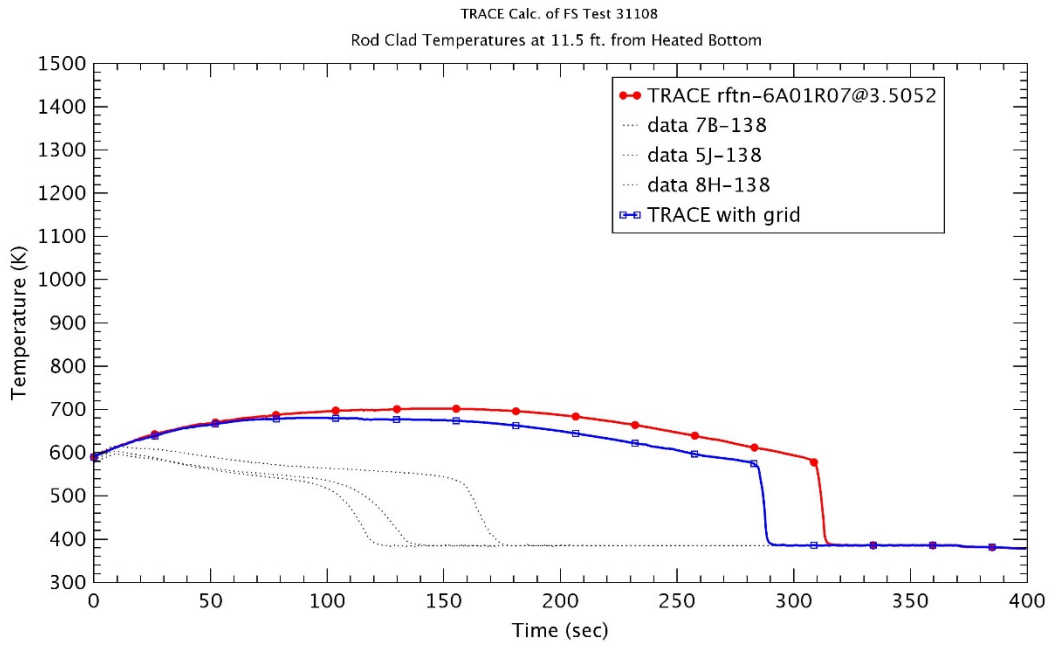


Figure 3-102 Heater Rod Temperature at 3.5 m – Run No.31108

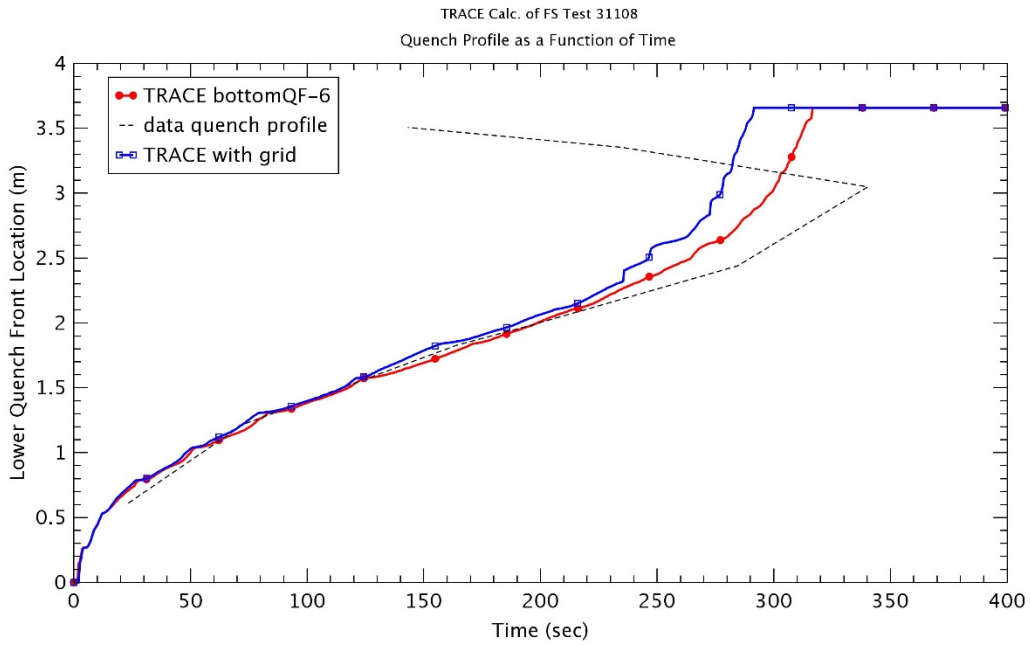


Figure 3-103 Quench Front Profile – Run No.31108

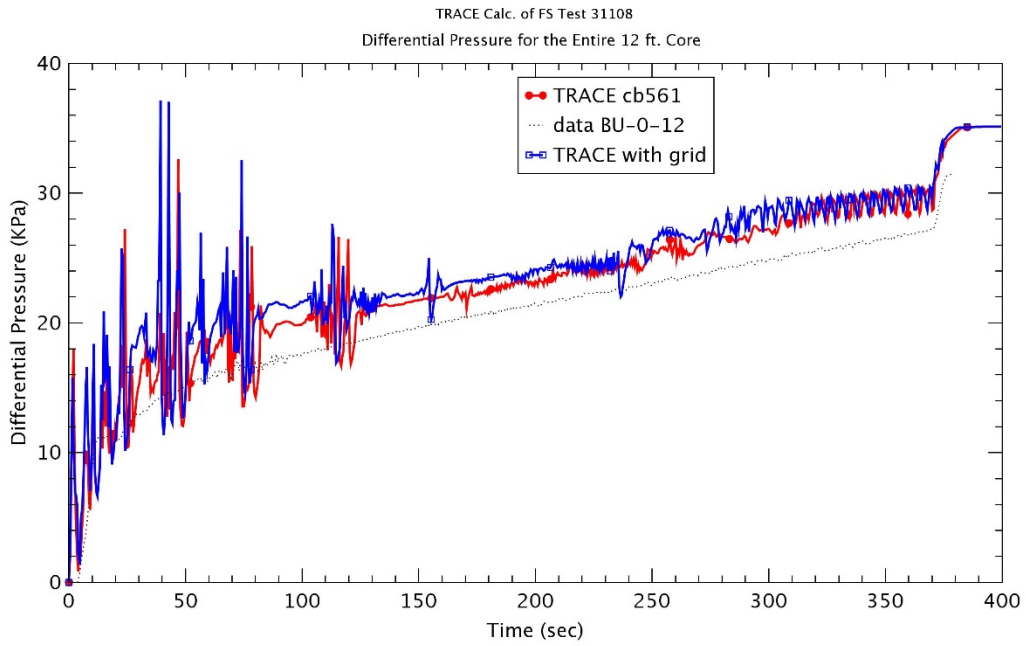


Figure 3-104 Differential Pressure for Entire 12 ft – Run No.31108

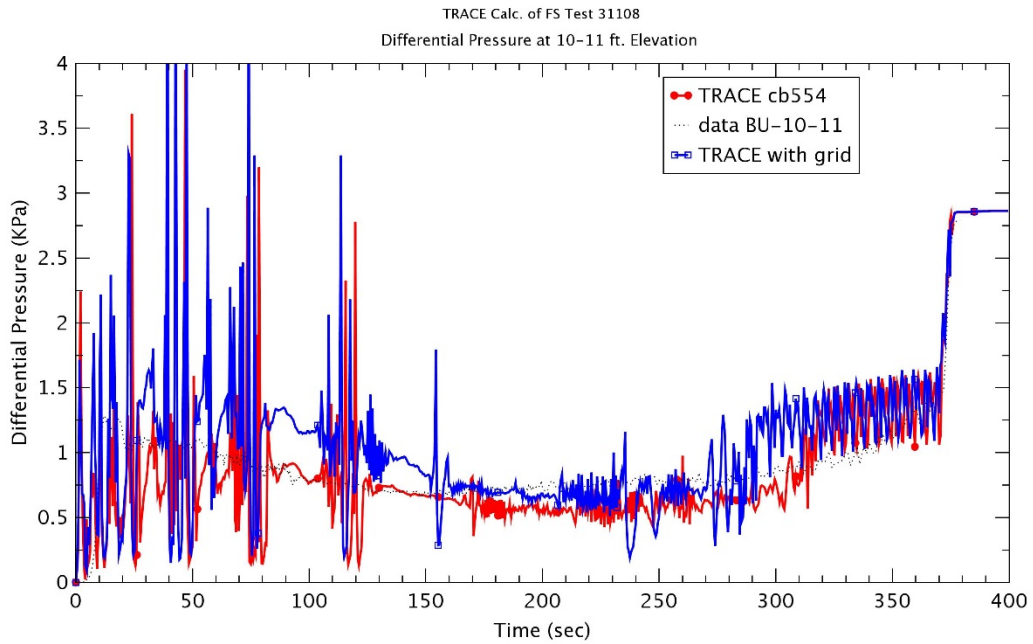


Figure 3-105 Differential Pressure at 10~11 ft Elevation – Run No.31108

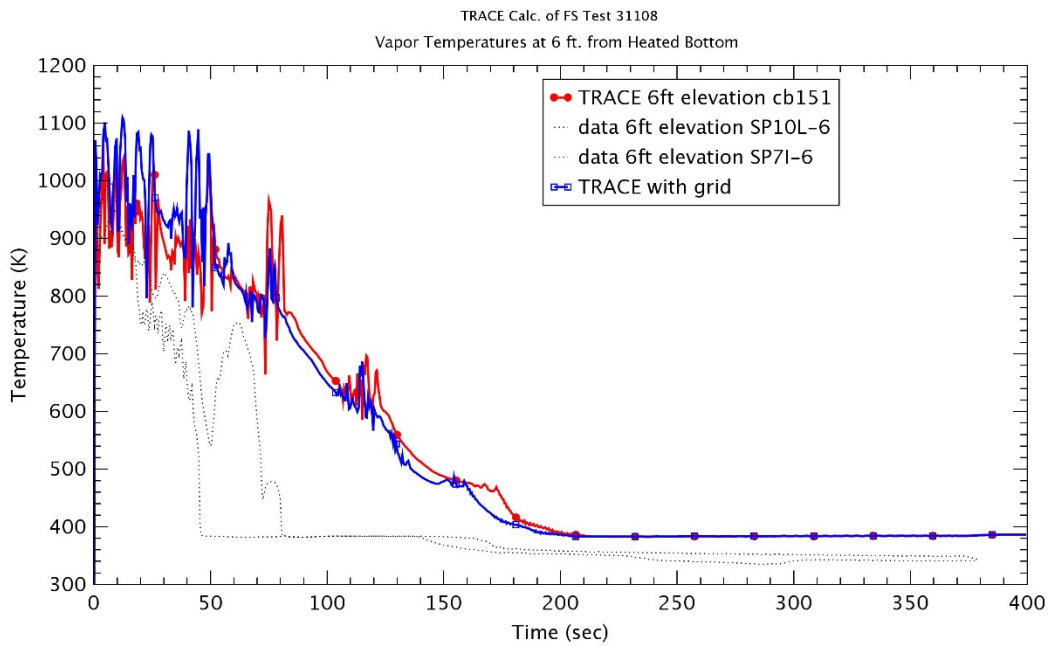


Figure 3-106 Vapor Temperature at 1.8 m – Run No.31108

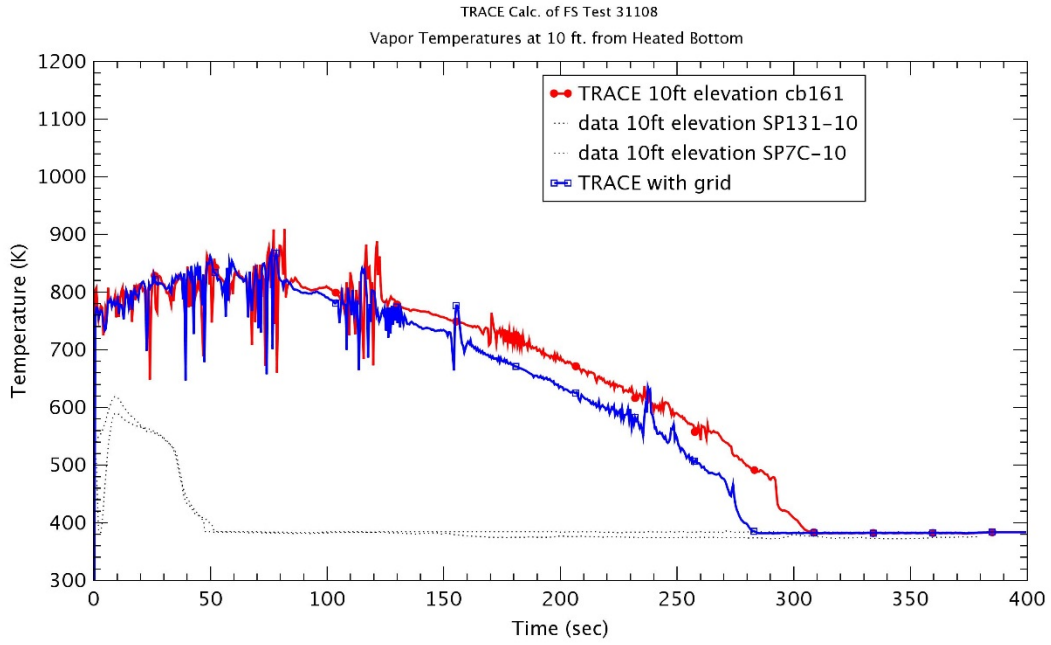


Figure 3-107 Vapor Temperature at 3.0 m – Run No.31108

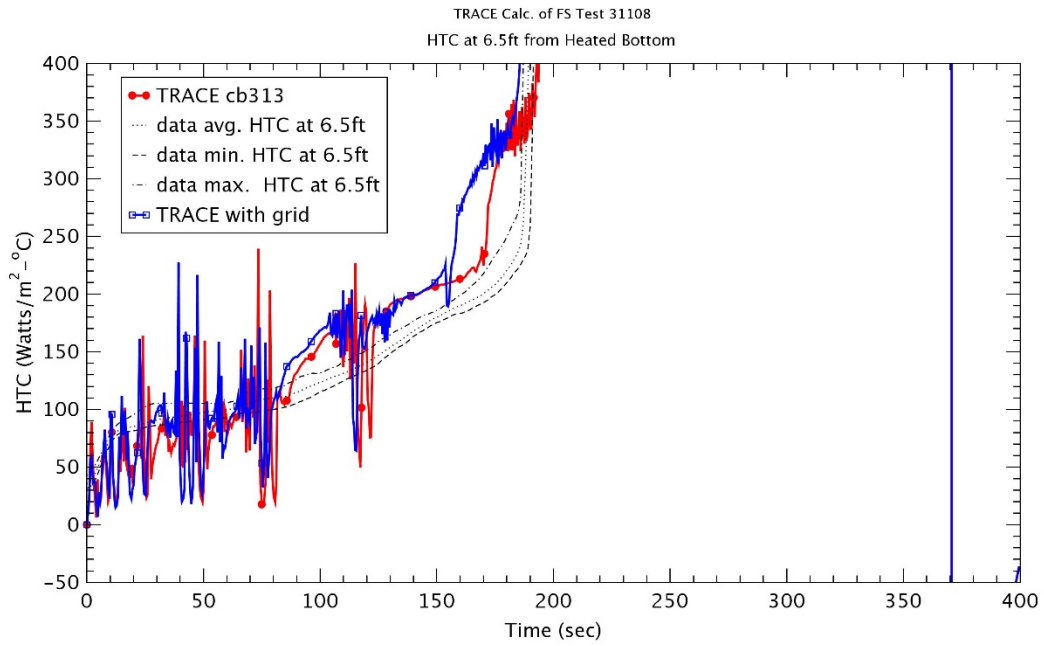


Figure 3-108 Heat Transfer Coefficient at 1.98 m – Run No.31108

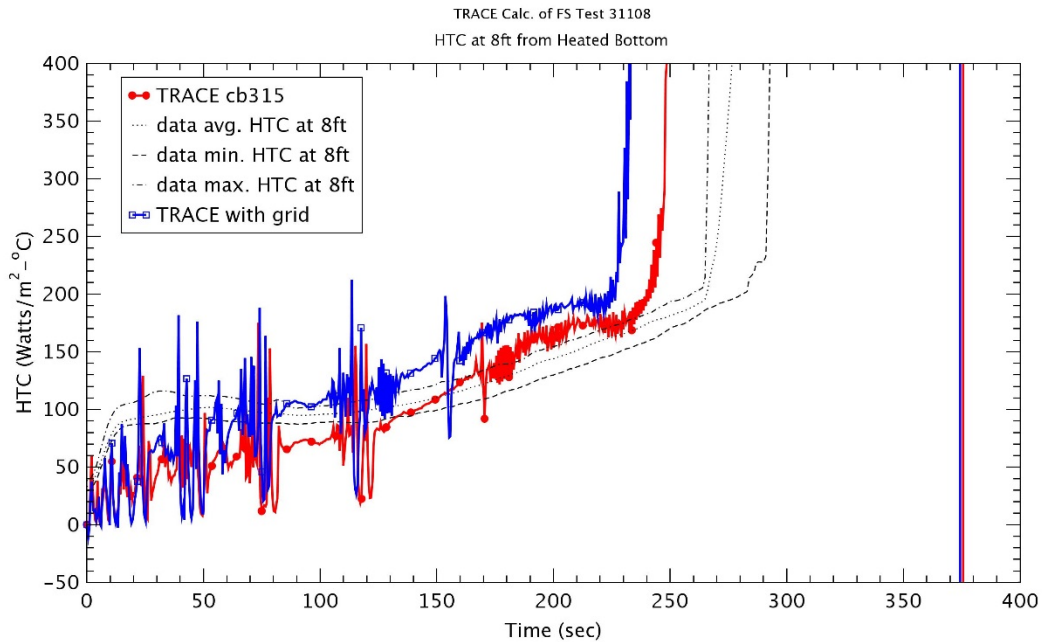


Figure 3-109 Heat Transfer Coefficient at 2.4 m – Run No.31108

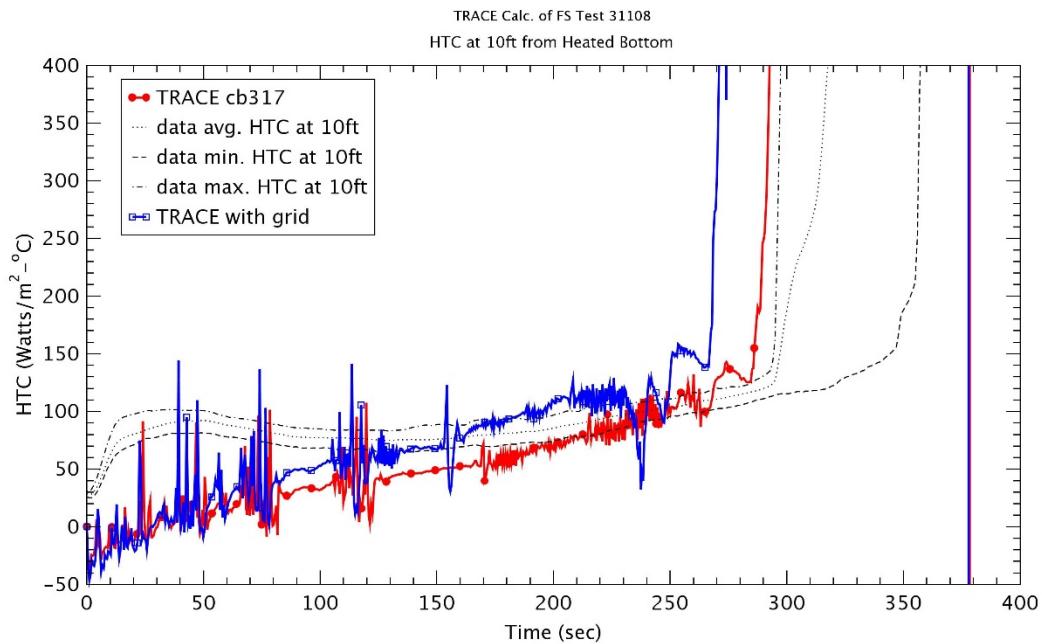


Figure 3-110 Heat Transfer Coefficient at 3.0 m – Run No.31108

3.2.1.6 Run No. 32013

Run No. 32013 was a test with a flooding rate of 2.64 cm/sec at 0.41 MPa and 79 oC inlet subcooling temperature as shown in Table 3-1. This was the same conditions as Run No. 31504, except for one

and a half times the pressure of the upper plenum. As described before, the actual input conditions changed largely with time and showed the big oscillations. Therefore, the inlet flowrate and temperature were considered as time-dependent variables as shown in Figures 3.111 ~ 3.112. Most initial conditions in the TRACE assessment manual [6] were applied in this study.

Figure 3-113 through Figure 3-120 plotted the rod temperatures at various elevations. These figures showed well the processes such as the heat up, turn-over of rod temperature during a reflood and a final quenching. In the case without the spacer grid model, the peak temperatures were reasonably predicted with the data at low elevations ($z \leq 2.4$ m), but were over predicted at higher elevations (3.0 m ~ 3.3 m). The maximum peak clad temperature was shown at elevation $z=1.98$ m (6.5 ft). The quenching times were fairly agreed with the data beside of higher elevations ($z > 3.3$ m). This test had 1.5 times the upper plenum pressure of Run No. 31504 and showed a similar trend with Run No. 31504. The lower rod temperatures and the earlier rod quench at all elevations were predicted as compared to Run No. 31504 since the saturation temperature would be relatively high due to the higher pressure. When the spacer model was applied, the rod temperatures were reduced and the quenching time was expedited at most elevations. During a heating up, the effect of the spacer grid model did not show at lower elevations ($z \leq 2.4$ m), but the rod temperatures at higher elevations were increased faster than the case without the spacer grid model. The turn-over time of rod temperature were predicted earlier than those without the spacer grid at all elevations since the spacer grid enhanced the increase of collapsed water level. The peak temperatures with the spacer grid model had the lower values at low elevations ($z \leq 3.0$ m) in comparison with those without the spacer grid model, while the peak temperature with the spacer grid model was a little higher than that at $z = 3.3$ elevation as shown in Figure 3-119. This might be resulted from the earlier rise of rod temperature during a heat up region. In the case with the spacer grid model, the decreasing temperature was ~ 2.7 K and the reduction of quenching time was ~ 5 sec due to the spacer grid model at elevation $z=1.98$ with the maximum peak cladding temperature.

As shown in Figure 3-121, the quench front without the spacer grid model showed the slightly under prediction results except for the upper region at all elevations, but it was reasonable. With the spacer grid model, the quench front was increasing slightly faster than that without the spacer grid model as the elevation was higher.

The differential pressure (DP) for entire 12 ft was shown in Figure 3-122 and the differential pressure between 11 ft and 12 ft was illustrated in Figure 3-123. The rise of DP for entire test section was related to the collapsed liquid level and the DP increased gradually with the injected water. The DP for entire 12 ft agreed fairly with the data and the DP between 11 ft and 12 ft was slightly over predicted for all times of test. If the spacer grid model was applied, the faster increase of DP for entire 12 feet was predicted which is similar to Run No. 31504. As shown well in Figure 124, the DP between 11 ft and 12 ft rose at elevation with the spacer grid and the pressure drop was predicted well.

Figures 3.124 and 3.125 represented the vapor temperatures at two elevations 1.8 m and 3.0 m, respectively. The vapor temperature at higher elevation 3.0 m was predicted well at the initial heat up period as compared to Run No. 31504 and it would be related to the lower rod temperature and the earlier quench time. The calculation with the spacer grid model showed the higher vapor temperature during the heat up and the faster quenching at high elevation.

The heat transfer coefficients (HTCs) at several elevations is shown in Figure 3-126 through Figure 3-128. As shown in Figures, the HTC was reducing or stagnant during the rod heat up, but TRACE did not predict well the experimental data for the heating up. However, the HTCs were fairly predicted during the reflood phase and the time of steep increase of HTC was agreed reasonably with the experimental data, especially at elevation $z = 2.4$. This would correspond with the behaviors of rod

temperature. With the spacer grid model, the earlier sharp rise of HTC was predicted due to the earlier rod quench.

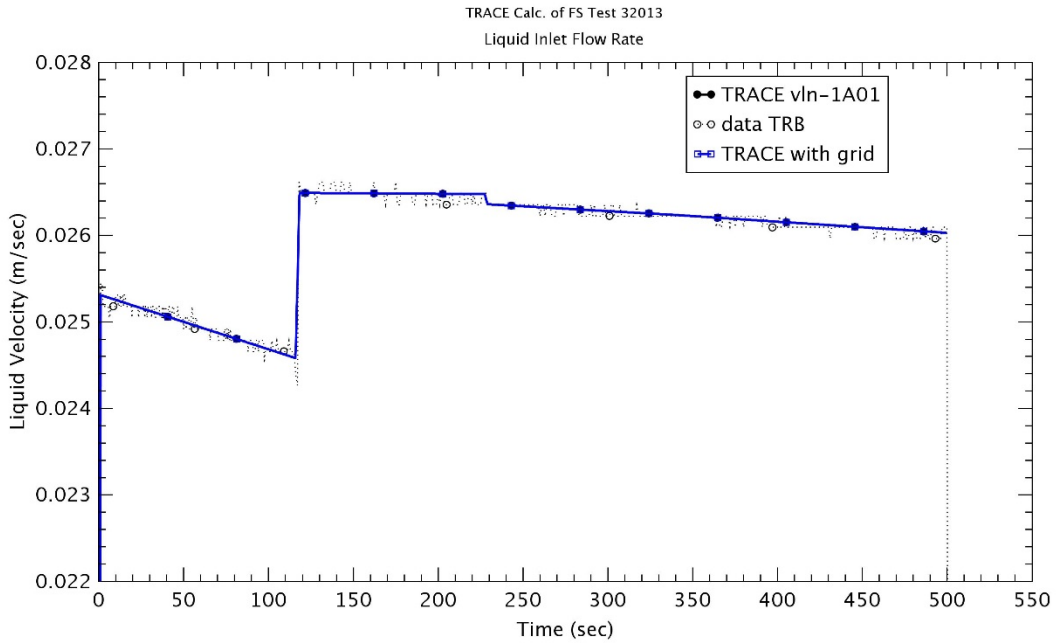


Figure 3-111 Liquid Inlet Flowrate – Run No.32013

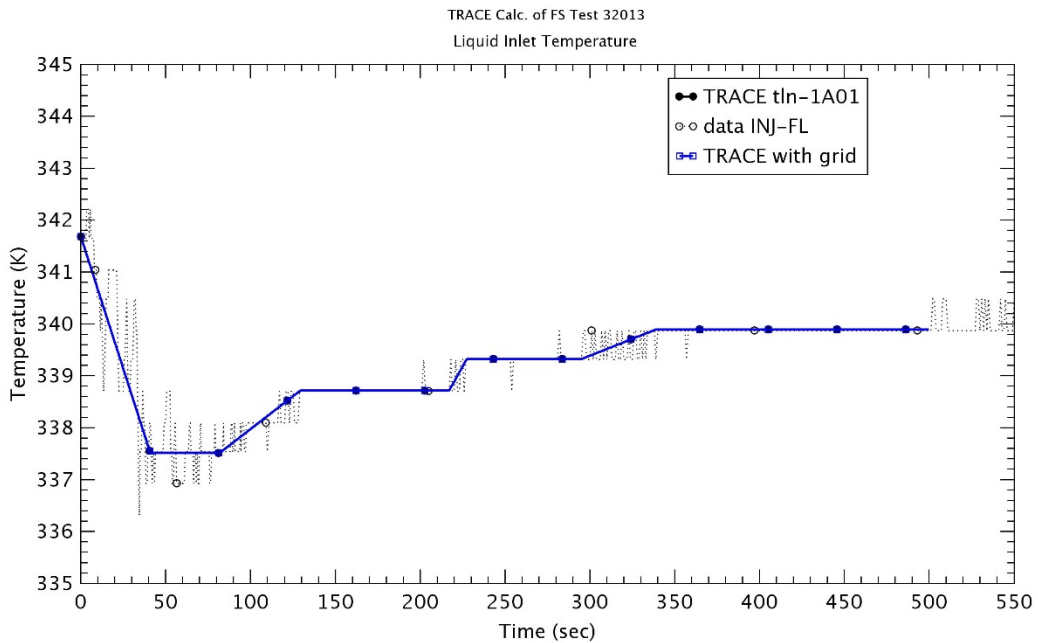


Figure 3-112 Liquid Inlet Temperature – Run No.32013

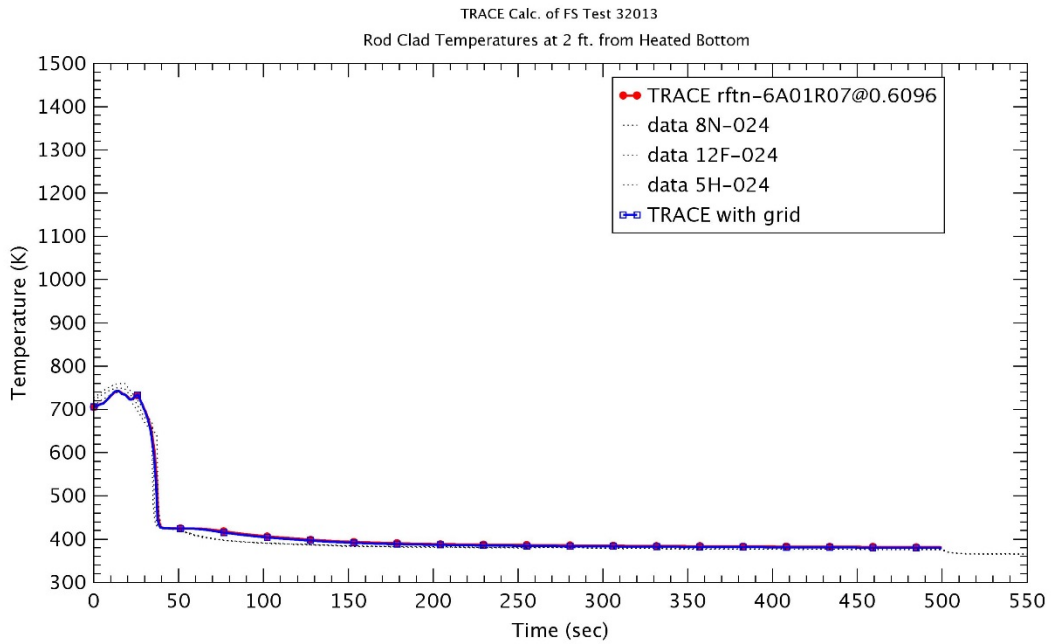


Figure 3-113 Heater Rod Temperature at 0.6 m – Run No.32013

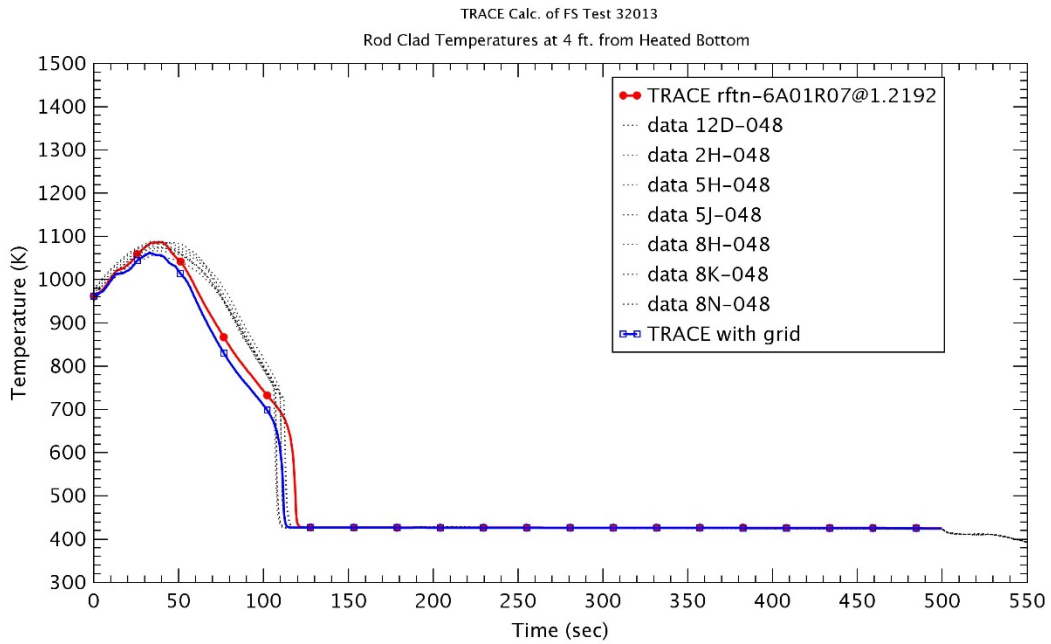


Figure 3-114 Heater Rod Temperature at 1.2 m – Run No.32013

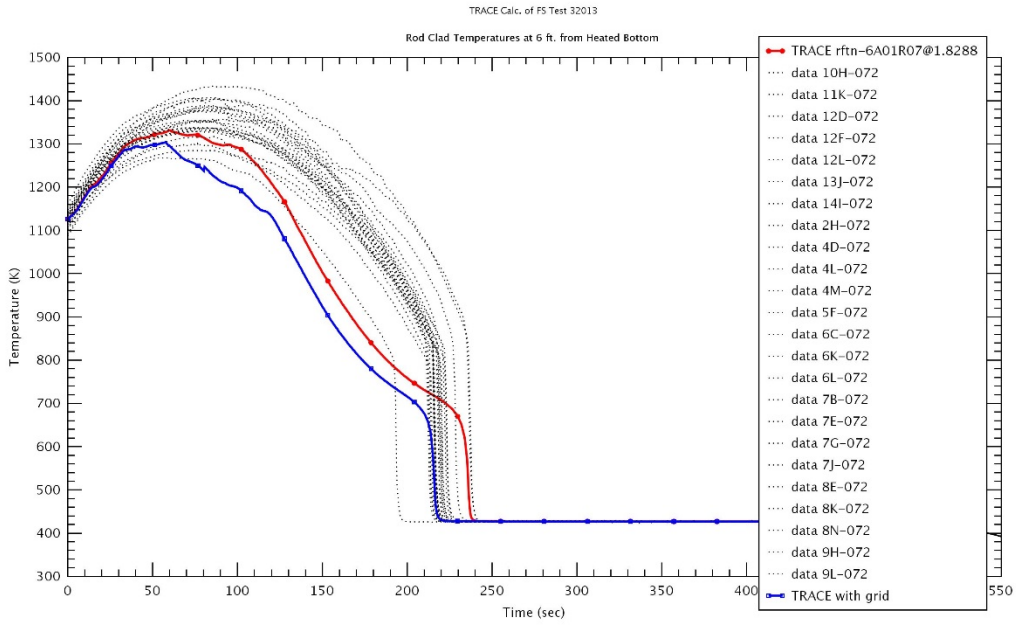


Figure 3-115 Heater Rod Temperature at 1.8 m – Run No.32013

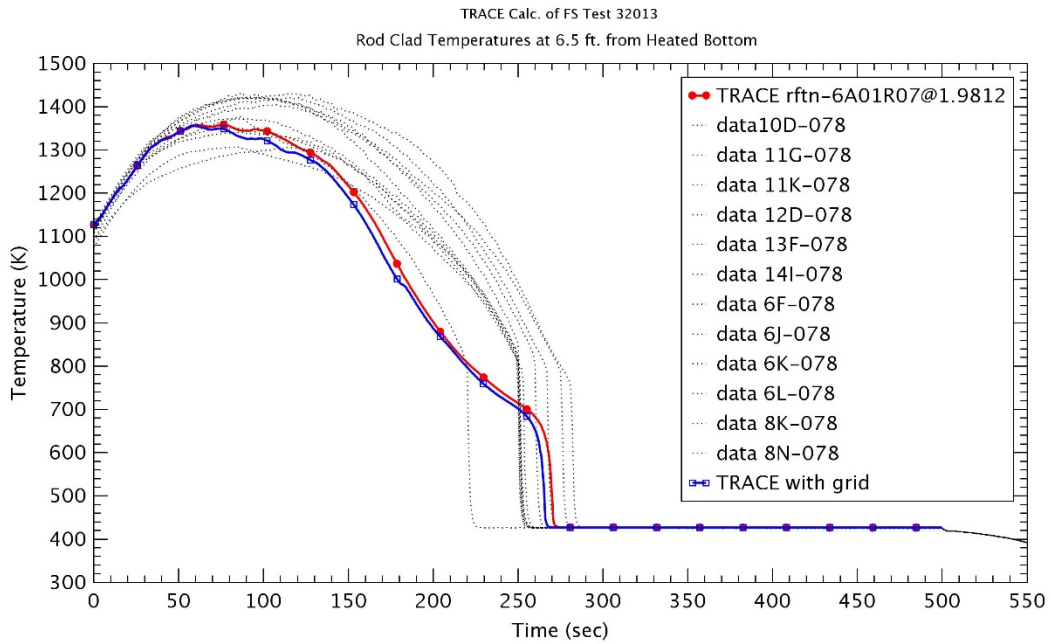


Figure 3-116 Heater Rod Temperature at 1.98 m – Run No.32013

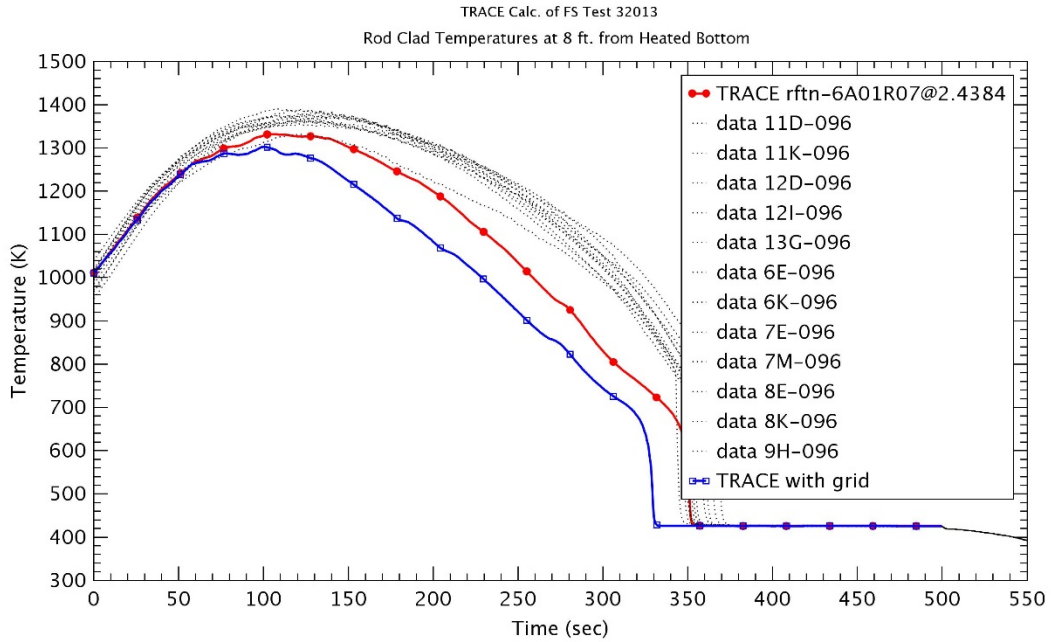


Figure 3-117 Heater Rod Temperature at 2.4 m – Run No.32013

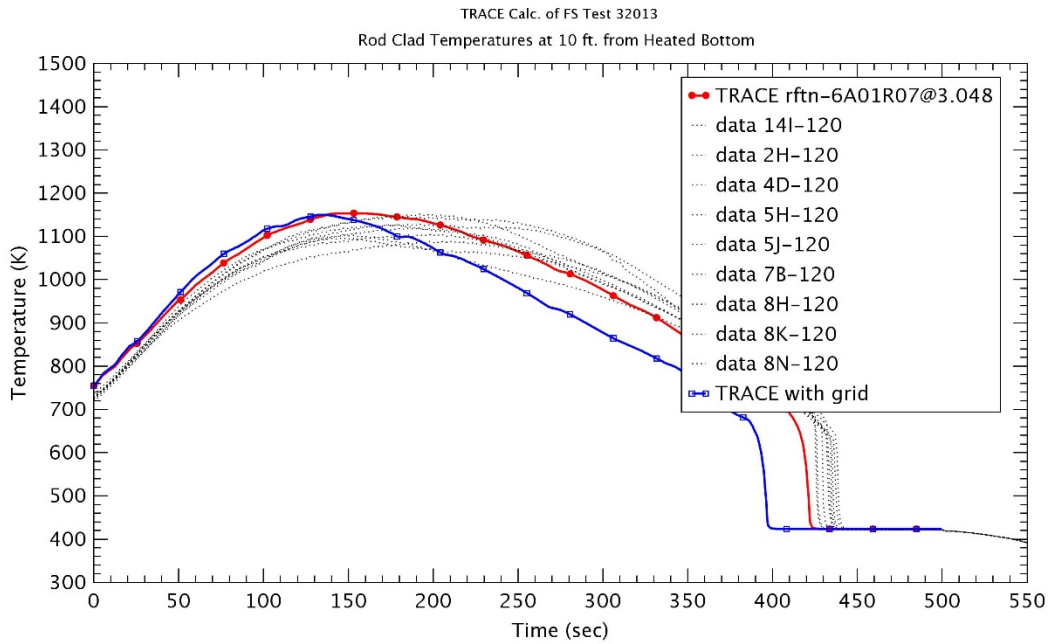


Figure 3-118 Heater Rod Temperature at 3.0 m – Run No.32013

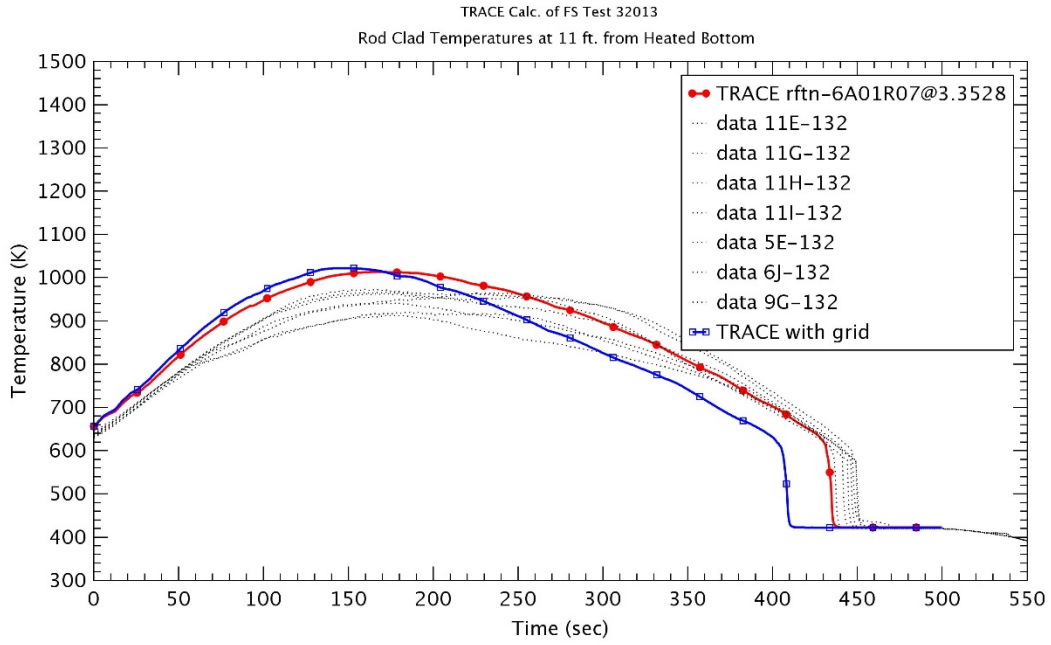


Figure 3-119 Heater Rod Temperature at 3.3 m – Run No.32013

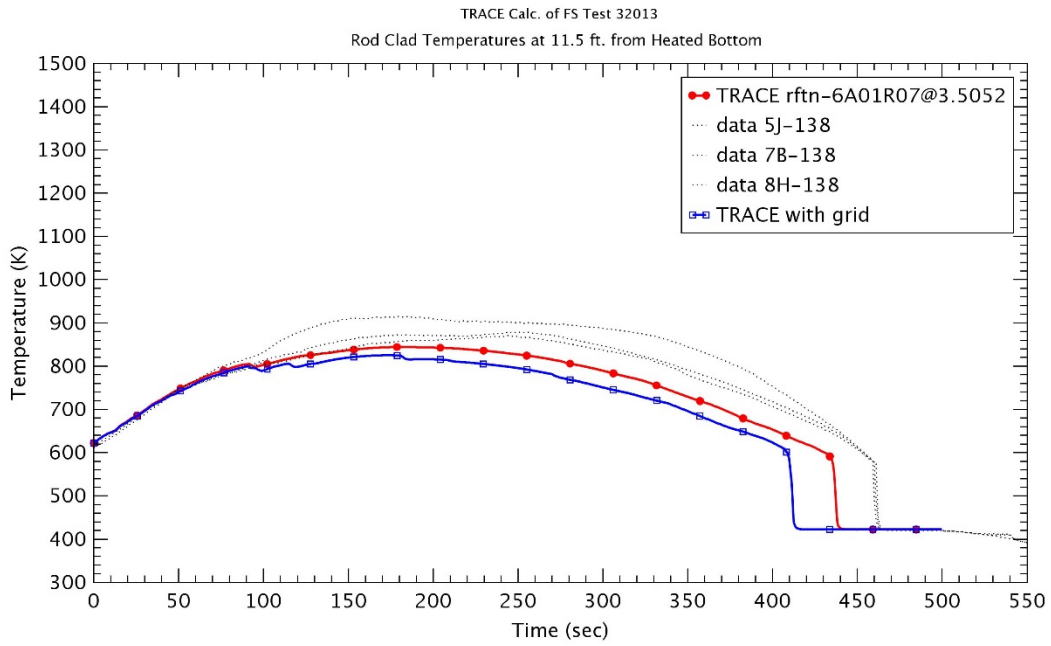


Figure 3-120 Heater Rod Temperature at 3.5 m – Run No.32013

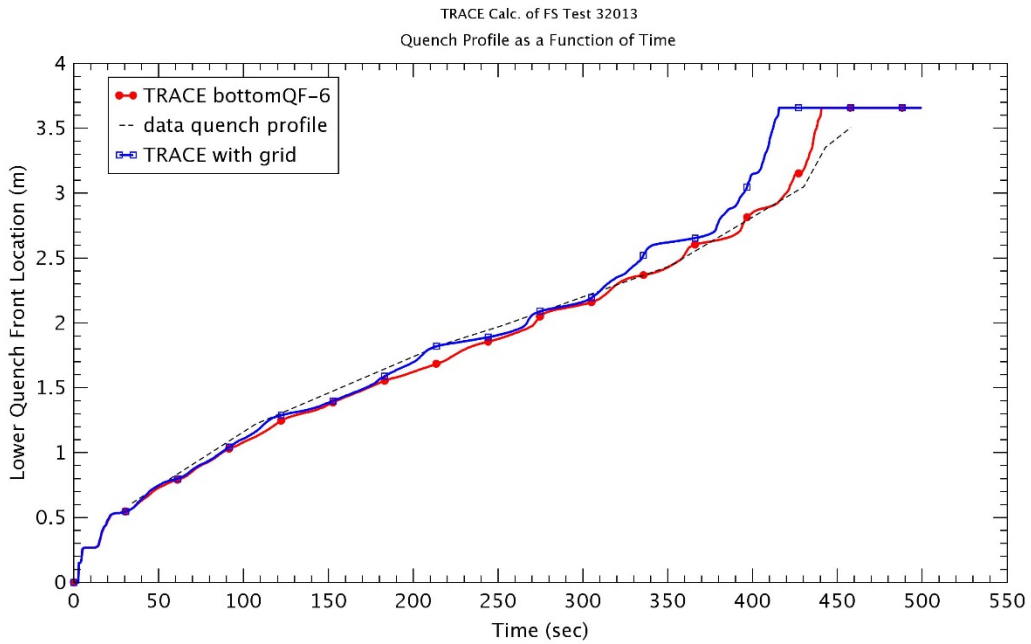


Figure 3-121 Quench Front Profile – Run No.32013

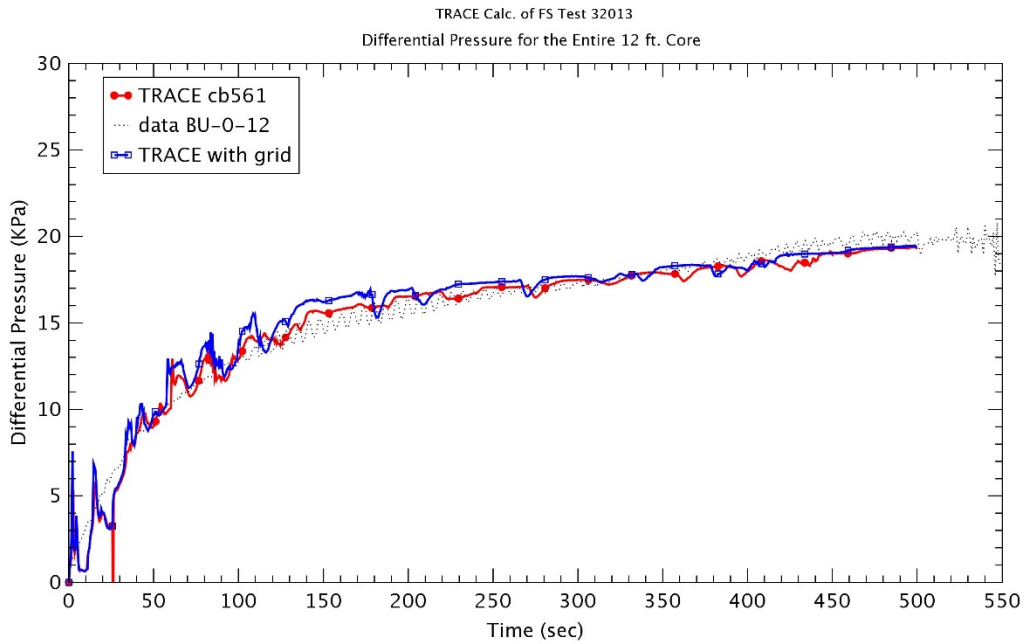


Figure 3-122 Differential Pressure for Entire 12 ft – Run No.32013

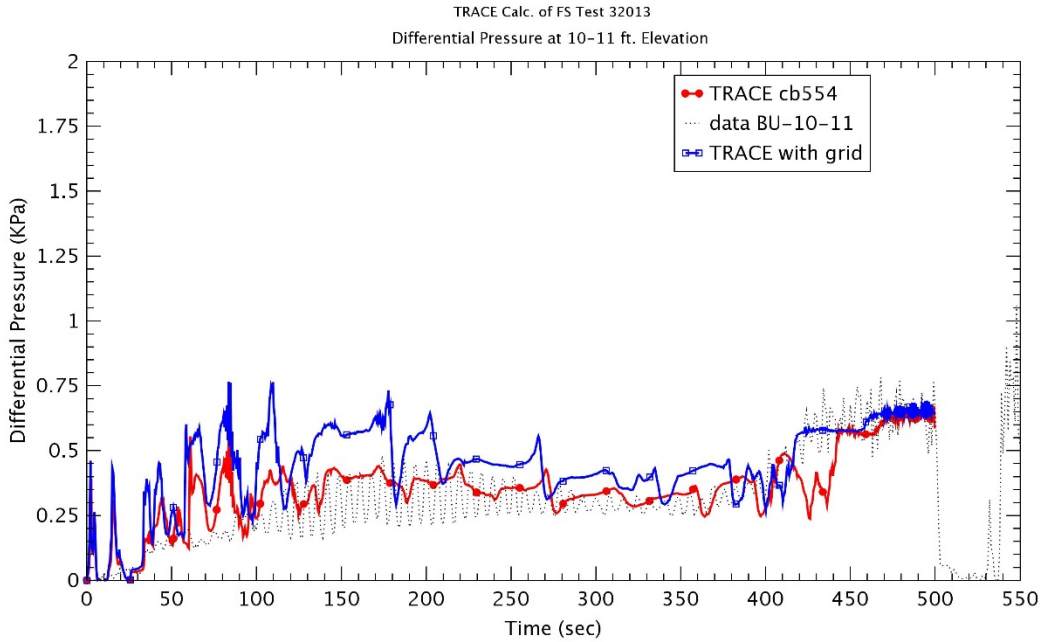


Figure 3-123 Differential Pressure at 10~11 ft Elevation – Run No.32013

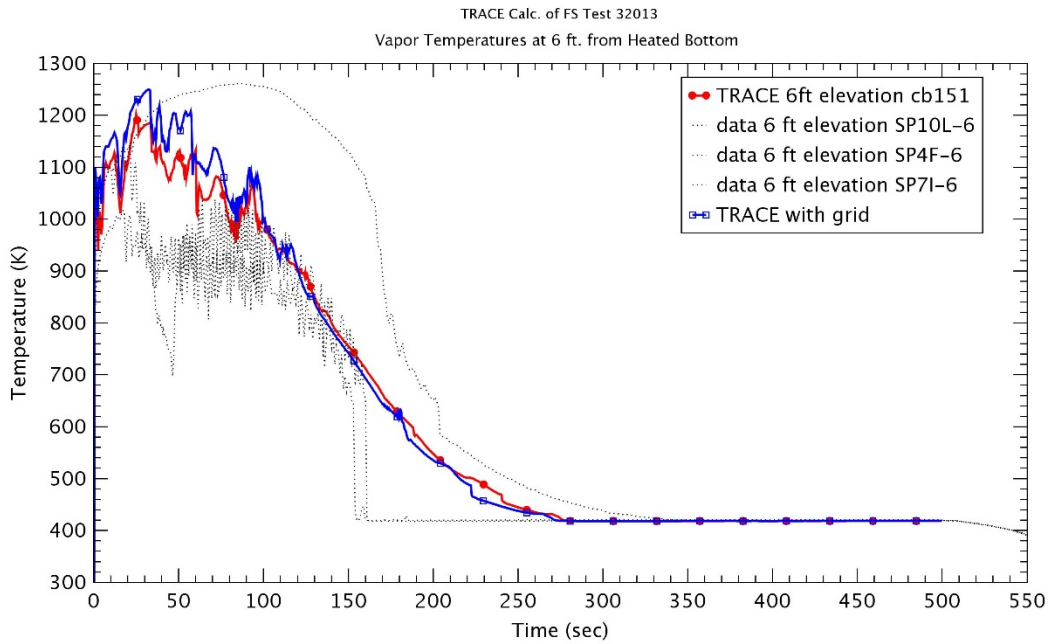


Figure 3-124 Vapor Temperature at 1.8 m – Run No.32013

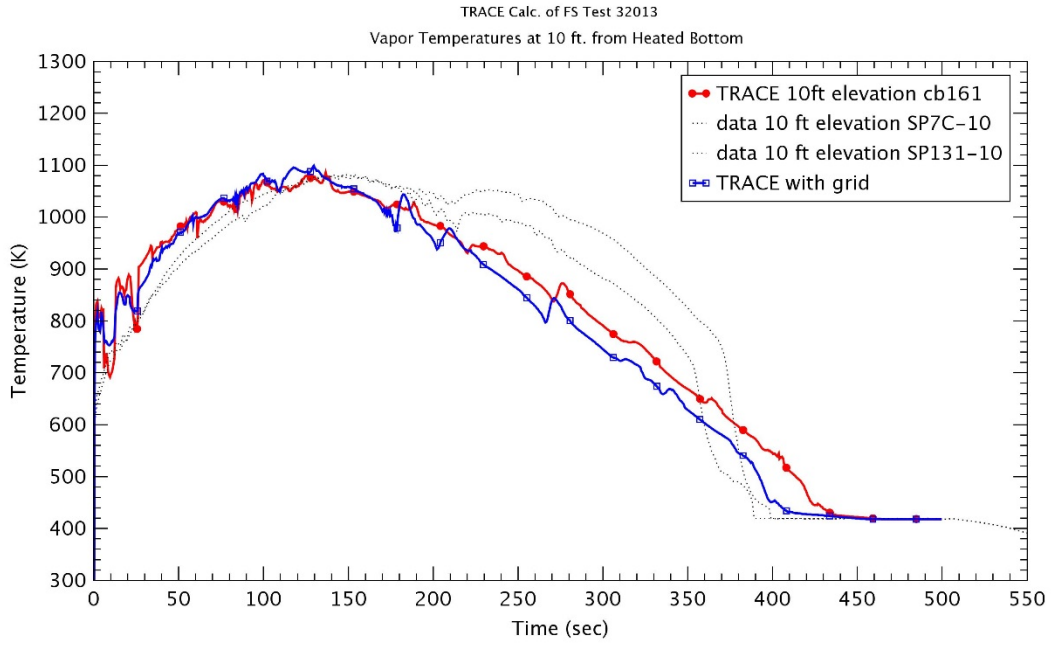


Figure 3-125 Vapor Temperature at 3.0 m – Run No.32013

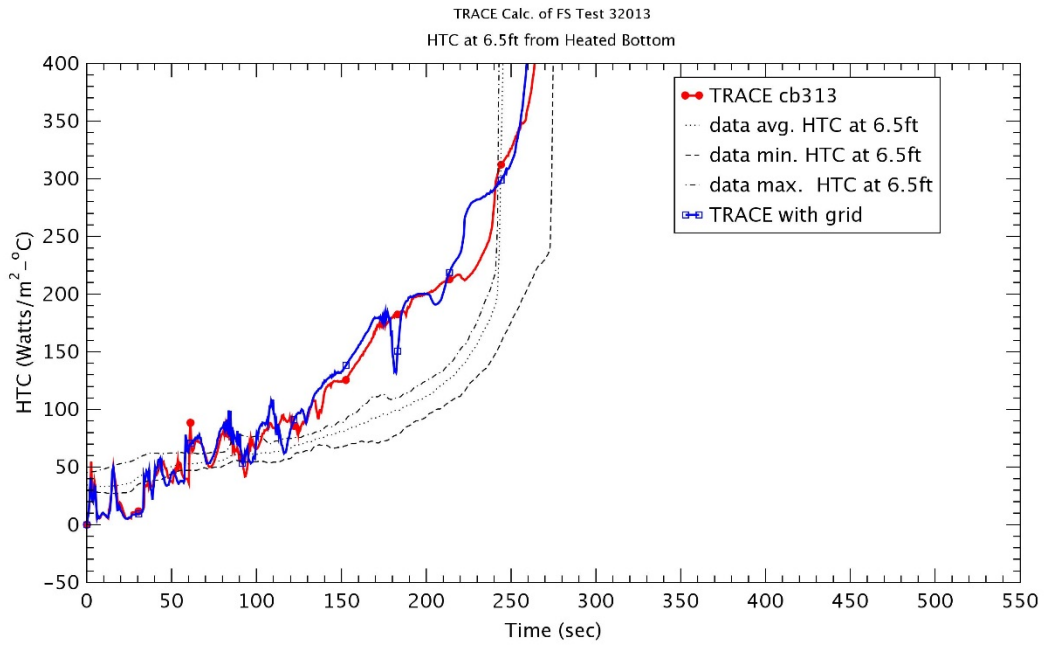


Figure 3-126 Heat Transfer Coefficient at 1.98 m – Run No.31701

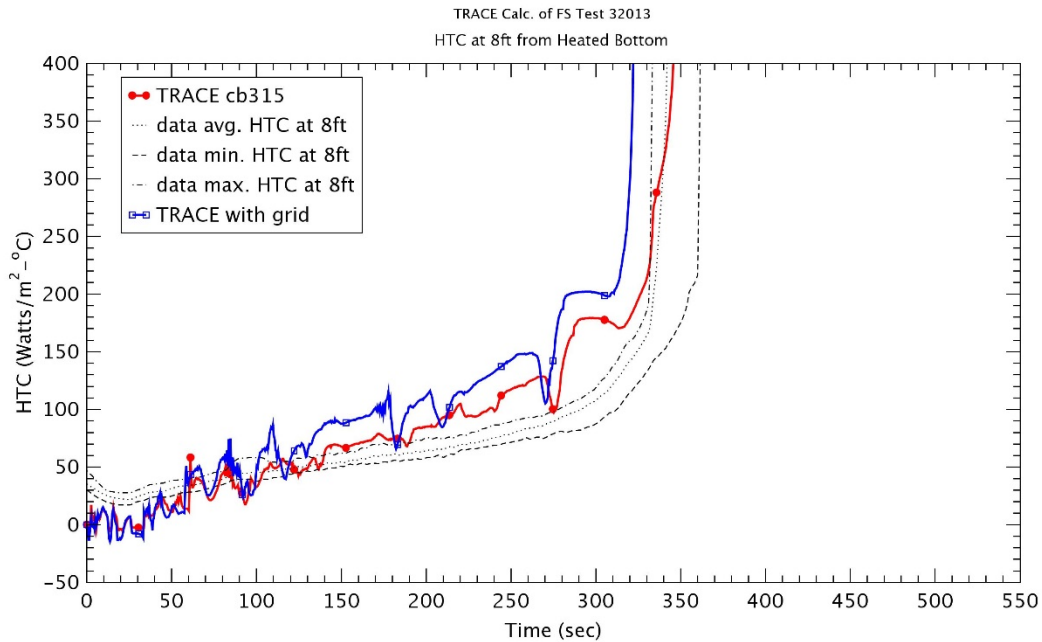


Figure 3-127 Heat Transfer Coefficient at 2.4 m – Run No.31701

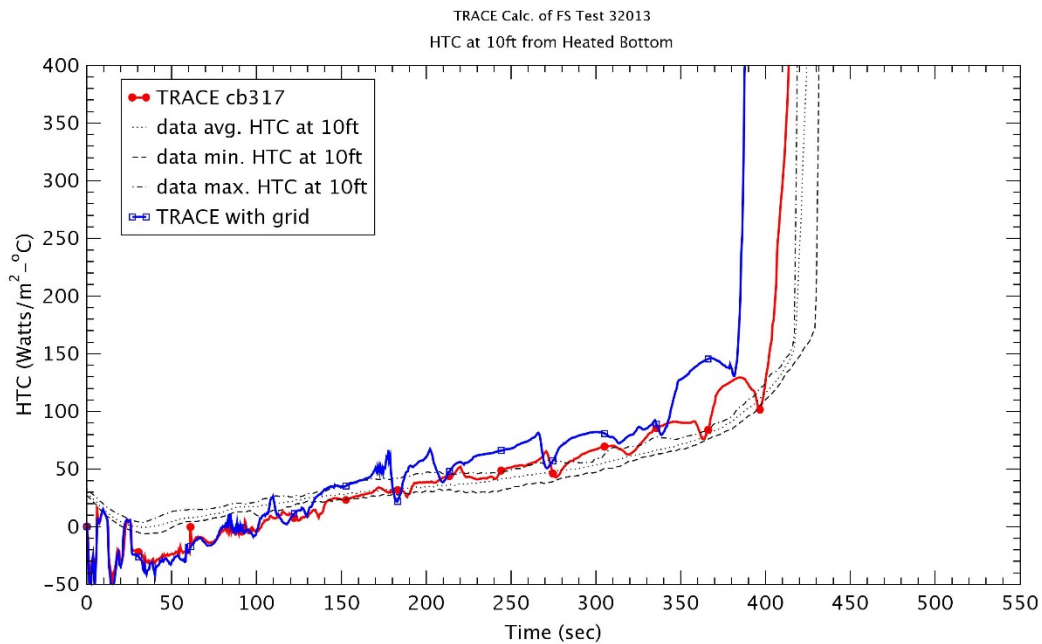


Figure 3-128 Heat Transfer Coefficient at 3.0 m – Run No.31701

3.2.1.7 Run No. 32114

Run No. 32114 was a test with a flooding rate of 2.5 ~ 3.1 cm/sec at 0.28 MPa and 5 oC inlet subcooling temperature as shown in Table 3-1. This was similar to Run No. 31504, except for a large

decrease of a subcooling degree. There was only test which used the low subcooling rate in Table 3-1. As described previously, the actual input conditions changed largely with time and showed the big oscillations. Therefore, the inlet flowrate and temperature were considered as time-dependent variables as shown in Figures 3.129 ~ 3.130. Most initial conditions in the TRACE assessment manual [6] were applied in this study.

The rod temperatures at various elevations were shown in Figures 3.131 ~ 3.138. These figures showed well the processes such as the heat up, turn-over of rod temperature during a reflood and a final quenching as in other tests. In the calculation without the spacer grid model, the peak temperatures were fairly predicted with the experimental data up to middle elevations ($z \leq 1.98$ m) and the calculated temperatures were located within the data spread range. However, the rod temperatures were over predicted at higher elevations (2.4 m ~ 3.3 m). The maximum peak clad temperature was shown at elevation $z=1.98$ m (6.5 ft) and increased largely due to a relatively higher inlet temperature as compared to Run No. 31504. Those predictions could be also induced well in Figures 3.142 ~ 3.143 with the relatively high vapor temperature. The quenching times were reasonably agreed with the data up to middle elevations ($z \leq 1.8$ m), but they were over predicted at higher elevations ($z \geq 1.98$ m). The quenching times were delayed due to the higher inlet temperature than Run No. 31805. When the spacer model was used, the rod temperatures were reduced and the quenching time was expedited at most elevations. During a heating up, the effect of the spacer grid model was not shown at all times of test. The turn-over time of rod temperature were estimated earlier than those without the spacer grid at all elevations since the spacer grid model enhanced the heat transfer. In the case with the spacer grid model, the decreasing temperature was ~ 20.2 K and the reduction of quenching time was ~ 27 sec due to the spacer grid model at elevation $z=1.98$ with the maximum peak cladding temperature.

As shown in Figure 3-139, the quench front without the spacer grid model showed a very good agreement results up to elevation $z \sim 1.5$ m, but it started deviating from the data above this elevation and over predicted due to the delayed prediction of rod quenching. With the spacer grid model, the quench front was increasing slightly faster than that without the spacer grid model as the elevation was higher.

The differential pressure (DP) for entire 12 ft was plotted in Figure 3-140 and the differential pressure between 11 ft and 12 ft was shown in Figure 3-141. The DP for entire test section was increased gradually with the injected water. The DP for entire 12 ft showed the over-prediction with the experimental data and TRACE predicted more water inventory in the test section compared to the data. The large oscillations of the DP, as in vapor temperatures, might be estimated due to the oscillation of upper plenum pressures. The slightly faster increase of DP for entire 12 feet was predicted as the spacer grid model was applied. As shown well in Figure 3-141, the DP between 11 ft and 12 ft was increased at elevation with the spacer grid and the pressure drop was predicted well.

The vapor temperatures were shown at two elevations 1.8 m and 3.0 m in Figures 3.142 and 3.143, respectively. The vapor temperature at higher elevation 3.0 m was largely over predicted during all times of test period and it would be related to the higher the rod temperature and the earlier turn-over time. The calculation with the spacer grid model showed well the faster quenching at high elevation.

The heat transfer coefficients (HTCs) at several elevations is illustrated in Figure 3-144 through Figure 3-146. As shown in Figures, TRACE under predicted the experimental data for the heating up, but the HTCs were fairly predicted during the reflood phase. The time of steep increase of HTC was delayed as the late prediction of rod quench in comparison with the experimental data at elevations $z \geq 1.98$. When the spacer grid model was applied, the earlier sharp rise of HTC was predicted due to the earlier rod quench.

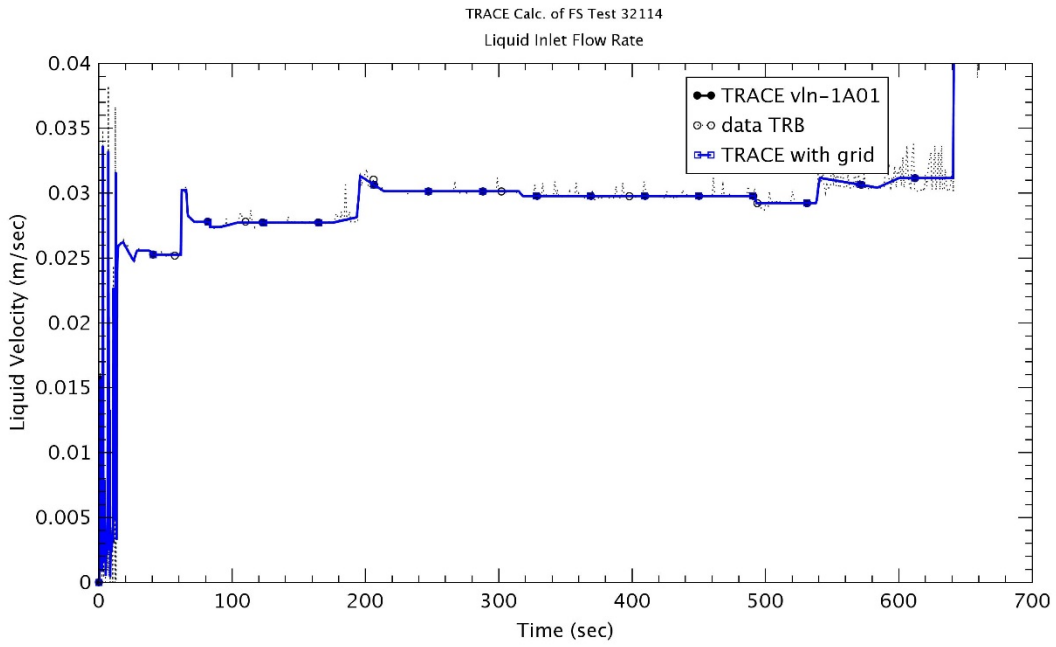


Figure 3-129 Liquid Inlet Flowrate – Run No.32114

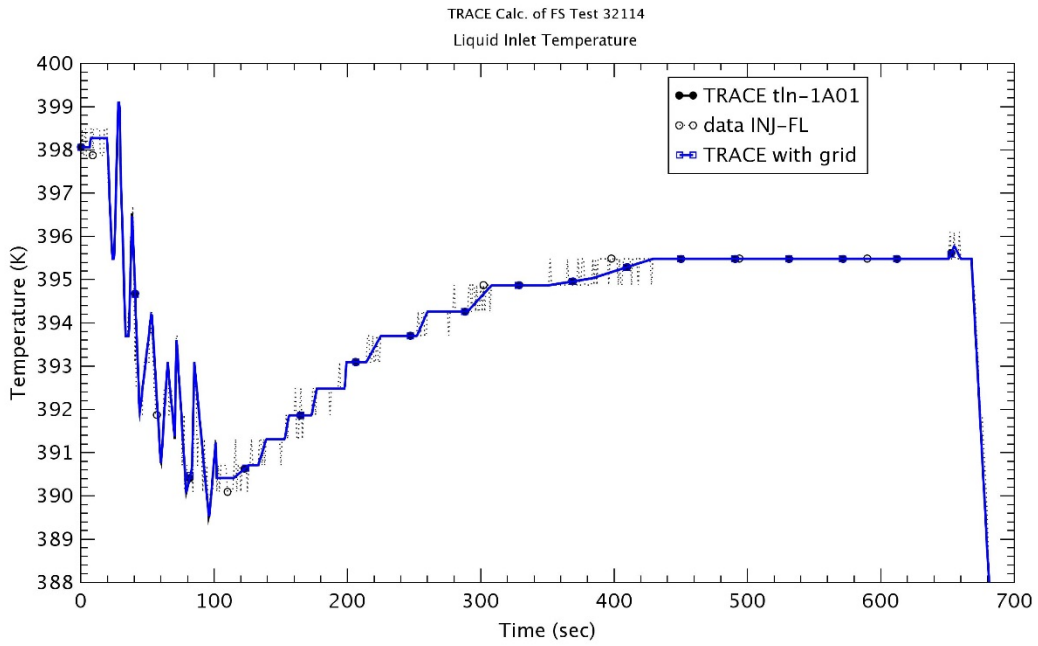


Figure 3-130 Liquid Inlet Temperature – Run No.32114

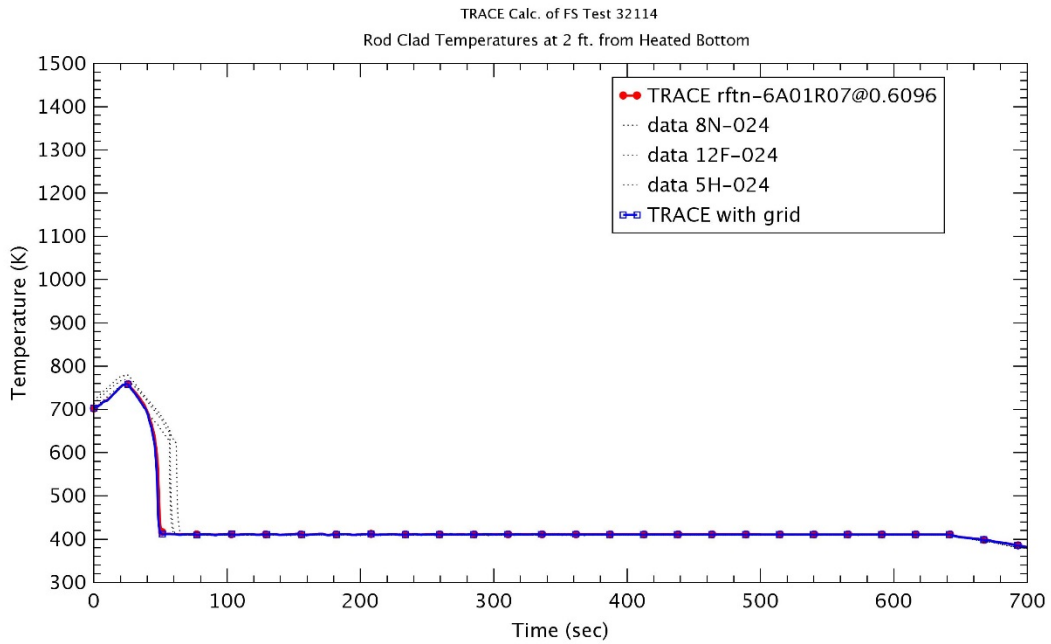


Figure 3-131 Heater Rod Temperature at 0.6 m – Run No.32114

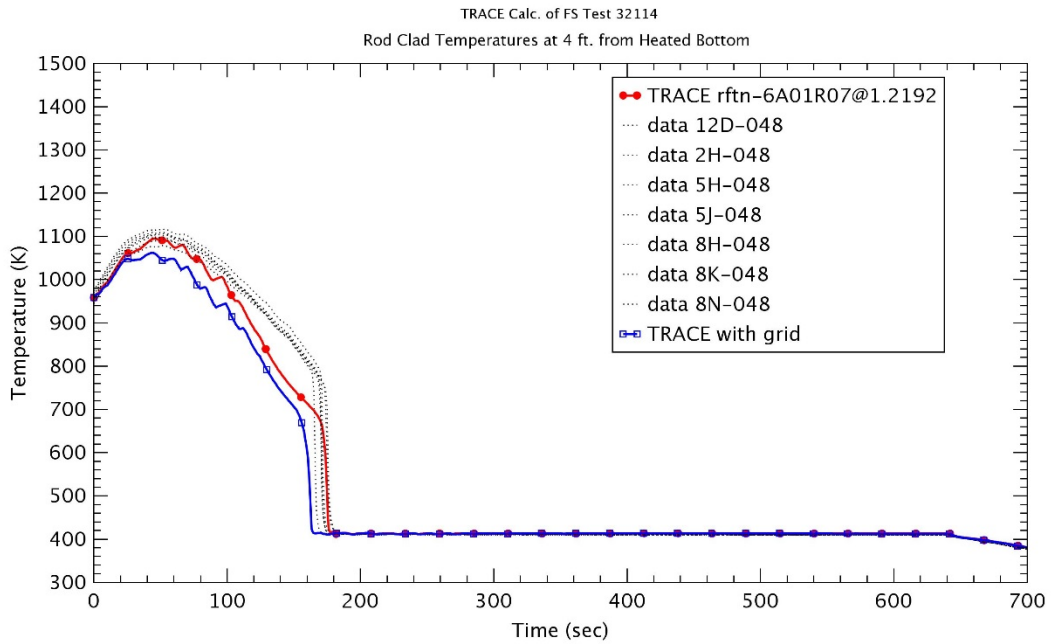


Figure 3-132 Heater Rod Temperature at 1.2 m – Run No.32114

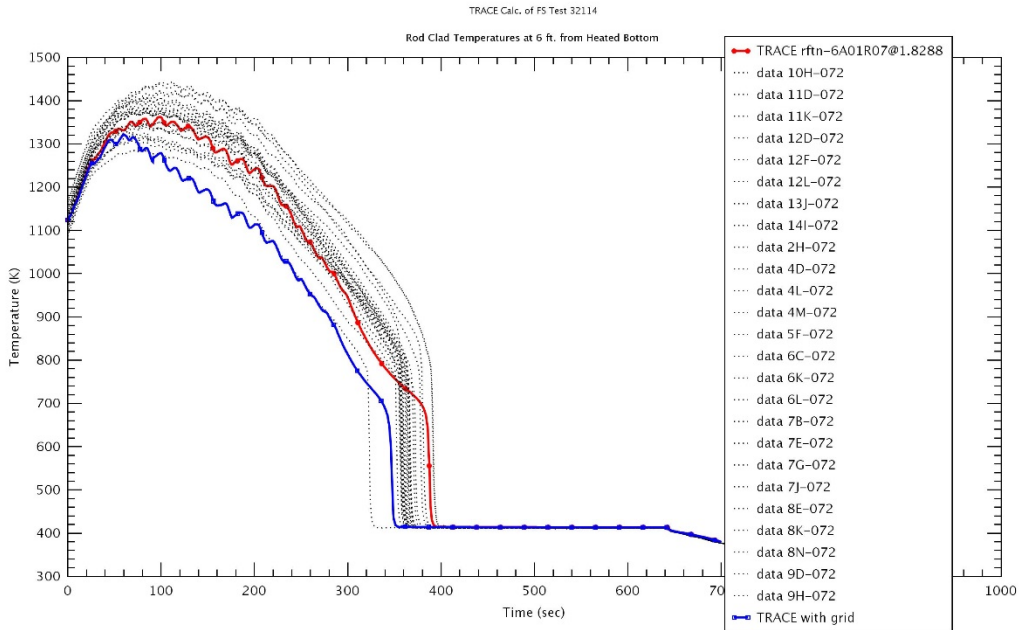


Figure 3-133 Heater Rod Temperature at 1.8 m – Run No.32114

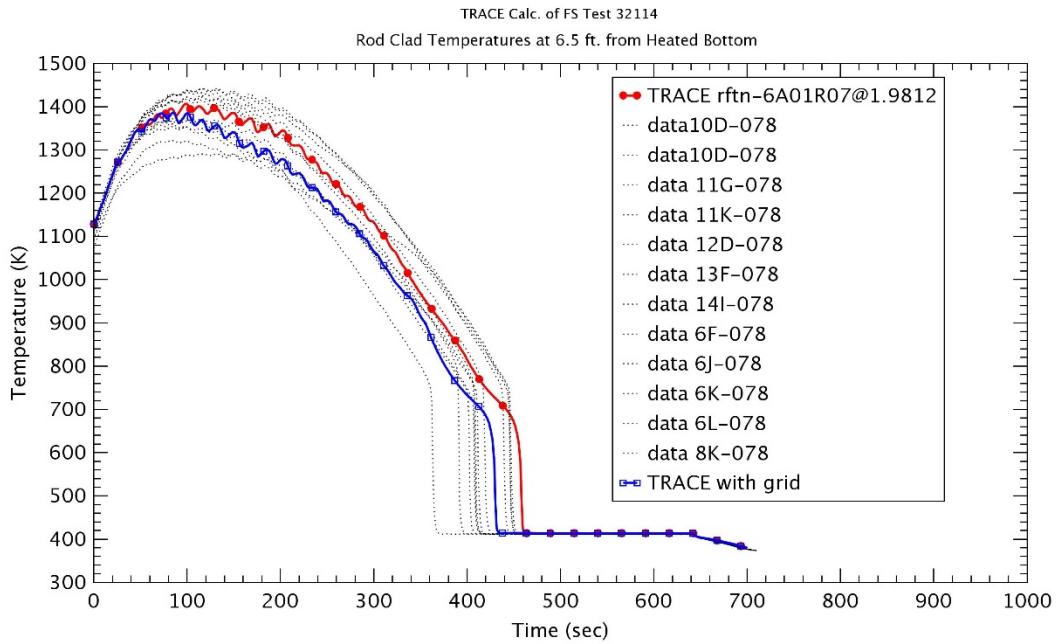


Figure 3-134 Heater Rod Temperature at 1.98 m – Run No.32114

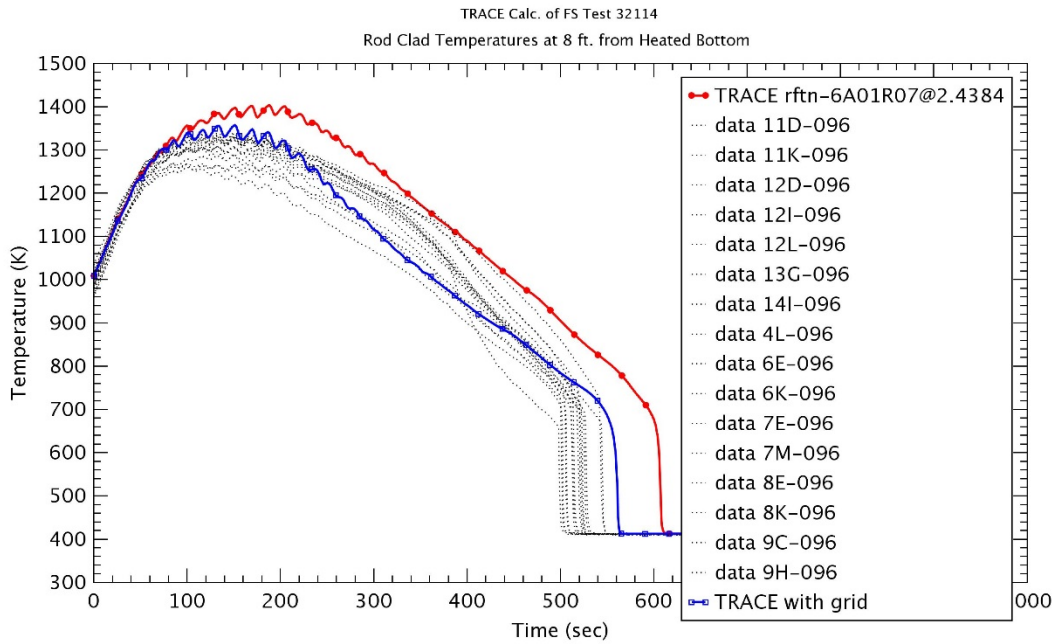


Figure 3-135 Heater Rod Temperature at 2.4 m – Run No.32114

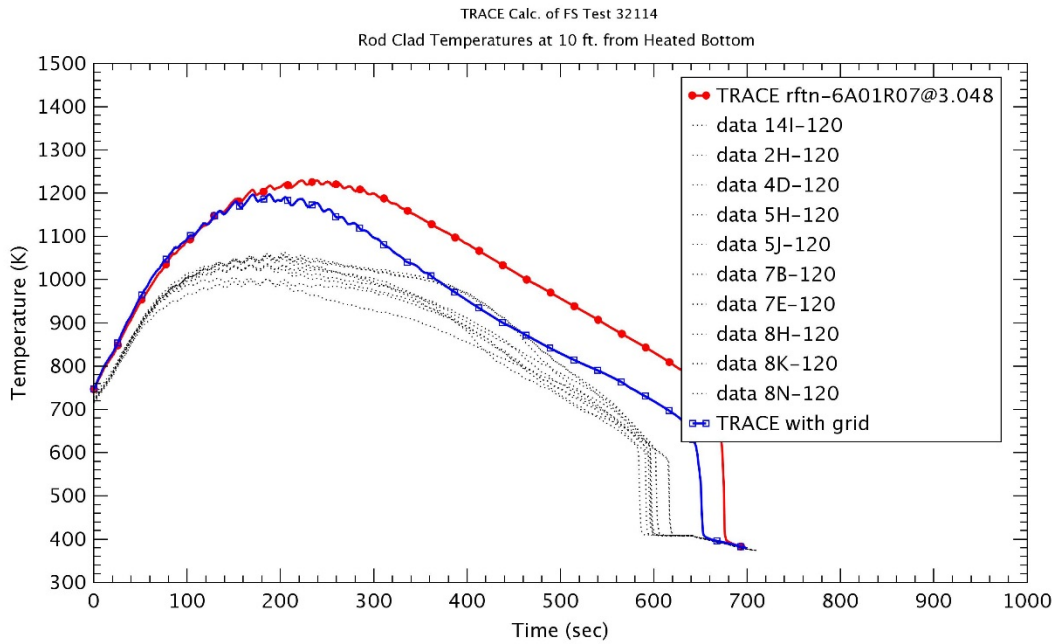


Figure 3-136 Heater Rod Temperature at 3.0 m – Run No.32114

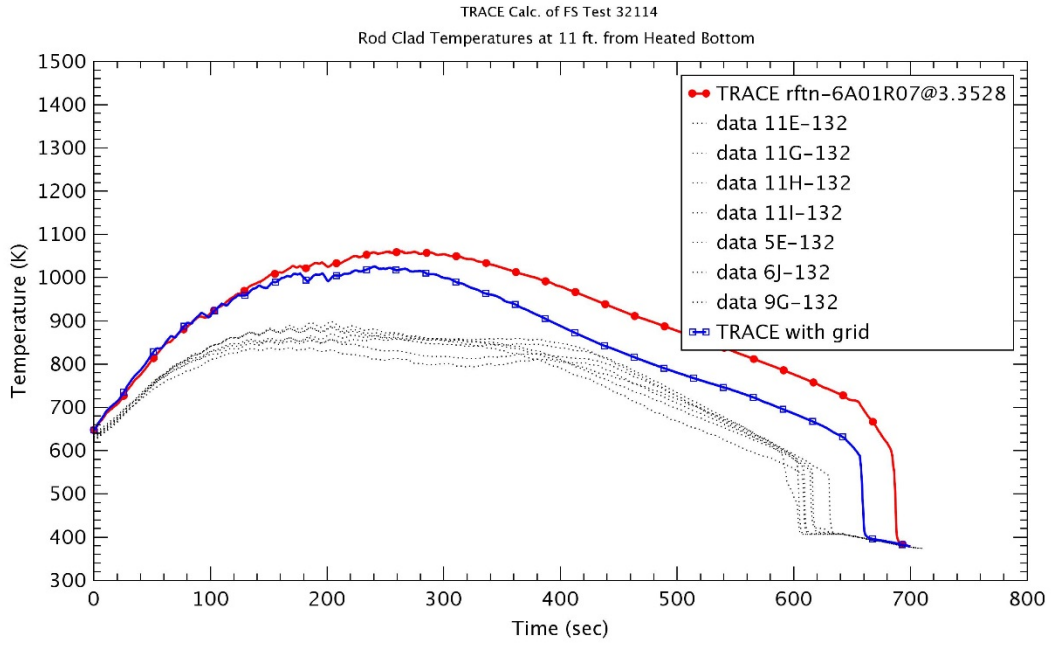


Figure 3-137 Heater Rod Temperature at 3.3 m – Run No.32114

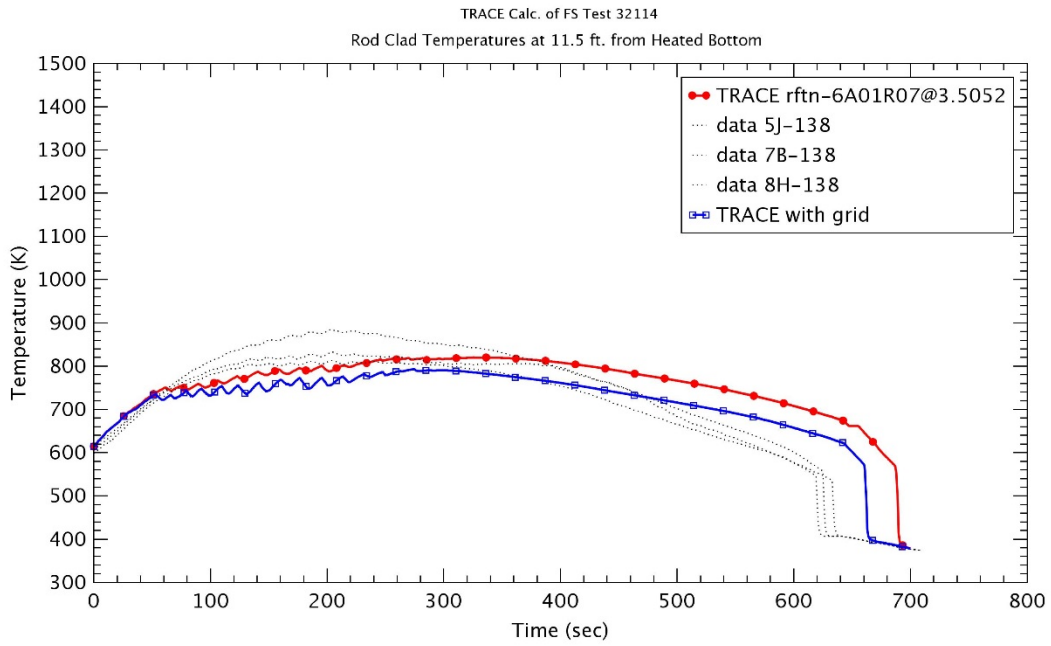


Figure 3-138 Heater Rod Temperature at 3.5 m – Run No.32114

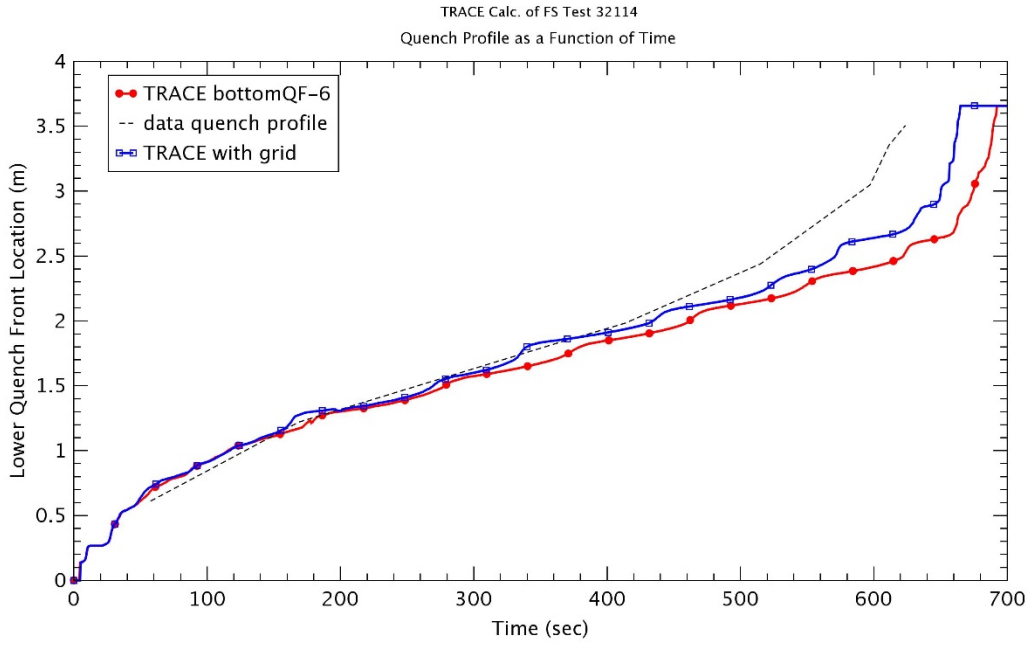


Figure 3-139 Quench Front Profile – Run No.32114

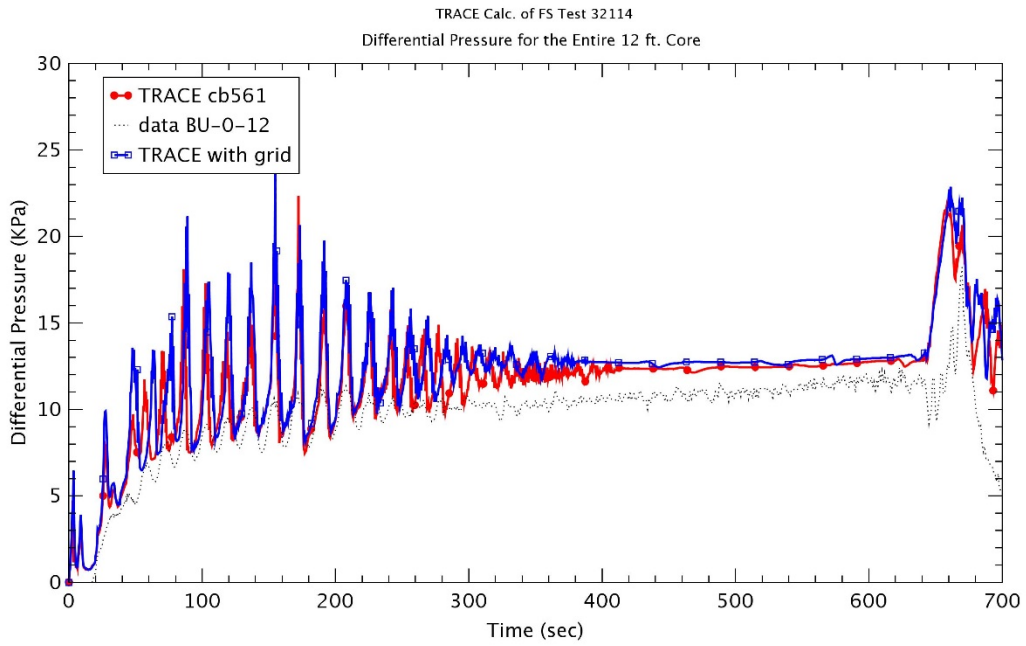


Figure 3-140 Differential Pressure for Entire 12 ft – Run No.32114

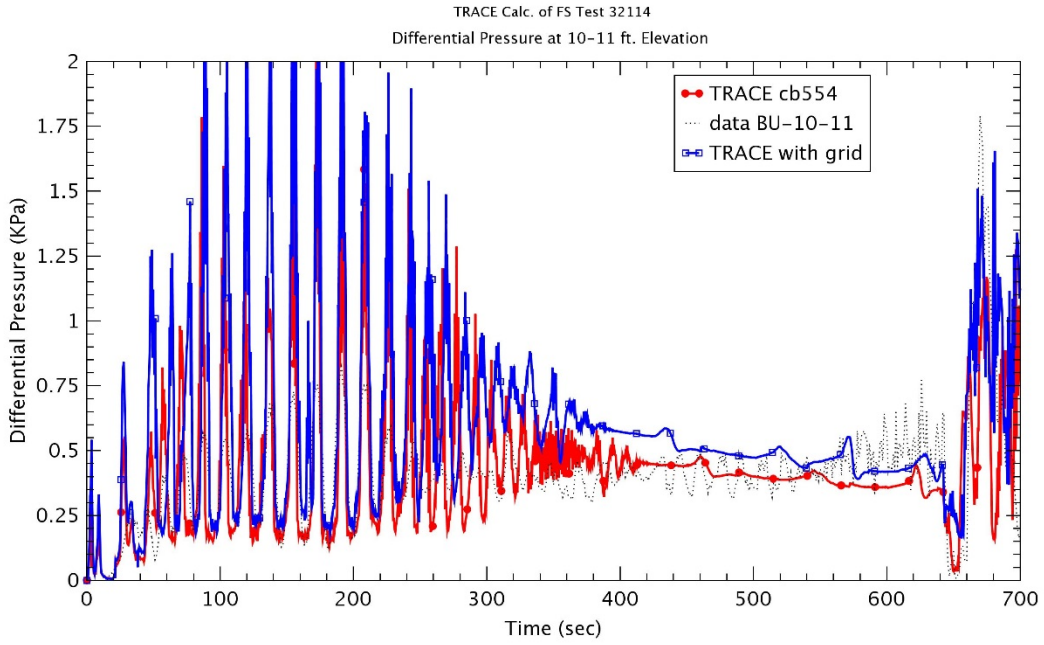


Figure 3-141 Differential Pressure at 10~11 ft Elevation – Run No.32114

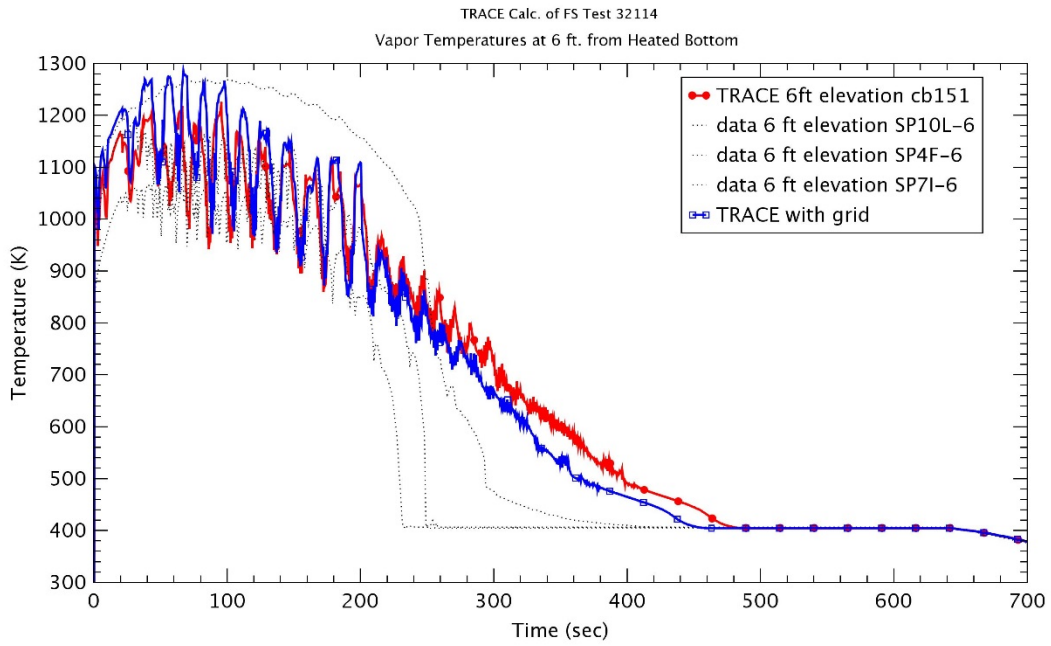


Figure 3-142 Vapor Temperature at 1.8 m – Run No.32114

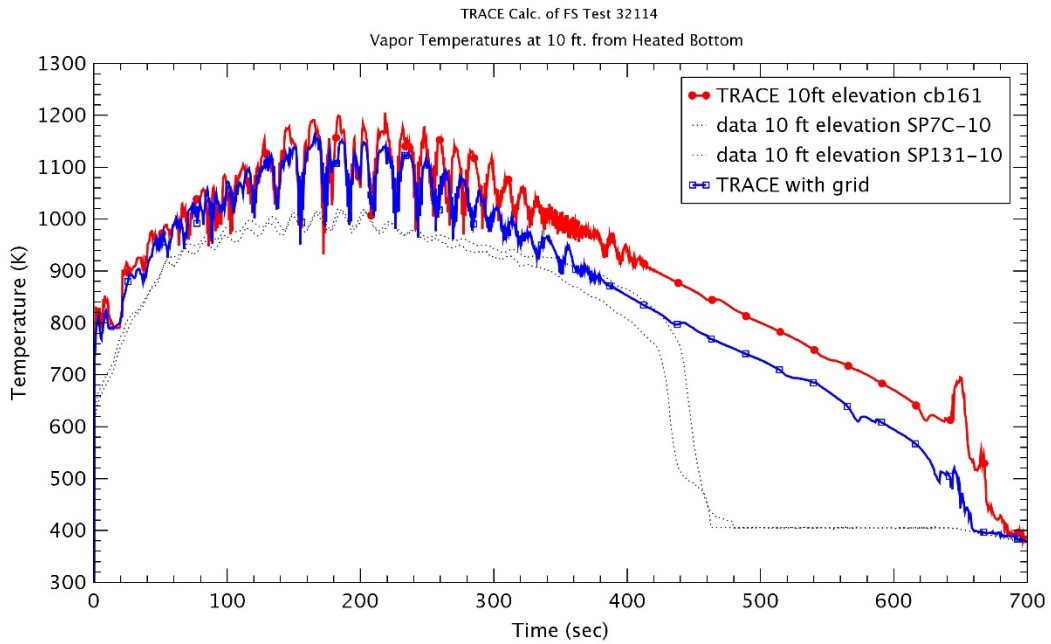


Figure 3-143 Vapor Temperature at 3.0 m – Run No.32114

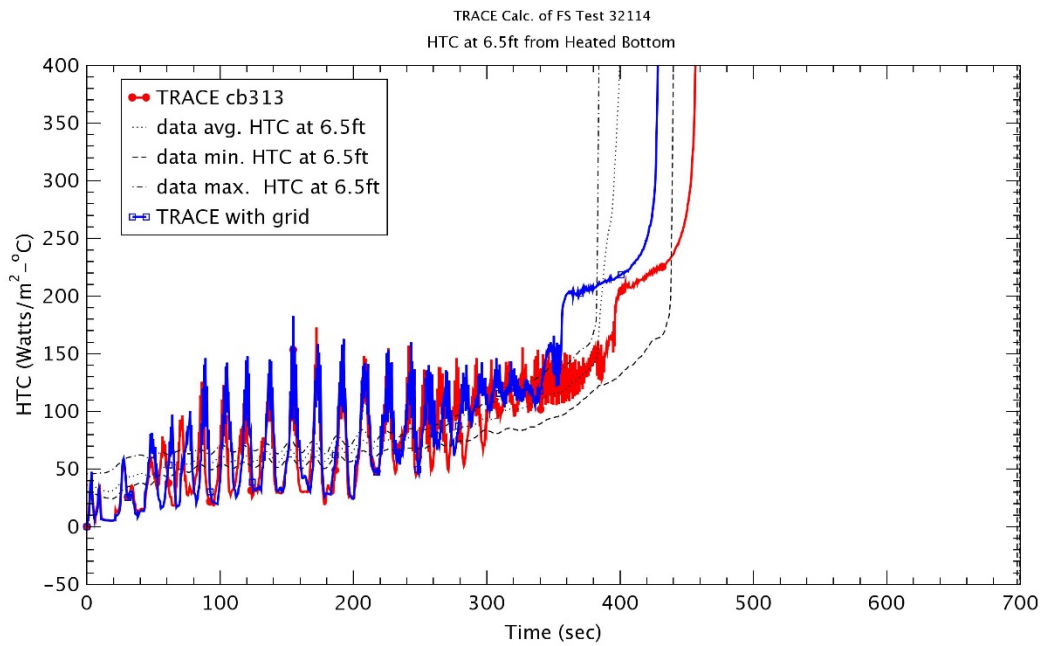


Figure 3-144 Heat Transfer Coefficient at 1.98 m – Run No.32114

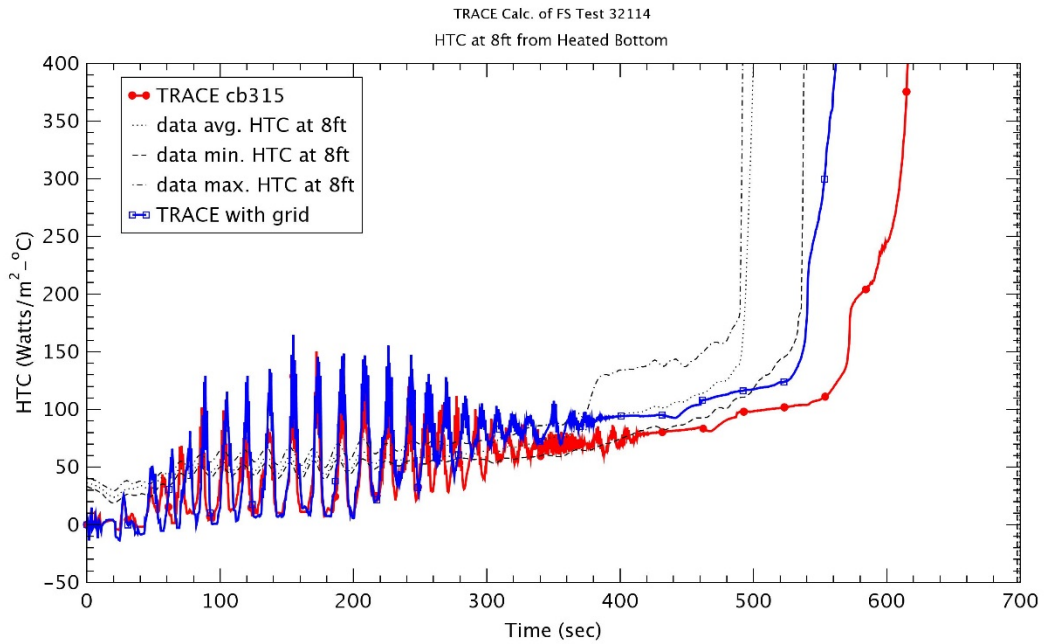


Figure 3-145 Heat Transfer Coefficient at 2.4 m – Run No.32114

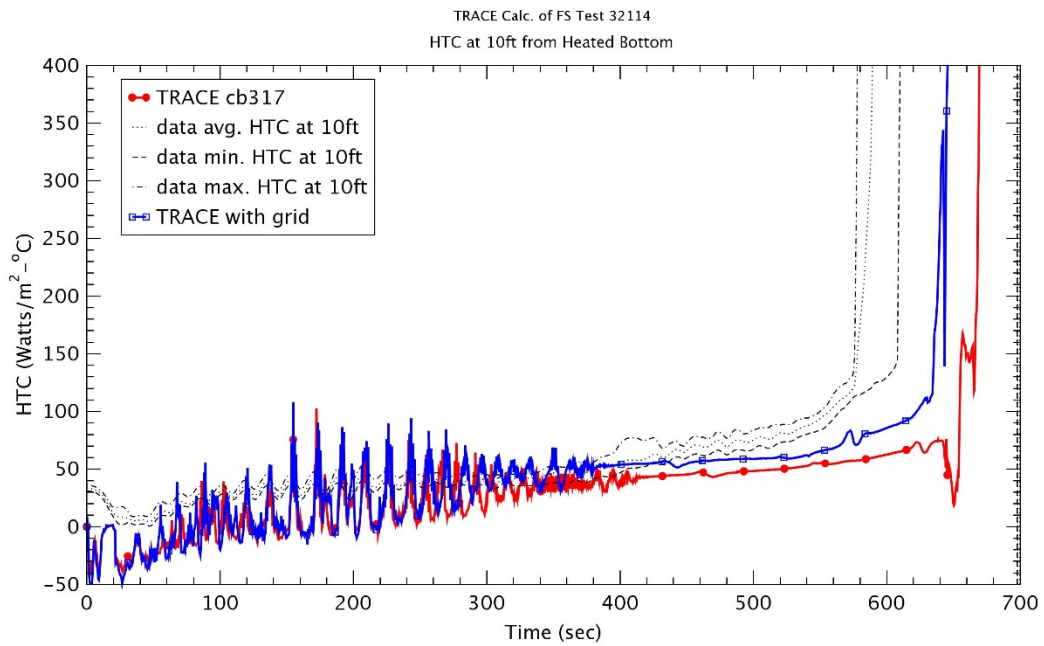


Figure 3-146 Heat Transfer Coefficient at 3.0 m – Run No.32114

3.2.1.8 Summary

In general, the spacer grid would enhance the convective heat transfer due to the flow acceleration and the turbulence increase downstream of grid. Currently, among 4 sub-models, the droplet breakup model is not activated and the grid re-wetting model is not fully implemented in TRACE. Therefore, the enhancement of convective heat transfer and the pressure drop due to the spacer grid could be only evaluated in this study.

As would be expected, the rod temperatures were decreased and the rods were quenched at the earlier time in most tests as the spacer grid model was used. From upper 5 tests of Table 3-2 that the reflood rate was only changed, it could be identified that the lower of the peak rod temperature and the earlier quenching time were predicted as the reflood rate was increased. For high reflood rate as Run No. 31701, the inlet flow is bigger than the quenching rate of rods and the heat transfer became very high. In tests with high reflood rate, the change of peak temperature due to the spacer grid was not large, which resulted from the short heat up period and the faster increase of liquid level by the high reflooding rate.

When the test pressure was lower, the higher rod temperature and the later rod quench were predicted since the liquid approached faster to the relatively lower saturation temperature. The use of spacer grid model predicted relatively larger differences for rod temperature, not for quenching time at lower pressure condition. Also, as the subcooling degree was higher, the decrease amount of quenching time due to the spacer grid was reduced since the high subcooling degree could enhance the heat transfer rate.

In all tests, Run No. 31805 with the lowest reflood rate was affected most significantly for the peak temperature and the quenching time by using the spacer grid model as shown in Table 3-2 and Figures 3.147 ~ 3.148.

Table 3-2 Peak Temperature and Quenching Time at Elevation z = 1.98

Run No.	Peak Temperature (K) (at time)			Quenching Time (sec)		
	W/O grid	With grid	Δ Temp	W/O grid	With grid	Δ Time
31805	1440.9 (113 sec)	1383.9 (65 sec)	57.0	379	347	32
31504	1371.4 (80 sec)	1360.6 (77 sec)	10.8	330	321	9
31203	1270.6 (57 sec)	1264.7 (37 sec)	5.9	252	248	4
31302	1196.4 (24 sec)	1194.0 (19 sec)	2.4	156	152	4
31701	1153.5 (7 sec)	1151.0 (7 sec)	2.5	85	83	2
31108	1202.8 (50 sec)	1186.5 (25 sec)	16.3	200	192	8
32013	1359.2 (60 sec)	1356.5 (58 sec)	2.7	273	268	5
32114	1406.6 (99 sec)	1386.4 (85 sec)	20.2	461	434	27

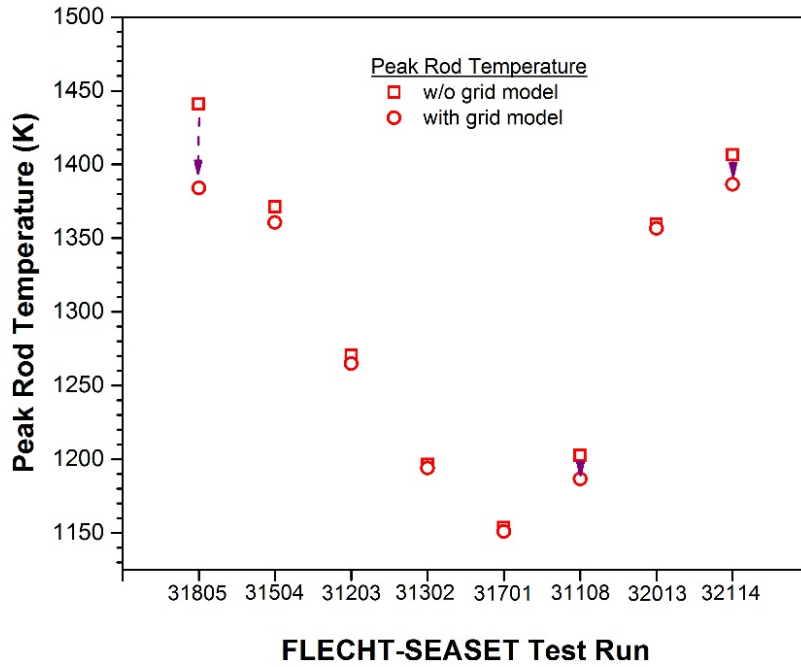


Figure 3-147 Variation of Peak Rod Temperature at Elevation $z = 1.98$

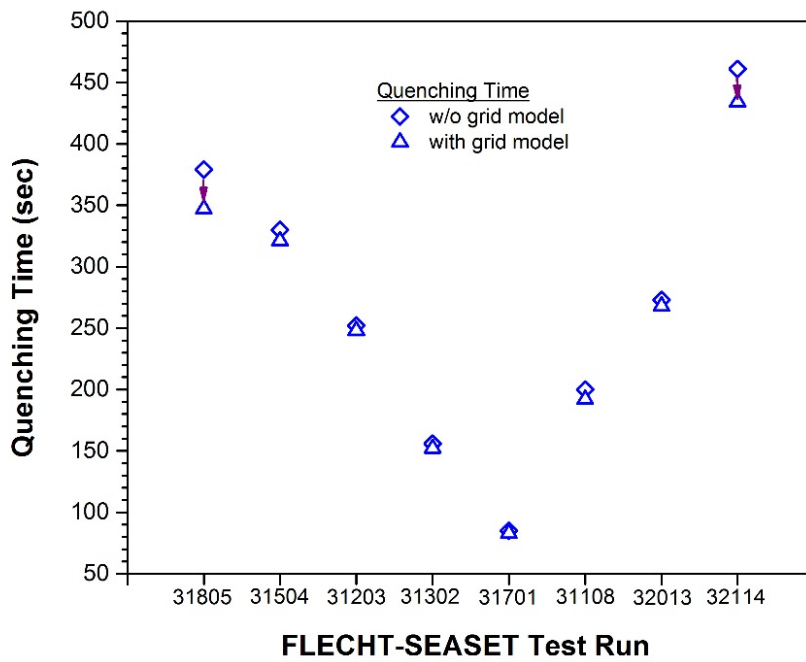


Figure 3-148 Variation of Quenching Time at Elevation $z = 1.98$

4 SENSITIVITY ANALYSIS

4.1 Effect of the Grid Location

From the input manual [2], the spacer grid input for the core region in the PIPE, CHAN, or VESSEL component would be internally considered in the core fuel rod HTSTR models (i.e., enhanced wall heat transfer due to the spacer grid) and in the fluid solution (i.e., additional additive flow loss due to the spacer grid). The HTSTR component could have only one spacer grid located within a given coarse mesh axial level, and then the renoding of a fuel HTSTR component might be required if the core region included a number of spacer grids.

Therefore, the selection of the proper grid location would be very significant in modeling the nodes for separate effect tests and actual plant analyses. Eight spacer grids were installed along 3.6 m heated length in FLECHT-SEASET. In chapter 2, each grid was modeled to locate in the bottom of every other node, and the first grid was located at the bottom of second node, which was just under the heated section. In this study, in order to perform the sensitivity study for the grid location, the locations of spacer grids would change to the top of every other node as shown in Figure 4-1. The first grid was located at the top of first node of test section, and then the lengths of first and last nodes were changed.

- Case-1 : Each grid was located in the bottom of every other node
- Case-2 : Each grid was located in the top of every other node

Among 8 tests in Table 3-1, Run No. 31805 and 31302 were selected for the sensitivity calculations for the grid location in low and high reflood test, respectively.

4.1.1 Run No. 31805

Run No. 31805 was a test with a flooding rate of 2.1 cm/sec at 0.28 MPa and 79 oC inlet subcooling temperature. This is a test with the lowest reflood rate in Table 3-1, and it could be identified that the effect of the spacer grid model was most dominant as described in previous chapter.

When the locations of spacer grids were varied (Case-1 → Case-2), the rod temperatures at various elevations were shown in Figure 4-2 through Figure 4-5. The effect of the grid locations would not be shown at lower elevation ($z < 1.2$ m) with low power density. However, the rod temperature of Case-2 had higher values at elevation $z = 1.98$ with the maximum peak cladding temperature as compared to Case-1. At elevation $z=1.98$, the temperature reduction for Case-2 was ~ 22.9 K, and the quenching time was decreased with ~ 13 sec in comparison to the case without the spacer grid model as shown in Table 4-1. It would be more reasonable to predict the experimental data and showed more conservative results. In TRACE, the heat transfer enhancement effects by the spacer grid were integrated over the downstream axial cells for 50 hydraulic diameters to consider the exponential decay of the enhancement downstream of a spacer grid [3]. The spacer grid enhancement effects for a given cell as well as design factors are multiplied by the original heat transfer coefficient predicted by TRACE for the given cell. Therefore, the HTSTR component had the effect of only one spacer grid located within a given coarse mesh. When the spacer grid was located at the top of node, the original heat transfer coefficient could be evaluated by the heat flux upstream of a spacer grid. The low heat flux upstream of a spacer grid would decrease the enhancement of heat transfer, and then it resulted in the relatively high rod temperature up to the elevation with the peak power. The delayed quenching was predicted due to high rod temperatures for Case-2. However, the difference for the rod temperatures was reduced, and the quenching time was just a little changed for the grid locations at higher elevations ($z > 2.4$ m). The effect of the grid location could depend on the power shape, the

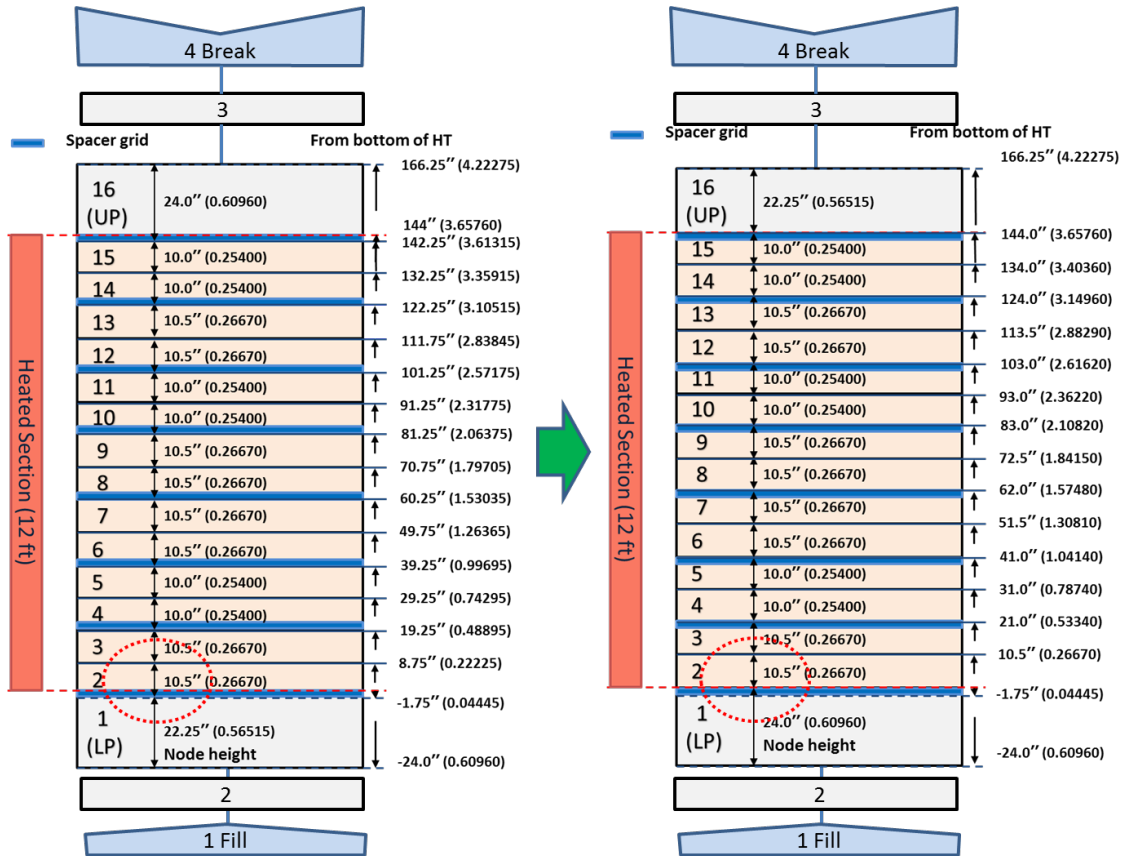
reflood rate, and the node modeling, and then the detailed sensitivity studies was required for various tests.

As shown in Figure 4-6, the quench front for Case-2 was increased rather late, but its difference was not big. Because the number of spacer grids was not changed, the pressure losses due to the spacer grids would be unchanged. The relatively high rod temperature could delay the rise of the quench front.

The heat transfer coefficients (HTCs) at elevation $z = 1.98$ m is presented in Figure 4-7. The average HTC for Case-2 during the reflood was under-predicted in comparison with Case-1. Those predictions were reflected in the relatively high rod temperatures. The steep increase of HTC for Case-2 was delayed since the rod was quenched late due to the high rod temperatures.

Table 4-1 Peak Temperature and Quenching Time at Elevation $z = 1.98$ for Run No. 31805

Case	Peak Temperature (K) (at time)			Quenching Time (sec)		
	W/O grid	With grid	Δ Temp	W/O grid	With grid	Δ Time
Case 1	1440.9 (113 sec)	1383.9 (65 sec)	57.0	379	347	32
Case 2		1418.0 (85 sec)	22.9		366	13



Case-1 Case-2
 Figure 4-1 Node Change for Sensitivity of Grid Location

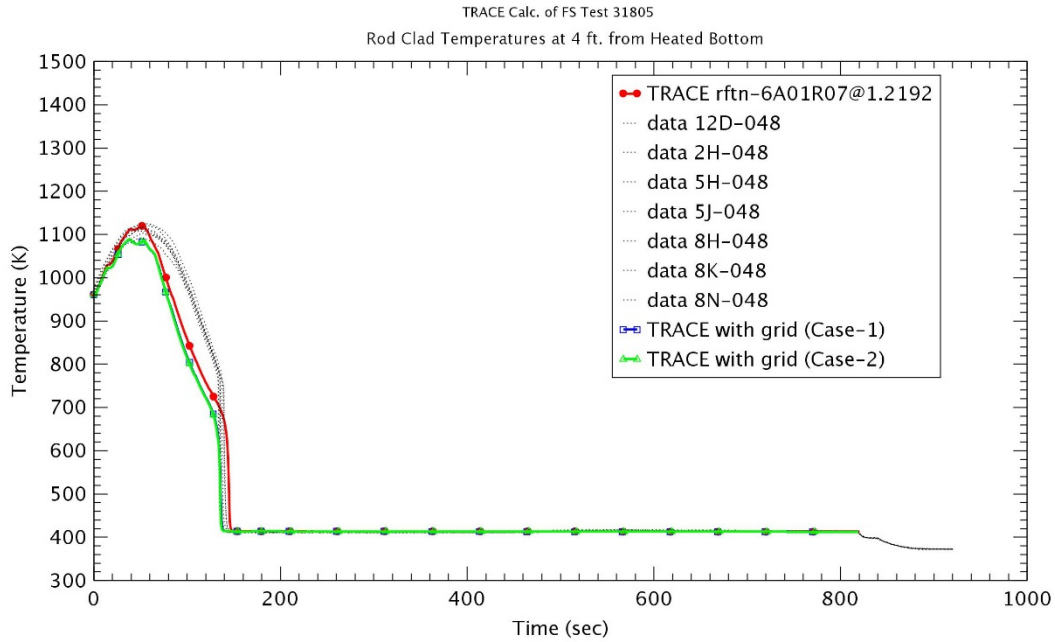


Figure 4-2 Heater Rod Temperature at 1.2 m – Run No.31805

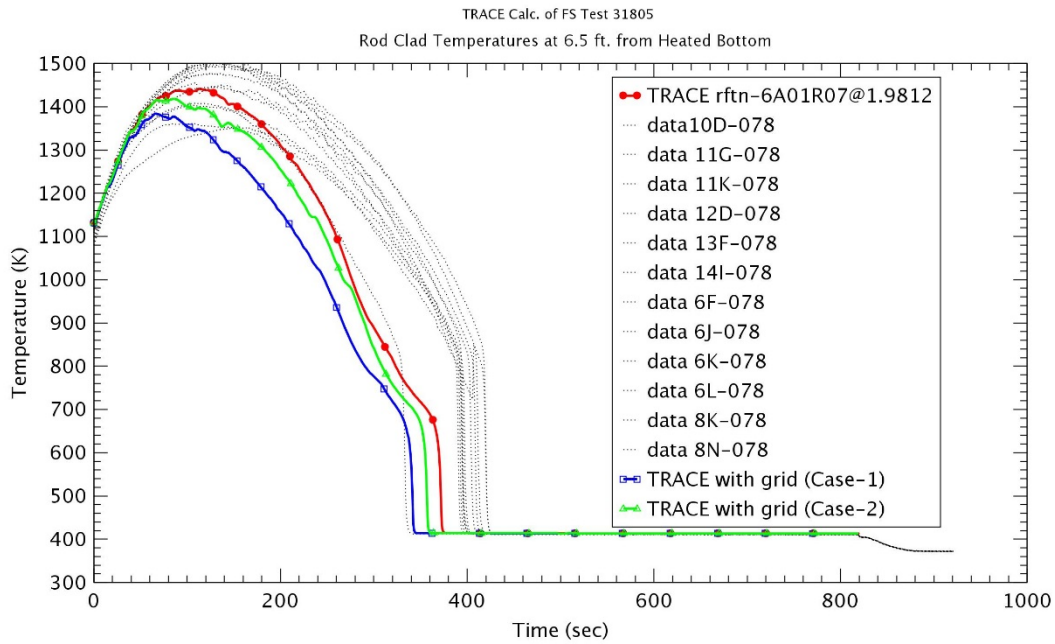


Figure 4-3 Heater Rod Temperature at 1.98 m – Run No.31805

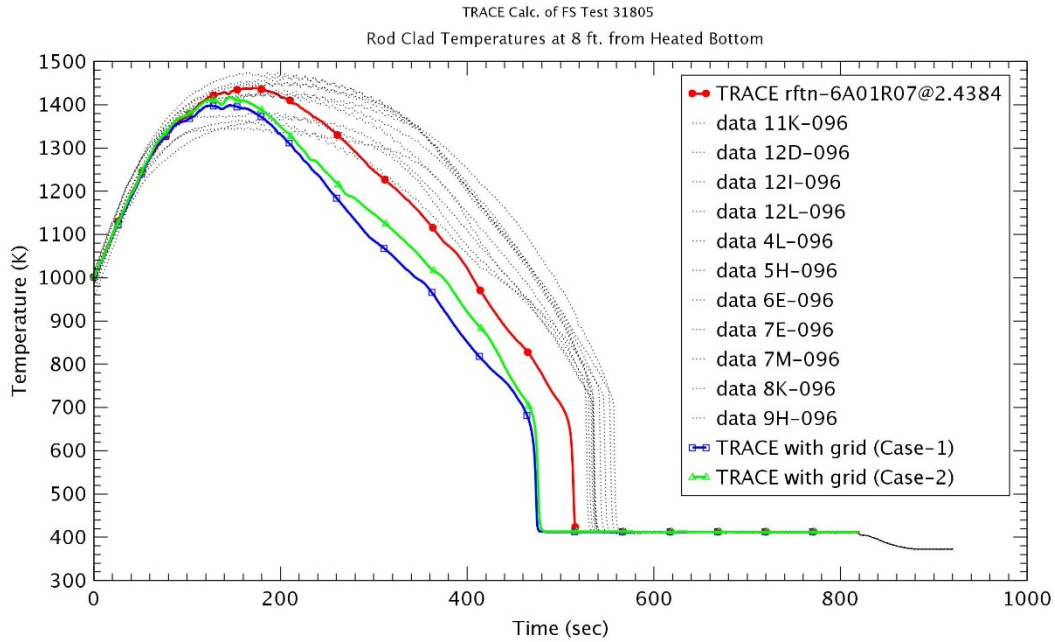


Figure 4-4 Heater Rod Temperature at 2.4 m – Run No.31805

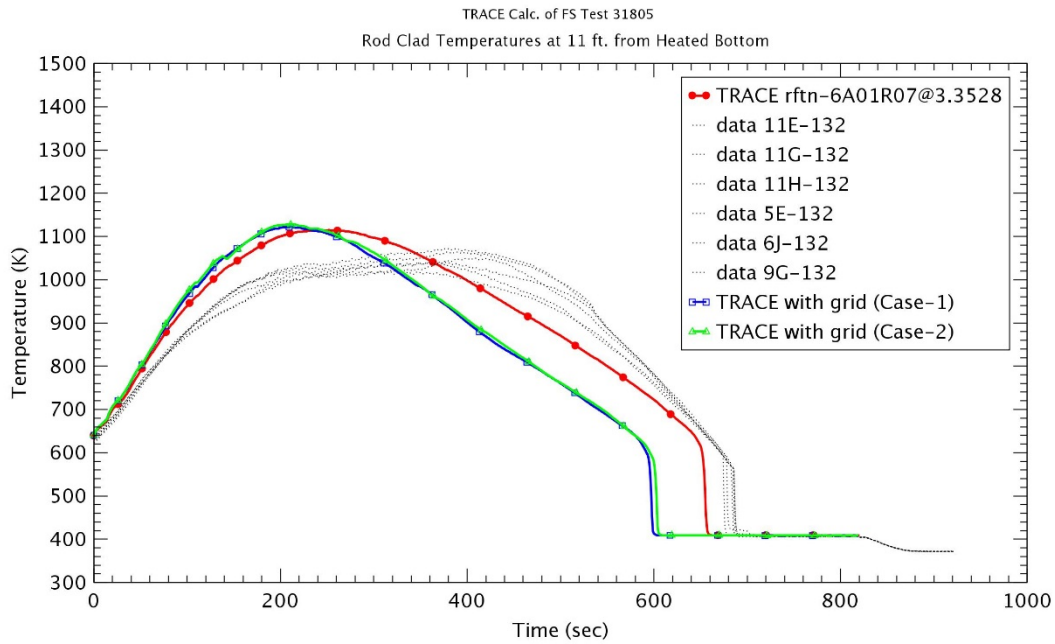


Figure 4-5 Heater Rod Temperature at 3.3 m – No.31805

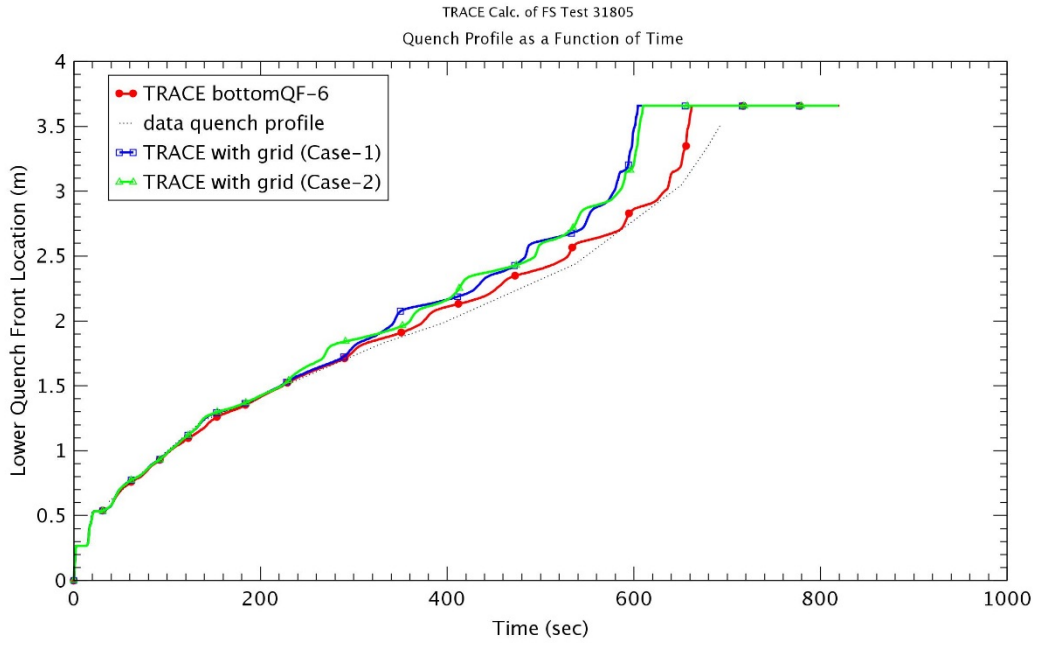


Figure 4-6 Quench Front Profile – Run No.31805

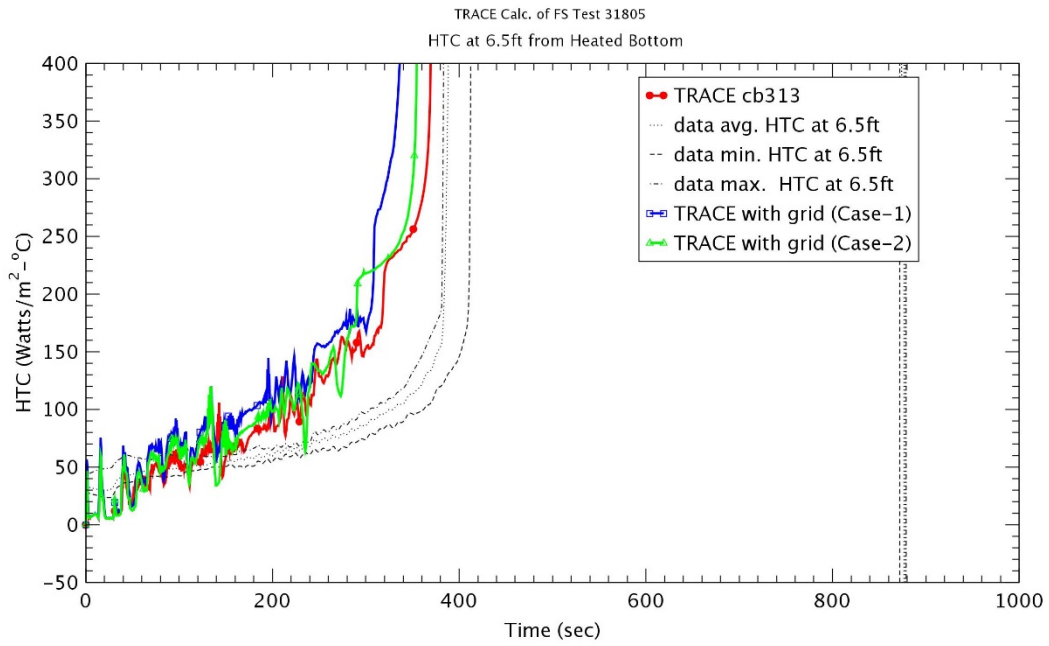


Figure 4-7 Heat Transfer Coefficient at 1.98 m – Run No.31805

4.1.2 Run No. 31302

Run No. 31302 was a test with a flooding rate of 7.65 cm/sec at 0.28 MPa and 78 oC inlet subcooling temperature as shown in Table 3-1. This was the same as Run No. 31805 except that it had three times over the reflood rate.

The rod temperatures at various elevations were shown in Figure 4-8 through Figure 4-11. The rod temperatures for Case-2 were similar to those for Case-1 at elevation $z < 1.98$ m (6.5 ft). The effect of the grid locations would be weakened by the high reflood rate which did not largely change the original heat transfer coefficient with time. However, the rod temperatures for Case-2 were predicted higher than those for Case-1 at elevation $z = 2.4$ m. This reflected the behavior of HTC as shown in Figure 4-13. The effect of the grid locations was not showed well for the rod temperature and the quenching time at elevation $z = 3.3$ m with low power density. At elevation $z = 1.98$ with the maximum peak cladding temperature, the temperature reduction for Case-2 was ~ 7.8 K, and the quenching time was decreased with ~ 5 sec in comparison to the case without the spacer grid model as shown in Table 4-2.

As shown in Figure 4-12, in Case-2 that the spacer grid was at the top of node, the quench front increased with almost same speed as Case-1. Because of the high reflood rate, the effect of the grid locations was not predicted for this test. The heat transfer coefficients (HTCs) at elevation $z = 2.4$ m was plotted in Figure 4-13. As shown in Figure, the HTC for Case-2 was under-predicted during the reflood phase as compared to Case-1. This might result from the use of the low original heat transfer coefficient since the spacer grid was modeled at the top of node. The steep increase of HTC for two cases occurred almost simultaneously since the rod quenching time was the same due to the high reflood rate.

Table 4-2 Peak Temperature and Quenching Time at Elevation $z = 1.98$ for Run No. 31302

Case	Peak Temperature (K) (at time)			Quenching Time (sec)		
	W/O grid	With grid	Δ Temp	W/O grid	With grid	Δ Time
Case 1	1196.4 (24 sec)	1194.0 (19 sec)	2.4	156	152	4
Case 2		1188.6 (18 sec)	7.8		151	5

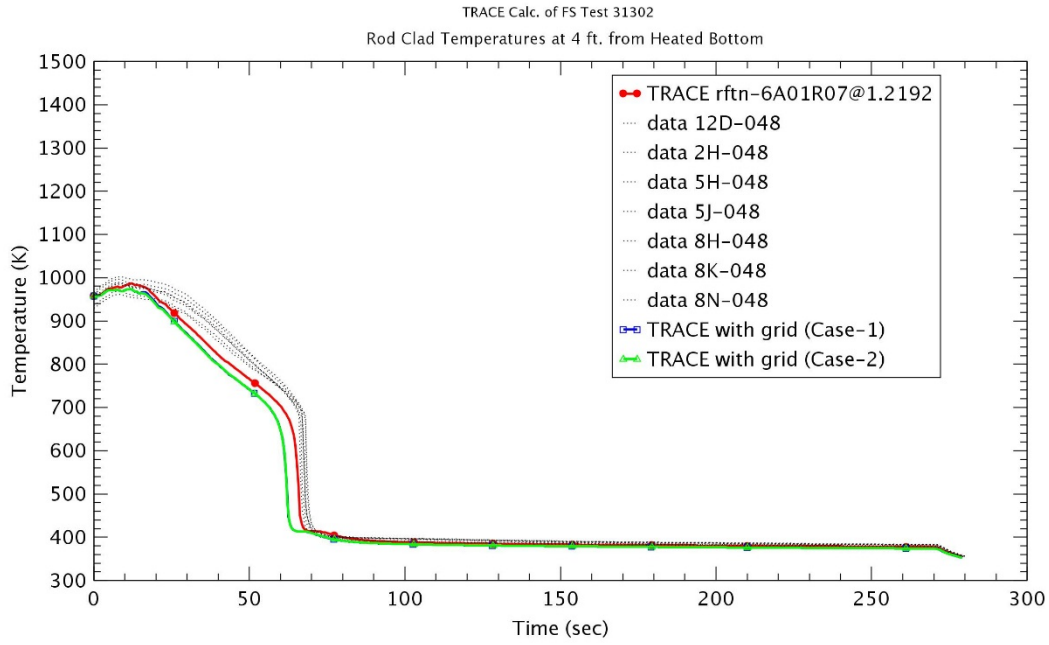


Figure 4-8 Heater Rod Temperature at 1.2 m – Run No.31302

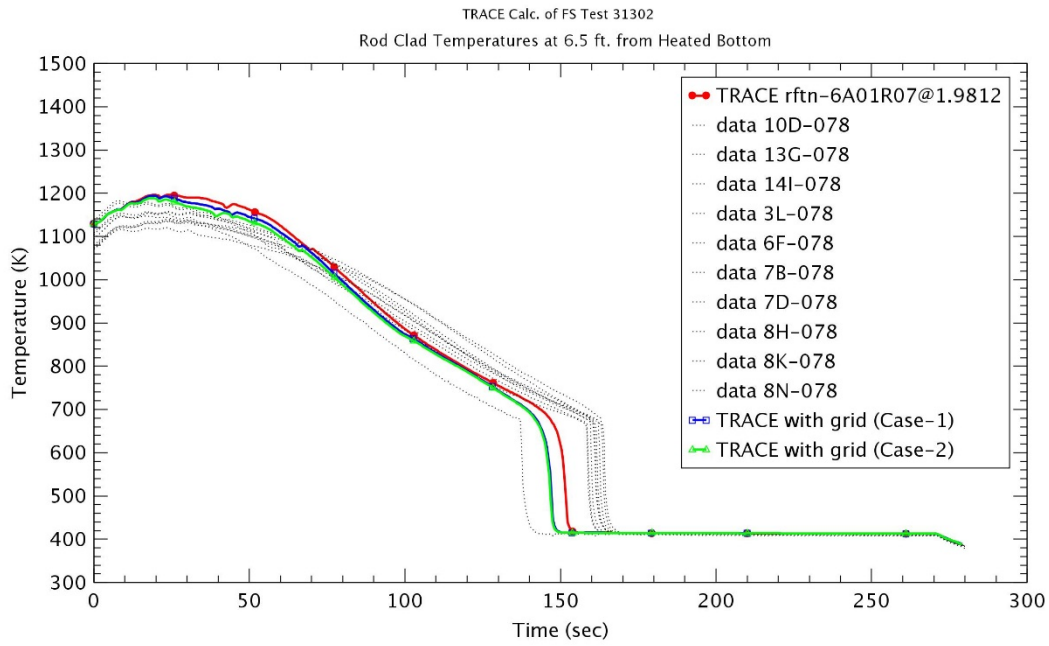


Figure 4-9 Heater Rod Temperature at 1.98 m – Run No.31302

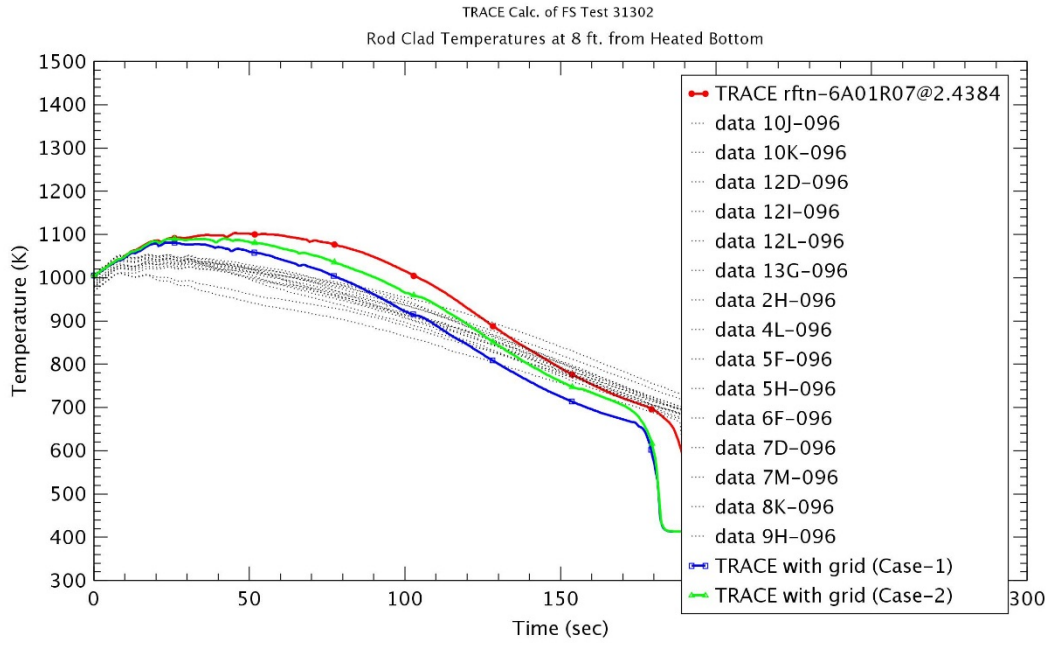


Figure 4-10 Heater Rod Temperature at 2.4 m – Run No.31302

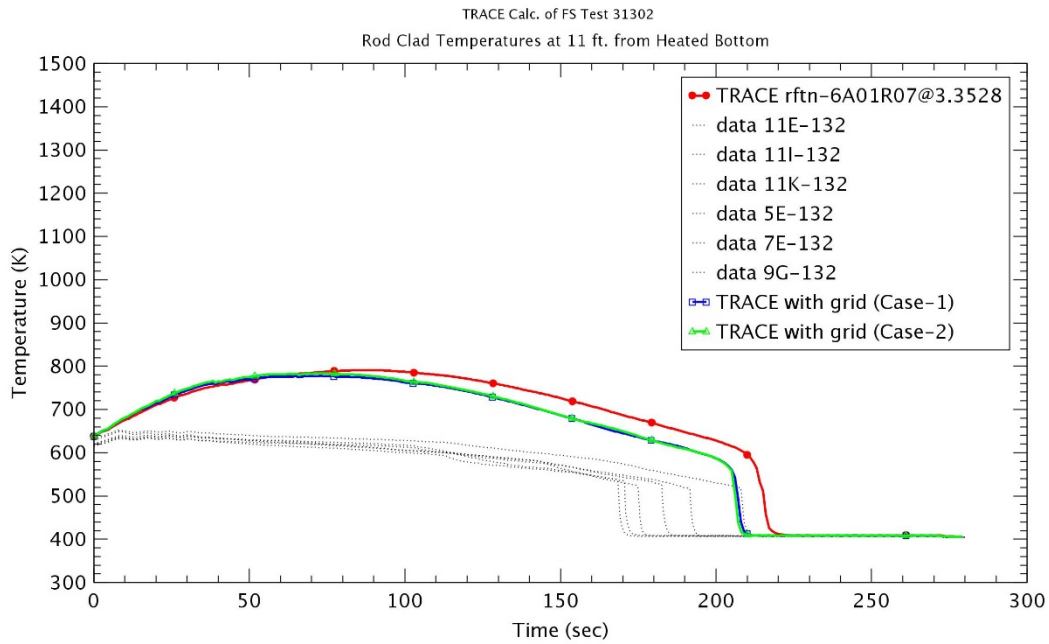


Figure 4-11 Heater Rod Temperature at 3.3 m – No.31302

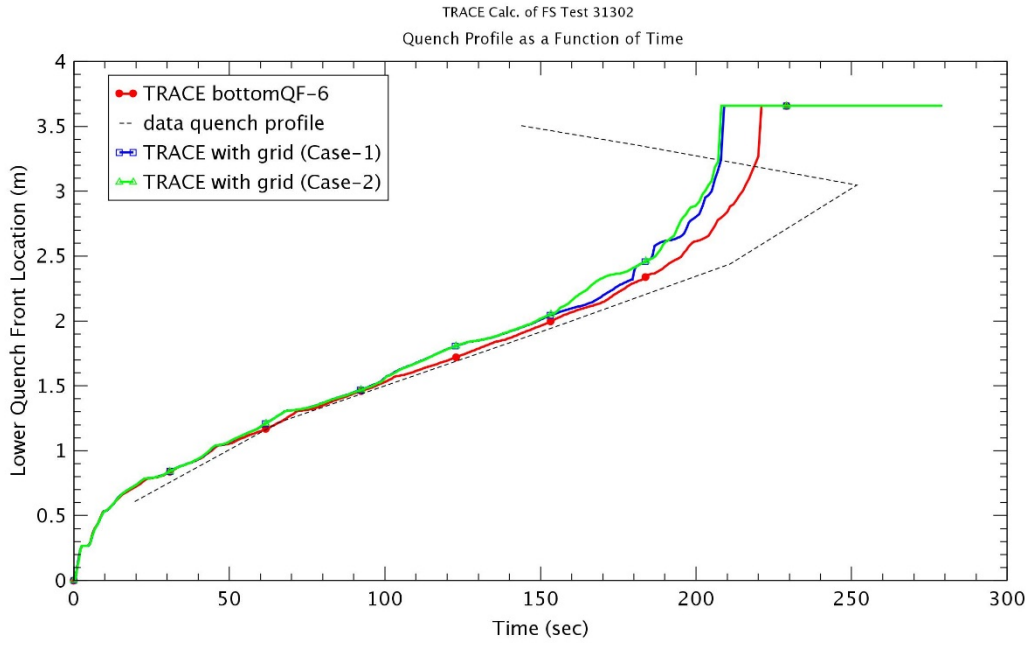


Figure 4-12 Quench Front Profile – Run No.31302

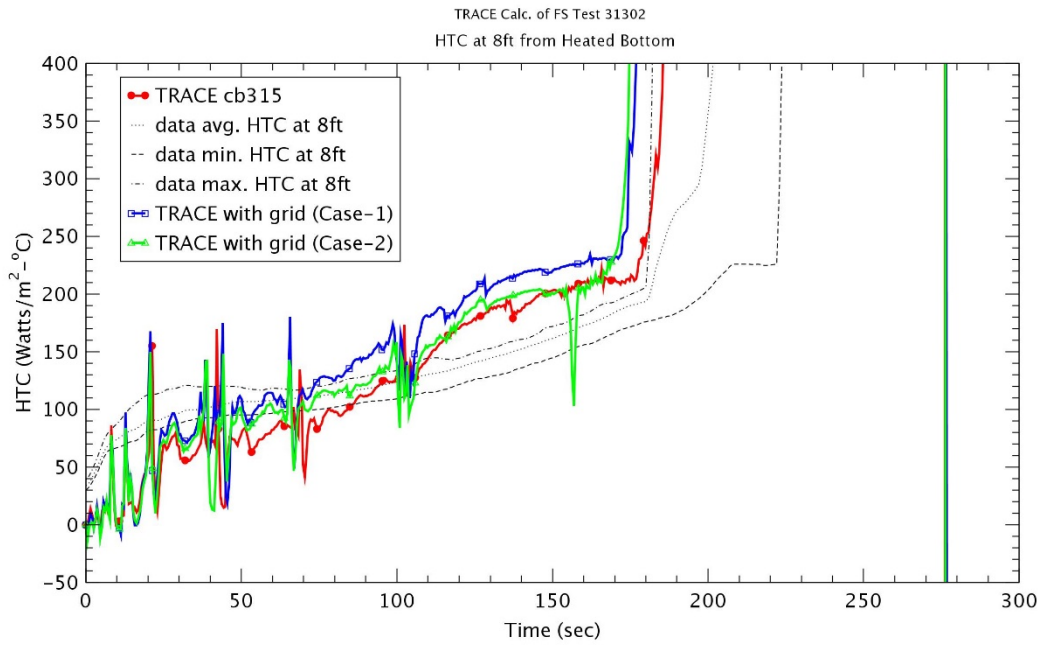


Figure 4-13 Heat Transfer Coefficient at 2.4 m – Run No.31302

4.2 Comparison with Spacer Grid Model of RELAP5

Currently, the RELAP5 [15] was updated as version 3.3jy by implementing the KNF (KEPCO Nuclear Fuel Co.) reflood model and the spacer grid model [16]. These models were theoretically based on the research was conducted by T.S. Choi [14]. Especially, the spacer grid model could be divided into three sub-models: Single-phase heat transfer enhancement, Grid rewet, and Droplet breakup.

The spacer grid model of RELAP5 is somewhat different from that of TRACE. For the convective heat transfer enhancement, the enhancement due to the acceleration of the flow (Part 1 of Eq. (1)) was only considered in RELAP5 that it has been used also in COBRA-TF [17]. The convective heat transfer enhancement could be under-estimated in tests with mixing vanes since Part 2 of Eq. (1) could be large enough to influence to downstream near to spacer grid. For fuel bundles with typical mixing vane, the enhancement for mixing vanes could be below ~ 20% of the enhancement due to the flow acceleration up to ~ 0.4 m downstream of the spacer grid. However, the effect for mixing vanes might be not shown in FLECHT-SEASET since the spacer grid without mixing vanes was installed in it. The laminar enhancement factor, F was used in TRACE, but it was not in RELAP5.

For the grid re-wetting model, the similar heat balance equation to Eq. (5) of TRACE was also implemented in RELAP5, but there were some differences in the detailed modelling. The radiation heat flux from the rods to the grid was obtained by using an electrical circuit analogy [3] in TRACE, but it was calculated explicitly in RELAP5 [14]. The correlation for the rewetting temperature in RELAP5 was also different from that in TRACE. The rewetting temperature in RELAP5 was selected as the maximum value between the homogeneous nucleation temperature and two other minimum film boiling temperatures, while it in TRACE was determined by the minimum film boiling temperature.

For the droplet breakup model, the suggested model by Yao, Hochreiter, and Cai [11] was used in TRACE, but the KAIST model [18] was used in RELAP5 since it could cover a wider range of the droplet Weber number, including Yao, Hochreiter, and Cai's data. As the droplet Weber number was larger, the smaller shattered droplets occurred. In the upper region where the droplet dispersed flow regime was long maintained in which the droplet velocity and the number of entrained droplet were large, the droplet Weber number was large, and then the vapor temperature could be reduced because of the higher interfacial heat transfer between the droplets and the vapor phase. This could decrease the rod temperature and expedite the quenching time at that region.

Currently, the droplet breakup model and the grid re-wetting model were not fully implemented in TRACE. Therefore, it was very difficult to compare directly to the effect of the spacer grid model between RELAP5 and TRACE. In this study, the results by RELAP5 could provide insights into the implementation and the modification associated with the spacer grid model.

The RELAP5 nodalization for the FLECHT-SEASET was shown in Figure 4-14 and was almost similar to the previous study [19]. The test section including a heater with 3.66 m length was divided into 20 nodes, and the upper and lower time-dependent volumes were modeled to define the fluid conditions, which represented the upper and lower plenums, respectively. Seven spacer grids were considered except for a first grid below the heater. Some initial conditions could be modified to use the same conditions as TRACE calculations in Chapter 3. Therefore, the actual inlet flow rate, temperature, and the upper plenum pressure were used as input with a function of time. The rod power was considered as a function of time.

Among 8 tests in Table 3-1, Run No. 31805 and 31302 were selected as low and high reflood test for the assessment for the spacer grid model of RELAP5, respectively.

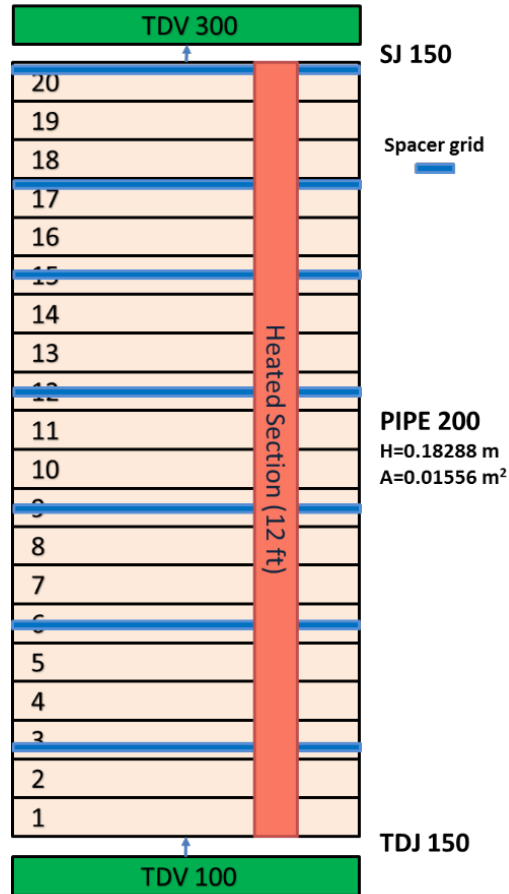


Figure 4-14 RELAP5 Nodalization for the FLECHT-SEASET Test

4.2.1.1 Effect of the new reflood model in RELAP5

RELAP5 has been broadly used in licensing LBLOCA analyses such as Westinghouse, OPR1000, and APR1400 plants in Korea. The KNF reflood model [14] was developed to improve the potential problems of RELAP5 Mod3.3 that the peak cladding temperature were under-predicted and the rod quenching occurred too early in FLECHT-SEASET tests. Therefore, the dry wall selection logic, the droplet size and inverted slug size, the post-dryout interfacial, film boiling heat transfer, and transition boiling models, etc. were modified in RELAP5. The effect of the new reflood model for Run. No 31805 was shown in Figure 4-15 through Figure 4-17. The developmental code version of KNF (r5m33p03rev0-F6.exe) was used in this calculation. As mentioned in previous study [14], it could be identified that the rod temperatures were increased and the rod quenches were delayed, especially at high elevations. It was confirmed that the KNF reflood model could show the more improved results in Run. No 31805 although the rod quenching time was over-predicted in elevation $z = 3.0$ m.

At that time, the spacer grid model was implemented together with this reflood model. It was modeled that the KNF reflood model could be invoked without the spacer grid input, but the spacer grid input could not be activated without the KNF reflood model. Figure 4-18 through Figure 4-20 plotted the relations between the KNF reflood model and the spacer grid input. As shown in Figures, if the KNF reflood model was not used, the calculation results were not changed with or without the spacer grid input. It could be found that the KNF reflood model should be required to activate the spacer grid input.

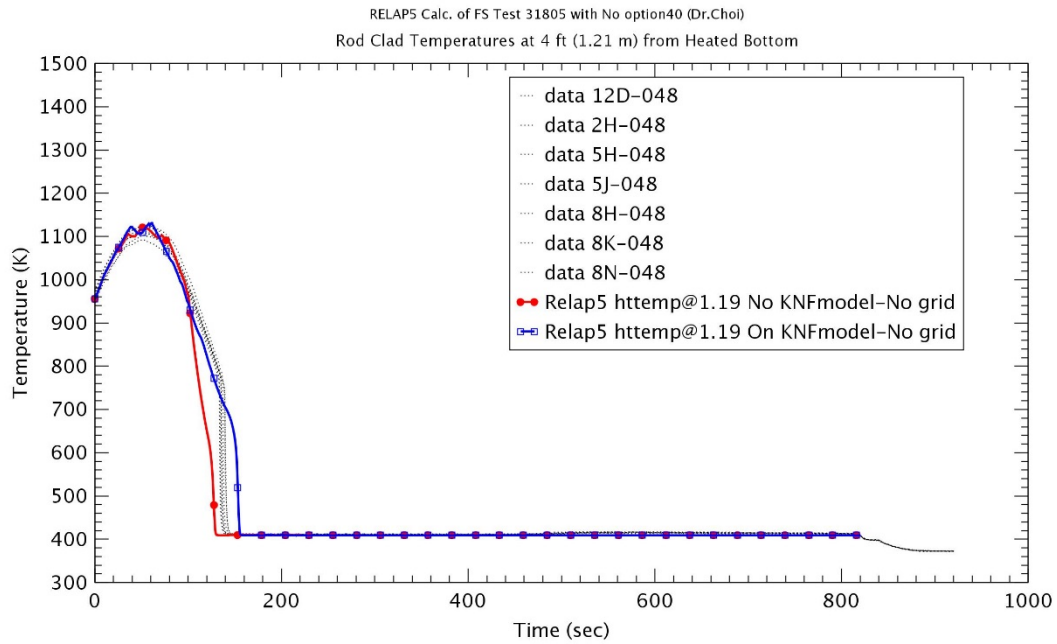


Figure 4-15 Heater Rod Temperature at 1.2 m – Run No.31805

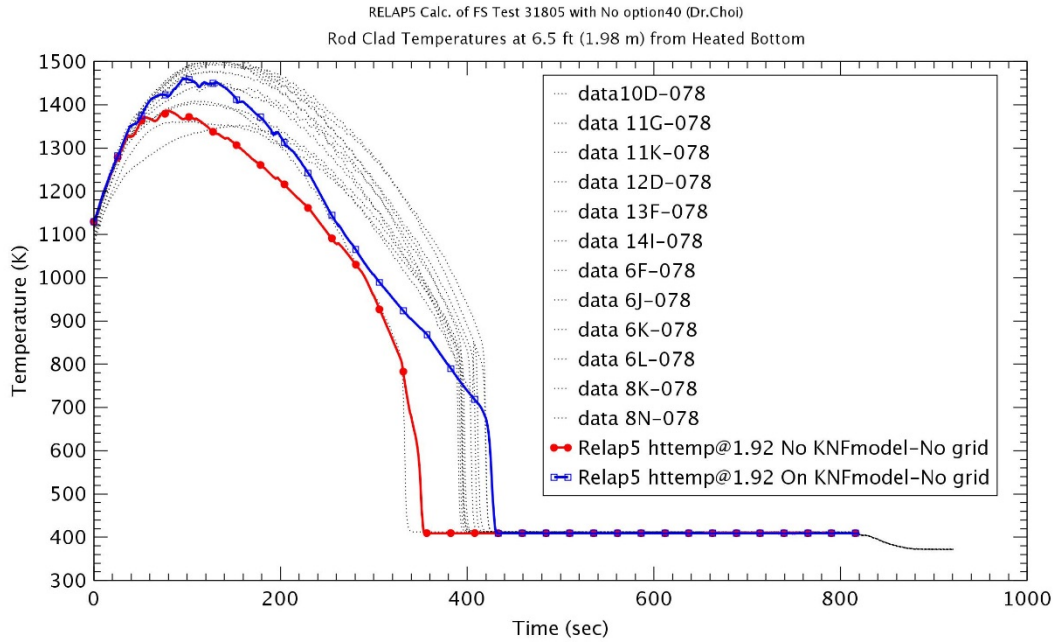


Figure 4-16 Heater Rod Temperature at 1.98 m – Run No.31805

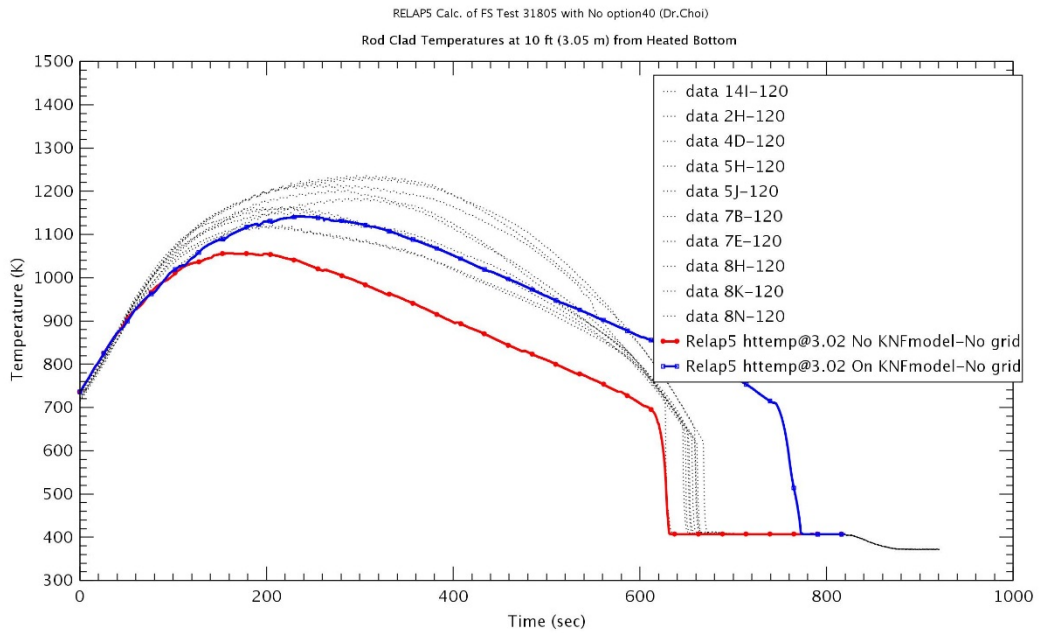


Figure 4-17 Heater Rod Temperature at 3.0 m – Run No.31805

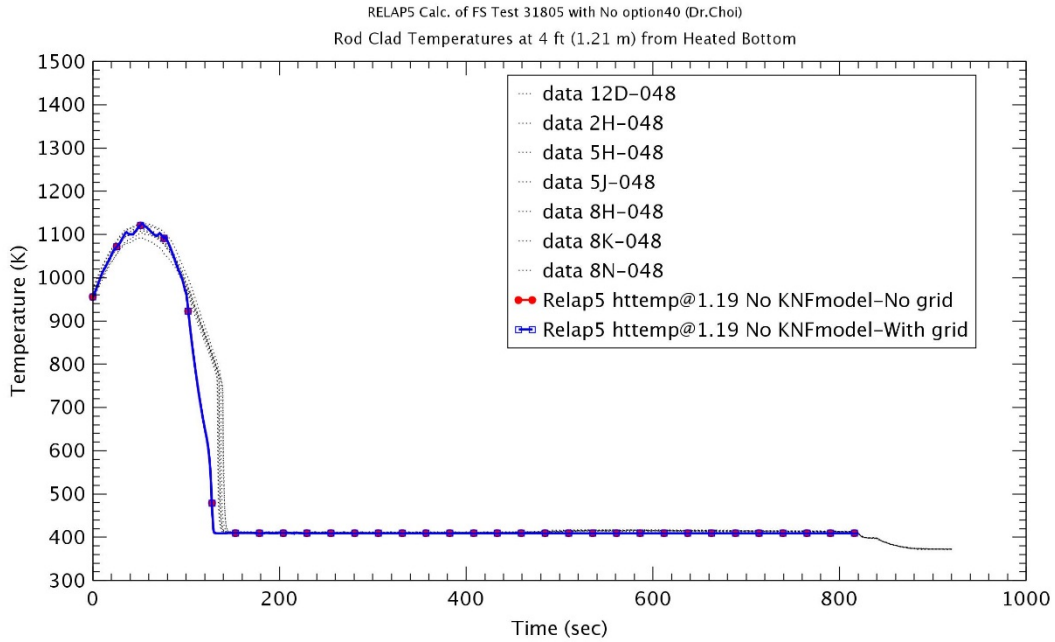


Figure 4-18 Heater Rod Temperature at 1.2 m – Run No.31805

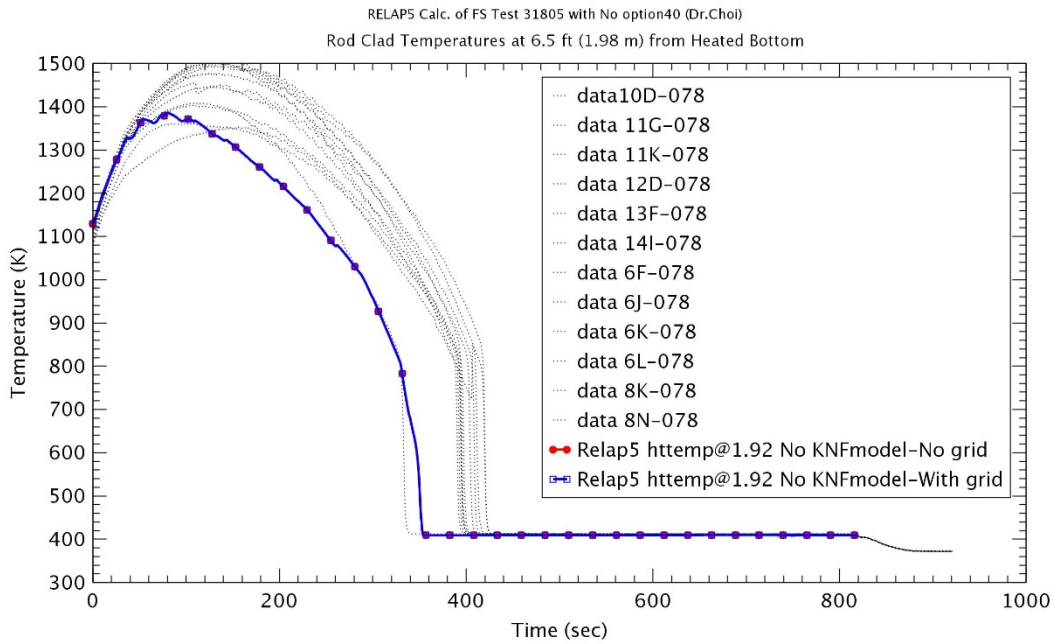


Figure 4-19 Heater Rod Temperature at 1.98 m – Run No.31805

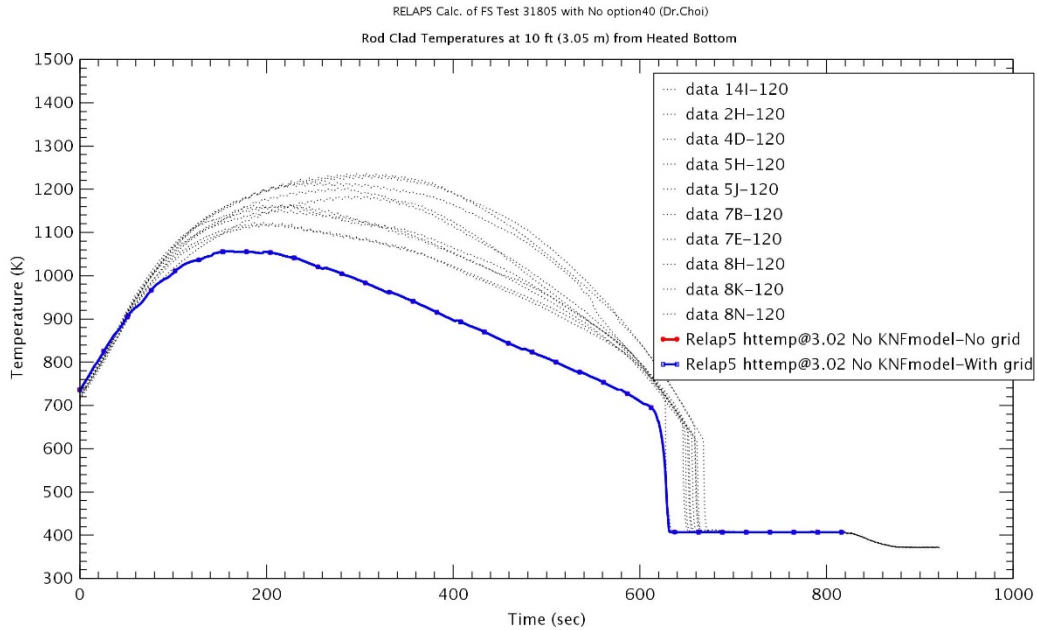


Figure 4-20 Heater Rod Temperature at 3.0 m – Run No.31805

4.2.1.2 Effect of the spacer grid model in RELAP5

In order to identify the effect of the spacer grid model of RELAP5 for Run No.31805, the rod temperatures at various elevations were shown in Figures 4.21 ~ 4.26. The typical reflood process was shown well that the rod was heating up in the initiation of reflood, turning to reduce during the reflood, and finally quenching. In the RELAP5 calculation without the spacer grid model, the predicted peak temperature along elevation agreed reasonably with the experimental data. Especially, the peak rod temperature at higher elevations ($z \geq 3.0$ m) had better prediction results as compared to those in TRACE. The maximum peak rod temperature was also shown at elevation $z=1.98$ m (6.5 ft). However, the quenching time was over-predicted even at the low elevation. This would show well the characteristics of new KNF reflood model such as the increase of rod temperature, the delay of quenching time as described in Figure 4-15 through Figure 4-17. When the spacer grid model was applied, the effect of mixing vane was not considered since the egg-crate grid was installed in the FLECHT-SEASET. As shown Figures 4.21 ~ 4.26, the effect of the spacer grid model did not show significantly up to elevation $z = 2.4$ m, but the peak temperatures with the spacer grid model had the lower values at higher elevations ($z \geq 3.0$ m) and were under-predicted the experimental data in comparison with those without the spacer grid model. The earlier rod quenches were also predicted in the case with a spacer grid model.

For the effect of the spacer grid model, it is difficult to find the meaningful comparison results between TRACE and RELAP5 in a quantitative perspective since they were different in the nodalization, the numerical scheme, and the applied thermal-hydraulic models. Therefore, several potential causes for differences of two codes could be considered in a qualitative point of view.

When the results of RELAP5 were compared with those of TRACE, the effect of the spacer grid model was more significantly shown in TRACE although the convective heat transfer enhancement was only considered in TRACE. The rod temperatures of TRACE started to reduce due to the spacer grid even

at elevation $z = 1.2$ m as shown in Figure 3-6. However, the rod temperatures of RELAP5 did not change at elevation $z \leq 1.98$ m except for the earlier quenching at elevation $z = 1.98$ m. As the elevation was higher over $z = 1.98$ m, the effect of the spacer grid in RELAP5 became larger as shown in Figure 4-27.

The axial temperature profile at 150 sec was shown in Figure 4-28 to identify the effect of sub-models in RELAP5. The droplet breakup model gave the biggest effect on the rod temperatures among three models taking into account the effect of spacer grids. The effect of the droplet breakup model was more significant at the higher elevation since the droplet velocity and the number of entrained droplet could be larger at the higher elevation. The rod temperature was locally decreased because of the increase of convective heat transfer immediately downstream of a spacer grid ($z \sim 2.1$ m), but the convective heat transfer enhancement did not have a significant effect on the rod temperatures during the entire transient as shown in Figure 4-28. This was the biggest difference between TRACE and RELAP5. For the spacer grid heat transfer enhancement, the effect of the convective heat transfer in TRACE was much larger than that in RELAP5.

This might be come from the modeling characteristics in TRACE and the use of the laminar enhancement factor. As explained above, the convective heat transfer enhancement effects in TRACE were integrated over the downstream axial cells for 50 hydraulic diameters to consider the exponential decay of the enhancement downstream of a spacer grid. In this test, 50 hydraulic diameters is about 0.5 m, and this effect could be considered for longer downstream cells in comparison with that of RELAP5. The distance from the grid location to the cell center was only considered in RELAP5 with an assumption being far enough apart between the spacer grids.

Secondly, the laminar enhancement factor was implemented in TRACE to take account for the additional enhancement effects that were observed for high void fraction, laminar flows. This factor can vary from 1.0 to 1.75 with Reynolds number, and the convective heat transfer enhancement of TRACE could be varied as shown Figure 4-29. Therefore, these differences between two codes could result in the more significant enhancement for the convective heat transfer in TRACE. As shown in Figure 3-6 ~ 3-12, the effect of the convective heat transfer enhancement in TRACE could be shown in the entire heated rod, but its effect in RELAP5 could be limited immediately downstream of a spacer grid. Actually, the convective heat transfer enhancement had a significant effect immediately downstream of a spacer grid, and its effect may be evaluated too much in TRACE. The detailed further studies would need to be performed to evaluate the effect of sub-models. The convective heat transfer enhancement ought to be also modified since the spacer grid could influence upstream convective heat transfer.

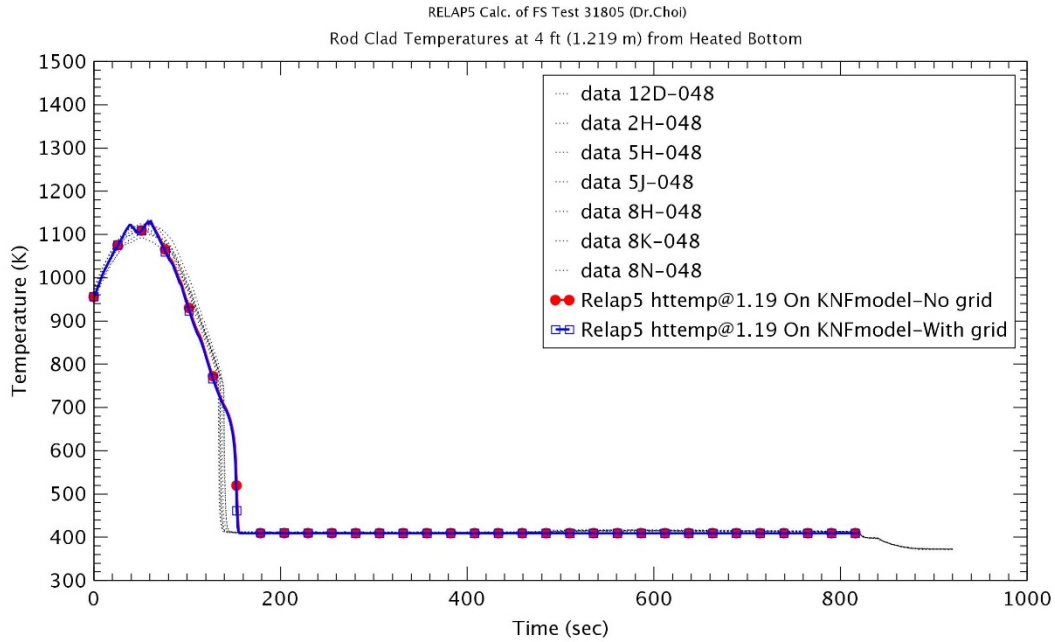


Figure 4-21 Heater Rod Temperature at 1.2 m – Run No.31805

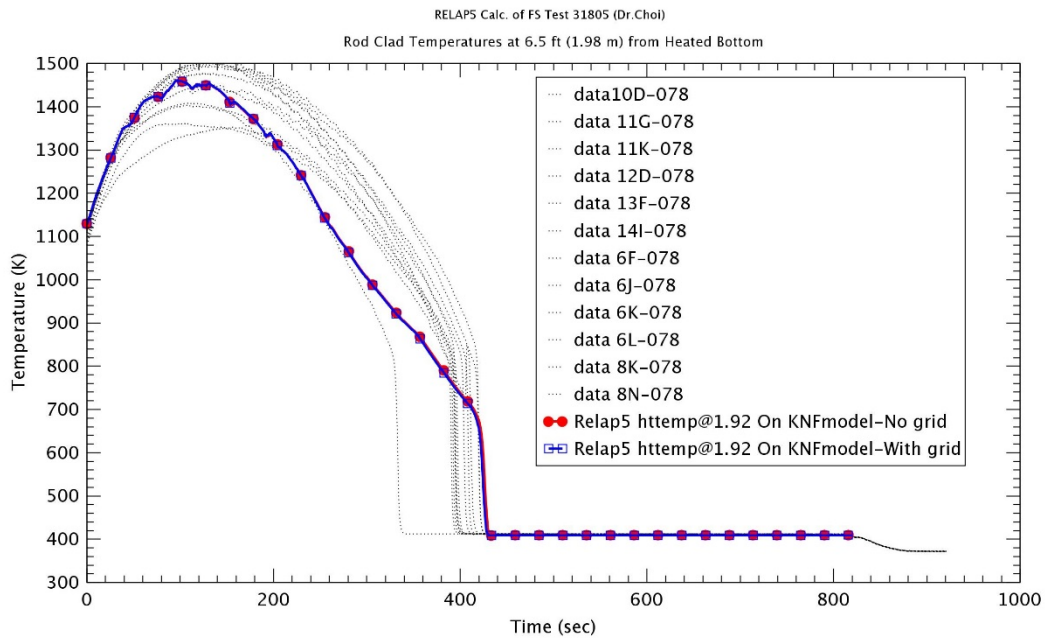


Figure 4-22 Heater Rod Temperature at 1.98 m – Run No.31805

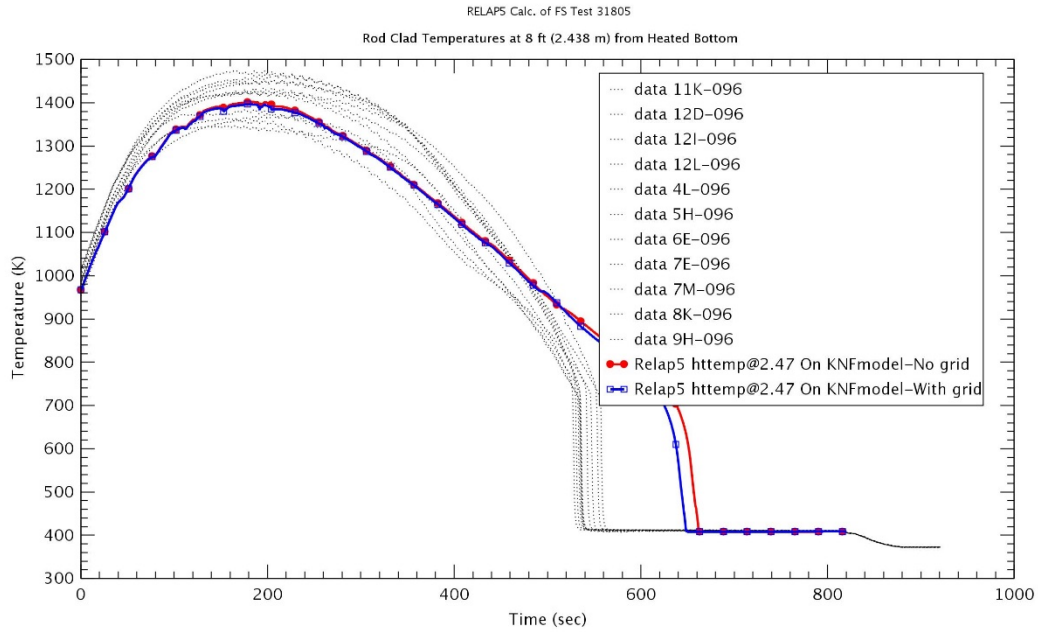


Figure 4-23 Heater Rod Temperature at 2.4 m – Run No.31805

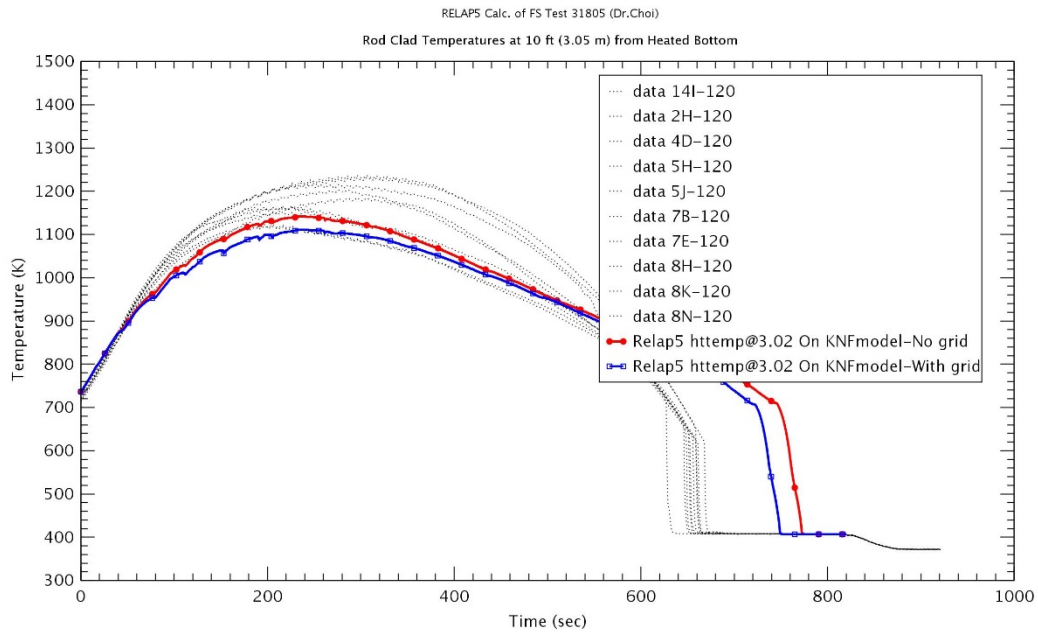


Figure 4-24 Heater Rod Temperature at 3.0 m – Run No.31805

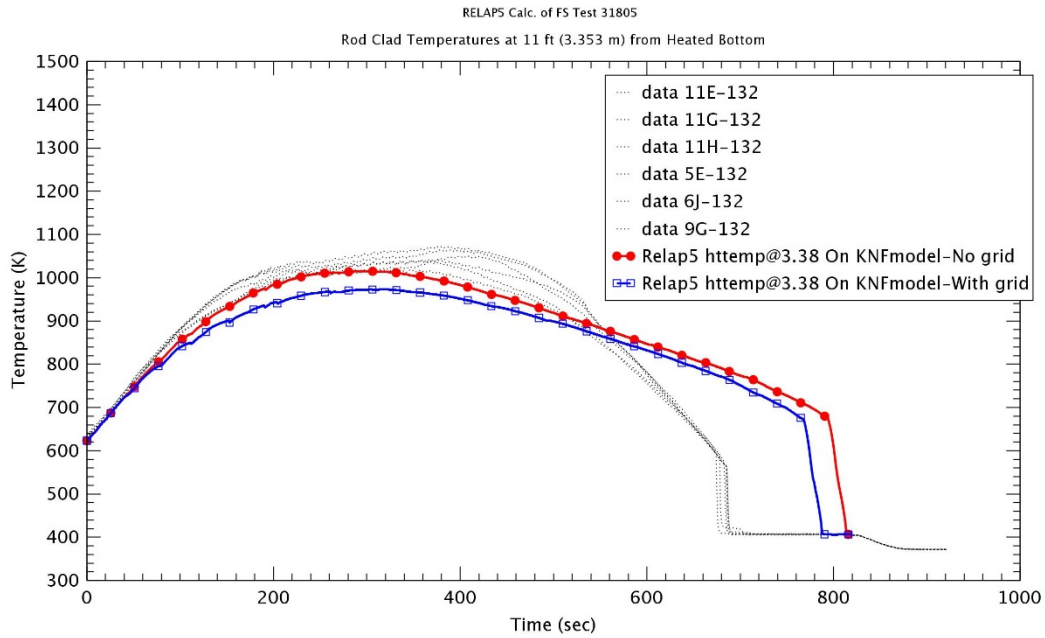


Figure 4-25 Heater Rod Temperature at 3.3 m – Run No.31805

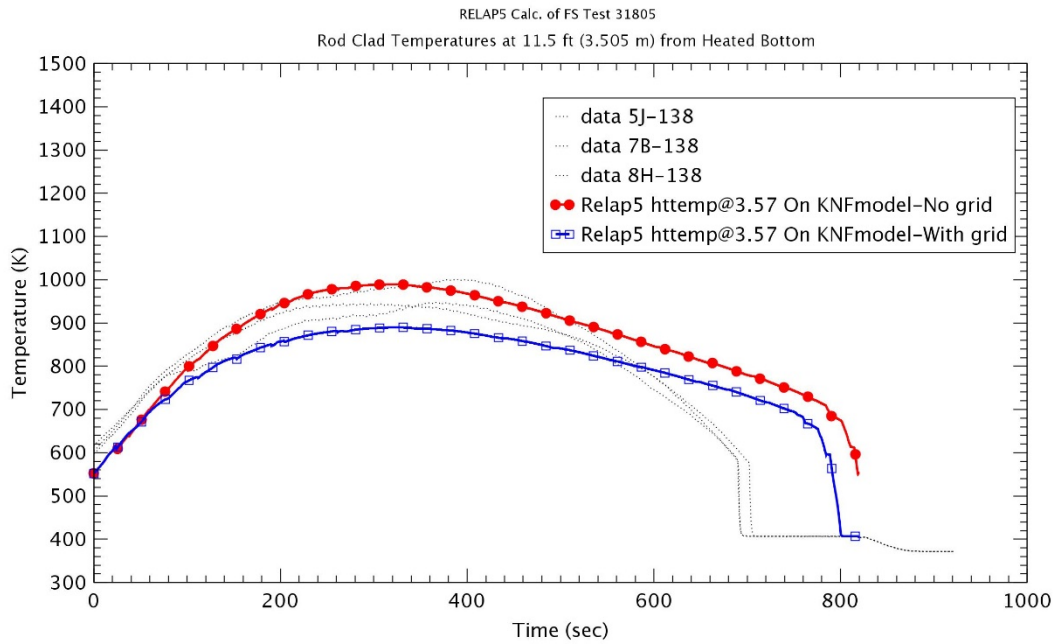


Figure 4-26 Heater Rod Temperature at 3.5 m – Run No.31805

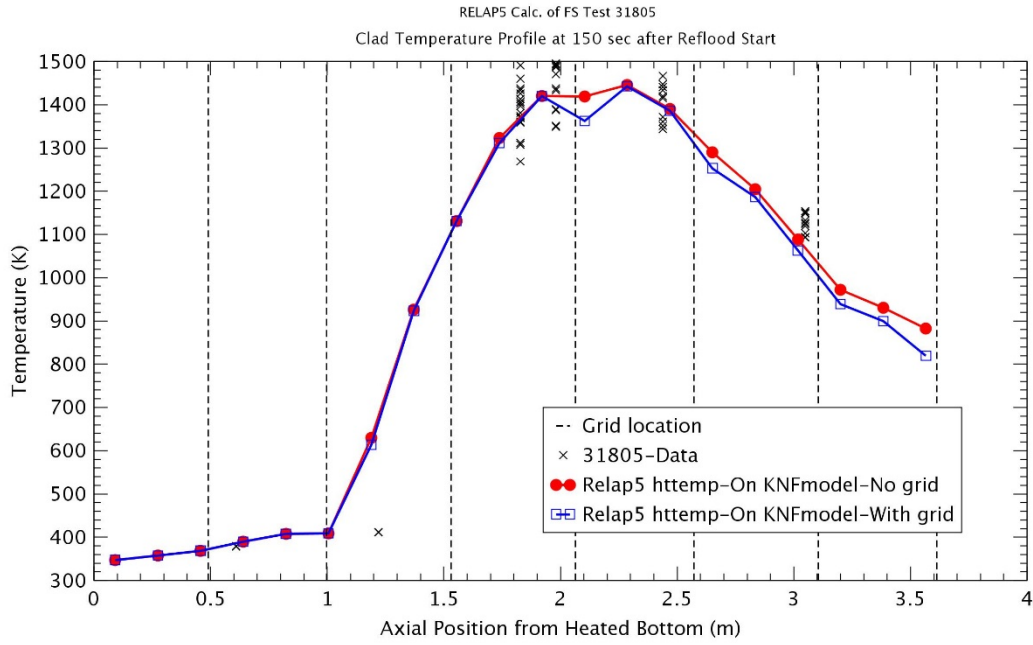


Figure 4-27 Axial Rod Temperature Profile at 150 sec – Run No.31805

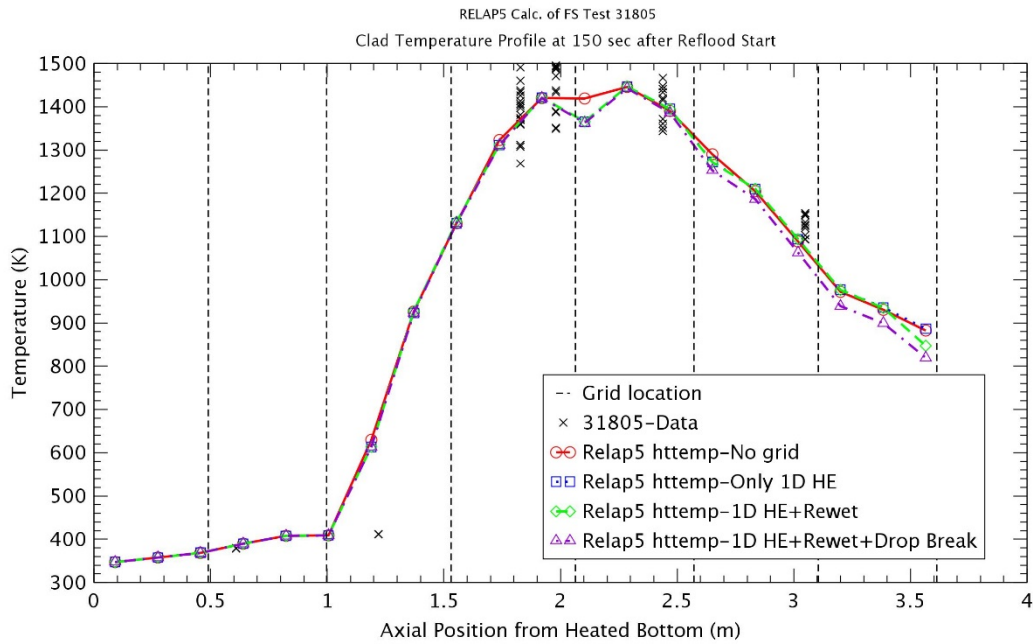


Figure 4-28 Axial Rod Temperature Profile for Sub-models at 150 sec – Run No.31805

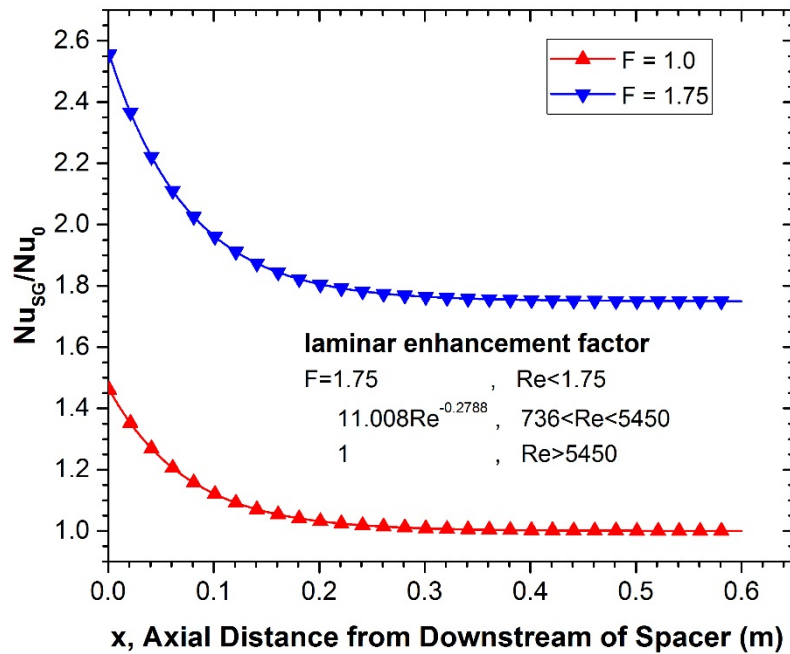


Figure 4-29 Variation of Heat Transfer Enhancement for Laminar Enhancement Factor

Figure 4-30 through Figure 4-35 represent the rod temperatures at various elevations for Run No.31302 with relatively high flooding rate. In the RELAP5 calculation without the spacer grid model, the rod temperatures along elevation were predicted well the experimental data. Especially, the peak rod temperature at higher elevations ($z \geq 2.4$ m) had better prediction results as compared to those in TRACE. The maximum peak rod temperature was also shown at elevation $z=1.98$ m (6.5 ft). The stepwise behaviors of the rod temperature could be showed at elevations $z \geq 2.4$ m due to the use of a coarse node and the relatively high reflood rate. The quenching time also showed a good agreement with the experimental data except for earlier quenching at some elevations. When the spacer grid model was applied, the rod temperatures did not changed significantly up to elevation $z = 1.98$ m. The peak temperatures with the spacer grid model had the lower values at higher elevations ($z \geq 3.0$ m), but they were not largely deviated from the experimental data in comparison with those without the spacer grid model. The rod quenches were also occurred at earlier time as a result of the heat transfer enhancement due to a spacer grid.

As compared to TRACE results in Figures 3.59 ~ 3.66, the effect of the spacer grid model in TRACE was more significantly shown, and it was also similar to the Run No.31805. As described above, these results may be come from the modeling characteristics in TRACE and the use of the laminar enhancement factor. The convective heat transfer enhancement may be excessively large if the laminar enhancement factor will be large.

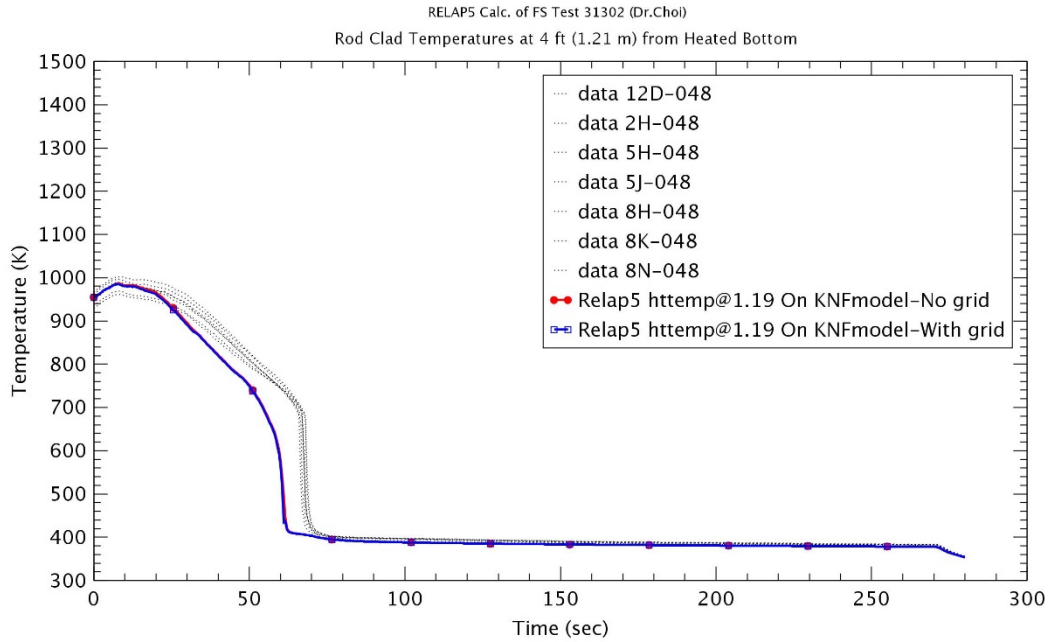


Figure 4-30 Heater Rod Temperature at 1.2 m – Run No.31302

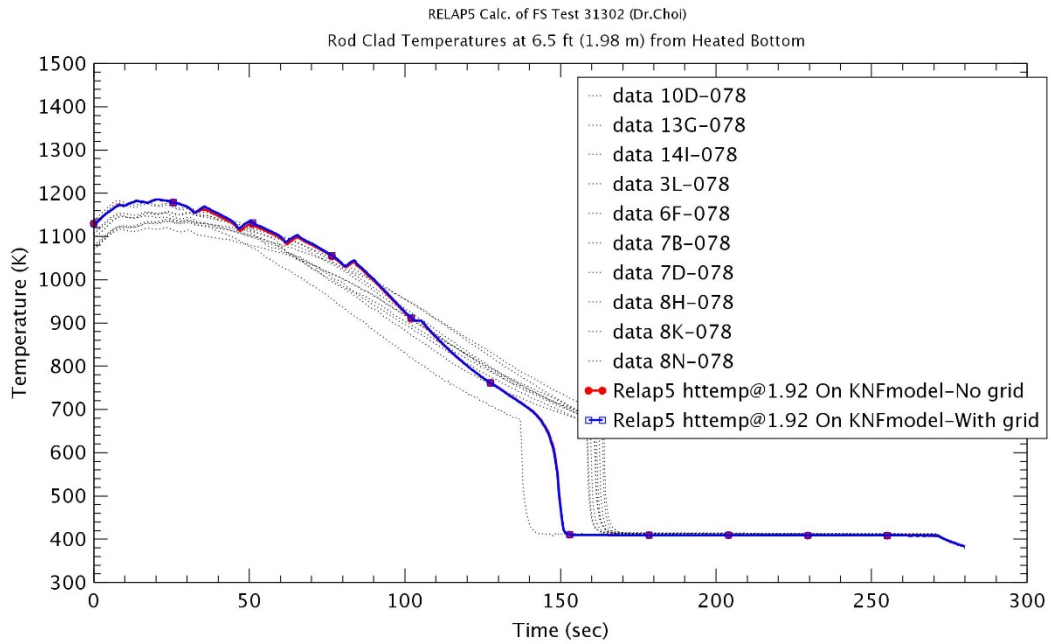


Figure 4-31 Heater Rod Temperature at 1.98 m – Run No.31302

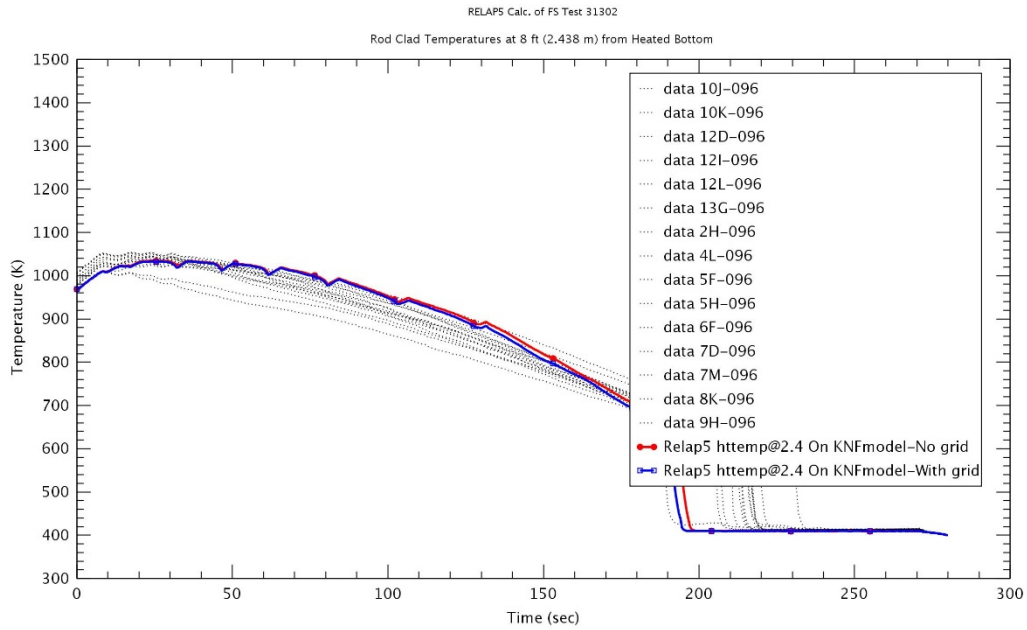


Figure 4-32 Heater Rod Temperature at 2.4 m – Run No.31302

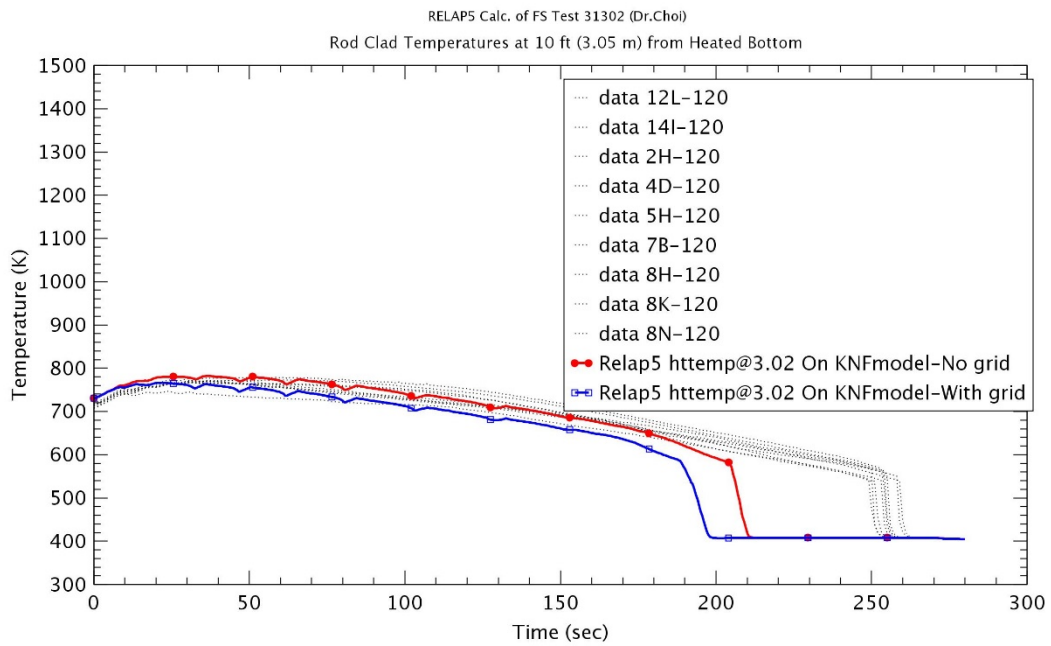


Figure 4-33 Heater Rod Temperature at 3.0 m – Run No.31302

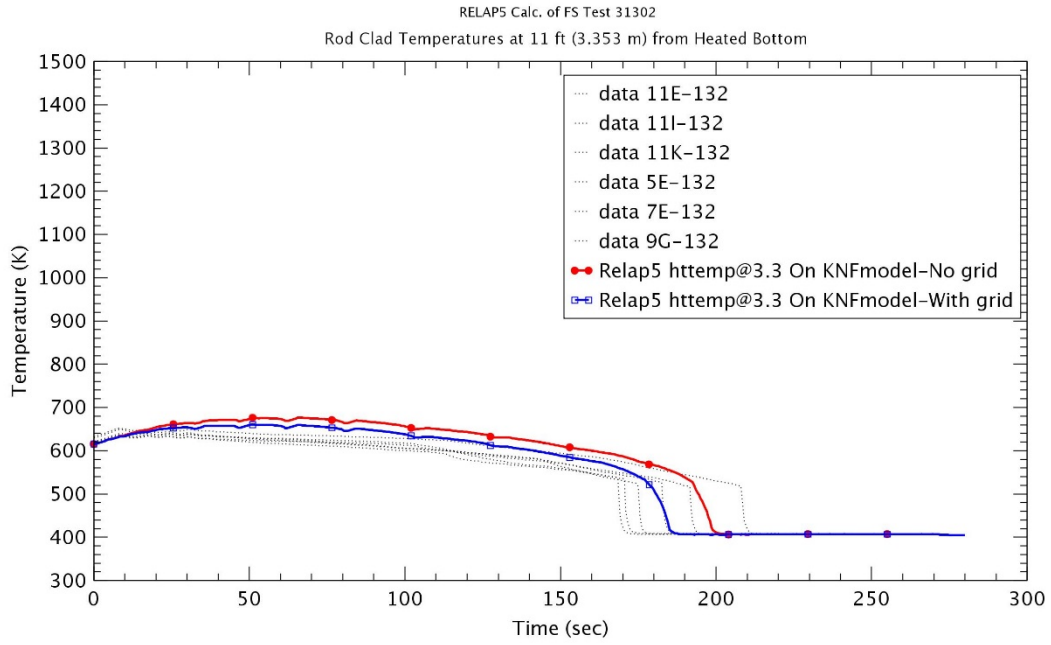


Figure 4-34 Heater Rod Temperature at 3.3 m – Run No.31302

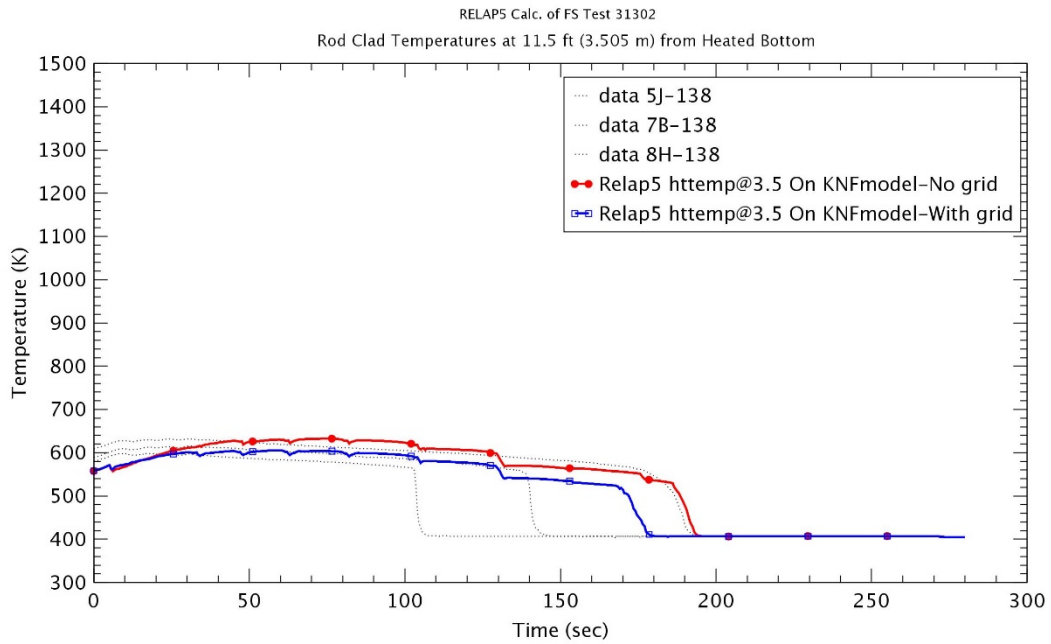


Figure 4-35 Heater Rod Temperature at 3.5 m – Run No.31302

Based on the theoretical study [14] and the developmental version of KNF, the KNF reflood model and the spacer grid model were initially implemented to RELAP5/MOD3.3 patch4 Version 3.3jy in October 2014, and they have been modeled in the latest developmental Version 3.3km (February 2016). According to RELAP5 input manual, the KNF reflood model could be used by Option 40 of Card 1 and invoked regardless of the KNF grid input (43000000 cards). However, the spacer grid model could be applied only when the option 40 was used in Card 1. This could be identified in the calculations of Figures 4.18 ~ 4.20.

In this study, the calculations for various FLECHT-SEASET tests were performed by the latest distributed RELAP5 versions (Version 3.3jz & 3.3kl), and two codes actually produced same results for this tests. The used input decks were the same as the calculations for a developmental version of KNF. The rod temperatures at various elevations for Run No.31805 were shown in Figures 4.36 ~ 4.38. When the spacer grid model was applied, the peak rod temperature had the higher values up to elevation $z = 1.98$ m. The peak rod temperature especially at elevation $z = 1.98$ m was largely increased due to the spacer grid. It is not the expected result. When the spacer grid was applied, the flow area is reduced and the convective heat transfer is promoted due to the flow acceleration and the turbulence increases and then the rod temperature would be usually decreased and the rod quenches were expedited. However, this decrease of the rod temperature was not shown in Figures 4.36 ~ 4.38. The results were contrary to those in Figures 4.21 ~ 4.24 using the same input decks.

Figure 4-39 through 4.41 showed the results for the use of KNF reflood model (Option 40) and spacer grid input (43000000 cards). The results with a spacer grid and no Option 40 (Green line) were completely in accord with those with a spacer grid and Option 40 (Cyan line). It was also an unusual thing that the effect of spacer grid model was significantly shown in Figures 4.39 ~ 4.41 even though Option 40 was not used in Card 1. For example, in the case with a spacer grid model (Green line), the growth of rod temperature and the delay of quenching time were predicted as compared with the case without it (Red line). It was also contrary to what we expected.

Consequently, as these results were compared to those in Figures 4.15 ~ 4.26, the current RELAP5 version (Version 3.3jz ~ 3.3kl) including the KNF reflood and spacer grid models may have some troubles to implement these models. Therefore, the detailed errors should be found and corrected in the further study.

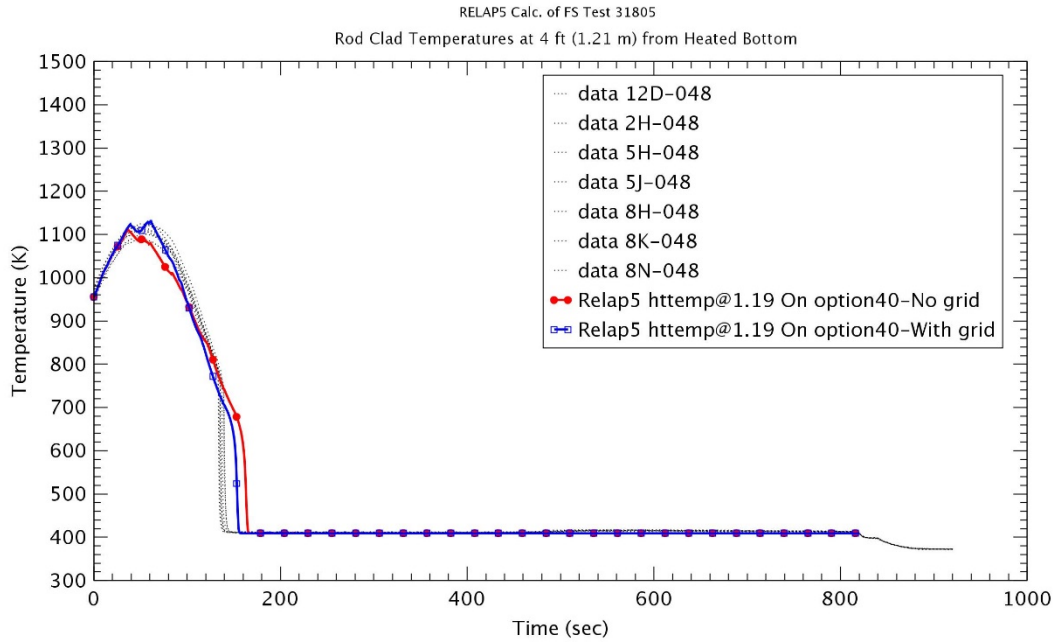


Figure 4-36 Heater Rod Temperature at 1.2 m – Run No.31805

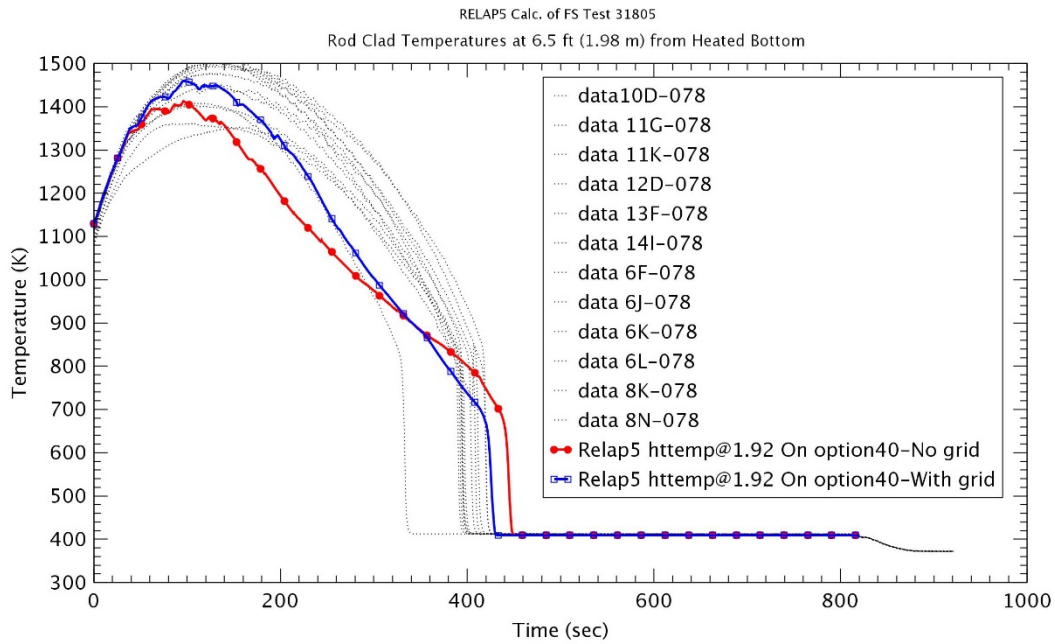


Figure 4-37 Heater Rod Temperature at 1.98 m – Run No.31805

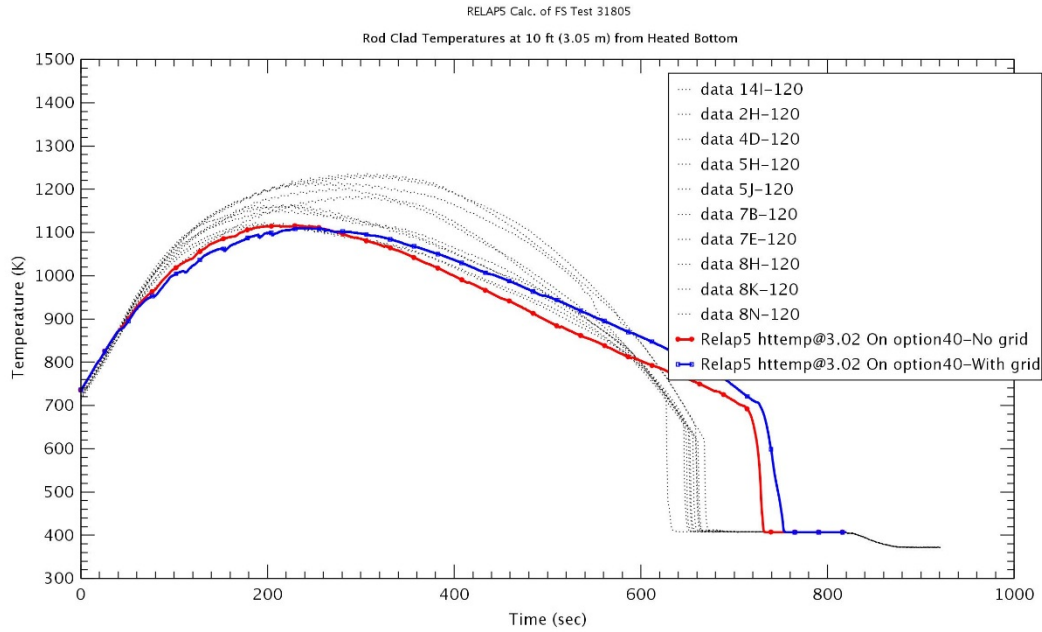


Figure 4-38 Heater Rod Temperature at 3.0 m – Run No.31805

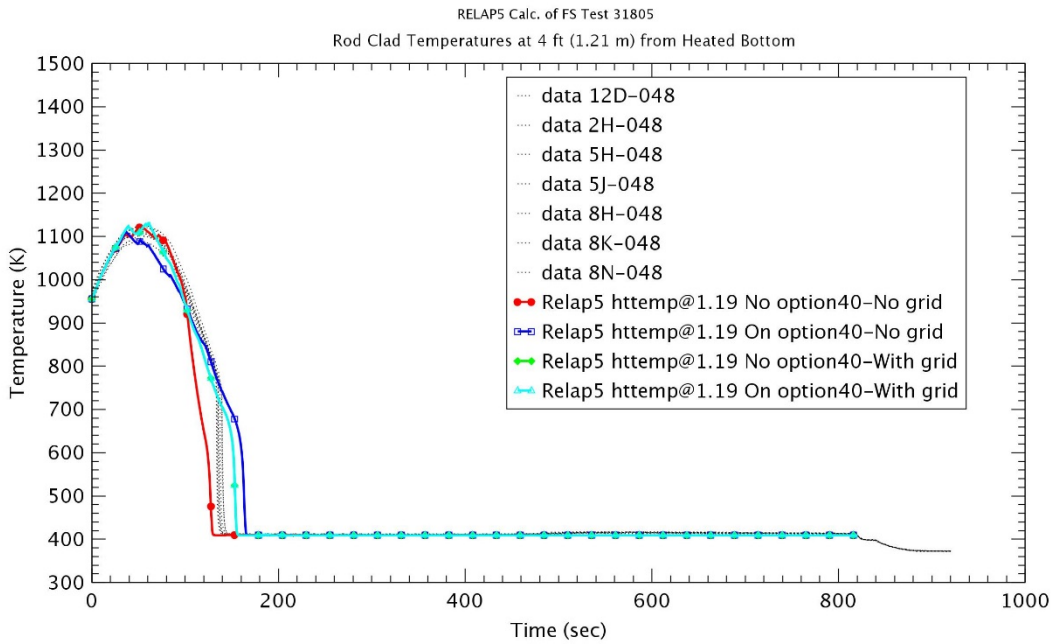


Figure 4-39 Heater Rod Temperature at 1.2 m – Run No.31805

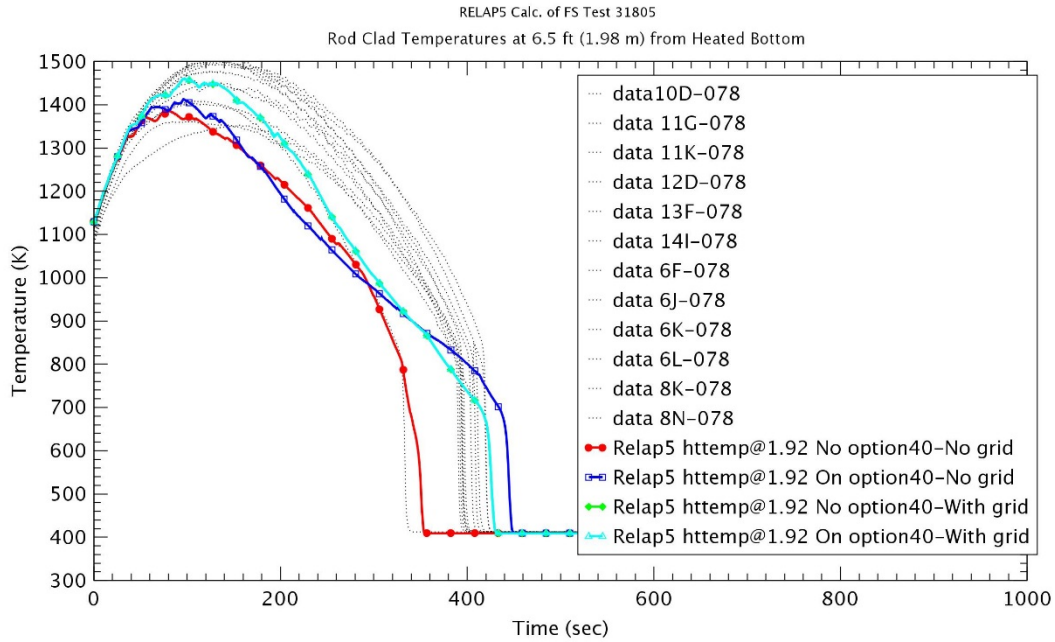


Figure 4-40 Heater Rod Temperature at 1.98 m – Run No.31805

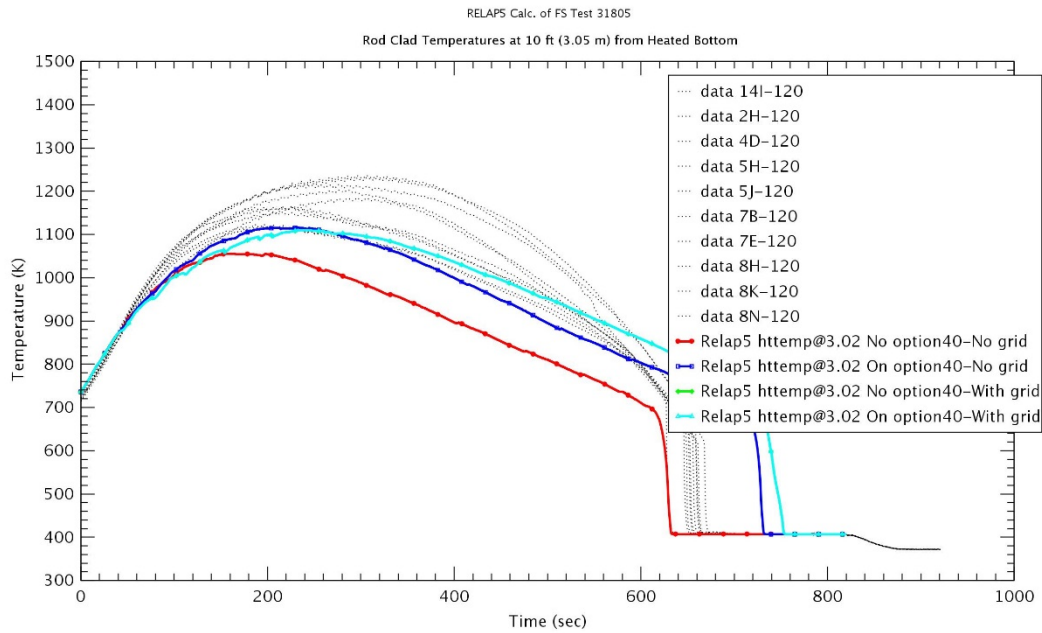


Figure 4-41 Heater Rod Temperature at 3.0 m – Run No.31805

5 CONCLUSIONS

The Full-Length Emergency Core Heat Transfer Separate Effects and Systems Effects Tests (FLECHT-SEASET) was conducted to identify the thermal hydraulic phenomena of forced and gravity reflooding in a 161-rod bundle without flow blockage. In this study, the spacer grid model of TRACE was evaluated for the FLECHT-SEASET test by the TRACE V5.0 patch4. The FLECHT-SEASET test section was modeled in the VESSEL component of TRACE. The test section was divided into 16 axial nodes; one node for lower plenum, fourteen nodes for heated section and one node for upper plenum and there were two cells between each grid. The 161 heated rods in 17x17 assemblies were modeled as a single HTSTR component. The injected flow rates and temperatures was provided as a function of time by FILL component connecting to the bottom of the lower plenum. The BREAK component was used to set the pressure boundary at the top of the test section. The egg-crate grids without the mixing vane were located in the bottom of every other node. The grid parameters were determined by the experimental design data [5,7] and the general fuel data.

Eight tests were chosen in this study and tests were covering a range of flooding rate from 2.10 cm/sec to 15.50 cm/sec, subcooling temperature from 5 °C to 79 °C and upper plenum pressure from 0.13 MPa to 0.41 MPa. The initial rod power at the peak location is 2.3 KW/m (0.7 KW/ft) in all tests. As would be expected, the rod temperatures were decreased and the rods were quenched at the earlier time in most tests if the spacer grid model was used. In addition, as the reflood rate was increased, the lower of the peak rod temperature and the earlier quenching time were predicted. In tests with high reflood rate, the change of peak temperature due to the spacer grid was not large, which resulted from the short heat up period and the faster increase of liquid level by the high reflooding rate. As the test pressure was lower, the higher rod temperature and the later rod quench were predicted since the liquid approached faster to the relatively lower saturation temperature. The use of spacer grid model showed relatively bigger differences for rod temperature, not for quenching time at lower pressure condition. As the subcooling degree was higher, the decrease amount of quenching time due to the spacer grid was reduced since the high subcooling degree could enhance the heat transfer rate.

The sensitivity studies were performed to identify the effect of the grid locations and the difference from the spacer grid model of RELAP5. When the locations of spacer grids were changed into the top of every other node, the rod temperature had higher values and the rod quenching was delayed at elevation with a high power as compared to the case which the spacer grids were located in the bottom of the node. It would be more reasonable to predict the experimental data and showed more conservative results. The RELAP5 code currently implemented the KNF reflood model and the spacer grid model. This reflood model considered three sub-models such as single-phase heat transfer enhancement, grid rewet, and droplet breakup. However, the current RELAP5 version (Version 3.3jz ~ 3.3kl) may have some error to implement the KNF reflood & spacer grid model. It may be because there are some troubles in the use of KNF reflood model (Option 40) and spacer grid input (43000000 cards). Therefore, the developmental version of KNF ([r5m33p03rev0-F6.exe](#)) was used to identify the effect of sub-models and then the droplet breakup model gave the biggest effect on the rod temperatures among three models. The effect of the droplet breakup model was more significant at the higher elevation since the droplet velocity and the number of entrained droplet could be larger at the higher elevation. When the RELAP5 results were compared with the TRACE results, the effect of the spacer grid model in TRACE was more significantly shown even though the single-phase heat transfer enhancement was only implemented in TRACE. These results may be come from the modeling characteristics and the use of the laminar enhancement factor in TRACE. The convective heat transfer enhancement may be excessively large if the laminar enhancement factor will be large.

In conclusion, the effect of the spacer grid model in TRACE was shown well to simulate the FLECHT-SEASET reflood heat transfer experiments. However, there are some limitations to quantitatively predict the effect of the droplet breakup and the grid rewetting models. From the comparison with the RELAP5, it may be found that the current RELAP5 version had some errors to implement the spacer grid model, and the effect of the spacer grid of TRACE could be over-estimated for the rod temperature behaviors. Therefore, the current RELAP5 needs to be modified to correct their errors for the spacer grid model and the TRACE code should be improved to implement the droplet breakup and the grid rewetting models in the future study.

6 REFERENCES

- [1] USNRC, "Improvement of RELAP5/MOD3.3 Reflood Model Based on the Assessments against FLECHT-SEASET Tests", NUREG/IA-0251, 2011.
- [2] USNRC, "TRACE V5.840 User's manual, Volume 1: Input Specification", 2014.
- [3] USNRC, "TRACE V5.840 Theory Manual, Field Equations, Solution Methods, and Physical Models", 2013.
- [4] RBHT IA reportssss.....
- [5] USNRC, "PWR FLECHT SEASET Unblocked Bundle, Forced and Gravity Reflood Task Data Evaluation and Analysis Report", NUREG/CR-2256, 1982.
- [6] USNRC, "TRACE V5.0 Assessment Manual, Appendix B: Separate Effects Tests", 2007.
- [7] USNRC, "PWR FLECHT SEASET Unblocked Bundle, Forced and Gravity Reflood Task Data Report", NUREG/CR-1532, 1980.
- [8] Yao, S. C., L. E. Hochreiter, and W. J. Leech., "Heat-Transfer Augmentation in Rod Bundles Near Grid Spacers", Journal of Heat Transfer, 104, 76-81, 1982.
- [9] Yao, Shi-Chune, M. Loftus, and L. Hochreiter., "Hydraulics of Blocked Rod Bundles", Nuclear Technology, 65, 444-453, 1984.
- [10] Rehme, Klaus, J. Marek, and K. Maubach. "Heat Transfer and Pressure Drop Performance of Rod Bundles Arranged in Square Arrays", International Journal of Heat and Mass Transfer, 16, 2215-2228, 1973.
- [11] Yao, S. C., L. E. Hochreiter, and K. Y. Cai. "Dynamics of Droplets Impacting on Thin Heated Strips," 23rd National Heat Transfer Conference, American Society of Mechanical Engineers, Heat Transfer Division. New York, 1985.
- [12] USNRC, "Analysis of FLECHT-SEASET 163-Rod Blocked Bundle Data Using COBRA-TF", NUREG/CR-4166, 1985.
- [13] USNRC, "NRC Regulations (10 CFR) Appendix K to Part 50-ECCS Evaluation Models", 2015.
- [14] T.S. Choi, "Development of an Improved Reflood Model for RELAP5 and SPACE", PhD Thesis of KAIST, 2013.
- [15] USNRC, "RELAP5/MOD3.3 Code Manual Volume II: Appendix A Input Requirements", 2010.
- [16] D. Barber., "RELAP5 Status and User Problem Report", Fall 2014 CAMP Meeting, Information Systems laboratories (ISL), Inc., 2014.
- [17] Thurgood, M.J., Kelly, J.M., Guidotti, T.E., Kohrt, R.J., and Crowell, K.R., "COBRA/TRAC-A Thermal Hydraulic Code for Transient Analysis of Nuclear Reactor Vessels and Primary Coolant Systems", NUREG/CR-3046, 1983.
- [18] Park, B.H., Kim, Y.S., Jeon, B.K., Kim, H.S., Choi, J.Y., and NO, H.C., "Models Evaluation of Reflood Heat Transfer by Spacer Grids in the Safety Analysis Code", KAERI/CM-1592/1211. 2012.
- [19] USNRC, "RELAP5/MOD3.3 Code Manual Volume III: Developmental Assessment Problems", 2010.

BIBLIOGRAPHIC DATA SHEET

(See instructions on the reverse)

NUREG/IA-0481

2. TITLE AND SUBTITLE

Evaluation of TRACE Spacer Grid Model with FLECHT-SEASET Reflood Test

3. DATE REPORT PUBLISHED

MONTH August	YEAR 2017
------------------------	---------------------

4. FIN OR GRANT NUMBER

5. AUTHOR(S)

Byung-Gil HUH, Ae-Ju CHEONG, Kyung-Won LEE

6. TYPE OF REPORT

Technical

7. PERIOD COVERED (Inclusive Dates)

8. PERFORMING ORGANIZATION - NAME AND ADDRESS (If NRC, provide Division, Office or Region, U. S. Nuclear Regulatory Commission, and mailing address; if contractor, provide name and mailing address.)

Korea Institute of Nuclear Safety
62 Gwahak-ro, Yuseong-gu
Daejeon, 34142, Korea

9. SPONSORING ORGANIZATION - NAME AND ADDRESS (If NRC, type "Same as above", if contractor, provide NRC Division, Office or Region, U. S. Nuclear Regulatory Commission, and mailing address.)

Division of Systems Analysis
Office of Nuclear Regulatory Research
U.S. Nuclear Regulatory Commission
Washington, D.C. 20555-0001

10. SUPPLEMENTARY NOTES

K.Tien, NRC Project Manager

11. ABSTRACT (200 words or less)

The effects of spacer grid model of TRACE V5.0 patch 4 were assessed for the Full-Length Emergency Core Heat Transfer Separate Effects and Systems Effects Tests (FLECHT-SEASET). The main parameters of the spacer grid were defined by the experimental design data and eight egg-crate grids were modeled in the VESSEL component of TRACE. The calculations for eight tests of FLECHT-SEASET revealed that when the spacer grid model was used, the rod temperatures decreased and the rods were quenched at an earlier time in most other tests. In addition, as the reflood rate increased, the lower peak rod temperature and the earlier quenching time were predicted. When the test pressure was lower, the higher rod temperature and the later rod quenching were predicted since the liquid approached a relatively lower saturation temperature faster. When the subcooling degree was higher, the reduced degree of quenching time due to the spacer grid was further decreased because the higher subcooling degree enhanced the heat transfer rate. Sensitivity studies were performed to identify the effect of the grid locations and the difference from the spacer grid model of RELAP5. In this study, the effect of the spacer grid model in TRACE is shown well to simulate the FLECHT-SEASET reflood heat transfer tests. However, since the droplet breakup and the grid rewetting models were not fully implemented yet, there were some limitations in quantitatively predicting their effects. The comparison with the RELAP5 revealed that the current RELAP5 version had some errors in implementing the spacer grid model, and the effect of the spacer grid of TRACE could have been over-estimated for the rod temperature behaviors as compared with RELAP5.

12. KEY WORDS/DESCRIPTORS (List words or phrases that will assist researchers in locating the report.)

Full-Length Emergency Core Heat Transfer Separate Effects and Systems Effects Tests (FLECHT-SEASET)
Mixing Vane Spacer Grid
Egg-crate Spacer Grid
TRACE Version 5.0 Patch Release 4
Reflood Heat Transfer
Droplet Breakup
Spacer Grid Rewetting

13. AVAILABILITY STATEMENT

unlimited

14. SECURITY CLASSIFICATION

(This Page)

unclassified

(This Report)

unclassified

15. NUMBER OF PAGES

16. PRICE



Federal Recycling Program



UNITED STATES
NUCLEAR REGULATORY COMMISSION
WASHINGTON, DC 20555-0001

OFFICIAL BUSINESS



NUREG/IA-0481

Evaluation of TRACE Spacer Grid Model with FLECHT-SEASET Reflood Test

August 2017